STUDIES OF A MICROPOROUS MEMBRANE FOR ANALYTE PRECONCENTRATION AND SEPARATION

by

Silvana do Couto Jacob, BSc, MSc

Thesis submitted in partial fulfilment of the requirements for the awards of

Doctor of Philosophy

of the

Loughborough University of Technology

January of 1994

Supervisor: Dr. Barry L. Sharp, BSc, PhD, DIC, CChem, FRSC

ACKNOWLEDGEMENTS

I would like to express a deep sense of gratitude to my supervisor and friend Dr Barry Sharp for his help, guidance. encouragement, valuable suggestions and constructive criticism wich contributed greatly to the production of this work.

I am grateful to the Brazilian government for the scholarship (Conselho Nacional de Desenvolvimento Cientifico e Tecnologico - CNPq), and to Fundação Oswaldo Cruz for financial support during my study.

I would also like to thanks Drs Phil Friedman and Tim Brockwell of VG-Isotech for their help and for allowing me to use the mass spectrometer at the VG-Isotech factory.

My time in the UK has been made richer by the support and friendship of Dr Arnold Fogg. Also by my research colleagues mainly: Ravinder, Ardinder, Paul, Ian, Ramin, Hellen, Derek, Steve and Dave.

Many thanks are due to the technical staff of the chemistry department , mainly Elaine Till, Bev Cooper, Alan Stevens, Burt Bower and John Spray for their friendship, help and cooperation.

Thanks are also due to Dr Peter Reid for his kind help and advice with the computer programs.

Lastly I thank my husband Josino for his love, care and understanding.

TABLE OF CONTENTS

ABSTRACT

A dual phase gas diffusion-FIA system containing a tubular PTFE-membrane was studied as a mean of producing gas samples for routine $^{15}N/^{14}N$ isotopic ratio mass spectrometry. The method is based on Rittenberg's reaction; the ammonium sample is injected into a liquid alkaline stream containing hypobromite and the N_2 gas produced in the reaction diffuses across a PTFE-membrane into a helium carrier stream which carries it to the detector.

Initially here, the use of a tubular microporous PTFE-membrane as a device for the preconcentration of samples in aqueous solutions was investigated. The performance of such a membrane was studied under a variety of operating conditions. A qualitative model of the membrane mechanism was developed based on the diffusion transport of vapour away from the contained liquid surface through the connected pore space. The dispersion undergone by the sample in the GD-FIA system containing this preconcentration unit was also studied and this FIA system was applied as a practical device for the determination and speciation of aluminium in a river water sample.

The procedure for generating nitrogen gas involved optimisation of the system parameters including the oxidation reaction step and the production on-line of the chemicals used. The nitrogen gas was generated easily and rapidly, allowing a sample throughput capability of the order of 20 h^{-1}. The system was applied to the determination of total nitrogen content in agricultural sample prepared by the Kjeldahl digestion. The method offered precision and accuracy comparable to those of the standard distillation-titration procedure. Isotope ratios were determined with good precision and means for obtaining accuracy comparable with established techniques were developed.

It was also shown that the DPGD-FIA system can be readily adapted to enable different forms of nitrogen e.g. NO_2^-, NO_3^- and NH_4^+ to be determined.

Keywords - Flow injection, gas diffusion, preconcentration, nitrogen speciation, nitrogen-15 isotope ratio mass spectrometry,

CHAPTER ONE
BASIC PHENOMENA IN MEMBRANE SEPARATIONS

1.1 Introduction

Although the utilisation of membranes for the separation of substances for analytical purposes can be considered comparatively rare [1], this method presents a series of advantages such as simplicity and compactness in the design of apparatus, ecological cleanliness, the continuous nature of the process and the possibility of automation. These advantages have led to the rapid development and use of membrane technology in industry, for example, in processes such as desalination, separation of gaseous mixtures, purification and concentration of impurities from waste, biotechnology and space science. Generally, membranes have been used as separation methods to replace well established methods such as evaporation, solvent extraction, adsorption and others.

A membrane is a semi-permeable barrier separating two phases. This barrier should selectively restrict the movement of chemical species (ions or molecules) across it to insure that a separation takes place. For practical uses, the membrane should have good mechanical and chemical stability and the transport rate for the permeating species must be high enough to assure reasonably fast separations. There are many ways in which a membrane can restrict molecular transport such as by: size exclusion, differences in diffusion coefficients, electrical charges and by differences in solubility. In general, membrane separation is a rate process. The separation is accomplished by driving forces, not by equilibrium between phases.

1.2 Types of membranes.

Membranes can be classified under several different schemes [2]. The most common classifications are by nature, by structure, by application and by mechanism of action. The most important are presented in Table 1.1.

Table 1.1 Schemes for classification of membranes[2].

by nature	natural	1. living membranes 2. natural substances
	synthetic	1. inorganic - metal, ceramic, glass 2. organic - films, tubing, hollow fibers
by structure	porous	1. microporous - inorganic, polymeric, filter 2. microporous
	non porous	1. inorganic 2. polymerics - films, tubes, hollow fibres, laminatedfilms
by mechanism	adsorptive	1. microporous -Vycor,compressed powder 2. reactive
	diffusive	1. polymeric 2. metallic 3. glass
	ion-exchange	1. cation-exchange 2. reverse osmotic 3. electro-osmotic
	non-selective	1. fritted glass 2. filter screens

This work is concerned only with synthetic membranes and these can be conveniently classified into four groups[3]:

1.2.1 Homogeneous membranes

1.2.2 Microporous membranes

1.2.3 Asymmetric membranes

1.2.4 Ion exchange membranes

1.2.1 Homogeneous membranes

This type of membrane comprise a homogeneous film or interface, Figure 1.1, through which a misture of chemical species is transported by molecular diffusion (permeation). The separation of various components in a mixture is directly related to their transport rates within the interface, which are determined by the diffusivities and the concentration of the individual components in the film.

Homogeneous membranes are prepared from polymers, metals, or metal alloys by film-forming techniques. Silicone rubber (poly[dimethylsiloxane]) is the most common substance used[4]. This material is chemically and mechanically stable and has a high permeation rate for a large variety of analytes, particularly for acidic gases and inorganic and organic compounds. It also has a high resistance to fouling, mechanical and chemical resistance and differences in selectivity and transport efficiency for different chemical species.

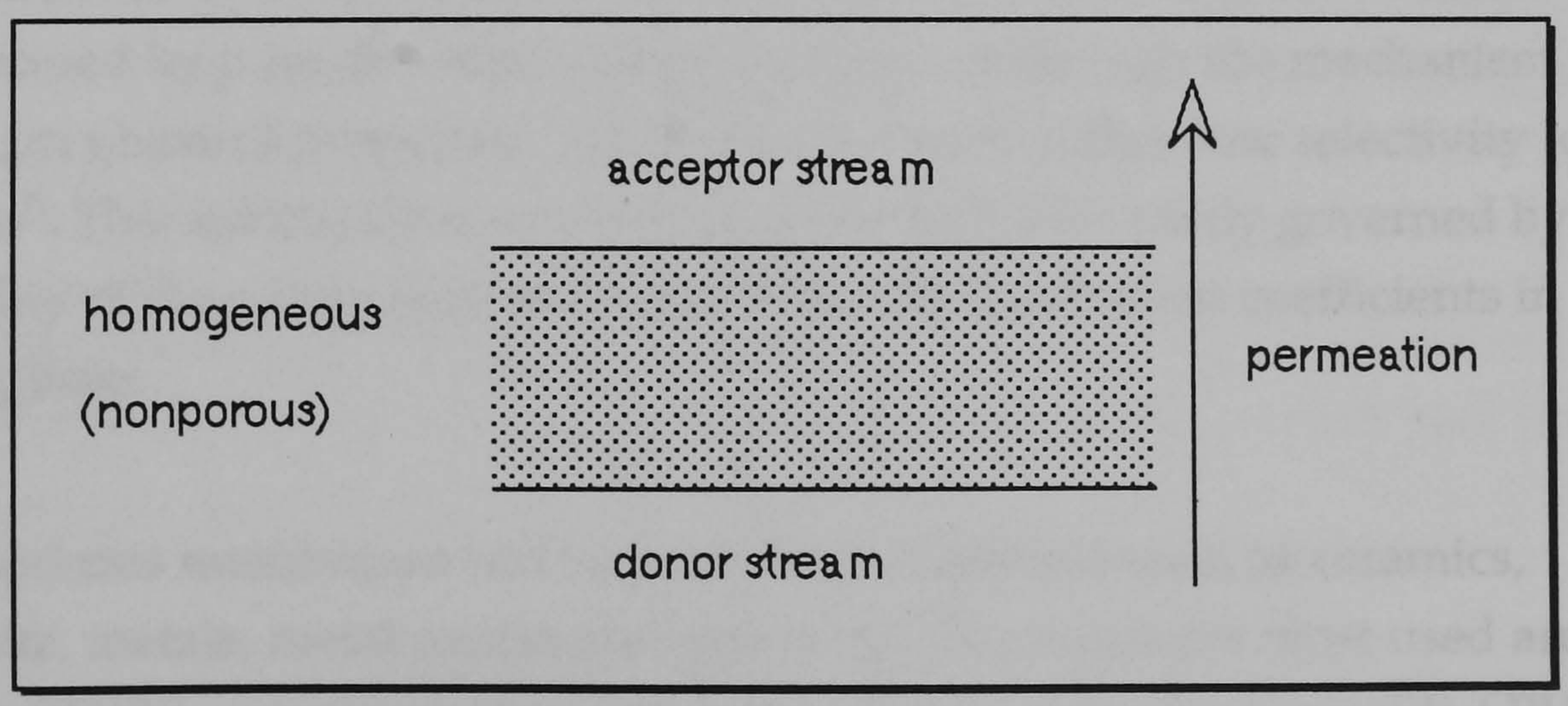

Figure 1.1 Structure of a homogeneous membrane.

An important property of these membranes is that chemical species of similar size, and hence similar diffusivity, can be separated efficiently when their solubility in the membrane phase differs. The overall separation process involves dissolution of the analyte in the membrane, diffusion transport in the condensed phase across the membrane and desorption (evaporation, diffusion) on the other side. Therefore, the selectivity is determined primarily by the solubility of the species (permeation), not by the volatility.

They are used to separate components that have similar size but different chemical nature in processes such as reverse osmosis, gas and vapour separation and pervaporation. Furthermore, due to the combination of solubility and diffusivity through the membrane matrix, homogeneous membranes exhibit higher selectivity than microporous membranes.

1.2.2 Microporous membranes

A microporous membrane has a very simple physical structure and consists of a solid matrix containing heterogeneous holes or pores, Figure 1.2. The size of the pores(about 20 μm) is extremely small in comparison to the classical filters. The smaller the pore size and porosity, the higher the resistance to leakage of water across the membrane due to much higher water permeable pressures which determine the pressure limits over which the aqueous solution starts leaking across the membrane.

Separation of chemical components is achieved by a sieving mechanism determined by pore diameter and particle size. Although the mechanism is based on physical properties, the membrane used adds some selectivity to the system[5]. This selectivity is consistently poor and it is mainly governed by the volatility of the compound and the differences in diffusion coefficients in the other phase.

Microporous membranes can be made from materials such as ceramics, graphite, metals, metal oxides and polymers. The polymers most used are: Teflon (PTFE), polyvinylidene difluoride (PVDF), polyvinyl chloride (PVC), isotactic polypropylene, cellulose ester (acetyl, nitro). Sometimes, polypropylene, nylon, vynil/acrylic copolymer and hydrophobized paper

represent economical alternatives to the more expensive PTFE and PVDF membranes.

The structure can be symmetric or asymmetric, depending on whether the pore diameters vary over the membrane cross section. Microporous membranes are used in processes to separate components that differ markedly in size or molecular mass such as micro or ultrafiltration and dialysis.

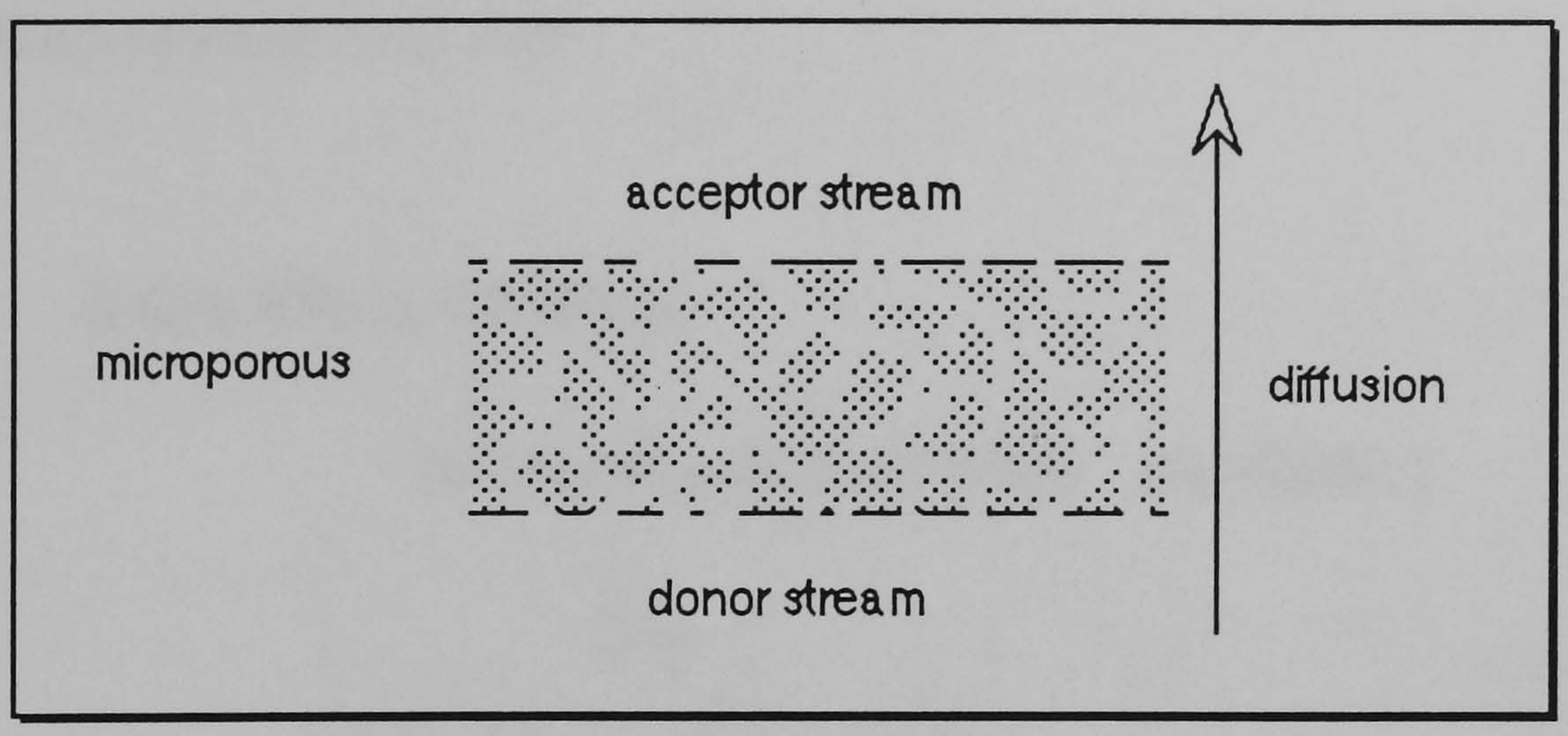

Figure 1.2 Structure of a microporous membrane.

1.2.3 Ion exchange membranes

These consist of highly swollen gels or a microporous structure with the pore walls carrying fixed positive (anion-exchange, alkylammonium groups) or negative (cation-exchange, sulfonic sulphate or carboxylic groups) charges. Membranes that consist of a mixture of negatively and positively charged segments are called *mosaic membranes* [4].

Separation in charged membranes is achieved not only by the structure of the membrane matrix, but also by exclusion of co-ion, i.e. ions which bear the same charges as the fixed ions of the membrane structure.

These membranes exhibit good thermal, chemical and ion transport properties. The separation properties are determined by charge and the concentration of the ions in the solution and in the membrane structure. Ion exchange membranes are generally prepared either by dispersing a

conventional ion exchange material in a polymer matrix, or from a homogeneous polymer in which electrically charged groups such as sulfonic, carboxylic or quaternary amine groups have been introduced. This type of membrane has been used in a limited scale due to problems involving the production of a stable and with high flux ion-exchange material.

However, in recent years, DuPont has developed a line of cation-exchange membranes based on a poly(tetrafluoroethylene) backbone with sulfonic acid groups attached at the end of short side chains based on the perfluoropropylene ether unit:

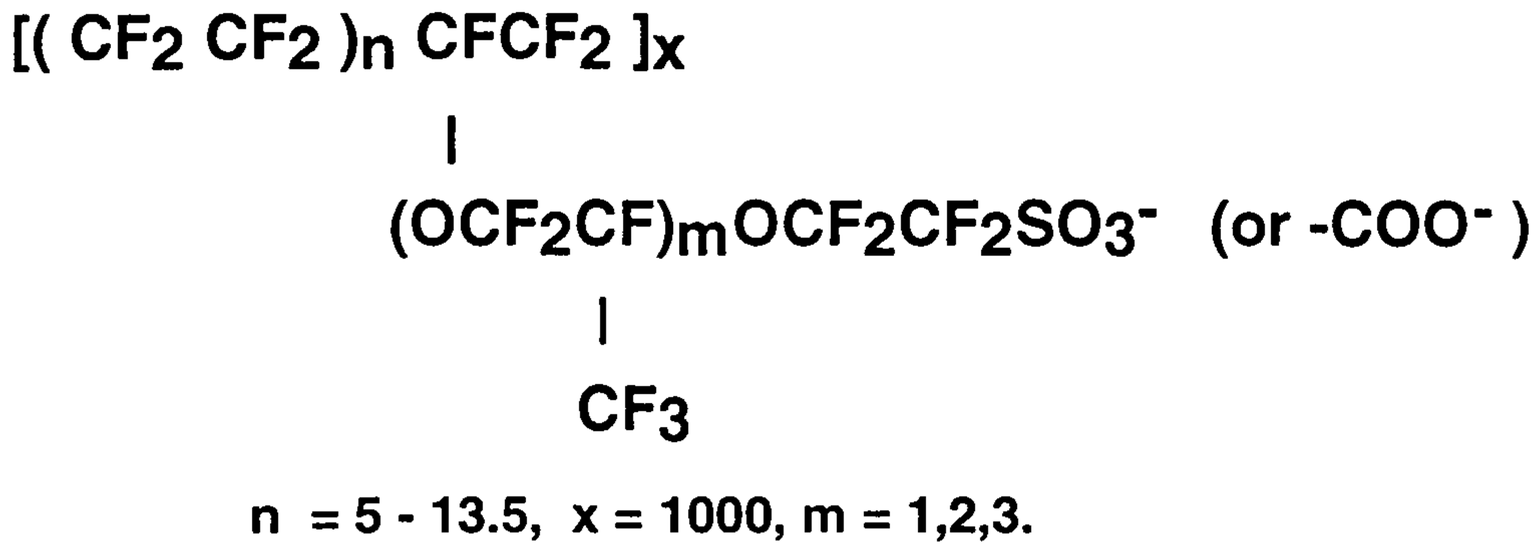

Membrane formed from this polymer is called Nafion® ionomer membrane[6]. It is a strong cation-exchange membrane with an active fluorosulfonic acid group. It consists of two phases, ionic clusters (domains) and perfluorinated matrix (hydrophobic backbone structure). Similarly, perfluorinated carboxylate membranes containing the -COOH group are rather strongly acidic in their H-forms because of the strong electron-withdrawing effect of the fluorine atoms.

In spite of the predominance of hydrophobic regions, the polymer has the ability to absorb relatively large quantities of water and other protic materials causing swelling of the polymer . Its unique structure is due to the molecular aggregation of hydrophilic and lipophilic segments of the polymer. It produces a more uniform exchange site environment and gives a dynamic nature to the cluster (large changes of water content for different forms of the material).

Its sulfonate groups essentially inhibit anionic constituents from penetrating across the membrane when either dilute solutions or gaseous streams are on both sides of the membrane. On the other hand, hydrophilic compounds, such as acid gases (HCl, SO_2, and HNO_3), aniline, cresols, etc., are efficiently and relatively rapidly transmitted through the membrane when an aqueous stream is on one side.

The mechanism of the transport is not clear, but it has been suggested[4] that it can occur through the aqueous channels (by dissolution of the species in the water forming ionic components), or it can occur through the lipophilic domains that have a structure similar to PVDF.

The main applications of ion-exchange membranes are in electrodialysis, electrolysis, batteries, fuel cells, and in pervaporation.

1.2.4 Asymmetric membranes

Transport rates through membranes are inversely proportional to membrane thickness. To achieve high transport rates it is desirable therefore to construct membranes as thin as possible, but these would lack mechanical stretch and be difficult to handle. Asymmetric membranes consist of a very thin (0.1 to 2 μm) polymer layer skin, supported on a highly porous 100-200 μm thick sublayer, Figure 1.3.

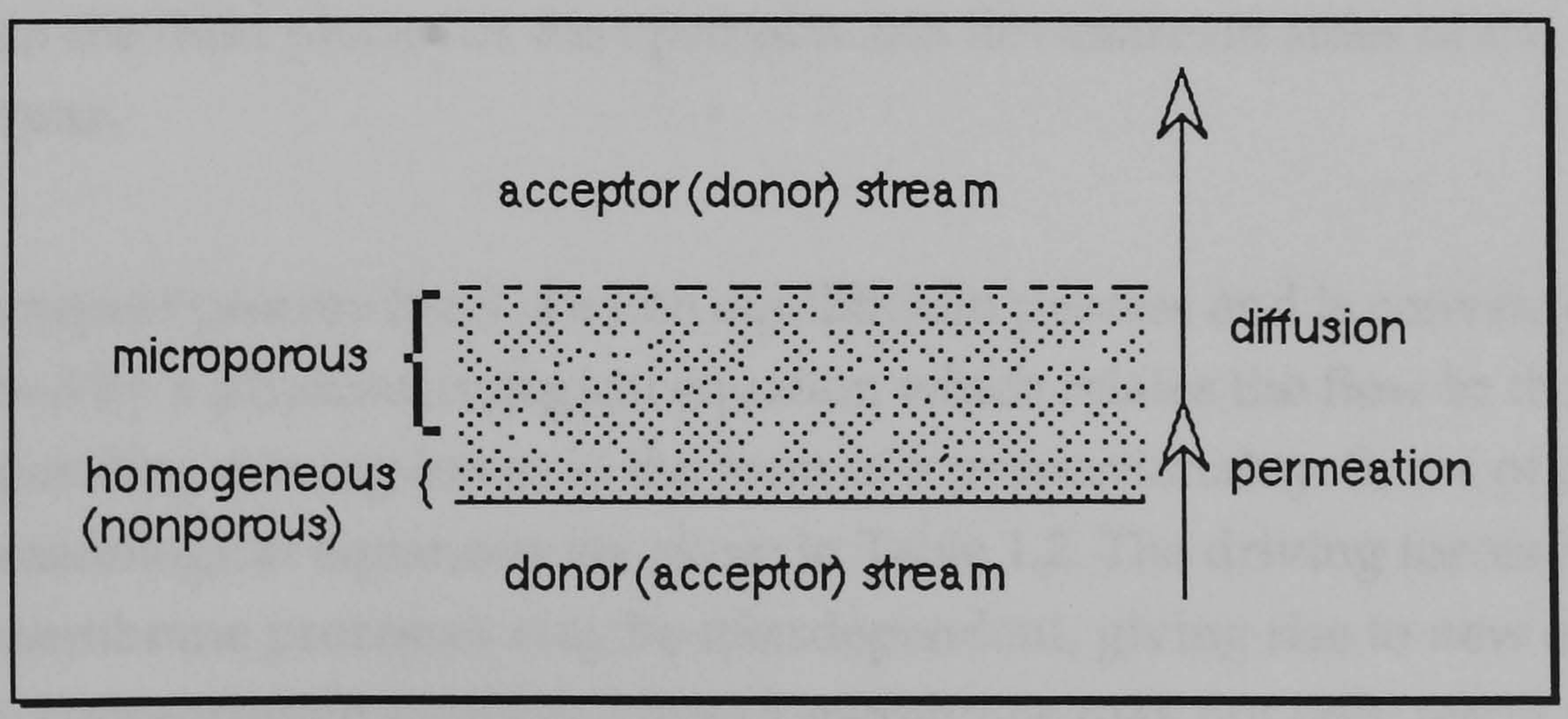

Figure 1.3 Structure of asymmetric membranes.

The skin, which is the discriminating part, may be a porous or homogeneous material and may be neutral (silicone rubber) or charged (ion-exchanger). The sublayer (nylon, PTFE, PVDF,etc.) acts only as a support for the thin, fragile membrane and has little effect on the separation characteristics or the mass-transfer rate of the membrane. The double-layer structure combines the selectivity of both materials. The separation characteristics are determined by the nature of the membrane material or the pore size, whereas the mass transport rate is determined mainly by the skin thickness. Because of the thinness of the homogeneous material, the rate of permeation is much higher than for single-layer homogeneous membranes.

Asymmetric membranes are used in pressure-driven processes such as reverse osmosis, ultrafiltration, or gas separation because these can best utilise the high mass-transfer rates and good mechanical stability.

1.3 Fundamentals of Membrane separation processes

1.3.1 Mechanisms of transport

The transport of fluids or solutes through membranes can occur by several different mechanisms, depending on the structure and nature of the membrane. In all cases, transport of any species through the membrane is driven by a difference in the free energy or chemical potential of that species across the membrane. These driving forces may result from differences in pressure, concentration, electrical potential or a combination of these factors between the fluid phases or the upstream and downstream sides of the membrane.

The transport process itself is a non equilibrium process and is conventionally described by a phenomenological equation which relates the flow to the corresponding driving forces in the form of a proportionality. Some of the phenomenological equations are given in Table 1.2. The driving forces in some membrane processes may be interdependent, giving rise to new effects[7]. Thus, a concentration gradient across a membrane may not only result in a flow of matter but, under certain conditions, can also cause the build-up of a hydrostatic pressure difference, this phenomenon is called osmosis. Similarly, a gradient in hydrostatic pressure may not only lead to a volume flows but

may also result in the formation of a concentration gradient, this phenomenon is called reverse osmosis. Another example is the establishment of a temperature gradient across a membrane which may result not only in a flow of heat, but may also lead to the transport of matter. This process is called thermodiffusion or thermoosmosis. The reverse process, when a mass flow causes a temperature gradient, is known as the *Dufour effect*.

Most often, the transport of a permeant through a membrane can be specified in terms of a permeability coefficient **P**. This coefficient relates the driving forces and corresponding mass fluxes through a membrane. It is defined as:

$$\mathbf{P} = \frac{\mathbf{J}\,\mathbf{L}}{\Delta \boldsymbol{\phi}} \qquad \text{(eq. 1.1)}$$

where

J is the permeant flux (in appropriate units),

L is the membrane thickness, and

$\Delta \boldsymbol{\phi}$ is the difference in hydrostatic pressure, partial pressure, concentration or potential between the upstream and downstream fluid phases.

Permeability coefficients depend strongly on the chemical and physical nature of the membrane and on the properties of the chemical species in the mixture.

The mechanisms involved in the variety of possible membrane separation processes can be categorised as basic transport phenomena. Definitions for some of these specific phenomena become important to clarify the processes involved and to provide pertinent delineation of appropriate mass-transfer models for different systems.

Table 1.2 Phenomenological relationships between fluxes and corresponding driving forces[8].

phenomenological relationship	flux	driving forces	constant of proportionality
Fick's law coefficient $J = D \Delta C$	mass J	concentration differences ΔC	diffusion D
Fourier's law $Q = K\Delta T$	heat Q	temperature difference ΔT	heat conductivity K
Hagen-Poiseuille's law $V = hd\Delta P$	volume permeability V	pressure difference ΔP	hydrodynamic resistance

1.3.1.1 Diffusion

Diffusion is a universal phenomenon by which matter is transported from one point to another under a concentration gradient. The mathematical theory of diffusion is based on the fundamental principle of non equilibrium thermodynamics, that is, diffusional flux is proportional to the concentration gradient[2]. The diffusional movement of mass in one direction through a plane is expressed by Fick's law:

$$\mathbf{Jx} = -\mathbf{D}\,\frac{\mathbf{dC}}{\mathbf{dx}} \qquad \text{(eq. 1.2)}$$

where

Jx , the diffusional flux, is the rate of mass flow per unit area in the x direction (measured in g moles cm^{-2} s^{-1}),

D is the diffusion coefficient (in cm^2 s^{-1}), and

dC/dx is the concentration gradient of the solute (in g moles cm^{-4}) in the direction x, which is normal to the plane.

The negative sign indicates that the mass flows in the direction of lower concentration. This equation states that the flux (mass) is equal to the product of the driving force (concentration gradient) and a constant (diffusivity), that

is, the flux is directly proportional to the concentration gradient. For the purpose of our discussion of membrane diffusion, we can avoid the complicated vector notations, since the transport will be usually unidirectional and membranes are relatively thin.

Fick's first law is inadequate for the solution of most diffusion problems, because the concentrations are usually unknown. The fundamental equation for the mathematical treatment of diffusion processes is the diffusion equation known as Fick's second law:

$$\frac{dC}{dt} = \frac{d}{dx}\left(D \frac{dC}{dx} \right) \quad \text{(eq. 1.3)}$$

where
t is the time.

This equation describes the accumulation of material at a given point as a function of time. The above two laws are the most fundamental equations of diffusion but, for membrane diffusion processes, different equation must be deduced and additional terms introduced due to the presence of the membrane which acts as another component in the diffusion system.

1.3.1.2 Hydrodynamic flow

When the membrane is porous and the fluid flow is laminar, a simple hydrodynamic theory applies. In the case of gas-phase flow, the pores must be large enough compared with the mean free path of gas molecules to ensure viscous flow. For many membranes, the structures of pores are very complicated and frequently not known. Various models have been used introducing numerous pore structure factors, such as average pore diameter, pore size distribution, tortuosity, and specific surface area.

The basic law governing the flow through porous media was originally developed by Darcy[2]. It states that the flow rate is directly proportional to the pressure gradient causing flow. The linear relationship is once again an example of the general phenomenological equations of fluxes and forces in non equilibrium thermodynamics, Here the flow coefficient is divided by the viscosity of the flow, and K is called the permeability, so that,

$$\frac{V}{St} = \frac{K \Delta P}{\mu l} \qquad \text{(eq. 1.4)}$$

where

V = volume flow

S = area

K= permeability

μ = viscosity of the flow

l = thickness of the porous media

The viscosity of a fluid is a measure of internal friction between fluid laminae flowing at different velocities. If a fluid undergoes laminar flow, this friction yields shear forces. When a flowing fluid contacts a solid surface, it adheres to the surface, resulting in a zero fluid velocity at the surface. As a consequence of the viscosity and the adhering property of the fluid, the solid surface experiences a drag force. The viscous resistance is a counter force to this drag.

Darcy's law expresses that the flow resistance is due to viscous drag and the permeability K contains all properties of the porous medium. This definition of permeability is intended to separate the fluid property, that is, the viscosity, from the pore-structure properties in the overall flow coefficient. The unit of Darcy's permeability is a darcy, which is a flow of 1 $cm^3\ s^{-1} cm^{-2}$ with a pressure gradient of 1 atm cm^{-1} for a fluid with 1 cP viscosity. The expression of permeability as a function of pore-structure parameters will depend on the specific pore models.

When a porous membrane consists of straight cylindrical capillaries of equal size, the Hagen-Poiseuille equation[2], should apply directly describe the flow and

$$\frac{V}{t} = \frac{n S \pi r^4}{8 \mu} \frac{\Delta P}{l} \qquad \text{(eq. 1.5)}$$

In terms of molar units:

$$F = \frac{V}{t}\frac{P}{RT} = \frac{n S \pi r^4 P}{8 \mu R T}\frac{\Delta P}{l} \qquad \text{(eq. 1.6)}$$

where

F = total flow rate

r = radius of capillary,

n = number of capillary per unit area,

R = gas constant

Comparing Eq.1. 4 and Eq.1. 5, we can obtain the Darcy permeability for the capillary model. The porosity, **E**, for the capillary membrane will be

$$E = n \pi r^2 \qquad \text{(eq. 1.7)}$$

and the permeability becomes

$$K = \frac{r^2 E}{8} \qquad \text{(eq. 1.8)}$$

Other hydrodinamic equations for a porous membrane have been developed. Kozeny[2] assumed that for a membrane consisting of a capillary bundle with noncircular cross-section, the path of fluid flow would be tortuous. Using the concept of the hydraulic radius, he derived the following equation:

$$\frac{V}{St} = \frac{E^3}{K'(1-E)^2 S^2 \mu}\frac{\Delta P}{l} \qquad \text{(eq. 1.9)}$$

Where

K' is a dimensioneless constant, dependent only on the pore structure.

Comparing Eq.1.4 and Eq.1.9, the Darcy permeability becomes

$$K = \frac{E^3}{K'(1-E)^2 S^2} \qquad \text{(eq. 1.10)}$$

Numerous modifications of the original Kozeny theory have been developed, and all of these offer various structural theories of permeability for different pore models.

1.3.1.3 Knudsen Flow

When the pore size of a membrane becomes small and the mean free path is comparable or larger than it, the fundamental concept of viscous flow breaks down. In this situation, the collisions between gas molecules become much fewer than the collisions between gas molecules and the wall. This situation is known as a "free-molecular diffusion" or "Knudsen flow". In experimental work it has been shown that at high-pressure the flow obeys the Poiseuille equation. As the absolute pressure becomes lower, the flow for a given ΔP reduces to a minimum, but then increases again before becoming independent of the absolute pressure. In the extremely low pressure range, the flow becomes independent of pressure, which is the true Knudsen regime. Based on the kinetic theory of gases, Knudsen derived the following equation for free molecular flow through a long circular capillary:

$$F = \frac{8\pi r}{3(2\pi RMT)} \frac{P1 - P2}{l} \qquad \text{(eq. 1.11)}$$

where

r = the radius of the capillary,

M = is the molecular weight of the gas.

Basically, the same equation can be applied to all microporous membranes with the application of a geometric modification factor **G**.

$$F = \frac{GS}{(2\pi RMT)} \frac{P1 - P2}{l} \qquad \text{(eq. 1.12)}$$

Many authors have attempted to evaluate the geometric factor G for different pore models considering quantities such as tortuosity and porosity.

1.3.1.4 Electrochemical phenomena

When the solute or membrane is ionised, electrical potential can play a role in transport just as do concentration and pressure. This process involves two

separated driving forces, that is, concentration difference and electrical potential difference and an extension of Fick's law for an ionic species i in an electrical field **dø / dx** can be expressed as the sum of two flow rates:

$$J_i = D_i \frac{dC_i}{dx} + \frac{Z_i C_i F}{RT} \frac{d\phi}{dx} \qquad \text{(eq. 1.13)}$$

where

Zi = ionic valence

F = Faraday constant.

The first term in the Eq. 1.13 represents the flow rate due to simple diffusion under a concentration gradient. The second term represents the ion flux driven by electrical potential, which is directly proportional to the electric current across the membrane.

Applications of an electrical field on such a system may induce a transport flux of ions which, in general, is opposed by molecular diffusion from the concentration gradient induced. Oppositely, molecular diffusion by an imposed concentration gradient of ion i induces an electrical field, or streaming potential, that opposes this transport and affects all others ions in the system.

When the solution contains several different free ions, unequal distribution of ions will result across the membrane and an electrical potential difference called *Donnan effect* will be created. There are usually two cases in which the Donnan effect may occur. One is with ion-exchange membranes placed in a solution of strong electrolytes. The other is a system of colloidal solution. One important but simple example of the Donnan effect is as follows: if electrolyte solutions are placed on the right, R, and left, L, sides of a membrane permeable to cations but not to anions or water, then the anion concentrations of the two solutions will not change. However, the cations will redistribute between the right and left solutions until an equilibrium is established. If the cations are a mixture Na^+ and Ca^{2+}, then at equilibrium

$$\frac{[Ca^{2+}]_R}{[Ca^{2+}]_L} = \frac{[Na^{+}]_R^{\,2}}{[Na^{+}]_L}$$

Thus, by placing a dilute Ca^{2+} solution on one side of the membrane and a concentrated Na^{+} solution on the other, one can develop a more concentrated Ca^{2+} solution by what has been referred to as Donnan dialysis[9].

1.3.1.5 Other mechanisms

Temperature gradients may lead to species transport that can be explained in terms of non equilibrium thermodynamics. When the temperature gradient causes diffusion, this process is known as thermal diffusion. If the temperature gradient is responsible for the flow of solvent, it is called thermo-osmosis. If the flow is in the Knudsen regime it is called thermal effusion. The thermal phenomena do not play a significant role in any membrane separation process, since the magnitudes of the coupled phenomena are usually quite small.

When diffusional phenomena are coupled with chemical reactions, the resultant transport rates may be greatly affected. For example, in facilitated transport, carrier molecules present in a membrane react or complex with the permeating species to create an additional gradient that contributes to transport [9]. Facilitated transport does not affect the ultimate equilibrium state, but simply acts as a catalyst which increases the rate at which equilibrium is approached.

1.4 Membrane separation processes

Membrane separation processes differ greatly depending on the membrane, the driving force and the area of application. Table 1.3 summarises the most important of these separation processes. The driving force can be a concentration gradient, hydrostatic pressure gradient, or an electrical potential gradient and in some cases a pressure and concentration differences can be utilised.

Typical pressure-driven membrane processes are microfiltration, ultrafiltration and reverse osmosis. They are basically similar and differ only in the size of the particles to be separated and the membranes used. A mixture of components of different size is brought to the surface of a semipermeable membrane. Under the hydrostatic pressure gradient, some components permeate through the membrane, whereas others are retained. Microfiltration and ultrafiltration are based on a sieving effect and particles are separated because of their differing dimensions. The term microfiltration is used when particles with a diameter of 0.1-10 μm are separated from a solvent or other components with molecular masses < (0.1-1) x 10^6. In ultrafiltration, the components to be retained by the membrane are molecules or small particles ≤ 0.1 μm in diameter. In reverse osmosis (hyperfiltration), particles, macromolecules and low molecular mass compounds such as salts and sugars, are separated from a solvent, usually water. In this case, the osmotic pressure of the solution becomes significant and cannot be neglected in comparison with the hydrostatic pressure driving force.

In a gas permeation process, the feed mixture consists of gases or vapours. Asymmetric solution-diffusion membranes and a hydrostatic pressure driving force are used to transport components through the membrane. The membrane selectivity is determined by the solubility and diffusivity of the components in the membrane interface.

Dialysis involves selective transport of solutes through a membrane as a result of concentration differences between two fluid phases. It achieves the separation (or purification of a solution) of solutes that are transferred more rapidly than others as a result of the relative permeabilities of these species through the membrane. One of the most important commercial uses of this technique is haemodialysis in which human blood is cleansed of metabolic wastes, such as urea, creatinine, and uric acid, while retaining essential higher molecular weight constituents and blood cells[9].

Table 1.3 Important membrane separation process; operation principals and applications[8].

separation process	membrane type	driving force	method of separation	application
microfiltration	symmetric microporous membrane (0.1 -10) μm	hydrostatic pressure difference (10 -500)KPa	sieving mechanism and adsorption	sterile filtration clarification
ultrafiltration	asymmetric microporous membrane (1- 10) μm	hydrostatic pressure difference (0.1 -1) MPa	sieving mechanism	separation of macromolecular solutions
reverse osmosis	asymmetric skin-type membrane	hydrostatic pressure difference (2 - 10) MPa	solution diffusion mechanism	separation of salts and micro-solutes
dialysis	symmetric microporous membrane (0.01 - 1)μm	concentration gradient	diffusion in convection free layer	separation of salts and microsolutes from macromolecular solutions
electrodialysis	cation-and anion-exchange membranes	electrical potential gradient	electrical charge of particle and size	desalting of ionic solutions
gas separation	homogeneous or porous polymer membrane	hydrostatic pressure and concentration gradient	solubility diffusion	separation of gas mixture
pervaporation	asymmetric homogeneous polymer membrane	vapour pressure gradient	solubility diffusion	separation of azeotropic mixture

Pervaporation employs both a concentration gradient and pressure as driving forces for separation[8]. Volatile organic compounds are removed from a liquid into the gas phase. Because of the presence of both liquid and vapour phases, the term pervaporation is used to describe this process which involves selective sorption of a liquid mixture into the membrane, selective diffusion or flow through the membrane, and then desorption into a vapour phase.

Electrodialysis is a process in which solute ions move across membranes by application of an electrical field, involving two separated driving forces, concentration differences and electrical potential difference. Although electrodialysis, can be considered as a modification of ordinary dialysis, the two process are distinctly different in many ways. Dialysis depends on the concentration gradient and the flow of solute is always from the more concentrated to the less concentrated solution. In electrodialysis, the direction of transport can be either way, depending on the field direction. In electrodialysis, the external electrical potential can be easily maintained until the desired degree of separation is achieved ,while in dialysis, the concentration gradient may diminish gradually as a result of the mass transport. The types of membrane used in the two processes are also different. Usually, ion-selective membranes are employed in electrodialysis, while in ordinary dialysis, microporous membranes are used.

1.5 Membrane techniques in analytical chemistry.

In recent years, most of the known membrane separation processes have found application for the separation of molecular mixtures. Micro filtration, ultrafiltration, reverse osmosis, dialysis and electrodialysis, are now widely used to produce potable water from sea and brackish water sources, to recover valuable products from industrial effluents, or to perform various concentration, purification and fractionation tasks in the chemical food and drug industries[8]. Although membrane processes are being used in diverse fields, their application is still impaired by high costs and shortcomings in membrane performance. However, membrane technology is in a state of rapid development and new membranes with better separation characteristics and improved thermal, chemical and mechanical properties are being developed.

In analytical chemistry, membranes are used mainly for separation and preconcentration of materials into pure species. Membranes are also used in many cases as isolating barriers to protect sensitive systems from the ambient environment. The combination of these two roles are well utilised in ion-selective membrane electrodes and specific gas probes[2]. In both cases, reagent and electrodes are surrounded by ion-specific or permeselective membranes so that only specific ions or gases may permeate through the membranes while the electrode system is protected.

The application of membranes to separate two phases, such as organic and aqueous solutions or a gas and a liquid, has increased recently especially with the development of flow injection as an on-line sample treatment technique. In flow injection, a high degree of selectivity is desired and the use of a membrane interface may enhance selectivity, for example, by removing the analyte from the complex sample matrix and introducing it into a carrier stream free of matrix. It may also be employed as a means for dilution or preconcentration[10]. The most used processes are: dialysis and gas diffusion, but, pervaporation and electrodialysis processes have also been used in flow injection systems.

CHAPTER TWO
GAS DIFFUSION FLOW INJECTION ANALYSIS

2.1 Introduction

Membrane separation in conjunction with flow injection offers great potential for selectivityand /or sensitivity improvement . Gas diffusion is the most popular separation technique used and is well suited for incorporation into flow systems. Due its easily automation becoming simple, fast and reproducible, in contrast to equilibrium modes, which are normally time consuming and inappropriate for quantitative measurements.

This technique can be used for:

-separation of an analyte from a matrix
-separation of a matrix from an analyte
-preconcentration
-dilution
-speciation (different physicochemical forms of the analyte)
-separation of two imiscible phases (including hydride techniques)
-introduction of reagents and samples
-preparation of standards
-interfacing of hybrid techniques

The GD-FIA technique is based on the separation of the particular species from the original sample matrix to a new matrix, the acceptor stream, which contains no chemical or physical interferents thus increasing the sensitivity and selectivity of the detection [11, 12, 13].

A large number of volatile inorganic (gases, volatile compounds, and gas-evolving ions such as ammonium, carbonates, sulphides etc.) and organics (phenols, aldehydes, ketones, alcohols, carboxylic acids, etc.) species can be measured after their separation and/or preconcentration using the GD-FIA technique. A typical GD-FIA manifold is shown in Figure 2.1. The substance from the original matrix ,donor stream, is converted into a gas which diffuses to an acceptor stream under optimised conditions. The transport of through the gas/diffusion unit can be realised from from a gaseous , liquid, aqueous or organic donor stream (and also from solid samples in some special cases), in which the compounds of interest can eventually be chemically converted to

a transportable species, into a suitable gaseous or liquid(organic solvent or aqueous) acceptor stream. Thus, different combinations can be realised depending on the characteristic of the sample and of the analytical system.

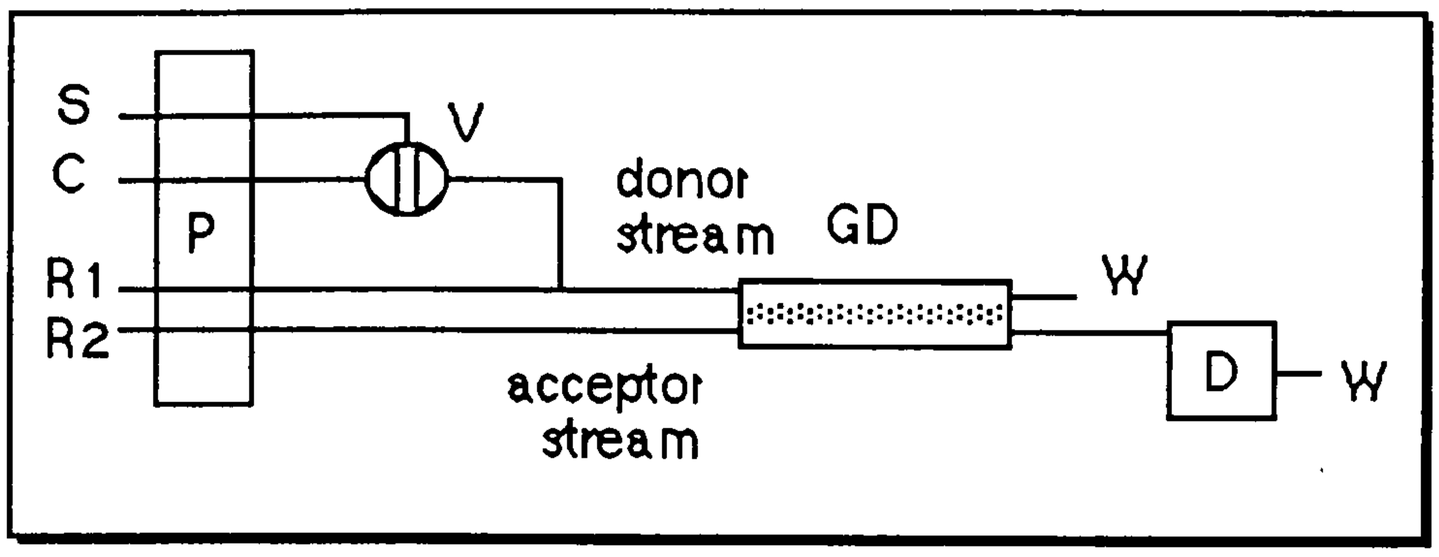

Figure 2.1 Typical manifold for a GD/FIA system. S = sample, C = carrier flow, V = injection valve, R1 and R2 = reagents, GD = separator unit D = detector and W = waste.

To chose a suitable acceptor stream, it must have enough absorption capacity to quantitatively and rapidly collect all of the diffused analytes. This capacity is directly related and dependent on experimental factors such as sample contact time with the membrane, contact area of the membrane, composition of the donor and acceptor fluids and the membrane properties. At given experimental conditions the transfer efficiency for different species is related to Henry's constants, the partial pressures, partition coefficients between the fluids and the membrane matrix and diffusion coefficients through the membrane matrix. Several theoretical models of mass transport have been discussed[14, 15, 16] but all appear to be of limited value for optimisation of the mass transport through membranes in a flow diffusion cell.

The analytes of interest, injected in a suitable form or generated on-line, can be detected directly based on their physicochemical properties. Peak heights or peak areas are commonly used for quantitation of the analytical signal which has a typical FIA profile corresponding to the concentration profile of the original reaction zone.

This chapter presents brief descriptions about the instrumentation involved and the experimental factors influencing the analytical sensitivity and selectivity when GD-FIA systems are used.

2.2 Instrumentation

2.2.1 GD-FIA manifolds

The material used to construct a GD-FIA manifold are the same as those needed for conventional FIA systems but with the addition of the separation unit. They must be chemically inert and not interact either with the analyte or reagents. A variety of the detectors, optical, electrochemical and others can be coupled to the system for quantitation of the analyte. Non selective detectors i.e., conductometric, potentiometric, etc. can often be used as the GD-FIA technique can offer high analyte selectivity.

Several manifolds of differing complexity have been utilised for determining gaseous, gas evolving, and volatile species. Kubán *et al.*[4] has described about 15 different manifolds. Generally, a defined volume of an untreated sample, aqueous or gaseous, is injected into either an inert carrier stream or a suitable modifier stream. The sample disperses into the carrier stream, or sample components react with the modifier in a mixing/reaction coil to form species that are transportable through the membrane in the separation unit. The geometry of the coil is dictated by the rate of the mixing process, the dispersion and the reaction rate. The presence of a modifier (a buffer for example) increases the efficiency and /or the selectivity of the separation. The transportable species from the donor stream penetrate across the membrane in the separation unit where they are collected in a stagnant, circulating or continuously flowing acceptor stream.

Two types of GD-FIA manifolds have been used:
- the continuous flow
- the stopped - flow.

In the first, Figure 2.2 a, the acceptor stream flows continuously to the detector, in the stopped -flow mode, a known amount of the acceptor fluid is enclosed inside the sample loop of the injection valve or it can be continuously circulated in a closed loop. In most cases a continuous flowing acceptor stream is used, but a considerable loss of sensitivity occurs even when the donor/acceptor stream flow rate ratio is large. In order to increase the sensitivity, and thus to increase the efficiency of transport through the

membrane the stopped- flow mode is used[17, 18, 19]. This combination produces a degree of preconcentration during the separation. The preconcentration factor reached depends on the total permeation through the membrane, the flow-rate of the donor stream and mainly on the time of permeation. A linear relationship exists between the time of exposure of the membrane to the sample and the concentration of the analyte in the sample [20]. Precise timing is therefore critical when running in the stopped-flow mode.

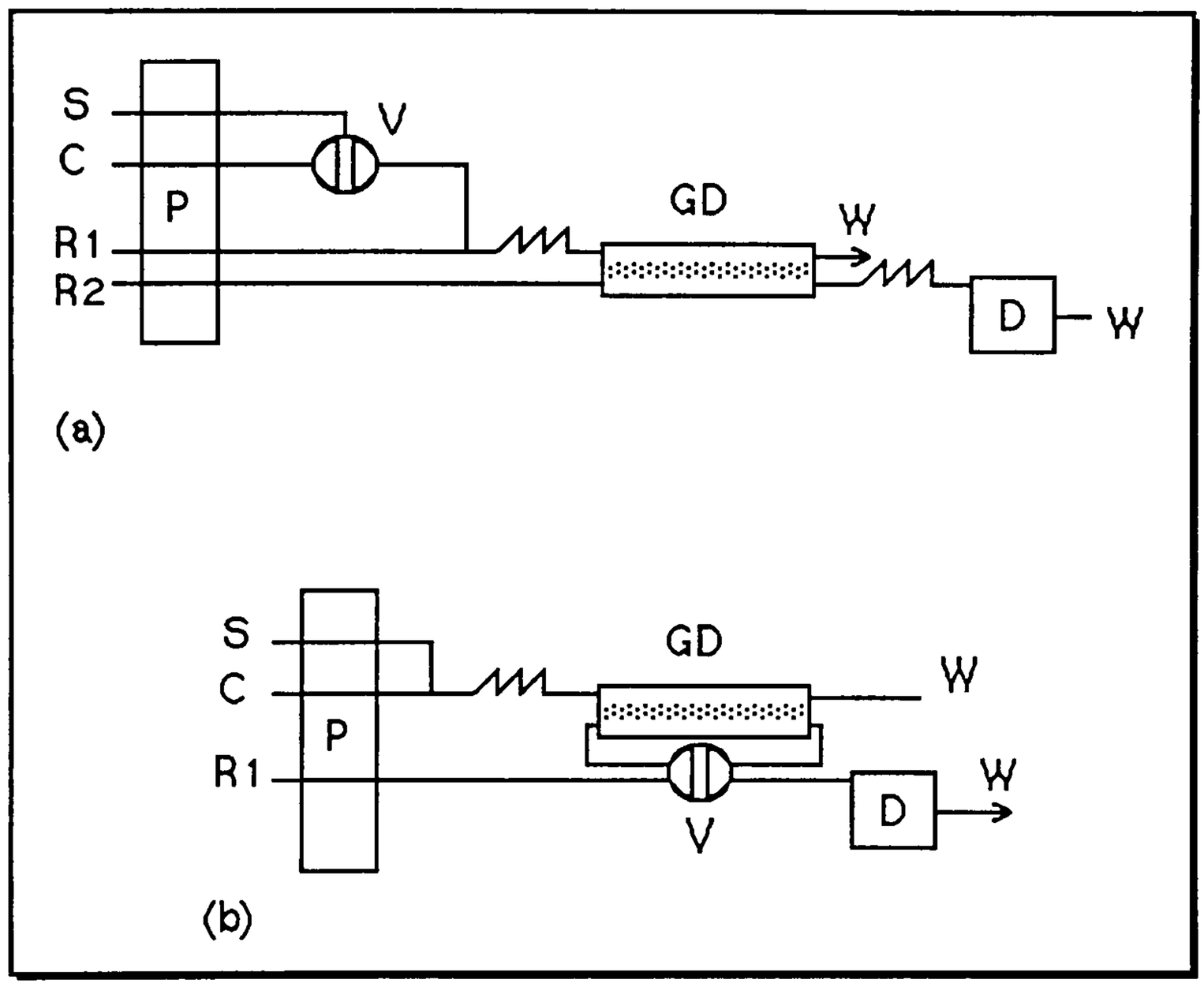

Figure 2.2 Examples of manifolds for continuous and stop-flow mode (a) and a closed loop mode (b). S = sample, C = carrier, R1 and R2 = reagents, P= peristaltic pump,V= valve, AC = acceptor stream, MC = mixing coil, RC = reaction coil, GD = gas diffusion separator unit, DS = donor stream and W = waste.

Another approach for the on-line preconcentration of gaseous and volatile analytes from fluid or gaseous samples is the closed-loop manifold[21]. This arrangement allows the acceptor liquid to be circulating in the loop while the carrier stream continuously enters the membrane device and is directed to the waste, Figure 2.2 b. The analyte is continuously separated and preconcentrated into a small volume of the acceptor fluid circulating in the closed loop. The detector can be situated on the closed-loop, Figure 2.3 a, monitoring the analytical signal continuously; or it can be located outside of the loop where the analytical signal is monitored after a preselected time period. The preconcentration factor in this case depends on the loaded

volume of the sample (time of sampling), the transfer efficiency and the acceptor loop volume.

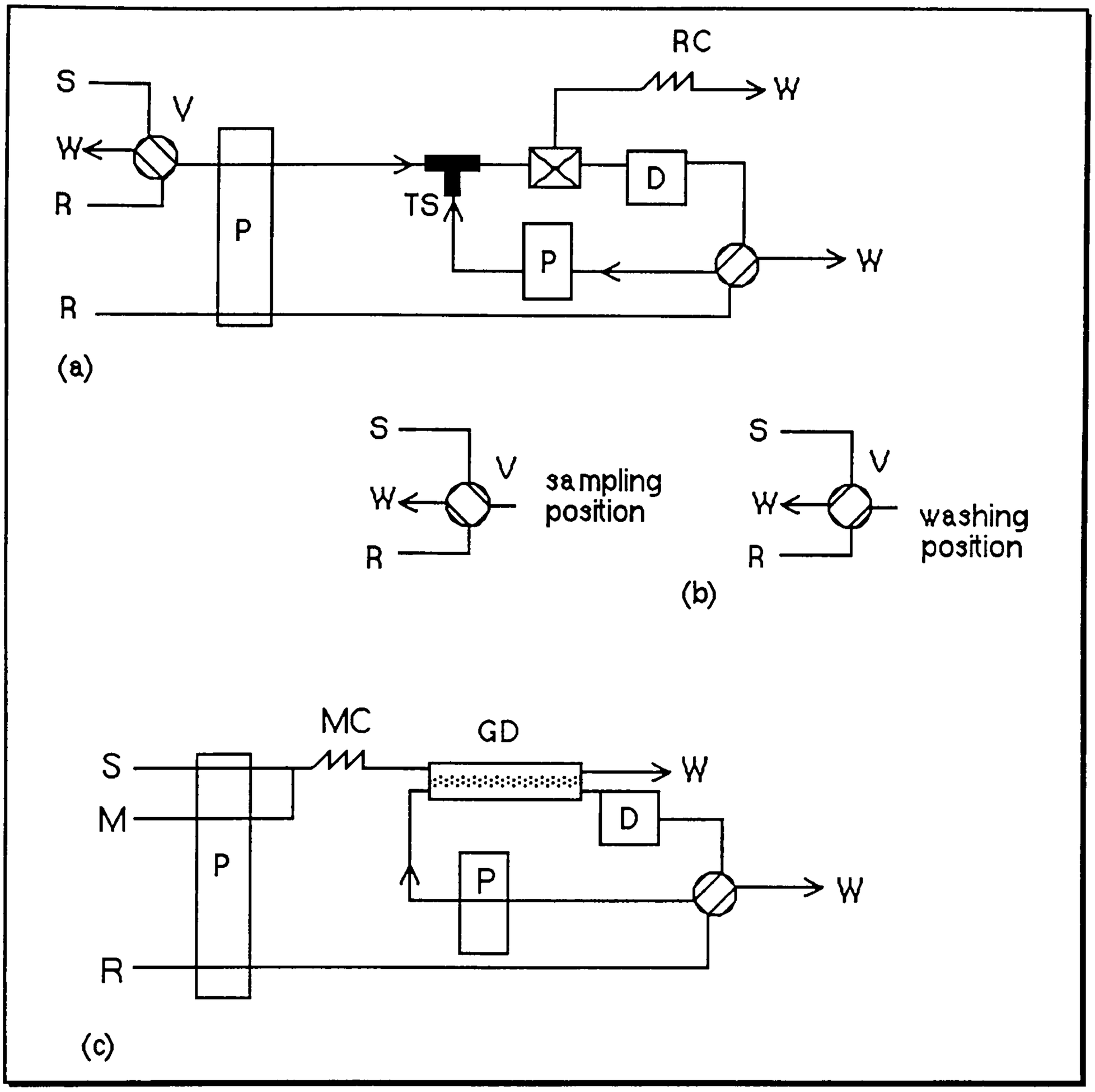

Figure 2.3 A closed-loop manifold for continuous introduction of a fresh gaseous sample into a continuous circulating acceptor stream. (a) A segmented mode containing a T-piece (TS) segmenter and a debubbler (PS) as a separator unit; (c) with a membrane device. The sampling and washing positions of the valves also are shown,(b)

A similar approach for gaseous samples is based on the continuous transport of gases into an acceptor flow across an open gas /liquid interface. The loop is connected to a fresh sample stream, which continuously enters the closed loop system via a four-way valve and leaves the loop after separation in the phase separator(a membrane type or a simple debubbler)[22, 23].

The incorporation of a second membrane into the manifold, (two separation units), can provide considerable additional selectivity for the determination, Figure 2.4. This approach is capable of producing practical solutions to problems requiring extraordinary discrimination between two similar analytes, e.g., two volatile acid gases[24]. The separation can be conducted both in the continuous flow mode or in the stopped-flow mode. A particular group of analytes can be pre-separated from the major components of the matrix in the first stage and subsequently selectively transported across the membrane in the second stage. A preconcentration step can then eventually be performed in either the first or second stage.

The separation units can contain either two identical or two different kinds of membranes. Each analyte is then collected in two separated acceptor streams of different composition. The two membranes can be arranged in series, as shown on Figure 2.4, or in parallel as shown in Figure 2.5.

This system can, for example, be used for the simultaneous determination of acidic and alkaline gases with two detectors in parallel, Figure 2.5 b or with a single detector situated after the confluence point, Figure 2.5 a.

Speciation of a particular analyte can be achieved using two membrane devices either in series or in parallel. The sample can be fed continuously into the first membrane, with the analytical signal being related to the content of free species. The acceptor stream is then, mixed with a suitable reagent (modifier) before it enters the second membrane unit. The combined analytical signals correspond to the total or available content of the analyte.

The sample can also be split or injected simultaneously into two separated channels passing two membrane units in a parallel configuration figure 2.6. Two detectors can be used to monitor the amount of the analyte Figure 2.6 a, or two separated peaks can be obtained using a delay coil of a suitable length in each particular line and a confluence point in front of a single detector , Figure 2.6 b.

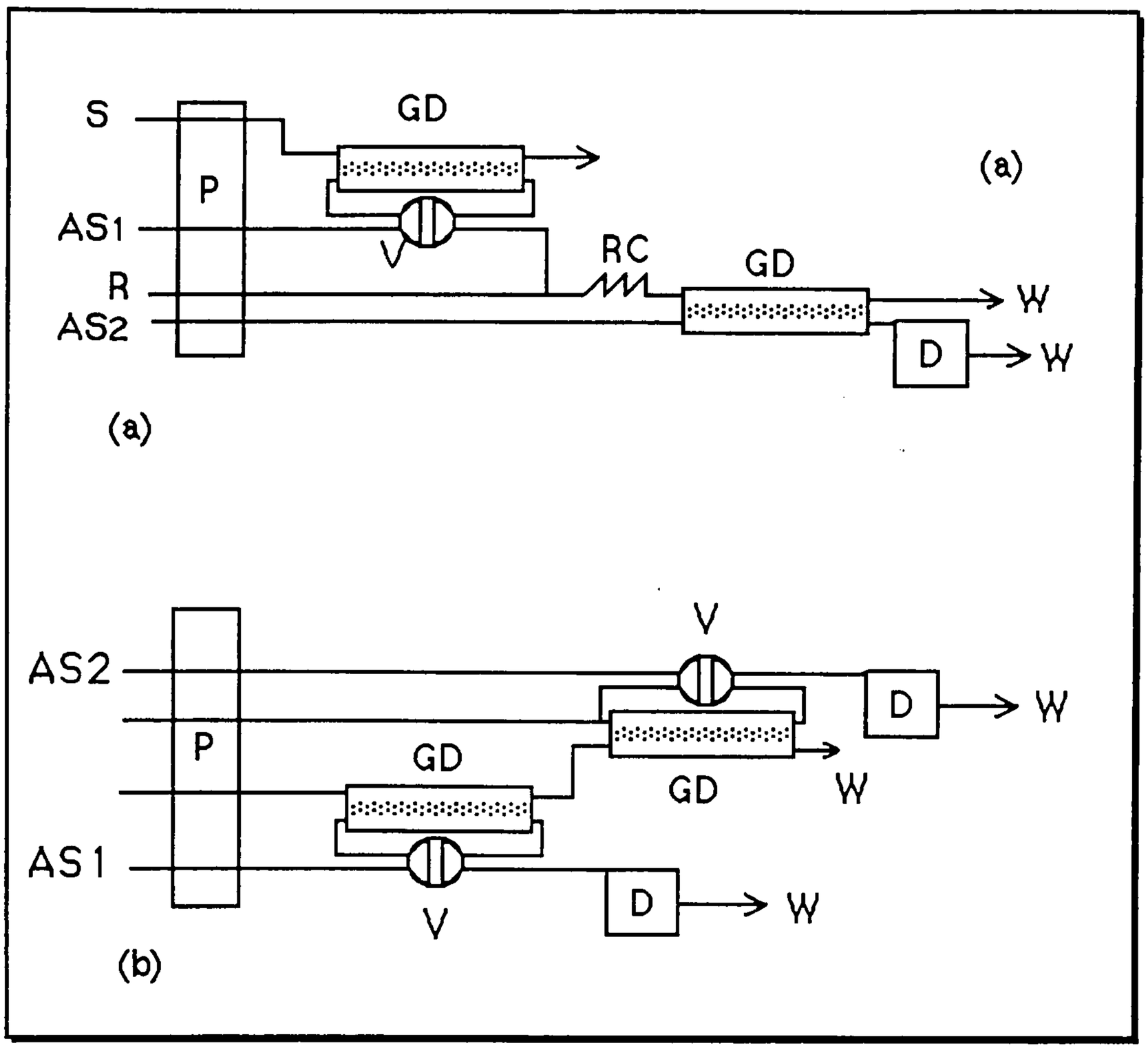

Figure 2.4 Manifold with two-stage separation and preconcentration in the first step (a) and in both steps, (b).

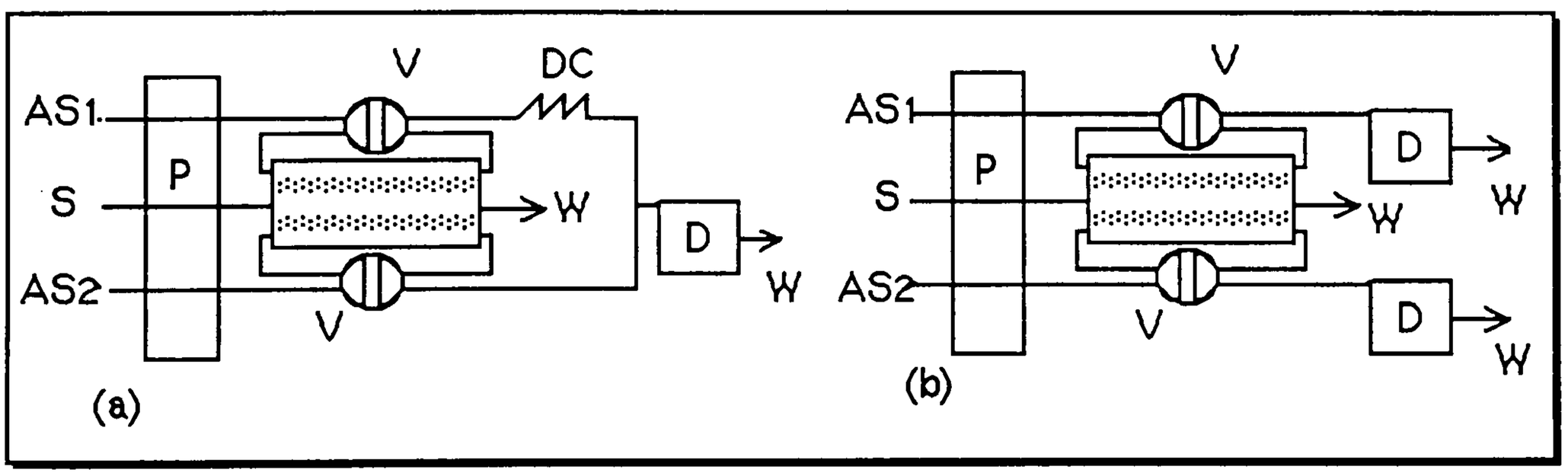

Figure2.5 FIA manifolds with parallel dual-membrane gas diffusion devices, with a single detector,(a), or two detectors in parallel,(b), and analytes preconcentration in both lines.

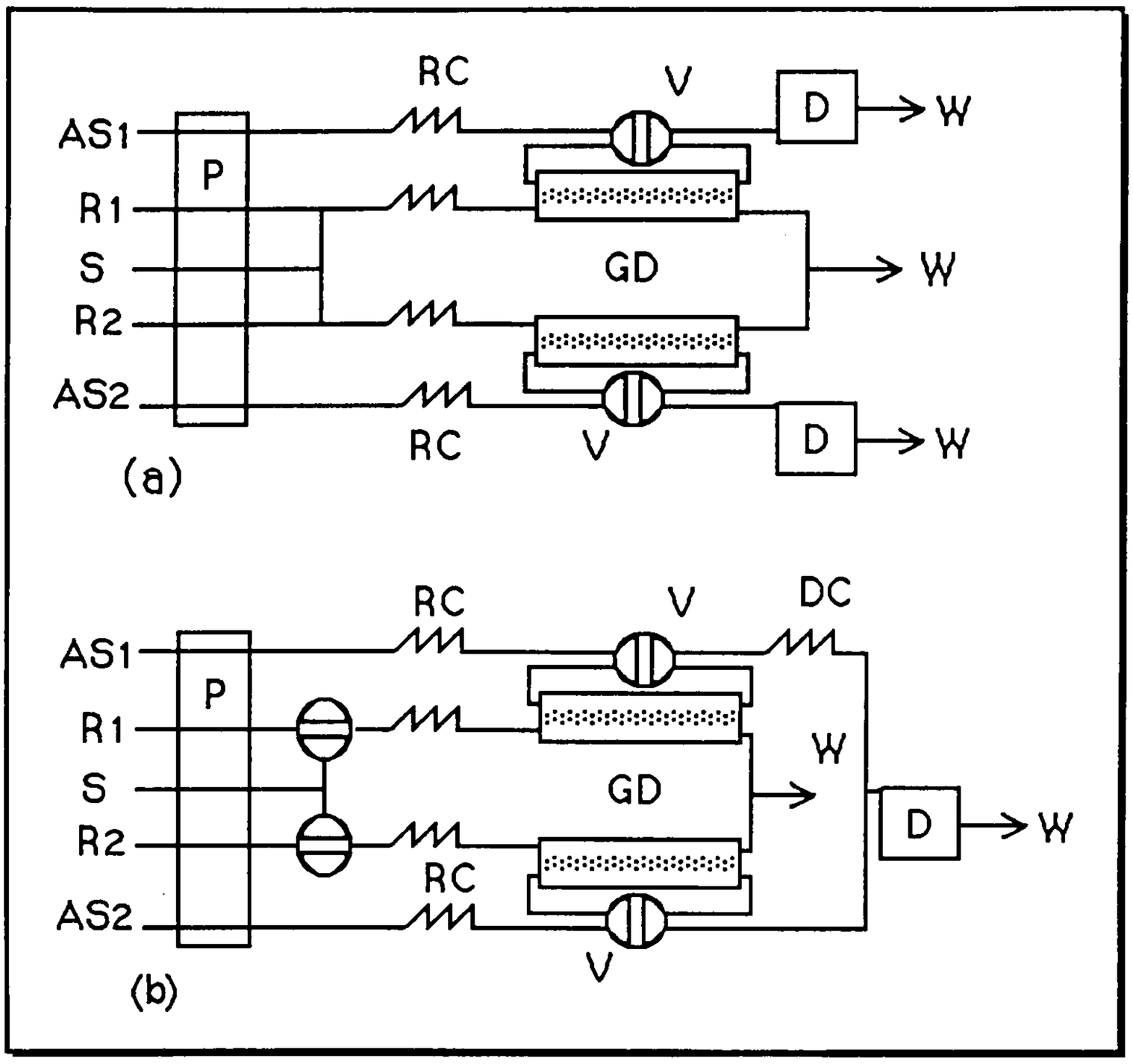

Figure 2.6 FIA manifold for the simultaneous determination of two components or species applying a single detector (b) and two detectors in parallel (a), the analyte preconcentration in both lines after splitting (a) or simultaneous injection (b) of the sample into two independent lines. R1 and R2 are modifiers of different composition in (b).

2.2.2 Gas diffusion separator unit - membrane devices

The separation unit in the GD-FIA systems is a special part of the manifold. In general, the donor and acceptor streams are separated from each other by a semipermeable membrane, although GD-FIA systems without membranes have been reported. The performance of the membrane separation/ preconcentration device is one of the keys for the success of the GD-FIA techniques. The membrane material, the area of the membrane exposed to the donor and acceptor streams and the volume and geometry of the grooves or the cavities on both sides of the membrane are some factors to be considered in order to design an efficient membrane device.

Some studies of cell designs and membrane properties have been published[24, 25]. To work properly, the membrane device has to continuously separate the analyte with stability of the mass transfer over a wide range of flow rate and flow rate ratios. It should also avoid any additional dispersion and unwanted dilution and provide, where appropriated, selectivity.

The material to make the membrane device must be chemically inert to prevent any reactions with the sample and reagents. The device can be made of a transparent material to allow observation of the correct functioning of the device. No adsorption should occur on the walls of the grooves or in the surface of the membrane to avoid any changes to the active contact area that could affect the efficiency of the separation.

The volume and geometry of the channels are fundamental to the transport process and should be as small as possible with the maximal contact area. The enlargement of the membrane area can be achieved either by making the grooves shallower and wider, or longer (or both), depending on the geometry of the membrane. Many kinds of membrane are suitable to be incorporated into a GD-FIA system. The selection of the membrane depends on many factors that may vary during experiments such as: the flow rate, the flow rate ratio, the physical and chemical properties of the donor and the acceptor streams, selectivity requirements, the mechanical properties of the membrane material, the nature and number of samples and the membrane separation cell design. Several different types of semipermeable membrane can be applied in flow analysis for each particular membrane separation process. The nonporous (silicone or natural rubber) and microporous (Teflon, PVDF, cellulose) membranes are most frequently used in GD-FIA systems, particularly for the determination of gases, gas-evolving species and highly volatile substances. Types such as, ion-exchange, modified supported liquid membranes and others, are less suitable for FIA purposes because of insufficiency of mechanical strength, availability in appropriates dimensions and reproducibility of preparation. Membranes are available in sheet (supported or unsupported) and tubular (capillary) forms of different sizes. Both types are manufactured with diverse porosity, pore size, and thickness. Sheet membranes with a mechanical support are sometimes necessary for best durability, ease of handling, and resistance to deformation under pressure.

The life time of the membrane is dependent on the nature of the samples, character of the membrane, and other factors. The membrane must not be stretched excessively when it is mounted because it could alter the diffusion properties and shorten the lifetime. In addition, sharp edges on groove channels, rough surfaces, and over tightening may damage the membrane during the mounting procedure.

The separation unit can be easily incorporated into a GD-FIA system according to the manifold configuration to be used. It can be connected straight to the donor/acceptor streams; it can be an integral part of the injection valve to allow preconcentration by stopping the acceptor flow or it can also be a part of a closed loop with the acceptor continuously circulating in the loop.

Sandwich modules for sheet membranes[18, 26], are the most frequently used designs, Figure 2.7). The classical sandwich device consists of two pieces, each one having a matching groove facing the gas semipermeable membrane.

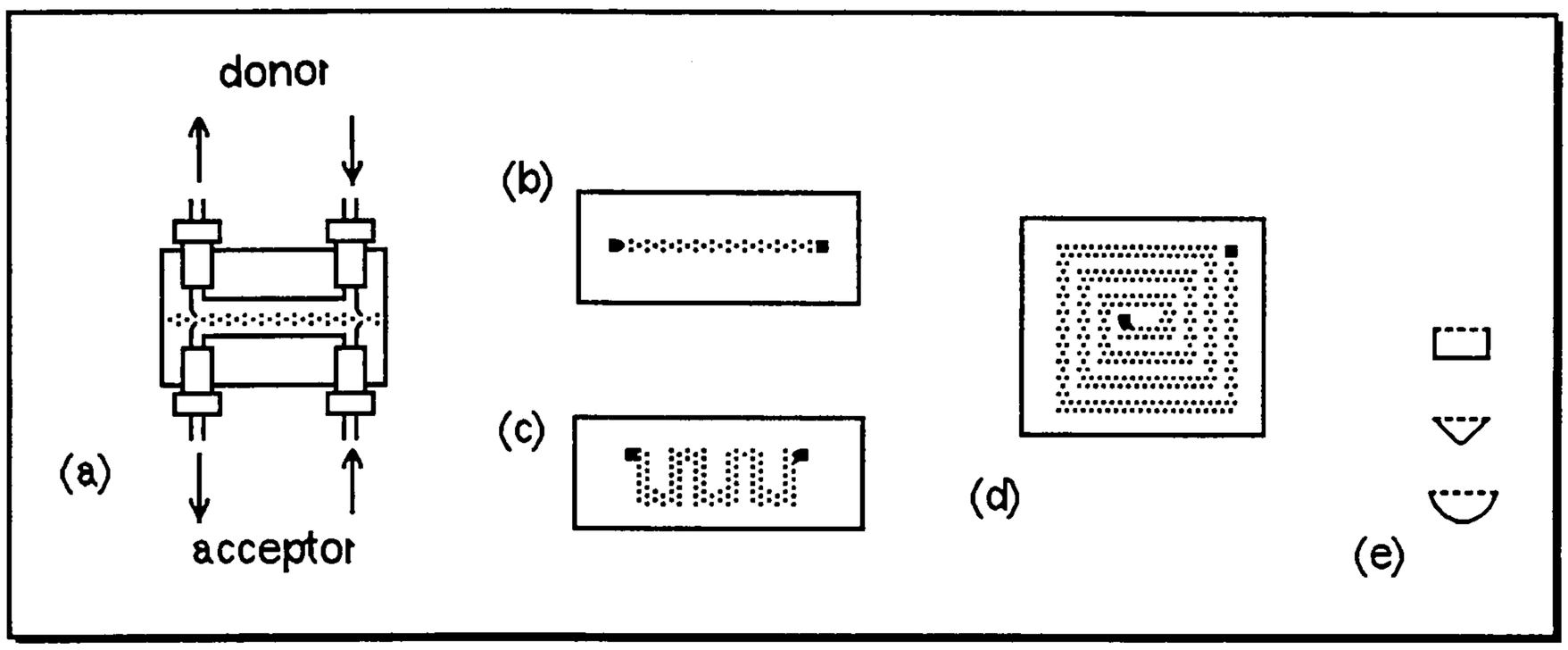

Figure 2.7 Sandwich membrane gas diffusion device;(a) with sheet (planar) membrane sandwiched between two bodies, having (b) straight, (c) meander, or (d) helical grooves. In (e), different possibilities for the cross-sectional area.

The two grooves can be of identical or different volumes, with a constant cross-sectional area and rectangular, triangular or circular profile. Straight, circuitous or concentric spiral grooves having several tenths of a millimetre depth and a 1-5 mm width have been used. The membrane also can be sandwiched between two spaces, made of silicone rubber, Teflon, etc., with straight grooves just fitting the inlet and outlet channels of the donor and acceptor bodies. The inlet and outlet tubes at the ends of the grooves can be oriented either perpendicularly or at an angle to the main axis of the device. Using a circular groove shape has the advantage to increase the contact area between the membrane and the donor/acceptor stream. When sheet membranes are used, specially with a circular groove shaped, a flat support for the membrane is desired. Teflon, nylon, or metallic net positioned on one or both sides can be placed into both channels for flat support of the

membrane. The use of a membrane support can bring advantages such as , better fluid mixing and a improvement on the radial transport of a solute in channels destroying the laminar flow and increasing the radial diffusion[24, 27]. Thus, they reduce the thickness of diffusion layers and the total volume of the cavities. Devices containing two membranes can be also employ a sandwich configuration. Two identical or different membranes are positioned on either side of a donor stream situated on the central body, Figure 2.8. The donor stream flows through the central channel and species of different properties pass across the particular membrane and are collected in suitable acceptor streams.

When the membrane to be used is tubular shaped, a coaxial configuration is used, Figure2.9 [26, 28, 30].

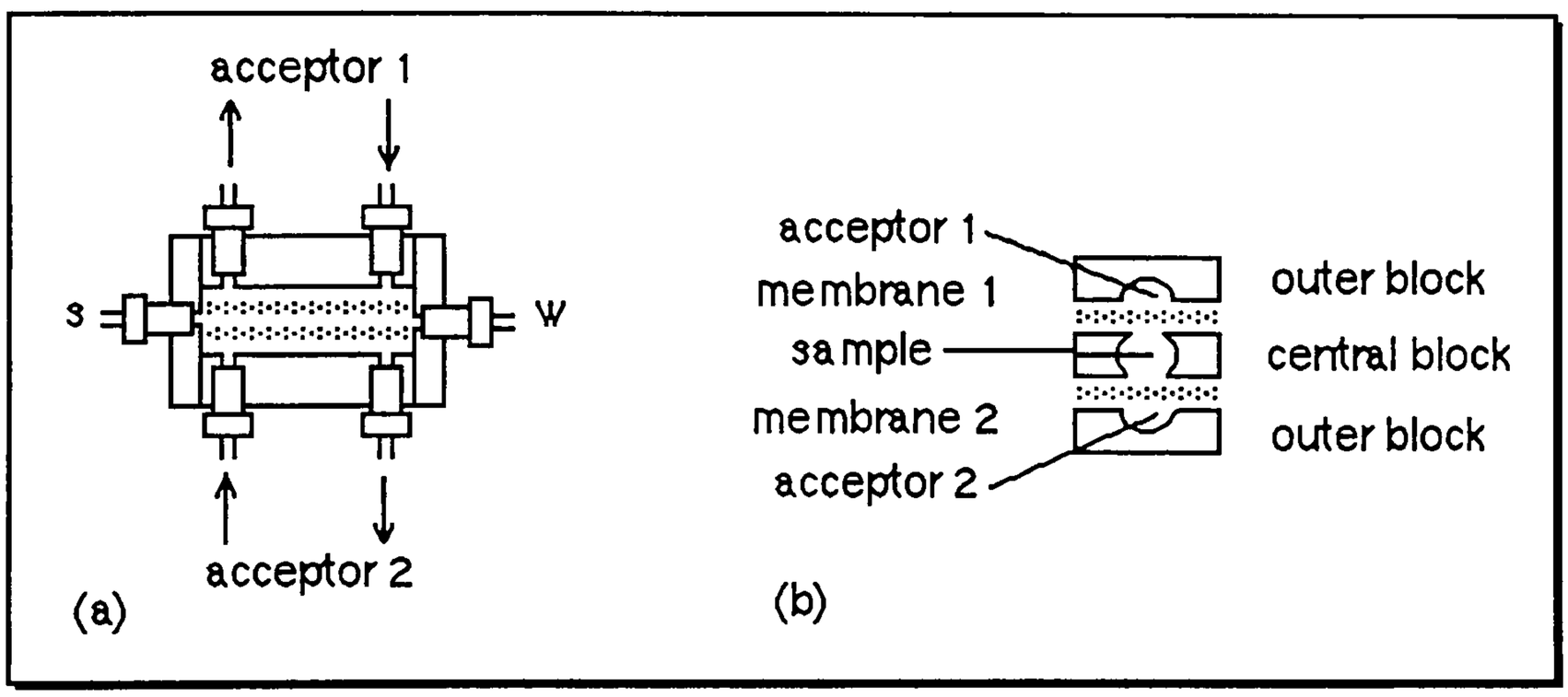

Figure 2.8 A dual- membrane device containing two identical or different membranes.

In these configurations, the donor stream can flow in either the annular space, Figure 2.9 a, or through the central membrane tube, Figure 2.9 b. The coaxial configuration has the advantages of being resistant to leakage of liquid and is easy to construct. It is preferred when gaseous analytes must be separated selectively from matrixes containing particles, solids, etc.

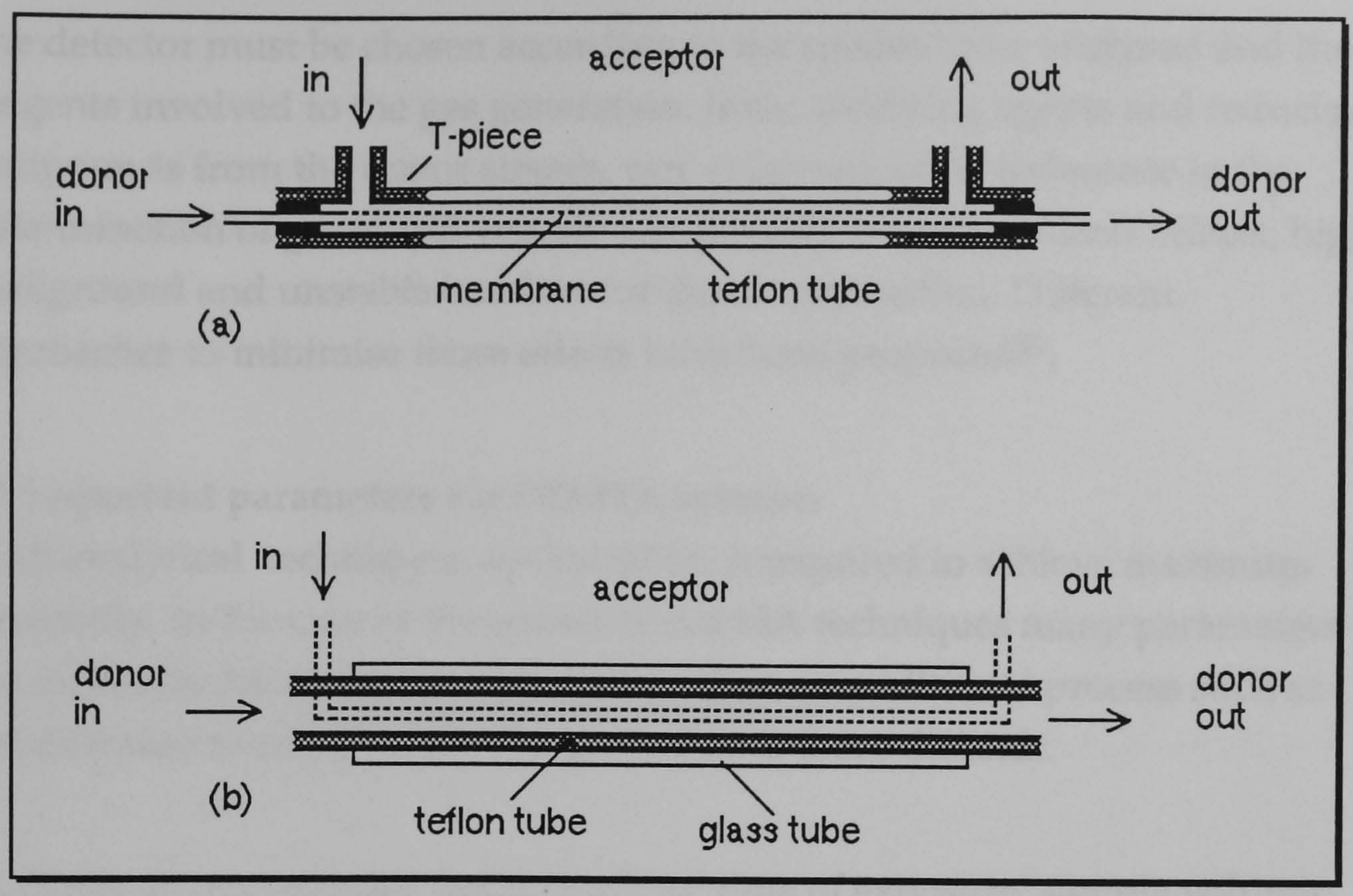

Figure 2.9 A coaxial devices for tubular membranes. Device constructed with polypropylene T-pieces (a), and a straight diffusion scrubber device (b).

2.2.3 Detectors

The GD-FIA technique needs high precision components in spite of the dynamic process occurring in the flowing streams; the concentration of detected species is continuously varying and highly reproducible pumping and injection systems are needed as in a conventional flow injection system. For this technique, is desirable that the detector has high sensitivity, low noise, rapid response and a minimum contribution to mixing processes in the flowing stream. The two first factors contribute towards the detection limit obtained by the particular analytical method, the second two contribute to the separation between successive peaks in the record of detector response vs. time. It is necessary to be able to make quantitative measurement of peak height or peak area free from contributions from neighbouring peaks.

Optical, electrochemical and others detectors coupled either with a chart recorder or a computer are commonly used for quantitation. Due to the high selectivity reached using the GD-FIA technique where the species to be analysed is previously separated, the sensitivity of the detectors can be intrinsically enhanced and non-selective detectors, i.e., conductometric, potentiometric, etc. can also be used to great advantage.

The detector must be chosen according to the species to be analysed and the reagents involved to the gas generation. Ionic, oxidising agents and reducing compounds from the donor stream, can cause serious interference in the determination of gases and volatile compounds, bringing matrix effects, high background and unstable baseline for the determination. Different approaches to minimise those effects have been proposed[30].

2.3 Important parameters for GD-FIA systems

In all analytical techniques, optimisation is required to achieve maximum sensitivity. In the case of the conventional FIA techniques many parameters can influence the analytical signal and, when an additional process such as gas diffusion is added, optimisation becomes more difficult.

In all transport processes factors such as: time of exposure, sample volume, concentration gradient and experimental conditions on both of the membrane side, i.e., temperature, pressure, flow rate must be examined in detail.

In the case of GD-FIA membrane techniques, the mass transfer depends on the resistance of the interface and that of the donor/acceptor streams. A relationship exists between the analytical signal and the concentration of the analyte, the volume of the acceptor solution inside of the donor stream (injector loop), the effective surface area of the membrane in direct contact with the sample, the permeability of the species and the temperature, etc. The sample and the acceptor flow rates, there time of exposure of the membrane to the sample, the volume of the sample, the length, the diameter, and the wall thickness of the membrane as well as the flow cell geometry, all affect the efficiency of the mass transfer through the membrane. For any specified membrane material, temperature, analyte concentration, etc., the amount of analyte penetrating the membrane is constant. The concentration profile depends on the distribution coefficient of this analyte between the membrane and the sample and acceptor stream.

2.3.1 Types of membrane

The type of membrane is an important factor determining the transition rate of the analyte as it affects its diffusion rate in the membrane, its solubility in the membrane matrix and diffusion through the two diffusion boundary

layers. For a good mass transfer efficiency, the analyte must have a high distribution coefficient from the sample into the membrane and from the membrane matrix into the acceptor fluid. The response time also varies for different membranes, being very short (less than seconds), for microporous membranes compared to the others type of membranes which enables rapid switching between sample and blank.

2.3.2 Distribution coefficients

The distribution coefficients between the membrane and the acceptor fluid governs the rapidity with which the analyte is removed from the membrane. A well defined concentration profile of the original sample plug and a short contact time of the sample zone with the membrane will result in a better shaped analytical signal.

Transport efficiency depends on these coefficients[14. 16.31]. This is the factor determining the slope of the trailing part of the signal and how rapidly the peak returns to baseline. A high value for the peak height/peak width ratio indicates that the analyte is removed efficiently from the membrane into the acceptor. The parameters of the peak maximum depend on the sample concentration, the diffusion rate and, both depend on the distribution coefficients.

2.3.3 Geometry of the membrane

Transport rates across membranes are nearly inversely proportional to the membrane thickness and proportional to the active surface area. The thinner wall membranes produce a better peak shape and a shorter response time. Smaller pore size is more effective in avoiding permeation of other species across the microporous membrane.

2.4 Experimental conditions

The factors connected with the experimental conditions on both sides of the membrane are the most important factors from the point of view of sensitivity and/or selectivity of determination.

2.4.1 Flow rate

Preconcentration factors depend on total permeation through the membrane and the flow rate ratio of the donor and the acceptor streams in the continuous-flow mode. A high flow rate of the acceptor stream can be used as a dilution scheme, and a low flow rate or stop-flow mode can be used to concentrate the sample. Usually, the amount of species transported across the membrane increases with the flow rate, but the results show some decrease of the signal when the contact time is too short. The contact time is longer at lower flow rates and, thus, more species can pass across the membrane.

2.4.2 Time of preconcentration

The magnitude of the analyte preconcentration factor depends linearly on the sample volume passing through the donor chamber and, of course, mainly on the time of preconcentration provided that the receptor fluid has sufficient absorption capacity. A linear relationship exists between the signal corresponding to the analyte transported across the membrane, the product of the time of exposure of the membrane to the sampling environment, and the concentration of analyte in the sample. Precise timing is thus critical when the stopped - flow mode is used.

2.4.3 Temperature

An increase in temperature will increase the diffusion rates, diffusion coefficients, and also the solubility of the analyte in solution and in the membrane material. Depending on the changes in distribution coefficient, this could result in either positive or negative change in the transition rate and the transport efficiency.

2.4.4 Pressure

The two different transport mechanisms for homogeneous and porous materials explain the differences in the influence of the gas pressure applied on the donor side of the membrane[24]. While an increase in the pressure increases the solubility of gases in silicone rubber and ion-exchange membranes, the pressure decreases the transport efficiency through the microporous membrane, probably widening the diffusion layer inside the membrane and making it protrude into the acceptor liquid. Some excess pressure on the donor side can be applied to improve the efficiency of the

transmembrane transport and the sensitivity of a procedure using nonporous silicone rubber membranes.

2.4.5 Composition of donor and / or acceptor streams

The actual composition of the fluids on both sides of the membrane is the most important factor affecting the selectivity of a determination. Appropriate chemical reactions, i.e., acid/base, complexation, oxidation, reduction, precipitation, etc., can improve the selectivity of the method significantly. Combining the different factors allows selectivity, and also sensitivity, to be simply changed over a wide range (several orders of magnitude).

2.5 Applications of GD-FIA technique

The GD-FIA technique has undergone extensive development as reflected in the large number of papers published on this topic over the last few years. Simplicity, speed and high sampling rates are qualities of the GD-FIA technique which persuade more and more research groups to become skilled in this technique.

Numerous examples of membrane-assisted flow injection determinations are given in the literature. They cover a wide range of methods and analytes. A summary of the variety of analysis in different areas where this technique has been successfully applied is given in Table 2.1.

The first application of GD-FIA was presented by Baadenhuijsen in 1979[32] when he decided to apply the flow injection technique to the well-stabilised Auto Analyzer technique for CO_2 as modified by Kenny and Cheng[33]. The same principle is used for all existing procedures for total carbonate and free carbon dioxide in different samples The procedure relies on adjustment of the sample pH to convert total carbonate to the free acid form, transport of a reproducible fraction of the CO_2 to a suitable receptor across an appropriate membrane and measurement of the transferred gas via spectrophotometry [14, 28, 32, 33], potentiometry[34]. and conductimetry[35, 36]. A fibber optic based fluorescence sensor, using a receptor buffer and hydroxypyrene trisulfonate as the acid- base indicator, has also been described[60]. Aoki *et al.*[54] have determined organic carbon from sea water samples using chemiluminescence

detection. Inorganic CO_3^{2-} is produced from the oxidation of organic species by $S_2O_8^{2-}$ reacts with H_2SO_4, and the CO_2 formed permeates through the microporous PTFE membrane and reacts with luminol reagent.

Similar methods have been developed for the routine determination of ammonia. The ammonium ion is injected into an alkaline solution and the ammonia formed diffuses across the membrane into a acceptor stream. The trapped ammonium has been determined spectrophotometrically [11, 14, 47, 61], with an acid-base indicator, by conductimetry measurements [43], by potentiometry with a liquid ion-exchanger ammonium selective electrode [37, 47, 61] and by fluorimetry[62].

Determination of total nitrogen in food and fertilizers has been reported by Pasquini *et al.*[43]. Organic nitrogen compounds of biological or agricultural samples are converted to ammonia after the classical Kjeldahl digestion and the digest is injected into a GD-FIA system using a conductimetric detector.A simple concentrator based on a microporous PTFE membrane and polymer net has been developed and combined with an ammonia-selective gas electrode for the continuous flow determination of low concentrations of ammonia ions in water[49]. The gas dialysis concentrator continuously gives about a ten-fold increase in the concentration of ammonium ions. the system was applied to the determination of residual concentrations of ammonium in water purified by destillation and/or de-ionisation and to natural water analysis.

A sophisticated GD-FIA conductimetric method, employing only one reagent, one FIA manifold and one detection system, for the determination of low levels of ammonia, total inorganic nitrogen and its two major forms of inorganic species, nitrite and nitrate was described by DeFaria *et al.* [26]. The method has been tested for water analysis. All nitrogen forms are transformed on-line into ammonia. The nitrite and nitrate samples are passed into a zinc reducing column. For nitrate determination, the sample is first treated with sulfamic acid. This way, all nitrite present is reduced to nitrogen gas and only nitrate remains in solution.

Table 2.1. Different areas of application for the GD-FIA techniques.

sample	species determined	system feature	detection	reference
CLINICAL				
blood plasma	CO_2	silicone rubber membrane	SP	32
	NH_3		P	37
serum	urea	immobilized enzyme PTFE membrane	SP	38
	salicylate		P	39
urine/blood	NH_3			40
FOOD				
milk	acetoacetate	PTFE tape	SP	41
	Cl^-		P	42
vegetable tissue	NH_3	PTFE tape 100 samples h^{-1}	C	43
wine and beverages	CO_2/SO_2	sheet PTFE membrane 25 samples h^{-1}	SP	34
	SO_2		SP	44
	ethanol	sheet PTFE membrane	P	45
	ethanol	immobilized PTFE membrane, 150 samples h^{-1}	A	46
ENVIRONMENT				
water	NH_3	PTFE tape, 100 samples h^{-1}	SP	47
	ozone	teflon membrane, 65 samples h^{-1}	SP	48
	$CN^- F^- NH_3$	PTFE membrane	SP	19
	NH_3	silicone rubber membrane	P	49
	$NO_3^- NO_2^-$ NH_3	PTFE tape, 60 samples h^{-1}	C	50
	Hg	nafion membrane	CV ICP-EAS	51
	Br^-	PTFE membrane, 30 samples h^{-1}	A	52
	As	tubular PTFE membrane	HG ICP-EAS	53

cont/...

sample	species determined	system feature	detection	reference
waste water	S^-	silicone rubber membrane	SP	18
	CN^-	silicone rubber, 20 sample h^{-1}	SP	17
air	SO_2		P	23
air and water	volatile compounds	silicone rubber	MS	31
	total organic carbon	PTFE membrane	CL	54
industrial effluent	Cl^- NH_3	PTFE membrane	SP	55
OTHERS				
metallurgical	CN^-	tubular PTFEmembrane	SP	56
chemical reagents	NH_3	teflon tape	P	57
	Hg	Nafion	CV ICP-EAS	51
synthetic samples	CN^- SCN^-	10 sample h^{-1}	SP	58
	BH_4		A	52
	NOx NO_2^-	sheet PTFE membrane, 30 sample h^{-1}	P	59

Note: SP, Spectrophotometry; P, potentiometry; C, Coulometry; A, amperometry; CL, chemiluminescence;

Recent applications of FIA-GD separation and preconcentration with a PTFE membrane include the determination of different anionic species such as sulphide, chlorine and cyanide.

Hydrogen sulphide evolved from an acidified sample was preconcentrated by permeation in a stationary alkaline acceptor solution enclosed in a silicone rubber sample loop[18]. Depending on the sample volume preconcentrated, the applicable analytical range spanned low μg l^{-1} to tens of mg l^{-1}. The sensitivity was increased by a factor of 30 compared with conventional methods, and it permitted practical determinations in the sub μg l^{-1} range using nitroprusside and methylene blue reagents. The same research group has also been used silicone rubber membranes for permeative transport of various sulphur anions, H_2S and SO_2, in sour water samples [63].

Bartroli *et al.*[44] determined total and free sulphur dioxide in wine by GD-FIA using *p*- aminoazobenzene as the colorimetric reagent.

Schulze *et al.* [57] has determined simultaneously ammonium and sulphide using spectrophotometric detection. They used a dual-detection manifold designed to enable estimation of the membrane efficiency. This configuration permit the determination of the volatile components in both the donor and the acceptor stream. A retardation loop was used in the case of sulphide. For ammonium, two gas diffusion units were coupled with each other. The transfer efficiency was ca. 40% for hydrogen sulphide and ca. 7% for ammonia. The effects of temperature and different type of membranes on the efficiency of separation were tested.

A GD-FIA method for the preconcentration and selective determination of sulphide has also been reported by Milosavljevic *et al.*[64]. The method is based on using the acceptor stream of the diffusion unit in a closed loop, mobile (recirculating) mode for the accumulation of the analyte. Part of the analyte present in the large sample volume (5ml) is effectively preconcentrated into a much smaller volume (0.15ml) of the recirculating acceptor loop. The analyte is subsequently injected into a sodium carbonated stream and carried to the amperometric detector. The sensitivity of this preconcentration method is directly proportional to the sample volume.

Barros *et al.*[65] used the GD-FIA technique to provide results in a much shorter time than the usual methods for determination of the volatile acidity in wines. The method involved injecting the wine sample into a de-ionised water stream which then flowed through a PTFE membrane separator. The acetic acid diffused through the membrane into another water stream that passed through a conductivity cell. Alternatively a spectrophotometric method was similar. The acetic acid diffused into a stream of bromocresol purple solution, at pH 7.0, which passed through a flow cell.

Rios *et al.*[24] have applied the GD-FIA technique to the determination of sulphur dioxide in air samples. They used electrochemical detection and a closed-loop manifold configuration.

Planar and tubular PTFE microporous membrane of different porosity, pore size and mechanical properties, have been employed to improve the selectivity of the reactions for cyanide determination[58, 66, 67]. Kubán[17] have

determined cyanide based on the reaction with highly selective sodium isonicotinate-3-methyl-1-phenyl-2-pyrazolin-5-one. This reaction was optimised and compared with other spectrophotometric methods based on Konig's reaction. Most interferences, including those of CNS^-, were eliminated by discrimination of mass transport through a non-porous silicone-rubber membrane.

Zhu and Fang [68], introduced a technique to improve the transfer efficiency of the gaseous species through the microporous membranes. It has been reported by Van Der Linden [14] that only a quarter of the total amount of gas generated, even under favourable conditions is separated on-line. For improvement of sensitivity in applications for which low detection limits are required, they arranged the gas diffusion unit as a part of the sample loop of the injection valve. The acceptor stream was kept stationary in the groove throughout the sampling/preconcentration sequence during which time sample containing the analyte was pumped continuously after been heated by passage through a Teflon tubing immersed in a 60° C water bath. Part of the analyte liberated was absorbed by the acceptor solution and injected into the manifold for reaction and detection. They applied this system for the determination of trace levels of total cyanide in waste waters. Zhu and Fang [19] used the same system , with some modifications, to determine traces of fluoride and ammonium ion. Tanaka *et al.*[29] have shown that both cyanide and thiocyanate can be determined rapidly by GD-FIA and spectrophotometric detection. A mixture of pyridine and barbituric acid was used as the chromogenic reagent and discrimination between cyanide and thyocyanide was achieved by differences in the transport of HCN and HSCN gases through a tubular microporous PTFE membrane at different pH values of the donor stream. In a similar way, Sweileh[58] has developed a method for both anionic species of cyanide. The method involves a two-step procedure in which the total concentration of both species is first determined spectrophotometrically using the same chromogenic reagent as Tanaka *et al.*[29]The cyanide is then complexed with Ni(II), and the thiocyanate is quantified separately and the cyanide concentration is then calculated by difference.

Figuerola et *al.*[69] used the GD-FIA technique to study interferences from metals and inorganic anions in the spectrophotometric determination of

cyanide. The results reveal the advantages on selectivity when the analyte is separated from Zn(II), Cu(I), Cd(II), NH_4^+ and some inorganic anions. The principle of diffusion of gaseous HCN across a tubular microporous PTFE membrane in different metallurgical samples has been applied by Marion *et al.*[56]. The membrane was directly immersed in an alkaline solution or in an aqueous mineral suspension for the on-line sensing of cyanide. The gaseous HCN diffuses through the membrane and is dissolved in a sodium hydroxide carrier solution which is then determined spectrophotometrically by the pyridine-barbituric acid method.

Hollowell *et al.* [70] studied either the possible interferences and the selectivity of the membrane for chlorine dioxide and chlorine. In the same way, Gord *et al.* [71] have shown that the GD-FIA technique provides elimination of interferences from ionic species including transition metals, chloride ions, chlorite ions and chlorate ions in routine determination of free chlorine (Cl_2, HOCl, OCl^-) in aqueous systems.

The permeation of halogens through microporous membranes has been studied by Motomizu *et al.*[72]. It was found that halogens such as bromine and iodine, which are not gaseous at room temperature, permeated through a microporous membrane. They reported that the permeability through a microporous PTFE membrane decreased in the order chorine > bromine > iodine. Iodine and bromine ions were determined by spectrophotometric methods coupled with oxidation by permanganate. Iodine was determined on the basis of the reduction of iodine to iodide . Residual chlorine was determined by spectrophotometric and by potentiometric detection with a coated-wire ion-selective electrode.

An important application for the membrane-assisted flow injection technique is as a gas-liquid phase separator for cold vapour /hydride generation atomic spectrometry, (FI-CVAAS, FI-HGAAS). In this technique, the gas-liquid interface is critical to achieve stable signals. The use of a gas-diffusion unit on-line avoids condensation on the transfer tube walls that causes a gradual loss of sensitivity and base line drift for AAS, AFS and ICP systems. In 1983, De Andrade *et al.*[73] made an important contribution to flow injection-hydride generation atomic absorption spectrometry, (FI-HGAAS)

with the development of a PTFE membrane phase separator for use in CV-AAS, (cold vapour atomic absorption spectrometry). The device was based on the permeability of PTFE tape to mercury vapour. Mercury vapour was formed in a carrier stream on one side of the PTFE membrane which then diffused directly into the absorption cell positioned in the light path of the spectrophotometer.

Many applications of gas diffusion, coupled to cold vapour or hydride generation techniques, have been reported in the literature, [53, 74, 75, 76]. All of them use planar or tubular microporous PTFE membranes in the separator unit. They have reported that the improvement in sensitivity achieved is not only due to a reduced dead volume in the gas liquid separator, but also that the use of the membrane decreases interferences from transition metals [77, 78].

A more effective way to remove moisture carryover in cold vapour mercury generation has been published recently by Corns *et al.*[79], and Fernandéz *et al.*[51]. The removal of moisture by using a semi-permeable Nafion membrane dryer tube is described. As the wet gas from the separator passes through the inner membrane, the moisture is removed and transferred to the outer tube. Meanwhile, a dryer gas, air, nitrogen or argon flows in a direction opposite to that of the wet gas removing the moisture on the outer surface of the membrane.

Canham *et al.*[80] have discussed the feasibility of determining arsenic and chloroform using GD-FIA and mass spectrometry.

Volatile organic species have been also determined using the GD-FIA technique. Oxidised ketones in milk were determined by Marstorp[41] acetoacetates were decarboxylated to acetone, which was separated from the sample by gas diffusion through a Teflon tape membrane and measured spectrophotometrically.

Melcher [31] has tried to apply GD-FIA to liquid chromatography. The ability of silicone rubber membranes to separate and concentrate organic compounds, even of low volatility, from sample matrices which could not be

directly injected into a chromatographic system has been demonstrated and the critical parameters for the system defined.

To increase the versatility of the GD-FIA technique, a novel method using enzyme modified membranes has been reported. In these, urease was immobilised onto a PTFE membrane. The immobilisation is possible as urease can undergo the addition of perfluoroalkil groups of the free amine residues of the enzyme. This modification generates localised areas of hydrophobicity on the enzyme, thereby converting a completely soluble enzyme into one with limited solubility which can then be adsorbed onto the gas-permeable membrane. The advantages offered by this method is due to the great specificity of enzymes. The method was used for the determination of urea in water and biological samples[38]. The urea is enzymatically converted to the ammonia, which is detected spectrophotometrically by changing the absorbance of a mixed pH indicator. It has also been used to enhance the specificity of ethanol determinations in beverages and medicines[46].

CHAPTER THREE
A MICROPOROUS MEMBRANE AS A PRECONCENTRATOR FOR AQUEOUS SOLUTIONS

This chapter describes the development of a preconcentration device containing a microporous PTFE membrane in which the species to be determined remains in solution and the preconcentration takes place based on the evaporation of the water from the aqueous solution which contains the analyte. The solution is pumped through the inside of a tubular microporous PTFE coil where under specific operating conditions, the vapour produced is separated through the microporous material.

Mass transport through the microporous membrane depends on many parameters of the system as stated before. Temperature, pressure, surface contact area, concentration of the species to be separated inside and outside of the membrane, must be intensively studied to be able to predict the capability of a device to preconcentrate aqueous solutions. Two systems have been built and used for these studies.

In an effort to characterise the membrane as a preconcentrator device, a model based on diffusion processes has been investigated. In this model, each pore of the membrane is considered as a diffusion tube and Fick's law has been applied.

Two possible arrangements are proposed to couple the preconcentration device in a FIA system and these systems were characterised. Practically, the device investigated was used for determination and speciation of aluminium in river water samples.

3.1 Characterization of the membrane

3.1.1 Experimental

The characterisation of a tubular PTFE-microporous membrane as a device for preconcentration involves a study of the behaviour of the system under different operating conditions. Parameters such as: temperature, surrounding air flow rate, length of the membrane and the air moisture outside the

membrane were considered and optimum conditions for achieving rapid removal of water vapour through the membrane were found.

The Apparatus used to carry out the studies necessary for the characterization of the membrane and the study of the operating conditions are shown in Figure 3.1. The first system in Figure 3.1a was composed of a 52 cm long piece of tubular membrane, enclosed in a glass tube in which air could flow at different rates. The glass tube which contained the membrane was kept in the water bath to allow temperature control. A heating glass coil, 5 mm bore size and 3 metres long, was used to raise the air temperature to the experimental temperature and a Teflon tubing coil, 0.8 mm i.d. and 3 m long, was used to heat the liquid before it passed through the membrane. Both coils were kept in a water bath. The efficiency of these heating coils was studied using a thermocouple.

In the second system , Figure 3.1b, a 10 m long membrane was mounted on a cylindrical cage and heated in a laboratory fan-assisted oven, (Gallenkamp). A switch was incorporated into the oven to allow the internal fan to be switched on or off. Plates containing silica gel were used inside the oven to produce a dry atmosphere.

Two Gilson peristaltic pumps, Minipuls 2 and Minipuls 3 were used to introduce the sample into the membrane. In the first system, a compressor produced the air flow surrounding the membrane.The air was passed through a drier column consisting of a Teflon tube, 8 mm bore size and 1 m long, filled with silica gel and its flow rate varied using a mass flow controller.

The parameters of the membrane used in both systems are described below.

membrane: tubular microporous-PTFE
maximum pore size: 10 µm
total porosity: 50% (based on relative density)
internal diameter: 0.45 mm
external diameter: 0.90 mm

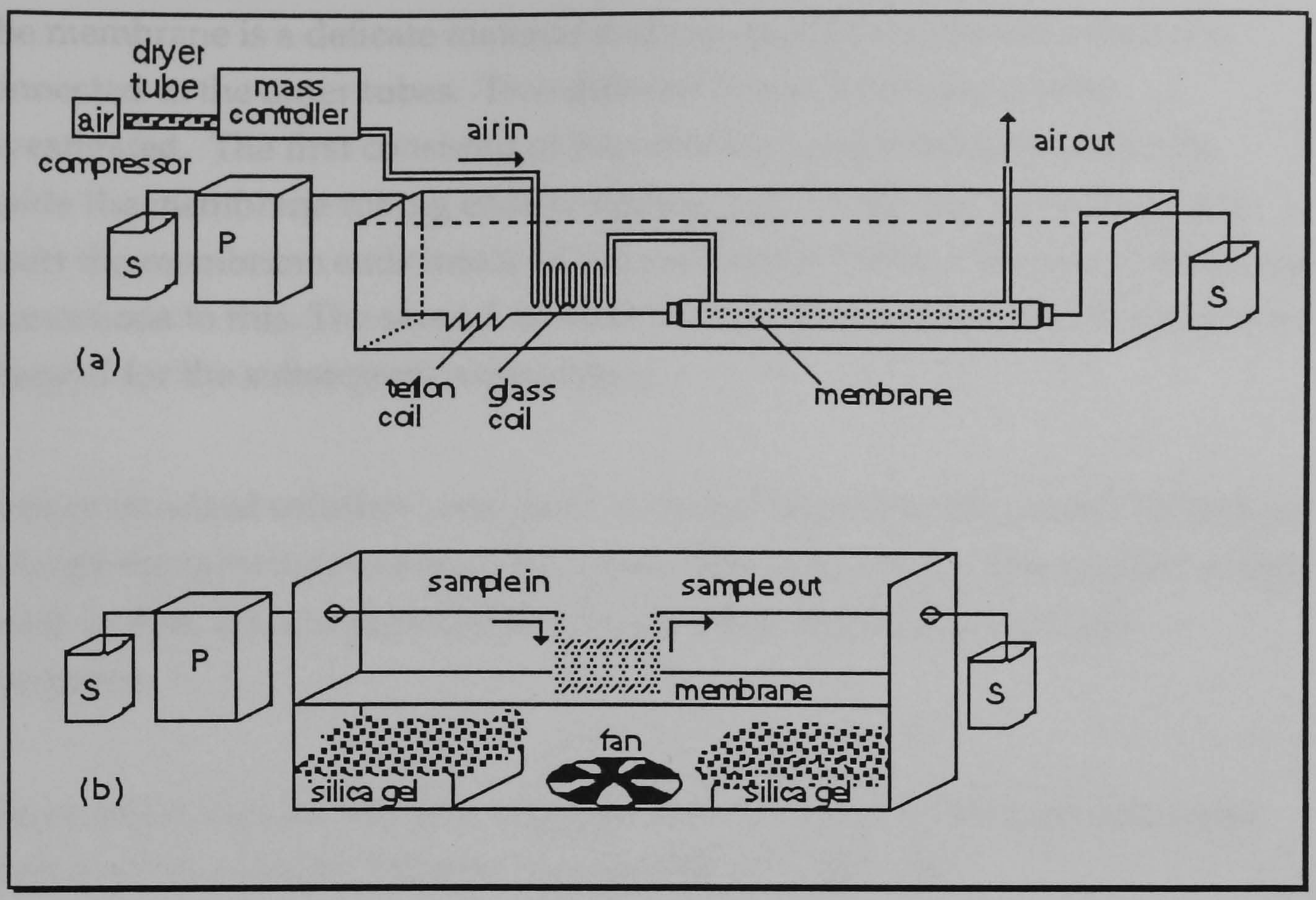

Figure 3.1 Systems used to investigate the optimum conditions for removal of water through the membrane. (a) System 1: using a water bath and a compressor; (b) System 2: using a fan-assisted oven.

An analytical balance Oertling model NA 114, was used for all weighing. Copper concentrations were monitored using an atomic absorption spectrophotometer, Phillips, model PU 9100, equipped with a Phillips copper hollow cathode lamp.

The first experiments were performed using the system shown in Figure 3.1a. Initially the amount of mass lost at different surrounding air flow at several temperatures was determined. Two different methods for monitoring the mass lost were used to study the performance of the weighing method. In the first, the solution was pumped from a reservoir flask through the membrane and collected in another flask. The mass of vapour lost through the membrane was calculated by the method of weighing by difference. The second, consisted of pumping the solution from the reservoir flask, through the membrane and back to the same flask. The reservoir /collector flask was weighed and the mass recorded at regular intervals. Each experiment took 15 minutes, and the liquid flow rate through the system was 0.5 ml/min.

The membrane is a delicate material and can easily be stretched when it is connected to the outer tubes. Two different ways to connect it were investigated. The first consisted of introducing a short stainless steel tube inside the membrane tubing ends to reinforce them. The second way was to insert the membrane ends into a wider and harder Teflon tube and to make the connections to this. The second method was easier and more valuable and was adopted for the subsequent experiments.

Copper standard solution was used to detect any mass lost caused by leakage through the membrane or from the membrane connections. The amount of this metal in both the source and collector solutions was determined and compared.

The practical data for the loss of water was compared with those calculated applying Fick's law of diffusion for a system of water /air.

3.1.2 Calibration of the instrumentation used and selection of weighing method

The results for the mass transfer using the two different methods to weigh the mass loss are shown in Table 3.1. The comparison of two methods was validated using the T-test and it can be concluded that there is no difference between the methods.

Table 3.1 Comparison between two different methods for monitoring the loss of liquid through the microporous PTFE tubular membrane. Method 1, interrupted flow . Method 2, uninterrupted flow. Time of sampling 5 min.

Temperature °C	mass loss, $gmin^{-1}$ method 1	mass loss,$gmin^{-1}$ method 2
20	0.015	0.020
50	0.057	0.060
70	0.106	0.116
80	0.131	0.139
90	0.168	0.160

3.1.2.1 Calibration of the peristaltic pumps.

Two different peristaltic pumps: Gilson Minipuls 2 and Gilson Minipuls 3, were used to deliver the liquid. Each was calibrated gravimetrically by the method of weighing by difference. The flow rate was calculated as the volume of water pumped in unit time. Water density was approximated to 1 g cm^{-3} over the temperature range 20-25° C. The flow rate capabilities of the two pumps for different tubing are shown in Figures 3.2 and 3.3.

The reproducibility of the pump flow rate was studied as it was a crucial factor in the present investigations. The Minipuls-3 pump, along with 1.65 mm i.d. pump tubing, was used in two different procedures for the studies. In the first one, the pump was run continuously and the amount of water pumped was measured by continuous weighing over a fixed time period for different pump rate settings. The results are shown on Table 3.2. The second procedure involved pumping water from a reservoir into a collector for a fixed time and then stopping the pump to weigh the reservoir and the collector bottles to find out how much water was pumped; Table 3.3.

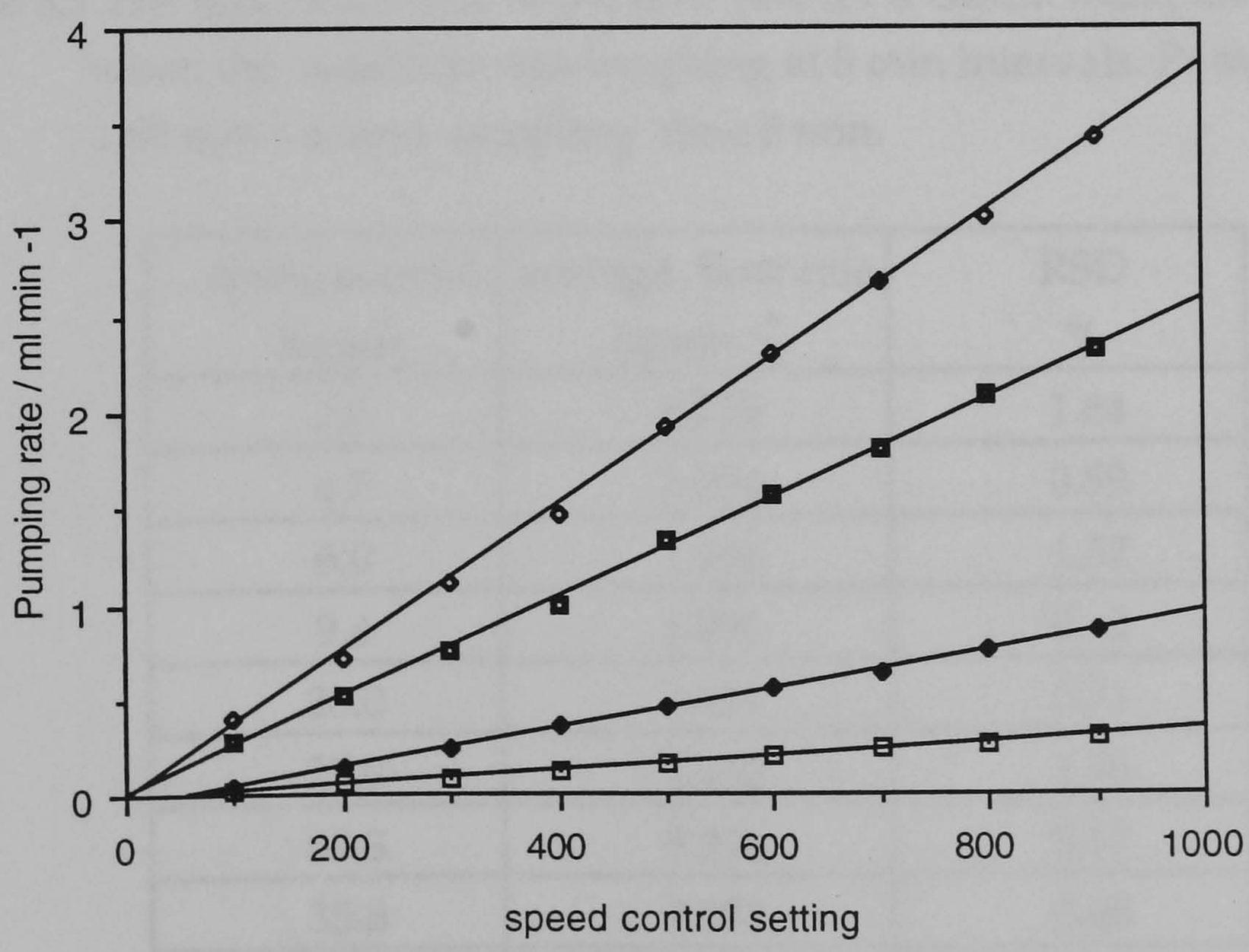

Figure 3.2 Calibration graph for Gilson Manipuls-2 pump peristaltic pump: pump tube dimensions: (▫) 0.38 mm id.; (◆) 0.63 mm id.; (■) 1.14 mm id.; (◇) 1.65 mm id.

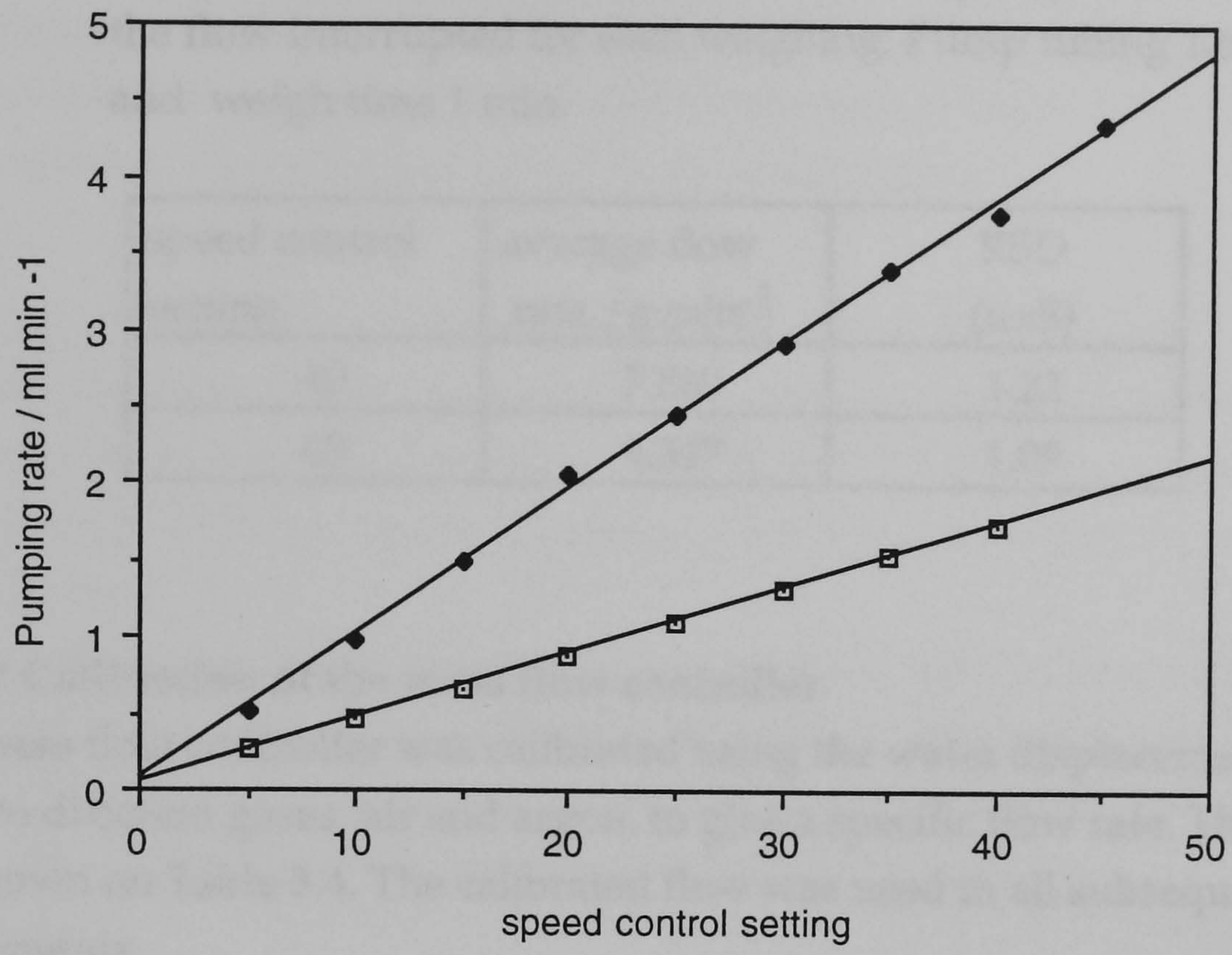

Figure 3.3 Calibration graph for Gilson Manipuls-3 peristaltic pump. Pump tube dimensions: (▣) 0.63 mm id.; (◆) 1.14 mm id.

Table 3.2 The reproducibility of the flow rate for a Gilson Minipuls-3 pump when the reservoir was weighing at 5 min intervals. Pump tubing 1.65 mm i.d. and sampling time 5 min.

speed control setting	average flow rate /gmin $^{-1}$	RSD %
3.7	0.792	1.64
4.7	1.004	0.59
6.0	1.266	1.57
9.4	1.891	0.42
20.0	3.951	0.71
25.0	5.162	1.36
30.3	5.926	0.17
35.8	7.001	0.68
40.1	7.759	0.41
46.5	8.954	0.48

Table 3.3 The reproducibility of the flow rate for a Gilson Minipuls-3 pump using reservoir and collector bottles. The pump was stopped and the flow interrupted for each weighing. Pump tubing 1.65 mm i.d. and weigh time 1 min.

speed control setting	average flow rate /g min^{-1}	RSD (n=5)
40	7.860	1.22
48	9.347	1.09

3.1.2.2 Calibration of the mass flow controller.

The mass flow controller was calibrated using the water displacement method for two different gases, air and argon, to give a specific flow rate. The results are shown on Table 3.4. The calibrated flow was used in all subsequent experiments.

Table 3.4 Calibration of the mass flow controller for two different gases.

meter flow /l min^{-1}	time to fill 2L flask/ s	practical flow /l min^{-1}
<u>air</u>		
2.5	48	2.50
5.0	28	4.28
6.0	24	5.00
10.0	15	8.00
<u>argon</u>		
1.0	111	1.08
3.0	36.69	3.27
8.0	14.16	8.47
10.0	11.97	10.02

3.1.2.3 Calibration of the thermocouple

A chromel-alumel thermocouple with a digital multimeter, Racal-Dana voltammeter, model 4009, was used for monitoring the temperature inside and outside the membrane. It was calibrated using a water bath and a mercury thermometer. The calibration graph is shown in Figure 3.4.

The thermocouple was inserted into the glass tube containing the membrane to measure the temperature of the carrier air surrounding the membrane. It was also inserted into the liquid stream via a Teflon T-piece placed just before the membrane to measure the temperature of the liquid emerging from the heating coil.

The air temperatures at different air flow rates are tabulated in Table 3.5. The 3 metre heating coil was shown to be efficient for flow rate as high as 10 l min^{-1}. Similar experiments showed the liquid heating coil to be efficient raising the liquid temperature to that of the heating bath.

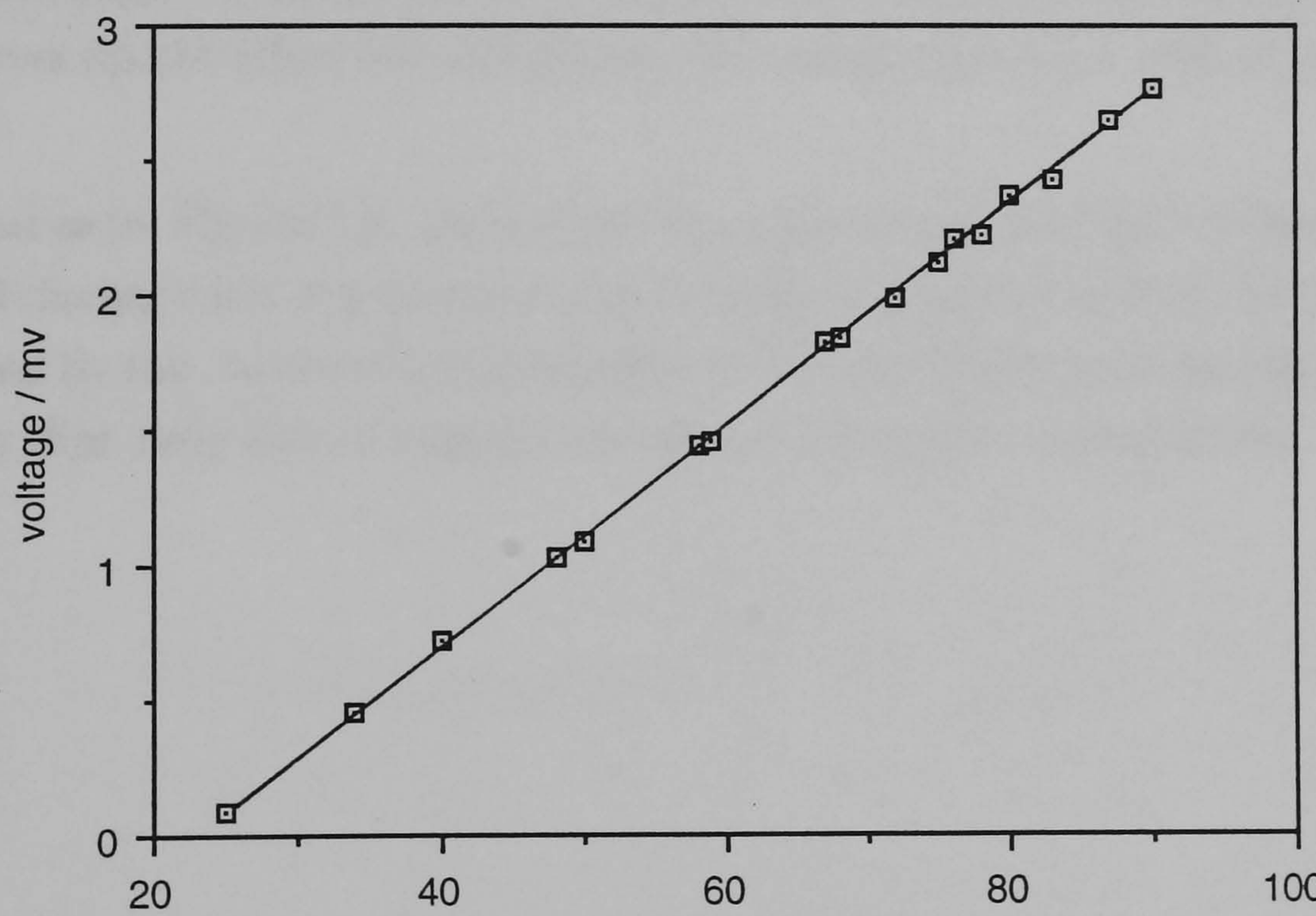

Figure 3.4 Calibration graph for thermocouple using a mercury thermometer and a water bath. Slope, 0.040872; y-intercept, -0.934772 ; correlation coefficient, 0.999.

Table 3.5 Air temperature thermocouple response for different flow rates and different water bath temperatures.

air flow /lmin^{-1}	temperature / °C				
	35 °C	44 °C	53 °C	75 °C	90 °C
2	32.7	39.5	49.8	74.9	88.2
4	33.4	40.0	49.5	74.7	88.9
5	33.1	39.9	50.0	74.9	89.2
7	32.7	39.7	50.2	74.9	89.7
8	32.4	40.0	50.5	75.2	89.7
9	32.4	40.2	50.2	75.2	89.7
10	32.4	40.0	50.2	75.2	89.7

3.1.3 Results and discussion

The results for the mass loss (gmin^{-1}) versus temperature using four different air carrier flow rates are shown in Figure 3.5. It can be observed that different air flows do not affect the loss greatly, but temperature is a critical parameter.

The curve in Figure 3.6 shows how the system was checked for leakage of liquid during each experiment. The amount of copper run into the system divided by the amount collected after each experiment must be equal to certify that only loss of vapour took place during the experiments.

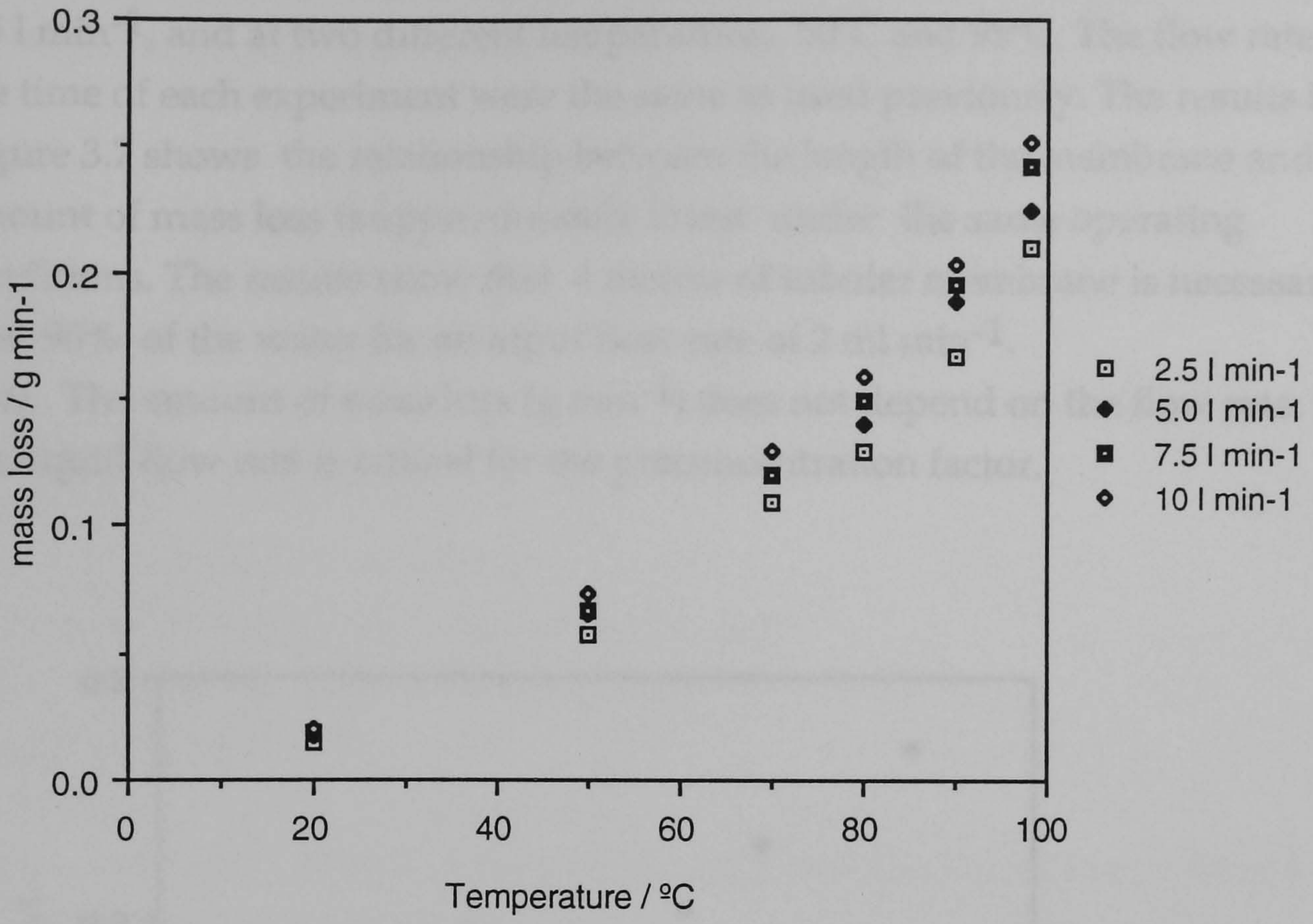

Figure 3.5 Influence of temperature and air flow on the liquid loss through 52 cm microporous PTFE tubular membrane.

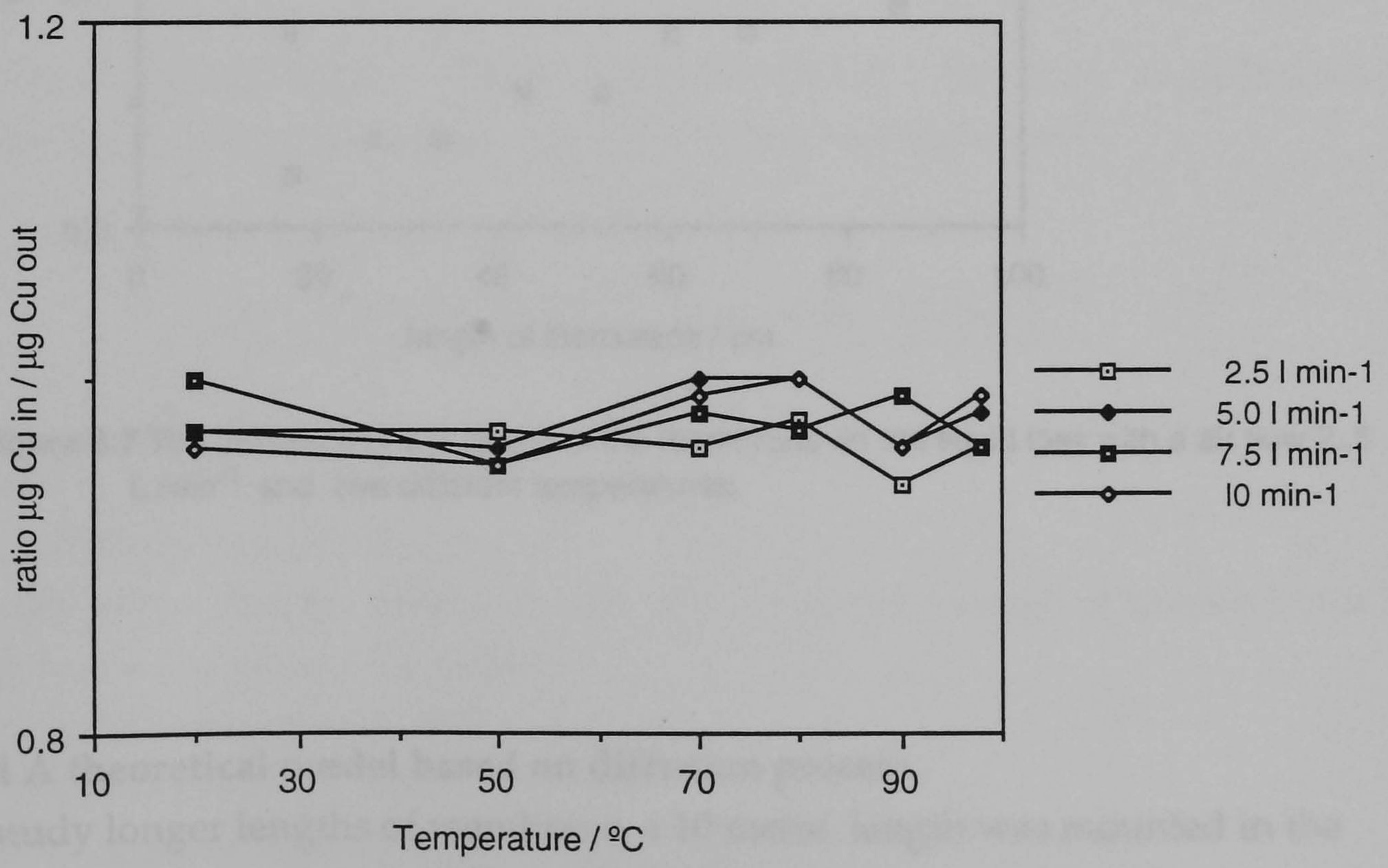

Figure 3.6 Verification of conservation of analyte mass during experiments to find the amount of vapour lost under different temperature and air flow conditions.

The influence of the length of the membrane was studied with an air flow of 2.5 l min^{-1}, and at two different temperatures, 50°C and 95°C. The flow rate and the time of each experiment were the same as used previously. The results in Figure 3.7 shows the relationship between the length of the membrane and the amount of mass loss is approximately linear under the same operating conditions. The results show that 4 metres of tubular membrane is necessary to lose 90% of the water for an input flow rate of 2 ml min^{-1}.

Note: The amount of mass loss (g min^{-1}) does not depend on the flow rate. But the liquid flow rate is critical for the preconcentration factor.

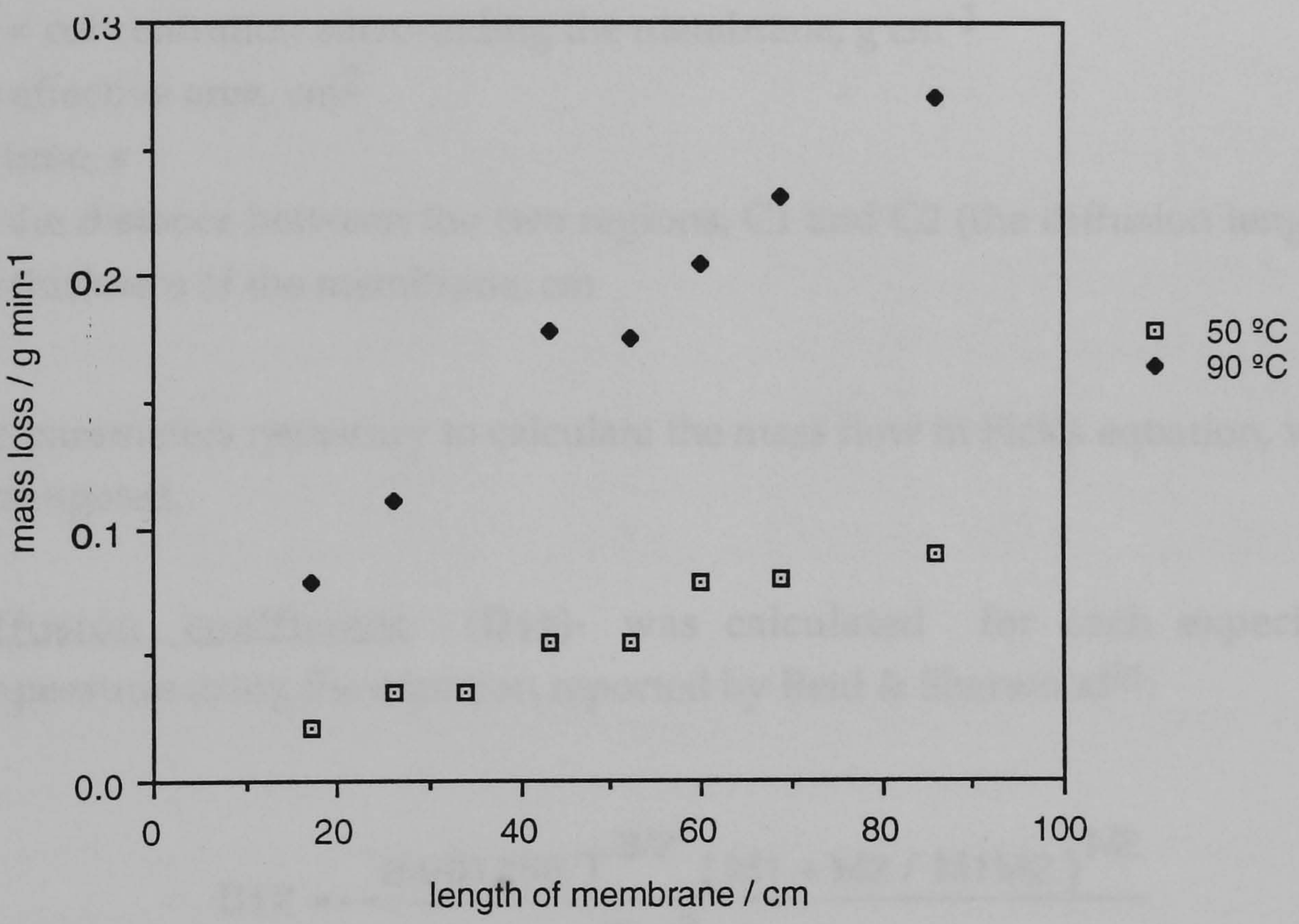

Figure 3.7 The influence of the length of the membrane on the liquid loss with a air flow 2..5 L min^{-1} and two different temperatures.

3.1.4 A theoretical model based on diffusion process.

To study longer lengths of membrane, a 10 metre length was mounted in the laboratory oven as shown in Figure 3.1 b. The water loss during a five minute period, at various temperatures, was investigated and the practical data used to test the diffusion model described in the following section.

A simple theoretical model based on a diffusion process was used to calculate the loss rate through the membrane. Fick's law, equation (1.2) was applied.

$$F = \frac{D12\,(C1 - C2)\,a\,t}{l} \quad \text{(eq.1.2)}$$

where

F = flow s^{-1}

$\mathbf{D_{12}}$ = coefficient of diffusion, $cm^2\ s^{-1}$

$\mathbf{C_1 - C_2}$= concentration difference, g cm^{-1}

$\mathbf{C_1}$ = concentration inside the membrane, g cm^{-1}

$\mathbf{C_2}$ = concentration surrounding the membrane, g cm^{-1}

a = effective area, cm^2

t = time, s

l = the distance between the two regions, C1 and C2 (the diffusion length), i.e. the thickness of the membrane, cm

The parameters necessary to calculate the mass flow in Fick's equation, were investigated.

Diffusion coefficient - ($\mathbf{D_{12}}$)- was calculated for each experimental temperature using the equation reported by Reid & Sherwood[81]:

$$D12 = \frac{0.001858\ T^{3/2}\ \{M1 + M2\ /\ M1M2\}^{1/2}}{P\ r_{12}^{2}\ I_D}$$

where

$\mathbf{D_{12}}$ = diffusion coefficient, $cm^2\ s^{-1}$

$\mathbf{M = M_1 + M_2\ /\ M_1M_2}$ where M_1 and M_2 = molecular weigh of species 1 and 2 (species1 = air; species 2 = water);

T = absolute temperature, (K)

P = absolute pressure, (atm)

$\mathbf{r_{12}}^{\mathbf{2}}$ = collision diameter, (Å)

$$r_{12} = \frac{(r_o)_1 + (r_o)_2}{2}$$

I_D = diffusion collision integral, dimensionless, function of Boltzman constant and energy of molecular interaction.

The quantities r_{12} and I_D are evaluated and tabulated for the gases in the mixture[81]. The diffusion coefficients calculated under those considerations are shown in Table 3.6.

Table 3.6 Calculation of diffusion coefficient for a system water/air under different temperatures.

T / °C	T / K	$T^{3/2}$ / K	I_D	r_{12}^2 / A	M	D_{12} / $cm^2\ s^{-1}$
20	293	5015.352	1.346	10.08698	0.3001	0.205971
50	323	5805.021	1.285	10.08698	0.3001	0.249816
70	343	6352.449	1.253	10.08698	0.3001	0.280247
80	353	6632.268	1.233	10.08698	0.3001	0.297338
90	363	6916.079	1.224	10.08698	0.3001	0.312341
98	371	7145.965	1.206	10.08698	0.3001	0.327404

Concentration on both sides of membrane - C_1 and C_2 - represent the water vapour concentration inside and outside the membrane.
Assumption that saturation occurs in the molecular layers immediately above the surface thus C_1 is the quantity of vapour produced when the saturated vapour pressure is reached and can be calculated using the ideal gas equation:

$$PV = nRT$$

where

P = vapour pressure , Nm^{-2}

V = volume, m^3

n = number of moles of vapour

R = gas constant, 8.314 J mol^{-1} K^{-1}

T = temperature, K

It is supposed that the air outside the membrane is not saturated by water vapour and the value for C_2 is close to zero. However, C_2 could also be estimated from the amount of vapour lost at each temperature. This calculation proves that the air is not saturated and the value for C_2 is small compared with the concentration C_1.

Table 3.7 Calculation for the concentration of water vapour inside the pore of the membrane at the liquid interface using the ideal gas equation and vapour pressure at different temperatures.

T/ °C	T / K	P_v / Nm^{-2}	PV /RT / mol	n / V / g cm^{-3}
20	293	2337	0.96×10^{-6}	17.27×10^{-6}
50	323	12334	4.59×10^{-6}	82.67×10^{-6}
70	343	31157	10.93×10^{-6}	196.66×10^{-6}
80	353	47343	16.13×10^{-6}	290.36×10^{-6}
90	363	70095	23.22×10^{-6}	418.06×10^{-6}
100	373	101325	32.67×10^{-6}	588.12×10^{-6}

Effective area -(**a**)- the effective area is the summed cross-sectional area of the membrane through which gas can pass. In practice, the effective area is made up of contributions from a very large number of individual and connected pores. The surface area of the membrane was determined using the system shown in Figure 3.8.

The flow rate generated when nitrogen gas was continually injected through the 52 cm membrane under several pressures inside and outside the membrane (differential pressure=ΔP) was measured. A water manometer was used to measure the ΔP applied for each experiment, and the flow was measured for each ΔP by the displacement method. The experiments were carried out at room temperature (25°C). The results for these experiments are shown in Table 3.8.

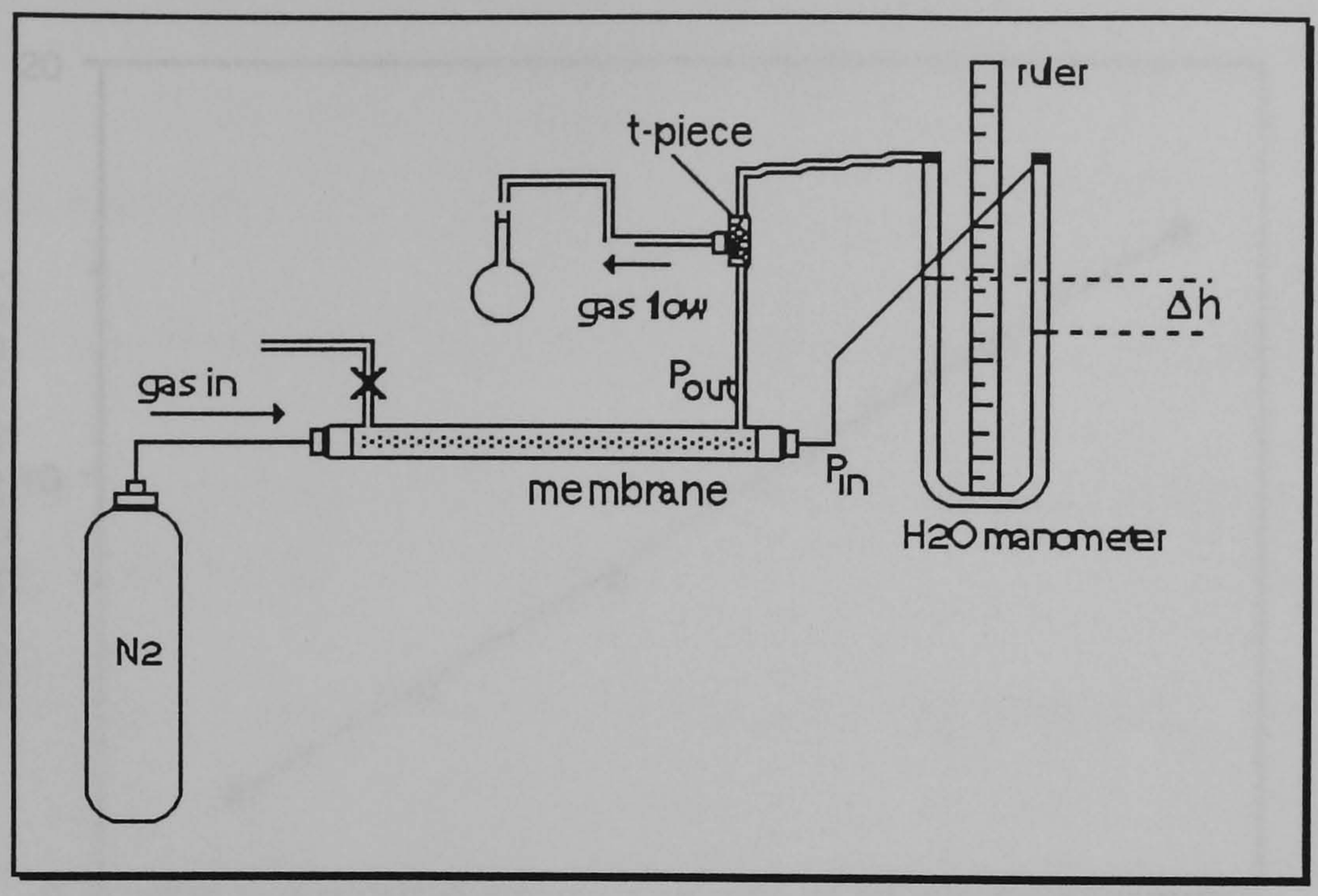

Figure 3.8 System used for measurement of differential pressure between both sides of the membrane and the flow through its pores. Length of the membrane, 52 cm.

Table 3.8 Flow of nitrogen through the membrane when several differential pressures were applied to the system. The flow was determined by measuring the time taken to empty a 250 ml volumetric flask.

ΔP /mmH_2O	ΔP /Pa	time /s	Q /ml min^{-1}	Q, /m^3 s^{-1}
14	137.3	108.81	137.85	2.3×10^{-6}
34	333.2	51.18	293.10	4.9×10^{-6}
54	529.2	33.32	450.18	7.5×10^{-6}
74	725.7	23.72	632.38	10.5×10^{-5}
94	921.8	19.00	789.47	13.2×10^{-5}
114	1117.9	15.75	952.38	15.9×10^{-5}

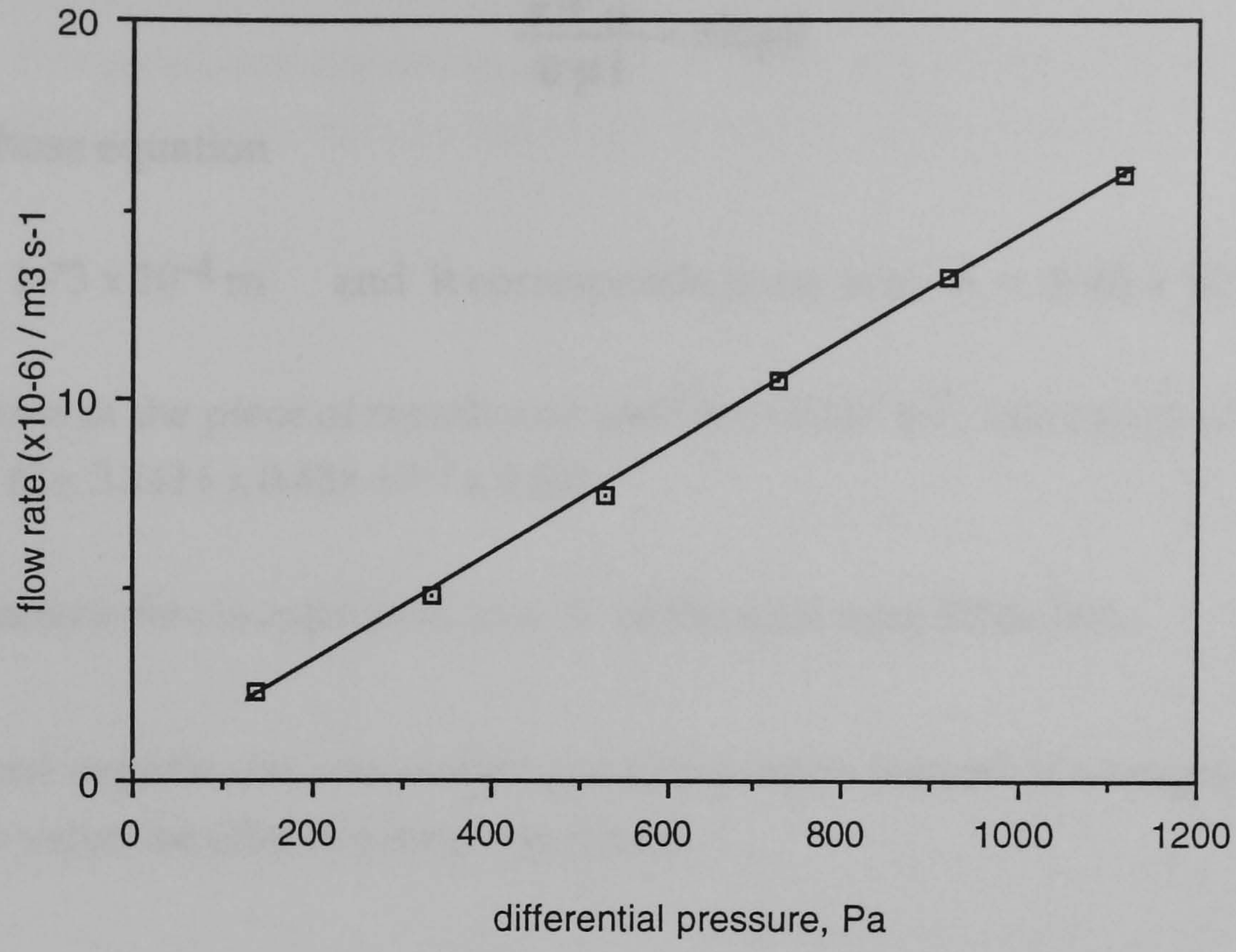

Figure 3.9 Variation of nitrogen flow through the microporous membrane under various differential pressures applied to the system.. Slope, 1.39 x 10^{-8}; y-intercept, 2.84 ; correlation coefficient, 1.00.

The slope of the ΔP x Q plot was used to calculate the effective area using Poiseuille's and Kozeny's equations.

calculation using Poisuille's equation:

$$Q = \frac{\pi r^4 \Delta P}{8 \mu l} \quad \text{(eq. 1.4)}$$

Q = flow, $m^3\ s^{-1}$

Δ**P** = differential pressure applied to the system, it is measured as Δh, cm H_2O and converted to Pa.

π = 3.1416

r = radius

μ = viscosity of the gas used. Nitrogen viscosity, 178.1x 10^{-7} kg $m^{-1}\ s^{-1}$; argon viscosity,

l = thickness of the membrane, 0.45 x 10^{-3} m

$Q/\Delta P$ = slope = 1.39 x 10^{-8} $m^3\ s^{-1}$ and

$$\frac{r^4 \pi}{8 \mu l} = \text{slope}$$

from those equation

$r = 1.73 \times 10^{-4}$ m and it corresponds to an area $A = 9.40 \times 10^{-8}$ m^2

Total area of the piece of membrane used is 0.00147 m^2, calculated as
$2\pi r L$ ($2 \times 3.1416 \times 0.45 \times 10^{-3} \times 0.52$).
hence
the effective area is expressed as a % of the total area: **0.00639%**

The same experiment was carried out using argon instead of nitrogen gas and a similar value for effective area was found.

The effective area calculated was very small and Kozeny's equation was applied to check if the tortuousity of the pore shape could have any effect on the present calculations.
Kozeny's equation:

$$V_k = \frac{m^2 \Delta P}{k_0 \mu l}$$

where
V_k = velocity
m = hydraulic radius
k_0 = Kozeny' s constante

Darcy stated that for sub-sonic flows for velocity less than 60 m s^{-1}:

$$V = \frac{Q}{A}$$

from Poiseuille's equation :

$$V_p = \frac{Q}{A} = \frac{r^2 \Delta P}{8 \mu l}$$

When the capillary pores are considered tube cylindrical ko = 2 and $V_p = V_k$. Under this consideration the hydraulic radius, can be calculated using Poiseuille's equation for any value for Q and ΔP from table 3.8:

$$\mathbf{r} = 1.73 \times 10^{-4}\ \mathrm{m}$$

$$V_p = \frac{Q}{A}$$

$$\mathbf{V_p} = 2.3 \times 10^{-6} / 3.1416 \times (1.73 \times 10^{-4})^2$$

$$\mathbf{V_p} = 24.46\ \mathrm{m^2\ s^{-1}}\ (= \mathbf{V_k})$$

using Kozeny's equation for a circular pore shape, $\mathbf{k_o} = 2$ **m** can be calculated: $\mathbf{m} = 5.3 \times 10^{-5}$ m and applying once more Kozeny's equation considering the capillary pores like granular beds $k_o = 4.5$ and

$$\mathbf{V_k} = 10.856 \qquad \mathbf{V_k = Q / A} \qquad \text{and} \qquad \mathbf{A} = 2.119 \times 10^{-7}\ \mathrm{m^2}$$

hence

the porosity = **0.0144 %**

The diffusion equation was applied and the theoretical data compared with the practical result carried out with the system in Figure 3.1b with 10 metre membrane. Table 3.9 presents the theoretical figures calculated when the simple diffusion equation was applied in a water/air system containing a 10 m long membrane.

The theoretical value were compared with those found practically and this is shown in Figure 3.10.

Table 3.9 The water loss flow by diffusion process through a 10 m tubular microporous membrane with a effective area 0.0144 % (calculated from Kozeny's equation); L, 0.045 cm; a, 0.041 cm^2; t, 15 min.

Temperature / °C	D_{12} / $cm^2\ s^{-1}$	$C_1 - C_2$ / $g\ cm^{-3}$	F / g
20	0.206	17.27×10^{-6}	0.0029
50	0.250	82.67×10^{-6}	0.0169
70	0.280	196.66×10^{-6}	0.0451
80	0.297	290.36×10^{-6}	0.0802
90	0.312	418.06×10^{-6}	0.107
98	0.327	588.12×10^{-6}	0.1577

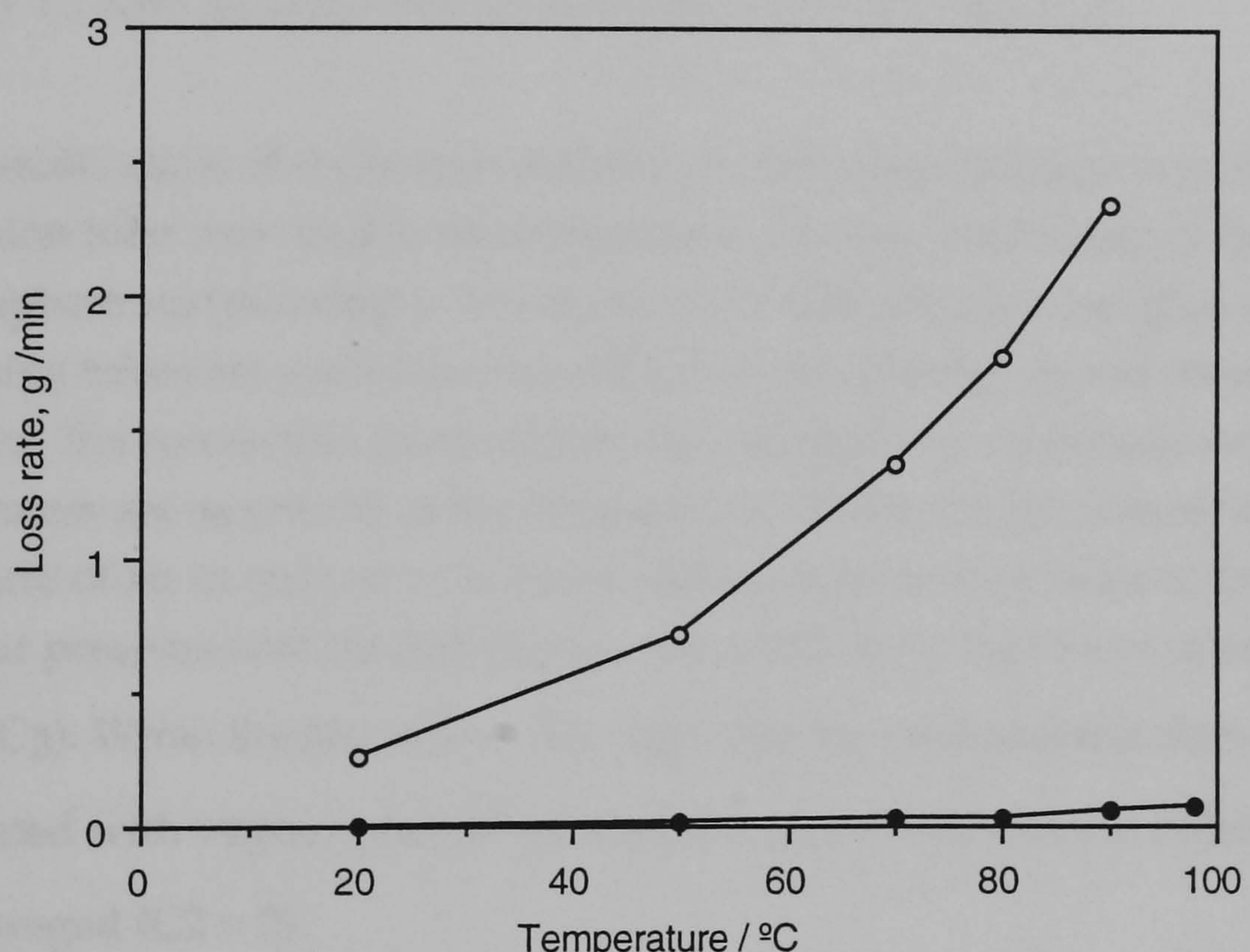

Figure 3.10 Comparison of the practical (o) and theoretical (●) liquid loss through 10 metre tubular PTFE -microporous membrane.

It is evident that significant quantities of water are lost and the actual quantities far exceed the calculated loss.

Experiments were therefore performed to compare the results obtained with the membrane to those of other systems in which a free liquid surface was used.. The parameters studied were temperature, the turbulence level in the oven and the water vapour pressure in the oven atmosphere.

To simulate a free surface in which mass transfer was affected only by the boundary layer resistance, a beaker of 15.9 cm^2 surface area was used. For a system in which diffusion occurs without convection, a tube of 1.13 cm^2 cross-section (with a length about 8 times the diameter) was used. The membrane had a total a total surface area 14.7 cm^2. In this case, the evaporation is affected by two resistances: one from the boundary layer and the other from the membrane body. The amount of water loss for these three systems with different mass transport processes involved are tabulated in Table 3.10. The results obtained for the diffusion tube were multiplied by 14, as its surface area is only 1.13cm^2,to allow comparison with the others systems.

The results show that the critical factor for the mass transport when the diffusion tube was used is the temperature and the conditions of the atmosphere surrounding it do not affect the diffusion process (this is why diffusion tubes are used for environmental monitoring). In the other systems studied, the convection produced by the atmospheric conditions surrounding the system are as critical as the temperature. When the fan was off the vapour pressure of air in contact with the boundary layer is very close to the saturated vapour pressure and the diffusion is restricted resulting in low mass loss ($C_1 = C_2$). When the fan was on, the opposite happens and the does not become saturated with vapour, due to the convection process, and the diffusion is encouraged ($C2 = 0$).

The high values obtained for mass loss through the membrane system compared with those for the free surface when the fan is off, are in agreement with the findings of Brown & Escombe[82]. They suggested that the evaporation from an open-water vessel surface is increased by placing a multi-perforated barrier over the surface.

Table 3.10 Comparison of the liquid losses for different diffusion processes at different temperatures. A 52 cm long tubular membrane was used in the system shown in Figure3.1 b.

temp. /°C	system	liquid loss by diferent processes / $gmin^{-1}$		
		membrane	free diffusion	diffusion tube
at 30 °C	silica/fan	0.031	0.032	0.0024
	silica	0.019	0.003	0.0013
	fan	0.027	0.033	0.0020
	none	0.017	0.004	0.0012
at 50 ° C	silica/fa	0.069	0.082	0.0059
	silica	0.046	0.012	0.0029
	fan	0.066	0.056	0.0047
	none	0.046	0.009	0.0034
at 80 °C	silica/fan	0.159	0.170	0.0887
	silica	0.106	0.051	0.0174
	fan	0.148	0.165	0.0274
	none	0.102	0.037	0.0141

This arise because the mouth of the tube or pore in which the static diffusion takes place is surrounded by a water vapour shell[82]. Depending on the distance between pores the shells may undergone free lateral diffusion or at lower pore separations, the shells interact and diffusion is slower. The resistance of the boundary layer is therefore increased. The data in Table 3.10 show that because of the small effective area of the membrane used, the pores are not close enough to increase the resistance for the diffusion stream. For the free surface, The shell from each incremental area interacts with those surrounding it and effectively the whole surface layer becomes saturated thereby greatly increasing the boundary layer resistance.

3.1.5 Theoretical model to fit the practical data

The basis of the refined model is shown in Figure 3.11. Not with standing the efficiency of arrays of pores in losing moisture, to explain the high levels of water vapour transport it is necessary to assume that the internal pore space of the membrane is saturated with the water vapour (i.e. the length, **l**, in equation 1.2 must be reduced). This situation will prevail provided that a monolayer of water molecules is sustained on the internal surfaces of the membrane. Precedence for this assumption is established in the literature [82, 83, 84] for flow through porous media.

The loss through the membrane is then determined by the following factors:
1. The vapour concentration difference between the internal vapour pressure inside the membrane (saturated value) and that in the surrounding atmosphere. This is the driving force for the diffusive transport.
2. A surface resistive component which opposes the diffusive transport through the outer pores of the membrane, (the equivalent diffusion length to this can appear to be of the order of the pore dimension, i. e. ca 10 μm).
3. A boundary layer resistance due to the static boundary layer of gas attached to the membrane surface.

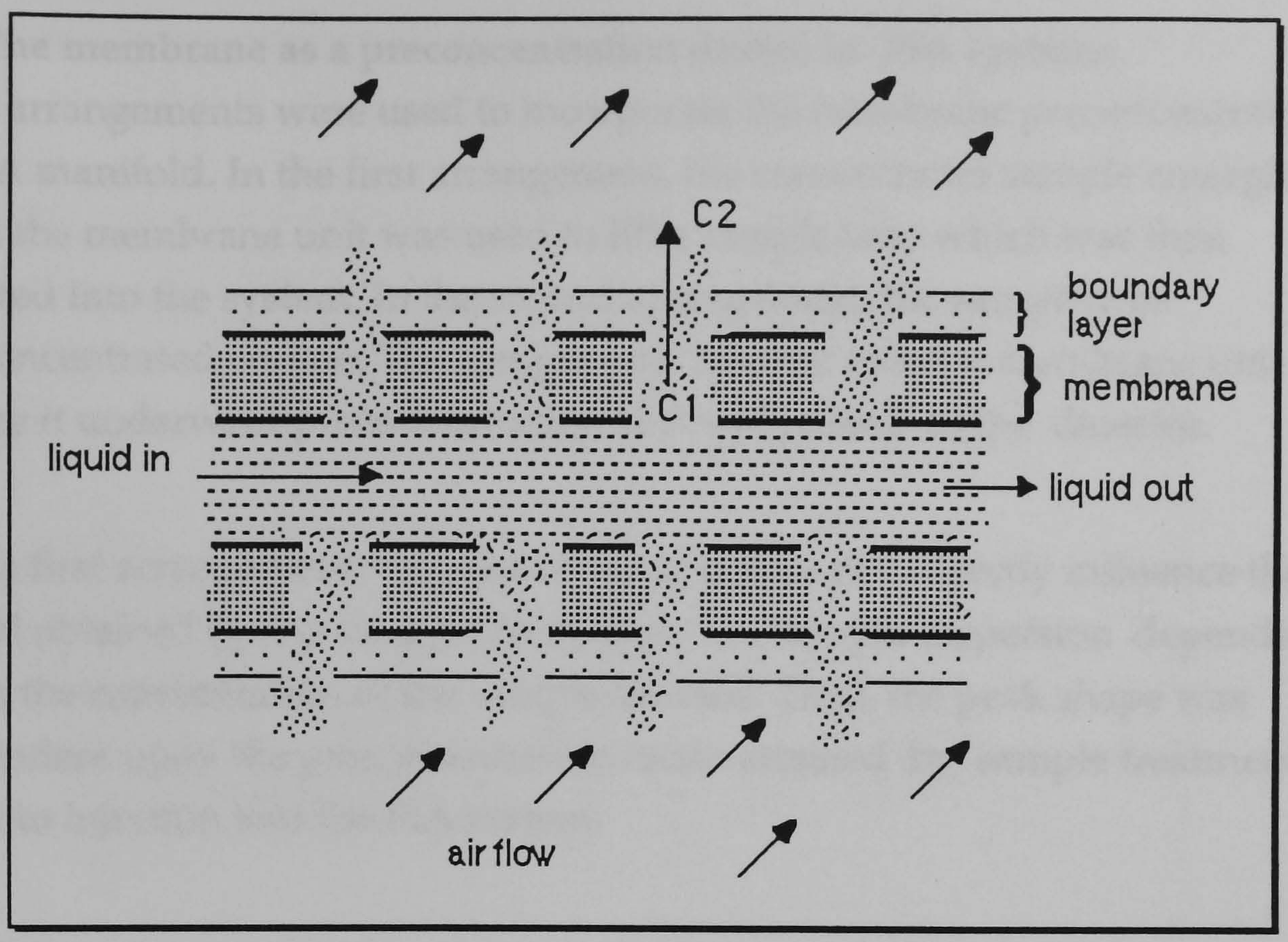

Figure 3.11 Cross- section view of a microporous membrane and its surface.

Using this model, it is possible to explain the data presented in Figure 3.10. Temperature is the most important parameter because it controls the saturated vapour pressure inside the membrane. However, the turbulence level in the oven is also important because it control the thickness of the boundary layer attached to the membrane. The importance of the boundary layer in controlling vapour loss has been extensively studied in relation to evaporation / transpiration from leaf surfaces[84, 85, 86]. Changing the concentration of water-vapour pressure inside the oven atmosphere does not appear to have a great effect. However, measurements show that the vapour pressure was only changed from 0.007 to 0.039 g/l, which is small compared with the saturated vapour pressure and therefore the change in C1 - C2 achieved was small.

3.2 The membrane as a preconcentration device in FIA systems.

Two arrangements were used to incorporate the membrane preconcentrator in a FIA manifold. In the first arrangement, the concentrated sample emerging from the membrane unit was used to fill a sample loop which was then injected into the system. In the second arrangement, the sample was preconcentrated on-line. The sample was injected into the membrane unit where it underwent preconcentration and was passed to the detector.

In the first arrangement, the membrane unit does not directly influence the signal obtained by the simple FIA system. The sample dispersion depends upon the concentration of the sample injected. Thus, the peak shape was dependent upon the preconcentration factor attained by sample treatment prior to injection into the FIA system.

In the second arrangement, due to the geometry of the long tubular membrane reactor, a large dispersion coefficient was anticipated. However, it is a situation in which two opposite effects are influential. These have been investigated and are discussed.

A FIA system is classified in accordance with the degree of sample dispersion within it. By definition, dispersion is the dilution undergone by a sample volume injected into a flowing stream [11]. It is characterised by the concentration profile adopted by a zone or plug inserted at a given point in the system without stopping the flow. The characteristics of this profile are important as the sample passes through the detector cell and the output signal is recorded. It is therefore representative of the dispersion at such a point, and can be used to assess the extent of it.

Two mechanisms contribute to the dispersion of the injected sample which is transported along the tube mainly by laminar flow. These are referred to as convective and diffusional transportation. When convective transportation occurs under laminar flow conditions a parabolic velocity profile is produced. Sample molecules at the tube walls have zero linear velocity and those at the centre of the tube have twice the average velocity. Dispersion occurs under diffusional transport due to the presence of concentration gradients in the

convective transport regime, giving rise to axial and radial diffusion, figure 3.12b.

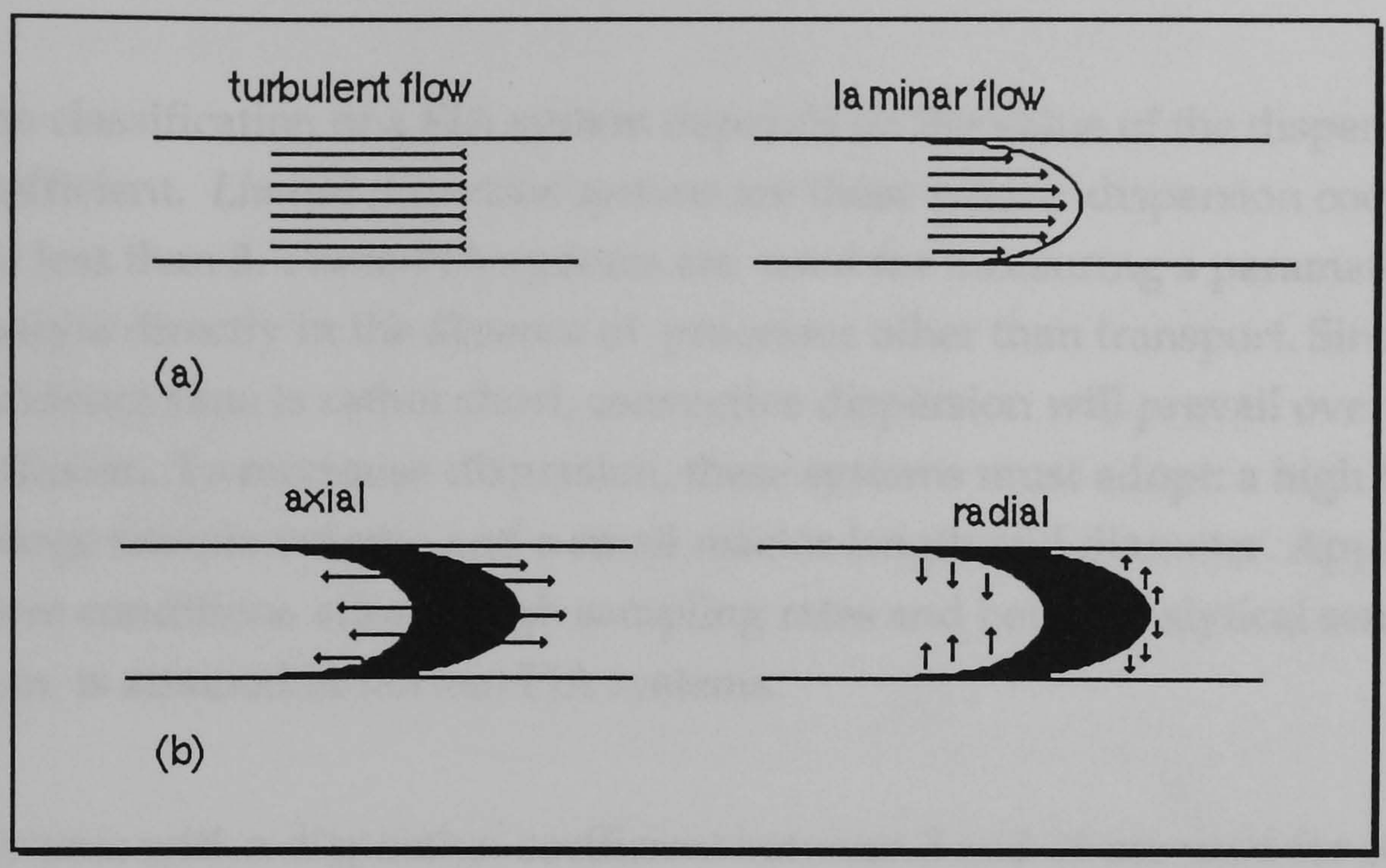

Figure 3.12 Dispersion mechanisms. (a) convective transport; (b) diffusional transport.

Axial diffusion is due to horizontal concentration gradients at the leading and trailing edges of the injected sample zone and contributes insignificantly to the overall dispersion. Radial diffusion, is caused by concentration gradients perpendicular to the direction of the flow and makes a significant contribution to the overall dispersion.

Various approaches have been proposed to relate theoretical considerations and experimental observations.

Ruzicka's dispersion coefficient (D) was the earliest parameter used to describe it. It is a direct measure of the extent of dilution undergone by a particular part of the sample zone between injection and detection and is defined as the ratio of the concentration before (C_o) and after (C) transport through a given FIA system:

$$D = \frac{C_o}{C}$$

Thus each point across the record signal has a corresponding dispersion coefficient. The maximum dispersion, D_{max}, in routine FIA ranges between 1 and 15.

The classification of a FIA system depends on the value of the dispersion coefficient. *Limited dispersion systems* are those whose dispersion coefficients are less than 3. These FIA systems are used for measuring a parameter of the analyte directly in the absence of processes other than transport. Since the residence time is rather short, convective dispersion will prevail over radial diffusion. To minimise dispersion, these systems must adopt: a high flow rate, a large sample volume and a small reactor length and diameter. Application of these conditions affords high sampling rates and better analytical sensitivity than is attained in normal FIA systems.

Systems with a dispersion coefficient between 3 and 10 are used for studies involving processes additional to transportation, for example a chemical reaction and are called *medium dispersion system*.

Large dispersion systems have dispersion coefficient greater than 10 and are characterised by the high degree of mixing between the carrier reagent and the sample, resulting in a well-defined concentration gradient. The residence time is rather long, so in some cases chemical equilibrium is attained.

The simplest way to measure the dispersion of a FIA manifold is by the injection of non-reactive species such as a dye into an inert carrier [86]. The dispersion is related to the sensitivity and sample throughput of the method. It is characterised by the concentration profile of the sample zone at a given point in time within the system. Four possible outcomes and their corresponding signals are shown in figure 3.13. As the dispersion increases, the peak height decreases. This means that the sensitivity decreases. Also, as the dispersion increases, the bandwidth increases causing the sample throughput to decrease.

The dispersion can be controlled by manipulating some of the variables of the system. The overall dispersion can be given by:

$$D = D_{injection} + D_{transport} + D_{detector}$$

Where $D_{injection}$ is the dispersion due to the sample volume and the geometric aspects of the system, $D_{transport}$ is the dispersion due to the reactor and the flow rate and $D_{detector}$ is the dispersion due to the flow cell geometry.

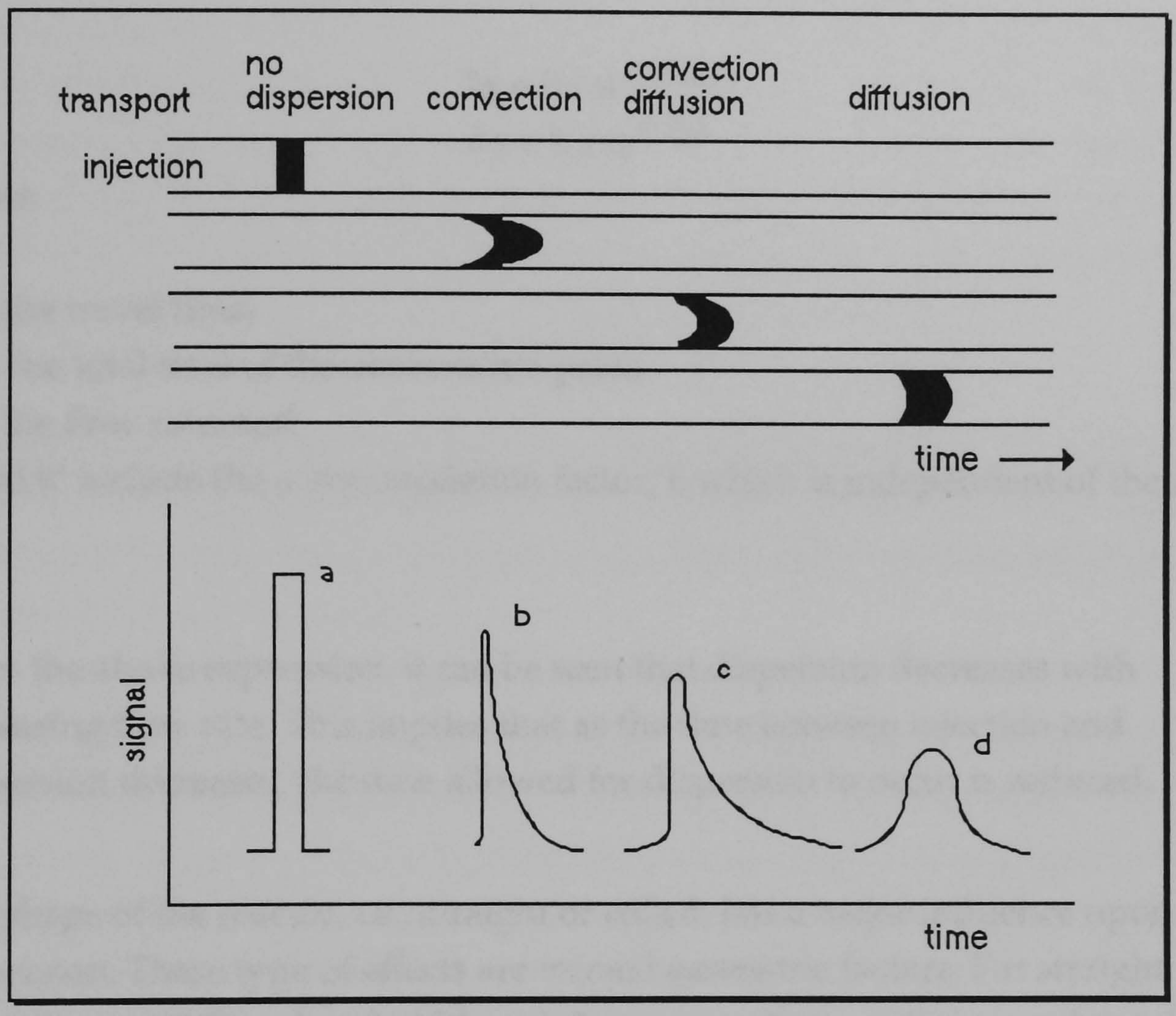

Figure 3.13 Sample dispersion and signal profiles.

Each variable in the above equation can thus be altered to obtain a change in dispersion. For example, in a typical FIA manifold it can be shown that the dispersion is inversely proportional to the sample volume (V)[12, 87];

$$D = k / V$$

The travel time, residence time and the bandwidth all vary with sample volume. A problem arises with very large samples in that the central portion

of the sample zone is not diluted. This implies that when this part of the sample passes through the detector, a signal corresponding to the original concentration of the sample, is obtained.

However, hydrodynamic factors such as the flow rate also influence dispersion. From Vanderslice's expressions, [88,89] the flow rate is related to the travel time and the bandwidth; for a given length of tubing:

$$t_a = k / q^{0.125}$$
$$\partial t = k' / q^{0.64}$$

where

t_a isthe travel time;
∂t is the total time of the observation peak;
q is the flow rate; and
k and **k'** include the accommodation factor, f, which is independent of the flow rate.

From the above expression, it can be seen that dispersion decreases with increasing flow rate. This implies that as the time between injection and dispersion decreases, the time allowed for dispersion to occur is reduced.

The shape of the reactor, i.e., straight or coiled, has a major influence upon dispersion. These type of effects are termed geometric factors. For straight tubes the travel time, bandwidth and dispersion all rise with increasing tube length and diameter.

For coiled reactors (tube is coiled helically) the centrifugal force caused by the circulation of the liquid[11] results in a radial flow. At low flow rates this centrifugal force is only slightly significant, and the velocity profile produced is virtually parabolic. However, at higher rates the velocity profile is altered since the molecules at the centre of the tube travel slower than those at the tube walls. This has a similar effect to radial diffusion in that it tends to reduce the dilution of the injected sample.

A third type of reactor can be made knotting end to end a length of flexible tubing. This markedly reduces dispersion, because the knots act as very tight coils.

Other devices such as packed tubes and single bead string reactors (SBSR) have also been used to control the dispersion. The behaviour of packed reactors is well known in chromatography. When the ratio of tube diameter to particle diameter lies between 5 and 20, the axial dispersion is directly related to the particle size. This implies that the smaller the diameter, the smaller the dispersion. The SBSR consist of ordinary Teflon tubes packed with tiny glass beads of slightly lower diameter than the id. of the tube. These beads increase radial diffusion, reducing dilution of the sample in the flow line, and therefore decrease dispersion.

Temperature is an influential factor and requires consideration [90]. Stults et al. have been investigated systems with and without chemical reactions. They have observed that temperature has a significant and predictable effect on the dispersion of a sample plug.

In a GD-FIA system, all factors influencing the mass transport through the membrane (as discussed in chapter 2) will influence the peak shape via dispersion. In such systems, these factors plus all other physical factors dependent upon the manifold design require to be studied in characterisation of the system.

3.2.1 Experimental

The system shown in Figure 3.1b, was used in a flow injection system in conjunction with flame atomic absorption spectrometry (flame-AAS). The emergent flow from the membrane was used to fill a sample loop which was then injected into the nebuliser uptake stream. This arrangement, shown in Figure 3.14 a , was necessary because the emergent flow rate from the membrane may be as low as 200 µl/min which is not directly compatible with typical nebuliser uptake rates, 4.5 ml/min.

Copper standard solutions were utilised and the absorbance at 324.8 nm was measured using a flame atomic absorption spectrometer (AAS), Phillips PU

9100. and a chart recorder, Phillips PM single pen . Air/acetylene flame and a copper hollow cathode lamp operating at 3 mA. The flame-AAS was calibrated by the calibration curve technique, using standards in the range 1 - 4 ppm. The oven temperature was held at 90°C, the oven fan was activated and drying agent was present.

Various lengths of Teflon tubing were used to prepare sample loops of the desired size. The volume of those were pre-determined by injecting a dye solution into a known final volume. The absorbance obtained were compared with those in a calibration graph of volume versus absorbance previously prepared by serial dilution of the same solution.

The effect of sample size on the absorbance was measured by injecting standard Cu solutions into the flame-AAS from sample injection loops of different volumes. These absorbances were compared with those obtained when the same standards were aspirated directly into the flame-AAS. The dispersion factor for this simple FIA system was characterised.

Studies of dispersion were also undertaken with the system in figure 3.1 b coupled to a U.V. spectrophotometer fitted with a flow cell, Figure3.14 b. This arrangement, Figure 3.14b, used a FIA system Tecator incorporating a Tecator 5020 analyser, a Tecator 5022 detector controller and a Tecator 5023 U.V. spectrophotometer with a pen chart recorder, Phillips PM 8251.

The possibility of operating at higher temperatures and lower flow rates without generation of undesirable bubbles was investigated to determine the best conditions for the system.

To obtain an extended dispersion profile, various concentrations of $KMnO_4$ solution were injected. The absorbances for samples eluted from the membrane were measured at 525 nm and recorded using a chart recorder.

Studies were carried out at various oven temperatures using various sample volumes and carrier flow rates. Replicate injections were performed until reproducible peaks were attained.

Experiments were carried out by replacing the oven with an ice bath at 2 °C, to study the maximum dispersion caused by the 10 m straight reactor. Under such conditions it was supposed that no water loss occurred and all dispersion was due to the length of the membrane.

Study of the influence of the membrane unit preconcentration factor upon peak profiles was carried out using a 2 ml injection loop and a 2ml min^{-1}flow rate, over the temperature range 20°C - 76°C. The results obtained were compared with those for the same standard concentrations of $KMnO_4$ without use of the FIA system.

In order to obtain a full illustration of the extent of dispersion, large volumes of 8 ppm $KMnO_4$ solution were injected into the FIA system. The maximum concentration zone was observed on the wider peaks. The volume of sample necessary to achieve the maximum concentration zone were calculated for each temperature.
In both arrangements used in this section the system shown in Figure 3.1b was used.
In the first FIA manifold, Figure 3.14a. a The absorbances were obtained using a wavelength of 324.8 nm and a copper hollow cathode lamp operated at 3 mA. The oven was set at the required temperature, the oven was fan assisted and the drying agent was in place.

Reagents
A stock copper solution (100 ppm) was prepared by transferring 10 ml of Spectrosol 1000 ppm standard copper solution to a 100 ml volumetric flask and making up to the mark with deionised water. The calibration standards of concentration 1,2,3 and 4 ppm and the test standard, 0.1 ppm were prepared daily from the 100 ppm stock solution.

A stock potassium permanganate solution (1000 ppm) was prepared by weighing out 1g of the salt (Fisons- analytical grade) and dissolving it in 1000 ml of water. The working solutions, 10 - 120 ppm, were prepared daily from the stock solutions.

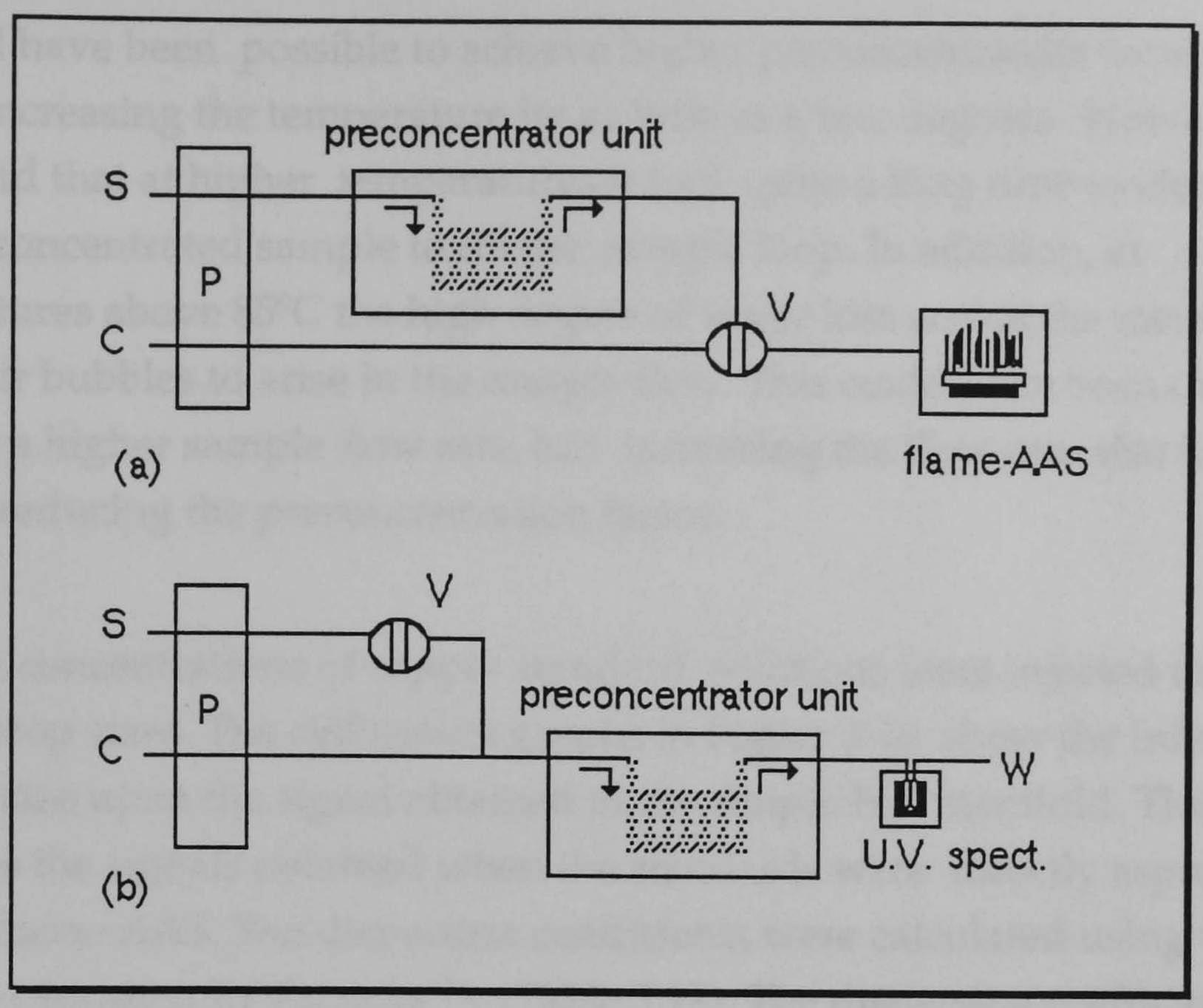

Figure 3.14 The two FIA manifolds arrangements used to study the sample dispersion in a flow system containing the preconcentrator unit. (a) Sample preconcentrated prior to introduction; (b) sample preconcentrated on-line.

3.2.2 Results and discussion

The peak profiles given in Figure 3.15 visually show the preconcentration capability of the membrane on running 0.1 ppm solution through the membrane at a flow rate of 1.87 ml min^{-1} at 90°C. At this temperature and flow rate, vapour bubbles appeared in the liquid stream emerging from the membrane. To overcome this the outflow was passed to an open topped ml sample cup and the injection loop filled simultaneously from this buffer reservoir. This arrangement is not practical for routine changing of samples, but served for the purpose of this experiment.

The preconcentrated sample gave an absorbance of 2.74 absorbance units corresponding to a copper concentration of 1.77 ppm . It may be observed that a preconcentration factor approaching 20 was attained. This simple experiment illustrates how the membrane may be used successfully as a practical preconcentration device for aqueous solutions.

It should have been possible to achieve higher preconcentration factors than 17.7 by increasing the temperature by as little as a few degrees. However, it was found that at higher temperatures it took quite a long time to elute enough concentrated sample to fill the sample loop. In addition, at temperatures above 85°C the high degree of water loss across the membrane caused air bubbles to arise in the sample flow. This could have been overcome by using a higher sample flow rate, but increasing the flow rate also had the effect of reducing the preconcentration factor.

Different concentrations of copper standard solutions were injected using various loop sizes. The calibration graphs in Figure 3.16 show the influence of the loop size upon the signal obtained in the simple FIA manifold. This figure also gives the signals obtained when the standards were directly aspirated into the flame-AAS. The dispersion coefficients were calculated using the equation proposed by Ruzicka [11], (Table 3.12). The dispersion coefficients for the different size samples are less than 3. Thus, the system can be classified as a limited dispersion system.

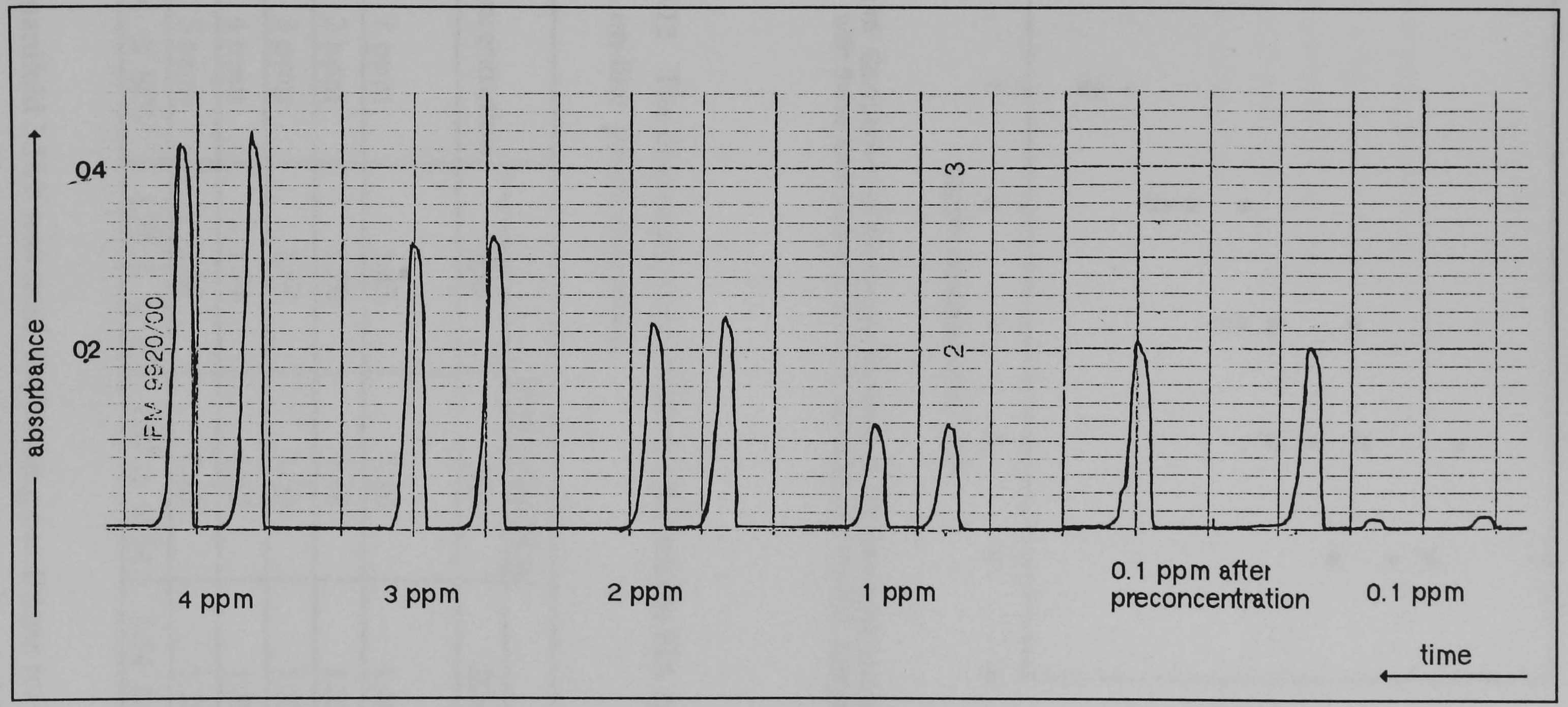

Figure 3.15 Characteristic peak profiles for 500 µl injection of 0.1 ppm of copper with and without preconcentration.

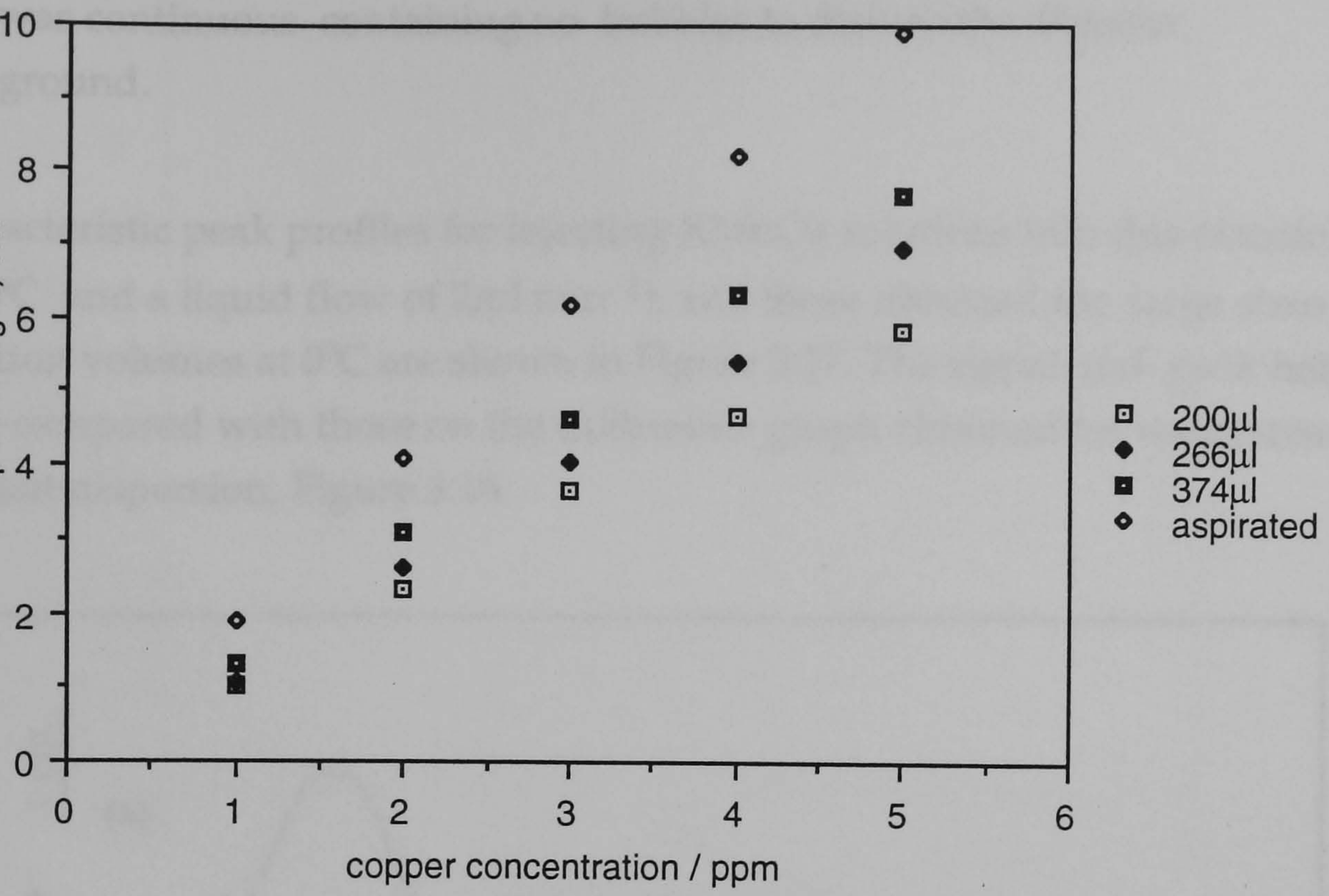

Figure 3.16 Comparison of the copper absorbance for standards aspirated into the flame with those for injection of discrete volumes into the FIA system.

Table 3.12 The dispersion coefficients for the simple FIA system without on-line preconcentration.

concentration	loop volume, µl		
	200	266	374
1 ppm	1.85	1.80	1.46
2 ppm	1.78	1.58	1.32
3 ppm	1.69	1.53	1.33
4 ppm	1.74	1.52	1.30
5 ppm	1.69	1.42	1.28
X ± SDV	1.75 ± 0.07	1.57 ± 0.14	1.34 ± 0.07

When the manifold 3.14 b was used, the limiting conditions for flow rate and temperature for operation were found to be 2ml min^{-1} and 76°C, respectively. Under these conditions the flow emerging from the membrane

unit was continuous containing no bubbles to disturb the detector background.

Characteristic peak profiles for injecting $KMnO_4$ solutions into this manifold at 76°C and a liquid flow of 2ml min^{-1}), and those obtained for large sizes of injection volumes at 0°C are shown in Figure 3.17. The signal and peak height were compared with those on the calibration graph obtained for the system without dispersion, Figure 3.18.

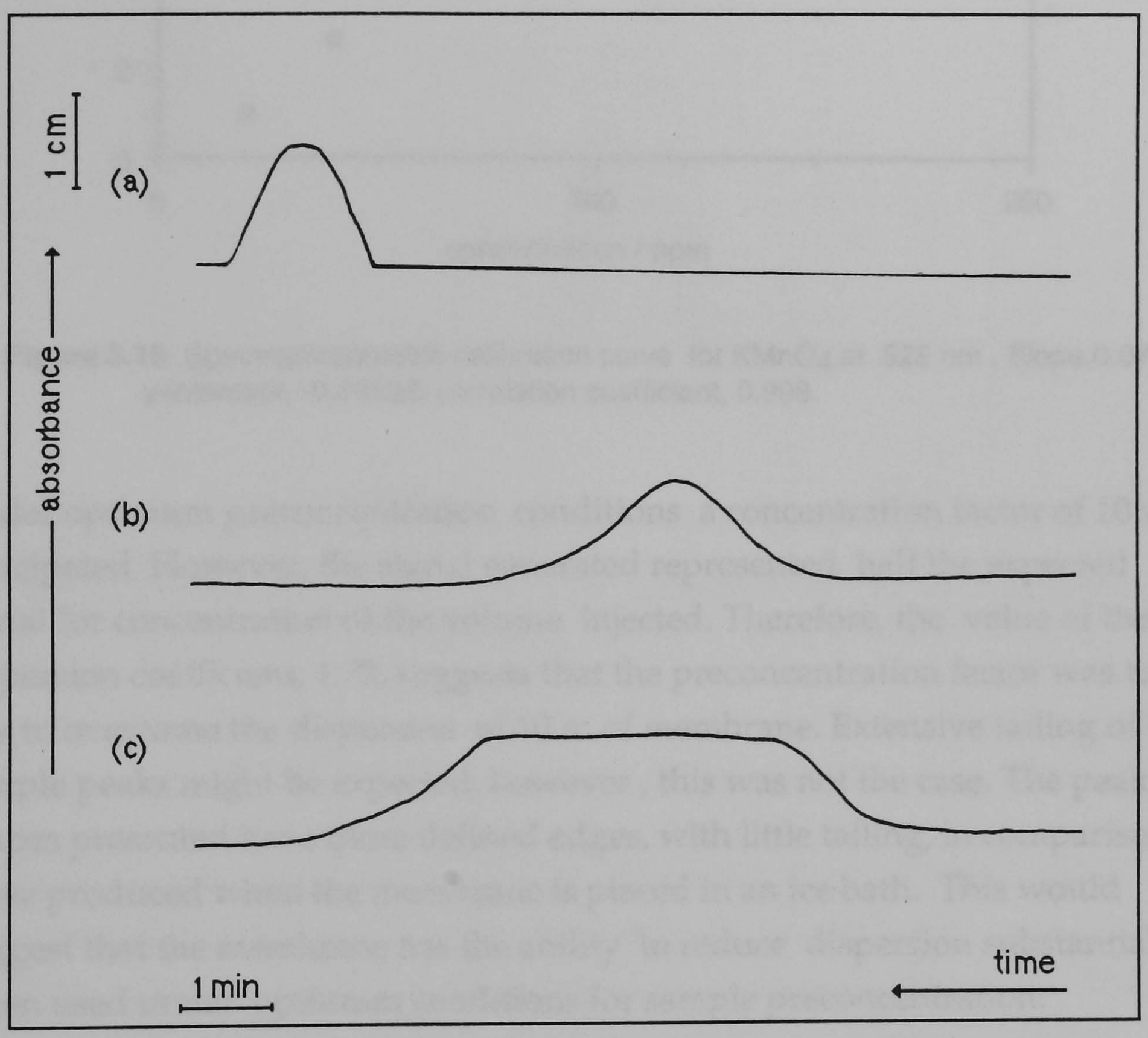

Figure 3.17 Characteristic peak profiles obtained for $KMnO_4$ solutions injected into the FIA system with a preconcentrator unit under various conditions. (a) 440 µl of 40 ppm standard solution injected in a carrier flow rate 2 ml min^{-1} at 76ºC; (b) and (c) 16 ml of 8 ppm and 20 ppm standard solutions injected in a carrier flow rate 2 ml min^{-1} at 0ºC respectively .

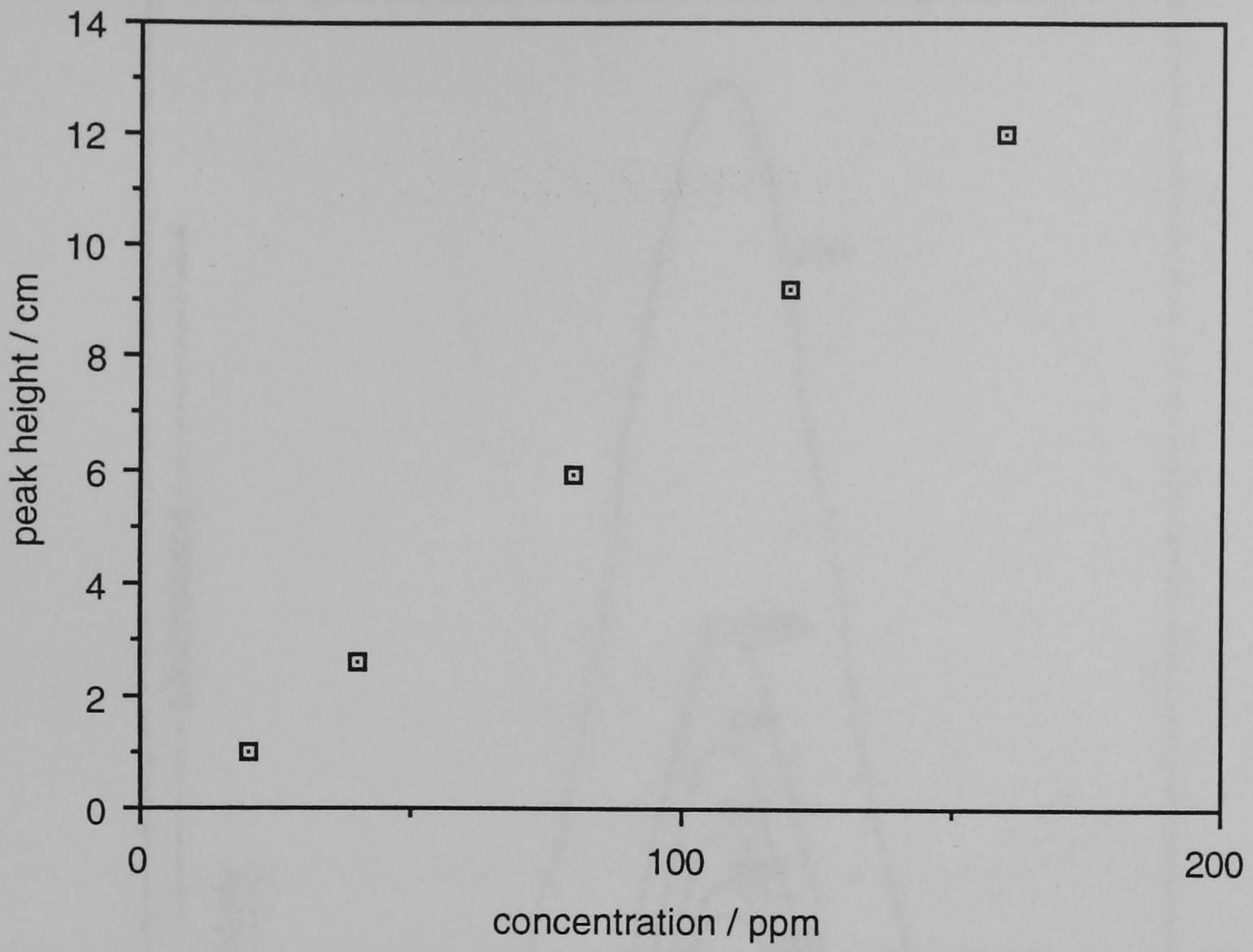

Figure 3.18 Spectrophotometric calibration curve for $KMnO_4$ at 525 nm . Slope,0.0793; y-intercept, -0.52622; correlation coefficient, 0.999.

Under optimum preconcentration conditions a concentration factor of 10 was anticipated. However, the signal generated represented half the expected signal for concentration of the volume injected. Therefore, the value of the dispersion coefficient, 1.79, suggests that the preconcentration factor was too low to overcome the dispersion of 10 m of membrane. Extensive tailing of the sample peaks might be expected, however , this was not the case. The peak shapes presented have more defined edges, with little tailing, in comparison to those produced when the membrane is placed in an ice bath. This would suggest that the membrane has the ability to reduce dispersion substantially when used under optimum conditions for sample preconcentration.

The effect of the preconcentration factor upon peak shape is shown in Figure 3.19. As the temperature increases, more well defined peaks are generated due to the increase in sensitivity. Similarly, as the carrier flow rate increases the peak height decreases as the mass loss efficiency is inversely proportional to the flow rate, Figure 3.20.

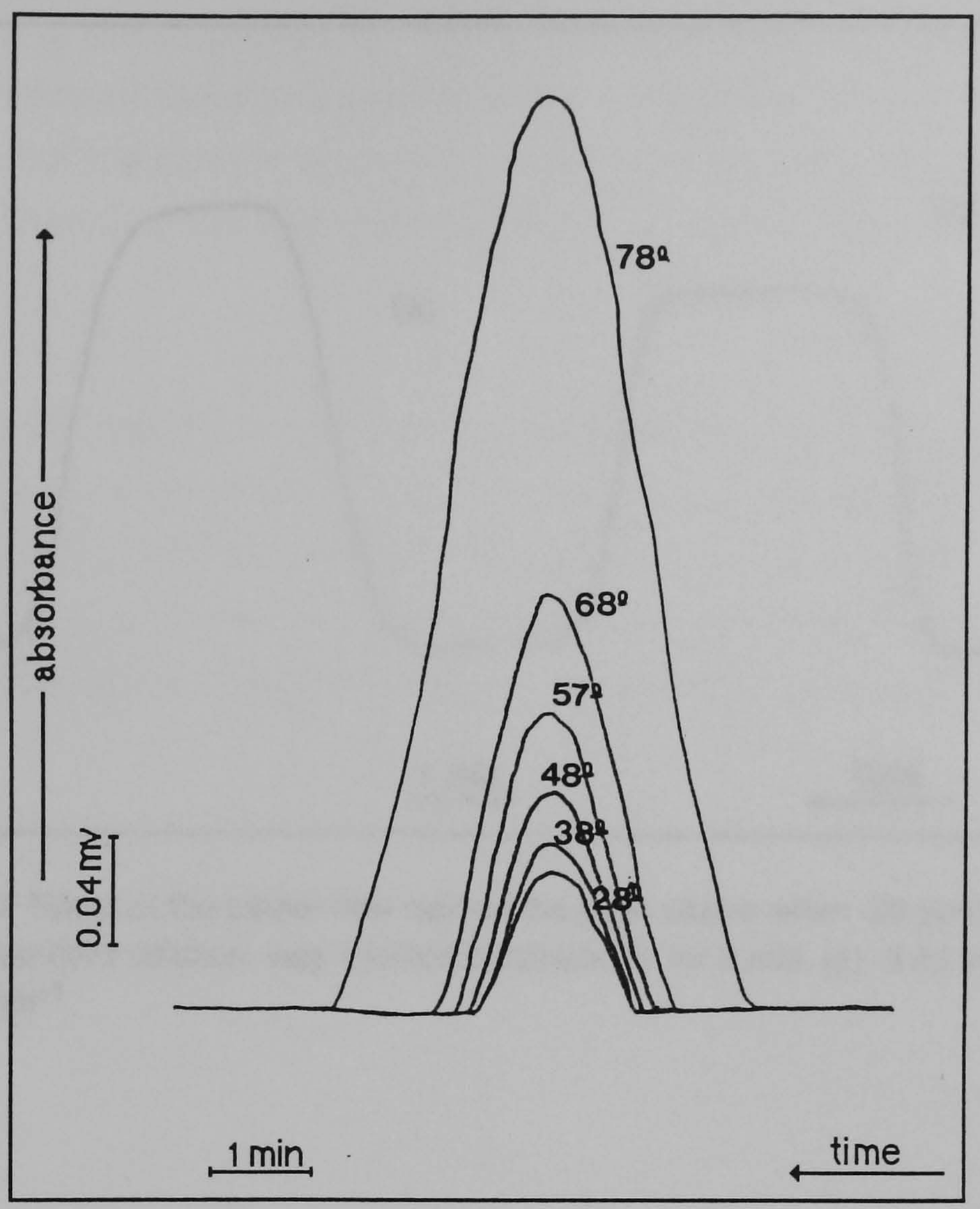

Figure 3.19 Effect of the temperature on the peak shapes obtained for 2 ml injection of 20 ppm $KMnO_4$ standard solution in a carrier flow rate 2 ml min^{-1}.

Figure 3.21 shows the peak profiles obtained when 8 ppm $KMnO_4$ solution was continuously injected to produce a maximum concentration zone. It can be clearly seen that the larger injection volumes yielded higher peaks. These peaks exhibit sharp well defined edges and there is an absence of tailing, showing that the concentration factor for the membrane reduced dispersion. The concentration of these samples were calculated using the calibration curve, Figure 3.18. The results are given in Table 3.13.

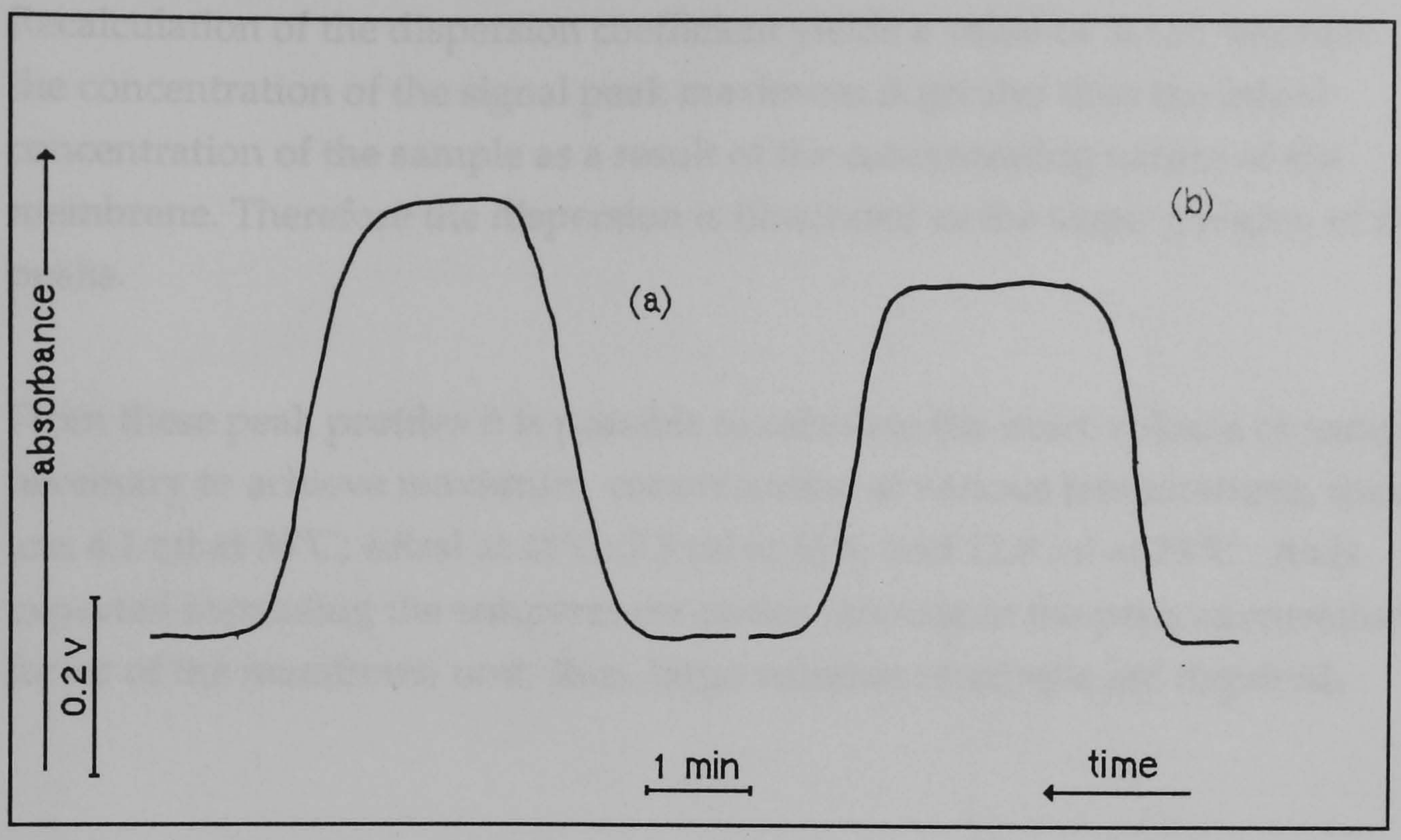

Figure 3.20 Effect of the carrier flow rate on the peak shape when 20 ppm $KMNO_4$ standard solution was injected continuously for 3 min. (a) 3 ml min^{-1}; (b) 5 ml min^{-1}.

These results successfully illustrate the dispersion reducing ability of the membrane, while concentrating the sample plug. The flat top region of the peaks represents the maximum concentration factor of the membrane. While the sloped edges represent the dispersion associated with each injection. There is little peak tailing reaffirming the conclusion that concentration process in the membrane substantially reduces the influence of the dispersion.

Table 3.13 Calculated concentrations for injection of when 8 ppm KMnO4 solution into the FIA system with preconcentrator unit at various temperatures.

temperature /°C	peak height / cm	concentration /ppm
34	0.9	18
48	1.2	22
61	2.2	34
76	5.1	71

Recalculation of the dispersion coefficient yields a value of 0.125 because the concentration of the signal peak maximum is greater then the initial concentration of the sample as a result of the concentrating nature of the membrane. Therefore the dispersion is illustrated as the sloping region of the peaks.

From these peak profiles it is possible to calculate the exact volume of sample necessary to achieve maximum concentration at various temperatures, these are: 4.1 ml at 34°C; 4.8ml at 48°C; 7.3 ml at 61°C and 12.8 ml at 76°C . As is expected increasing the temperature causes increase in the preconcentration factor of the membrane unit, thus, large volumes of sample are required.

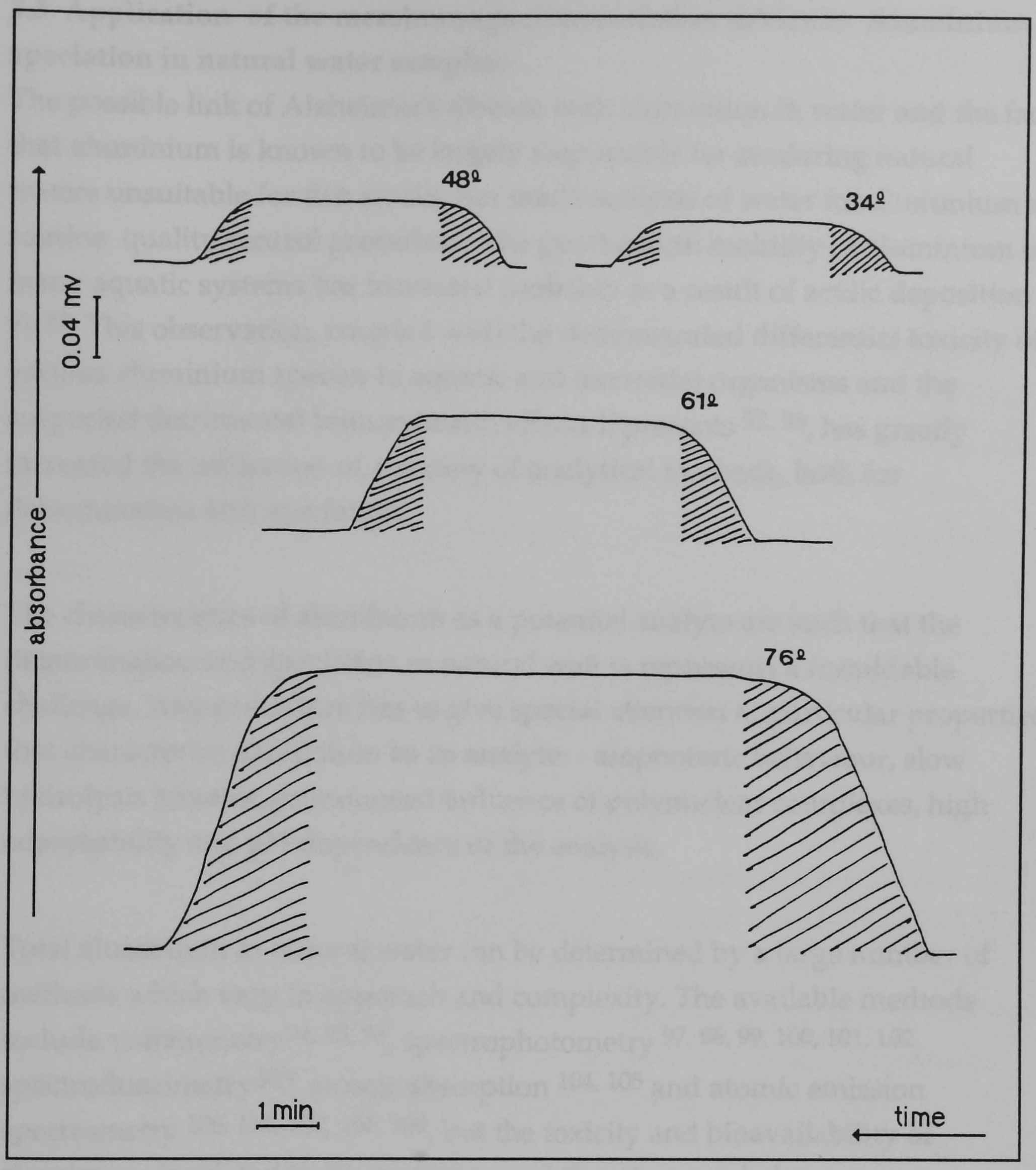

Figure 3.21 Characteristic peak profiles obtained for continuous injection of sample into the carrier flow at various temperatures.

3.3 Application of the membrane preconcentration device to Aluminium speciation in natural water samples.

The possible link of Alzheimer's disease with aluminium in water and the fact that aluminium is known to be largely responsible for rendering natural waters unsuitable for fish stocks, has made analysis of water for aluminium a routine quality control procedure. The geochemical mobility of aluminium in many aquatic systems has increased probably as a result of acidic deposition [91, 92]. This observation, coupled with the demonstrated differential toxicity of various aluminium species to aquatic and terrestrial organisms and the suspected detrimental human health effects it presents [92, 93], has greatly increased the utilisation of a variety of analytical methods, both for determination and speciation.

The characteristics of aluminium as a potential analyte are such that the determination and speciation in natural waters represents a formidable challenge. Any procedure has to give special attention to particular properties that characterise aluminium as an analyte: - amphoteric behaviour, slow hydrolysis kinetics, pronounced influence of polynuclear complexes, high adsorbability and pH dependence of the analysis.

Total aluminium in natural water can be determined by a large number of methods which vary in approach and complexity. The available methods include voltammetry[94, 95, 96], spectrophotometry [97, 98, 99, 100, 101, 102], spectrofluorimetry[103], atomic absorption [104, 105] and atomic emission spectrometry [106, 102, 107, 108, 109], but the toxicity and bioavailability of aluminium is related to its speciation and therefore total aluminium determination alone is of limited use for monitoring or assessing its environmental effects.

The possible aluminium species in solution are:

- alkaline pH: $Al(OH)_4^-$
- below pH ≈ 4: Al^{3+}
- pH range 4 -7: monomer and polynuclear complexes of hydroxide ions, fluoride anions, and certain chelating organic ligands.

Aluminium in natural water is normally found at trace levels and separating it into fractions further reduces its concentration in the various fractions. This inevitably creates a need for a preconcentration step to enhance sensitivity and detection.
Different preconcentration steps such as ion-exchange, solvent extraction and electro-deposition have been used in aluminium determinations.

West et *.al.*[110] proposed that for samples low in salts (e.g.potable waters), enrichment procedures may be considerably simplified to mere evaporation. The PTFE membrane takes advantage of this simple enrichment process due to its properties. It is hydrophobic and thus does not allow water to pass through it while water vapour formed by evaporation can pass through the porous media.

The ability of the membrane to improve detection limits has already been investigated and it is proposed to incorporate it in a scheme for the speciation of aluminium.

Even though detailed schemes for physical and chemical speciation of aluminium have been described, for routine purposes a simple analytical procedure has been suggested by Seip et *al.*[111] . The pyrocatechol violet method might be applicable for adaptation to speciation procedures and it is used as a standard method by Driscoll [93] and involves passing the water sample over a cation exchanger in the sodium form . The free labile aluminium is exchanged for the sodium ion and the column elute contains only organically chelated aluminium.

The three most important aluminium fractions produced by this method are:
1. Organically complexed (non-labile aluminium).
2. Inorganic (labile) monomeric aluminium. (this fraction includes free aluminium and soluble aluminium hydroxide, fluoride, and sulphate complexes).
3. Acid soluble aluminium.

In the present study, the total aluminium concentration was determined using electrothermal atomisation - atomic absorption spectroscopy (ETA-

AAS). The total monomeric aluminium was estimated by complexation with pyrocatechol violet, the total polymeric fraction being the difference between the two.

The monomeric fraction was further split into two by stripping the labile free Al fraction off, using Amberlite resin, and determining the non-labile part using the same method as for total monomeric aluminium. The membrane unit was used as a preconcentration technique.

3.3.1 Experimental

The scheme used for the aluminium speciation incorporating the membrane unit is described below:

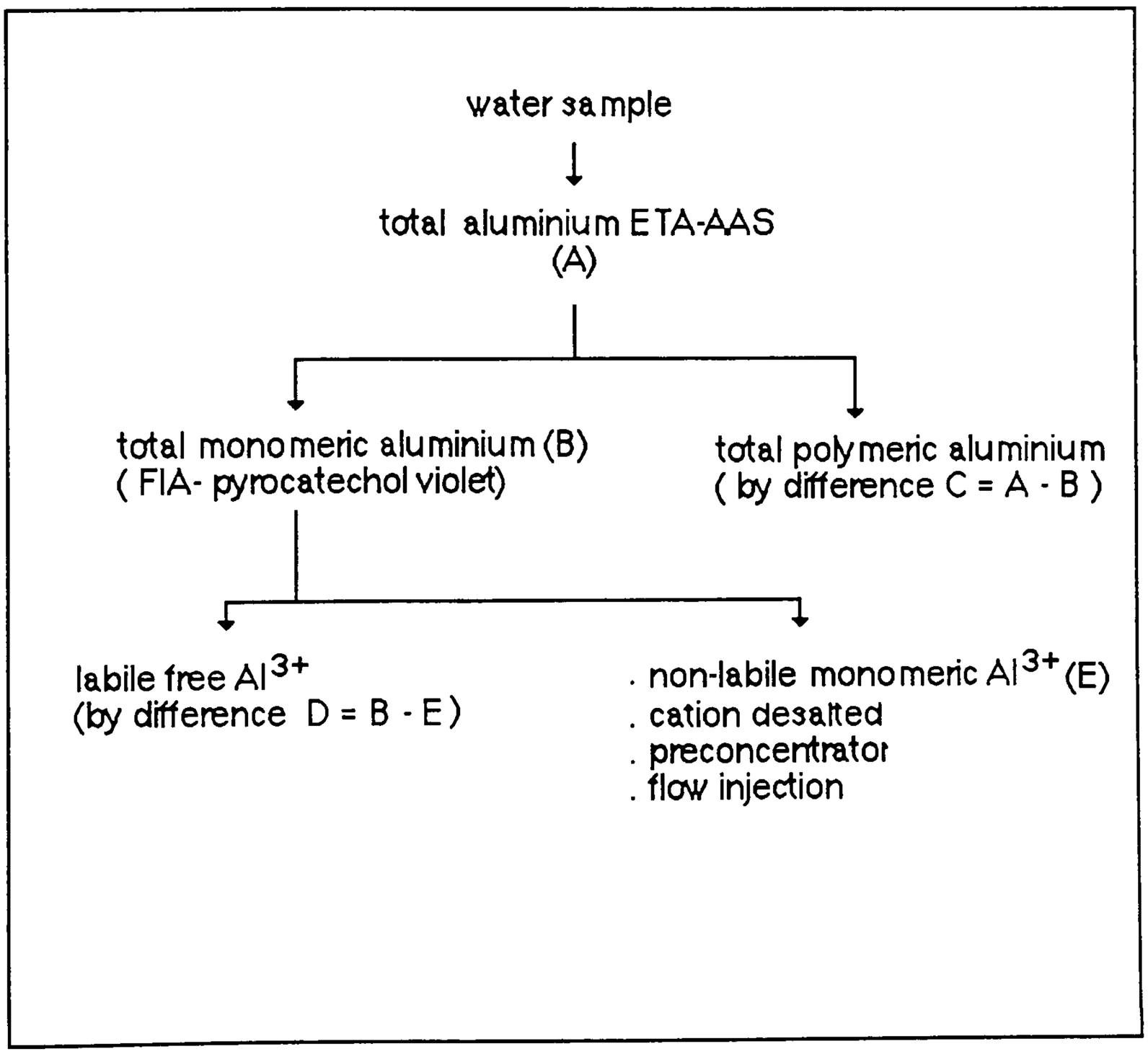

The flow-injection pyrocathecol violet method used is based on Royset's [100] optimised method . In this method inorganic aluminium was determined by reaction with pyrocatechol violet, followed by visible spectrophotometric detection of the coloured product.

The system shown in figure 3.1.b was coupled to a visible spectrophotometer, Phillips PYE UNICAM SP6-250, set at 585 nm, using a

Hellman flow-through cell (10 mm light path, 15 mm path height, 30 µl volume and made of quartz). The manifold is shown in Figure 3.22. It was built with 0.8 mm id. Teflon tube and a chart recorder, Tekman TE 200 . Two peristaltic pump, Gilson Minipuls2 and an Ismatec were used to pump sample and reagent. Flow rates of reagents were as shown in Figure 3.22.

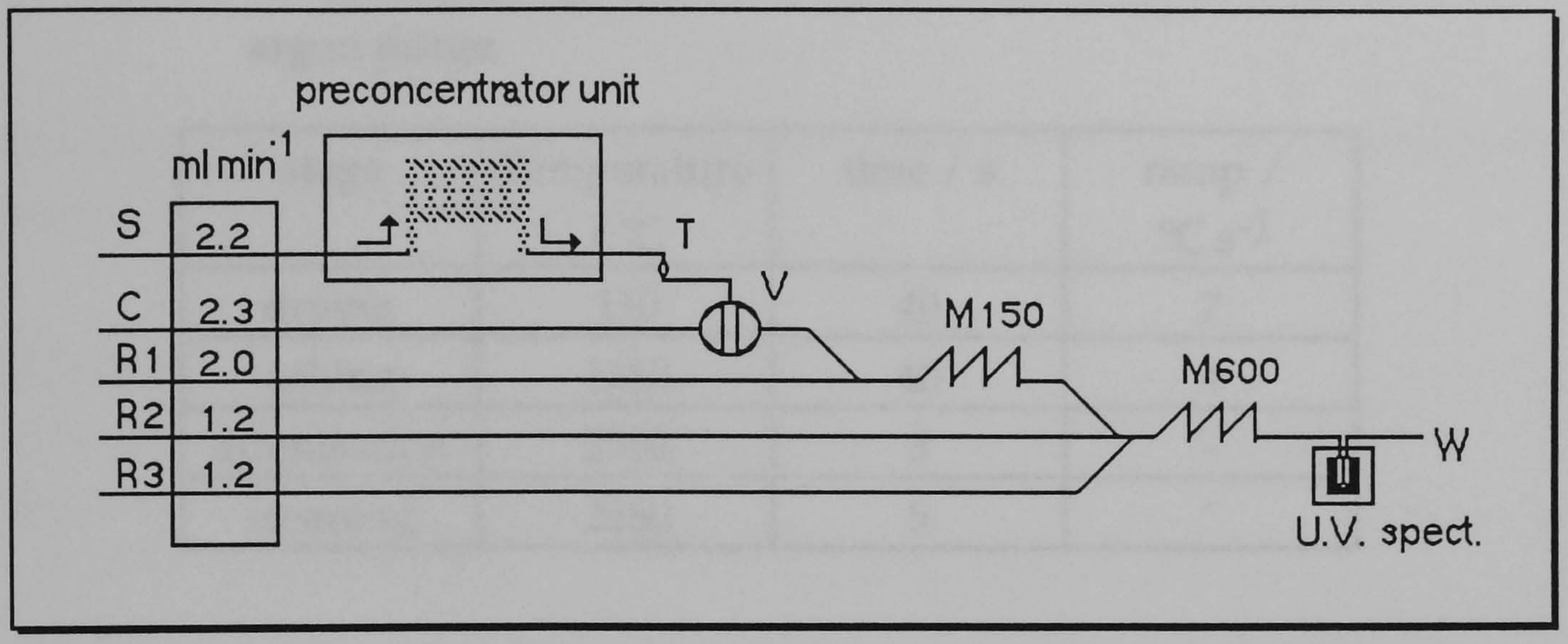

Figure 3.22 Flow injection manifold for the determination of aluminium by pyrocatechol violet. S, sample; W, waste; V, injection valve; M, mixing coil (length in cm); C, carrier; R1, iron-masking reagent; R2, PCV reagent; R3, buffer and T, condenser.

A micro condensing device was connected in between the membrane and the injection valve containing a sample loop, 200 cm. This device was used to recondense vapour formed in the membrane as it was heated and to avoid bubbles entering the detector. The preconcentrator unit was used with 8.85 m tubular membrane and the preconcentrator factor for this unit was checked up to 90°C at different sample flow rates.

For the aluminium total determination, an ETA-AAS was used as a detector instead of a visible spectrophotometer. A atomic absorption spectrometer, PYE UNICAM SP9, was used . It used an aluminium hollow cathode lamp with lamp current set at 7mA. The wavelength was set at 309 nm and the slit width was 0.2 nm. A D_2 lamp was used for background correction and the furnace was purged with argon . The preconcentrator unit was not on-line and samples and standards were collected manually from the concentration step and then analysed by ETA-AAS.

The furnace programme used is tabulated in Table 3.14. It is an adaptation of that described by Person *et al.*[112]. The effect of nitric acid and the phosphoric acid matrix modifier was studied by preparing the standards in 0.02 M nitric acid and 7 μM phosphoric acid solution. An autosampler was used for automatically inject 20 μl sample solution on the ETA-AAS furnace.

Table 3.14 Furnace programme. Cool down was about 30 seconds with argon purge.

stage	Temperature / °C	time / s	ramp / °C s^{-1}
drying	110	40	7
ashing	1250	40	4
atomisation	2300	8	-
cleaning	2550	5	-

The first experimental step was to prepare the resin Amberlite IR-120 to a sodium form. About 20g of resin in the hydrogen form, was stirred with 0.5M sodium chloride solution. The sodium chloride solution being changed daily. After a week the concentration of the sodium chloride was reduced to 0.005M and stirring has continued for another two days, until the pH of the supernatant was higher than that of the sodium chloride solution.

The resin was then transferred to a 1cm diameter, 20cm long column and adjusted so that 1×10^{-3}M sodium chloride solution eluent produced an eluent of pH 5.0. After this initial equilibration of the column with eluent, 50 to 60ml of sample was passed through the column to displace the eluent and was then discarded. An additional 60ml was then collected for analysis and the column was regenerated using 400ml of eluent[113].

The stability of the aluminium-PCV complex was studied by measuring manually the absorbance at different times of colour development using a static uv-visible spectrophotometer and employing reagents at the recommended concentrations [114]. The ability of the PTFE membrane to enhance detection limits was demonstrated by analysing standards before

and after passing them through the membrane, using both the pyrocatechol violet method and the ETA-AAS method.

Standards and samples were run with and without the preconcentrator. The pH range 6.1 - 6.2 is optimal to minimise changes in background and sensitivity and this range was attained by using a hexamine buffer at a concentration of 3 M.

Standards were analysed with and without having been preconcentrated and were all prepared in deionised water.

Reagents

Aristar - reagent grade materials and deionised water used throughout.

Reagents for cation desalting

- Sodium chloride 0.5 M
- Sodium chloride (29.22g) was dissolved in water and made up to a litre. Further dilution were made as and when required.

-Amberlite IR 120 Resin. The hydrogen form of the resin was converted to the sodium form by equilibrium with sodium choride solution .

Reagents for visible spectrophotometry

Reagents were prepared according to Royset's[100] optimised method.

-hydrochloric acid 0.1M - this acid solution was prepared by dilution of 5 M hydrochloric acid with water.

-1,10 phenanthroline solution 10 mM - hydroxylammonium chloride (34.75 g) was dissolved in approximately 800 ml of water. 1,10 phenanthroline hydrate (1.98 g) was then dissolved in the above solution. the solution was transferred to a 1000ml volumetric flask and made up to the mark with water, and was thoroughly mixed. The solution was then stored in a polyethylene bottle.

-pyrocatechol violet solution 5 mM - pyrocatechol violet (1.93 g) was dissolved in 75 ml of water, transferred to a 100 ml volumetric flask and made up to the mark. The solution was thoroughly mixed and stored in a polyethylene bottle.

-hexamine buffer solution 3 M - hexamethylene tetramine (420.57g) was dissolved in water and made to a litre, then 17ml of 37% w/v hydrochloric

acid was added to a litre of the buffer to give a final concentration of 0.2 M hydrochloric acid. The solution was then stored in a polyethylene bottle.
-standard aluminium solution 20 ppm - 10 ml of a 1000 ppm standard aluminium solution was transferred to a 500 ml volumetric flask and made up the mark with 0.1 M hydrochloric acid solution, and mixed. The solution was stored in a polyethylene bottle. Appropriate dilutions were then made as and when required

For the flow injection system, the carrier (C) and all standards were prepared in 0.1 M hydrochloric acid. To the samples, hydrochloric acid was added to a final concentration of 0.1 M.

Reagents for ETA-AAS

-nitric acid 0.01M - the nitric acid solution was made by dilution of Aristar grade 15.85M nitric acid.
-phosphoric acid 7 μM (7×10^{-6}M) - the phosphoric acid solution was made by dilution of Aristar grade 14.75 M phosphoric acid.
-standard aluminium solution 20 ppm - 10 ml of a 1000 ppm standard aluminium solution was transferred to a 500 ml volumetric flask and made up to the mark with water and mixed. The solution was stored in a polyethylene bottle and appropriate dilutions were made when required either with water or 0.01 M nitric acid.

Water sample

The water sample was collected from a small isolated clough on Hallam Moor, approximately half a mile from Moscar (GR 235875), and 6 miles from the Howden Reservoir site. On this occasion it was after spells of heavy rain and snowfalls and the sampling conditions were as follow:

pH	4.0
temperature of sample	3.5°C
weather	sunny, cold
date	4th January 1991

The sample was filtered through a 0.45 μm membrane within 3 hours of collection, to remove colloidal material and arrest bacterial changes.
Some of the water was cation desalted (removal of free Al^{3+}) by using a ion-exchange resin, Amberlite IR 120 as described under methods.

3.3.2 Results and discussion

Figure 3.23 shows the effect of the time on the coloured compound when prepared from standard aluminium and natural water sample respectively. The plots depict stabilisation of the absorbances for the natural water sample between 10 and 30 minutes of colour development (which are in agreement with other workers [115, 116] and 10 minutes was the chosen work time.

To check the preconcentration factor, the oven was set at 90°C and distilled water was pumped through at different flow rates. Results are shown in Table 3.14. To get a 10 fold concentration, an input of 2.2 ml min^{-1} at 90°C would be ideal. Figure 3.24 shows characteristic peaks obtained for 0.035 ppm aluminium standards without preconcentration and after 10 fold concentration.

Table 3.16 Concentration factors obtained at different flow rates through the system 3.1b with 8.85 m microporous PTFE tubular membrane.

input flow ml min^{-1}	output flow ml min^{-1}	concentration factor
3.46	1.34	2.58
2.3	0.44	5.77
2.28	0.26	8.80
2.20	0.21	10.48
1.55	0.13	11.63
1.56	0.12	13.56

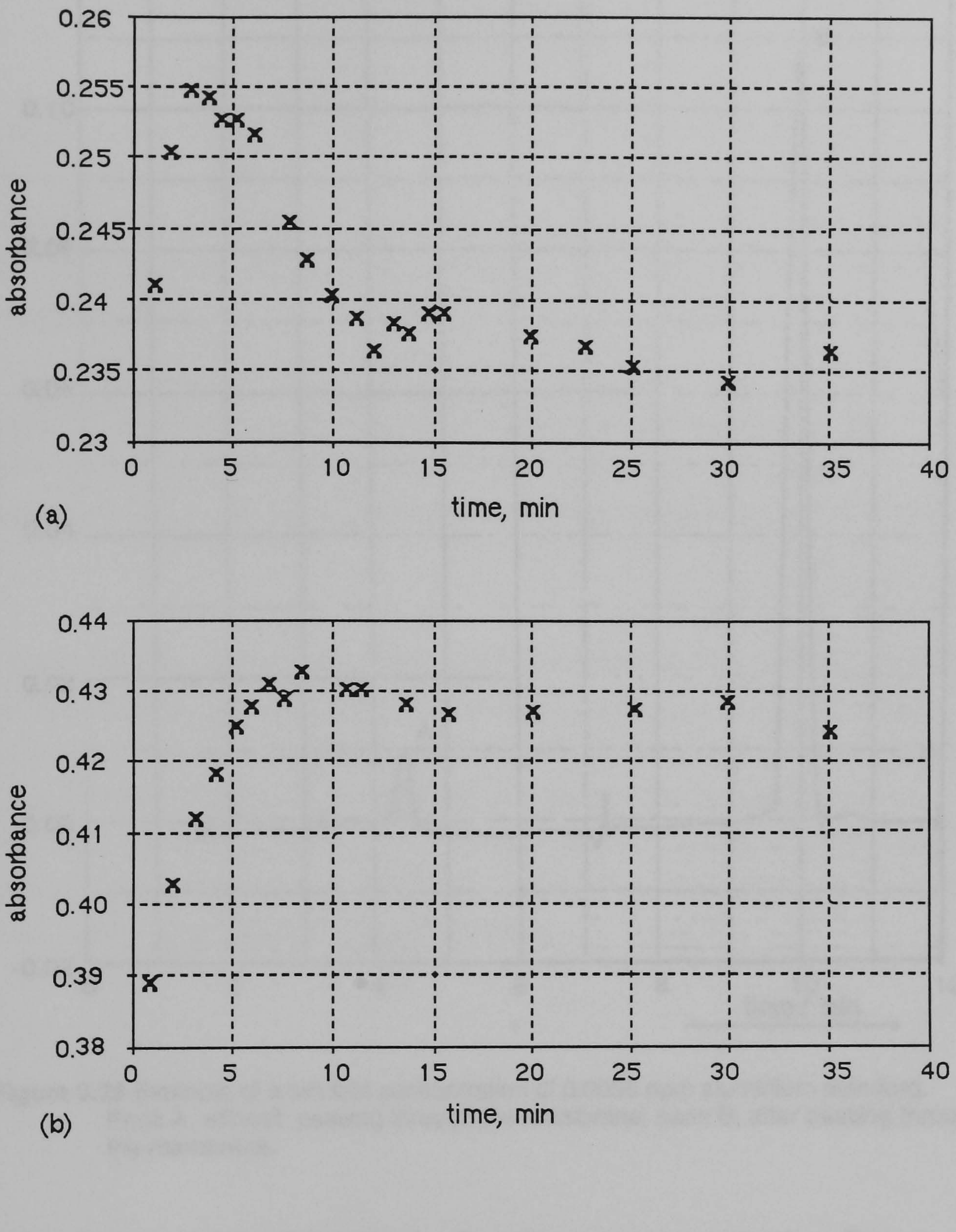

Figure 3.23 Stability testing of the coloured compound formed on reacting pyrocatechol violet (PCV) with (a) aluminium standard and (b) water sample.

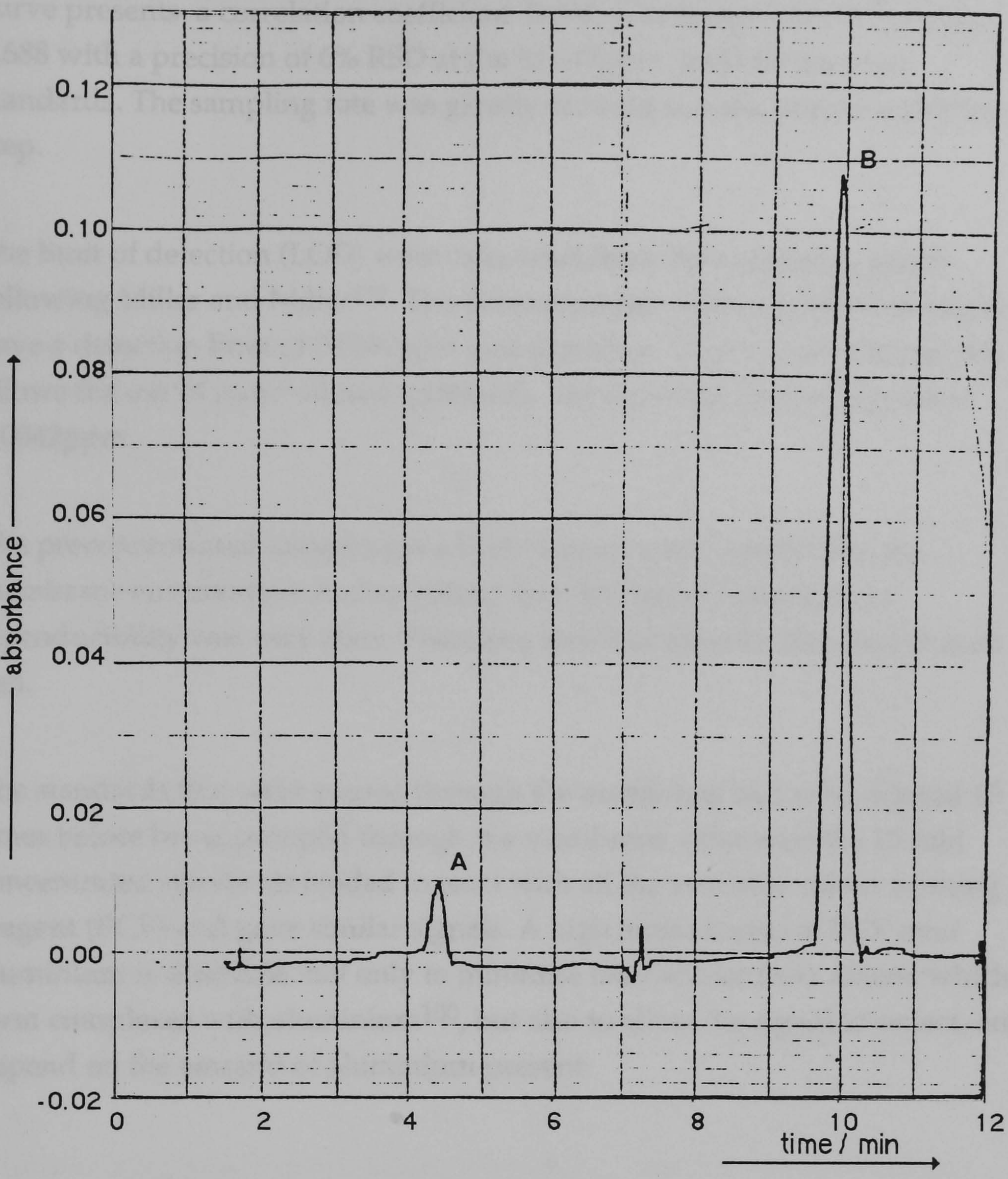

Figure 3.24 Example of a ten fold concentration of 0.0035 ppm aluminium standard. Peak A, without passing through the membrane; peak B, after passing through the membrane.

The absorbances obtained for standards without preconcentration, Figure 3.25, resulted in a calibration curve with a correlation coefficient 0.998, y-intercept -4.67×10^{-4}; slope 0.3455. Reproducibility was 9.4% RSD at the 0.114ppm level for aqueous standard and sampling rates of 10 samples an hour could be attained.

For the standards that were preconcentrated, Figure 3.26, the calibration curve presents a correlation coefficient 0.998, y-intercept 2.21×10^{-2}; slope, 1.688 with a precision of 6% RSD at the 0.0447ppm level for aqueous standards. The sampling rate was greatly reduced due the preconcentration step.

The limit of detection (LOD) were calculated from the calibration graph following Miller and Miller[117]. The determination without preconcentration gave a detection limit of 0.0397ppm and that after preconcentration, which allows the use of more diluted standards, the detection limit improved to 0.0042ppm .

The preconcentrated samples gave fairly reproducible results once the membrane environment had stabilised, but the between experiment reproducibility was very poor. Therefore standard must be included in each run.

The standards that were passed through the membrane had to be diluted 10 times before being pumped through the membrane, otherwise the 10 fold concentrated standards tended to react with all the available colour forming reagent (PCV) and gave similar signals. A high molar excess of PCV over aluminium is desirable, not only to minimise interference from anions which form complexes with aluminium[100], but also to allow the signal to reflect, and depend on the amount of aluminium present.

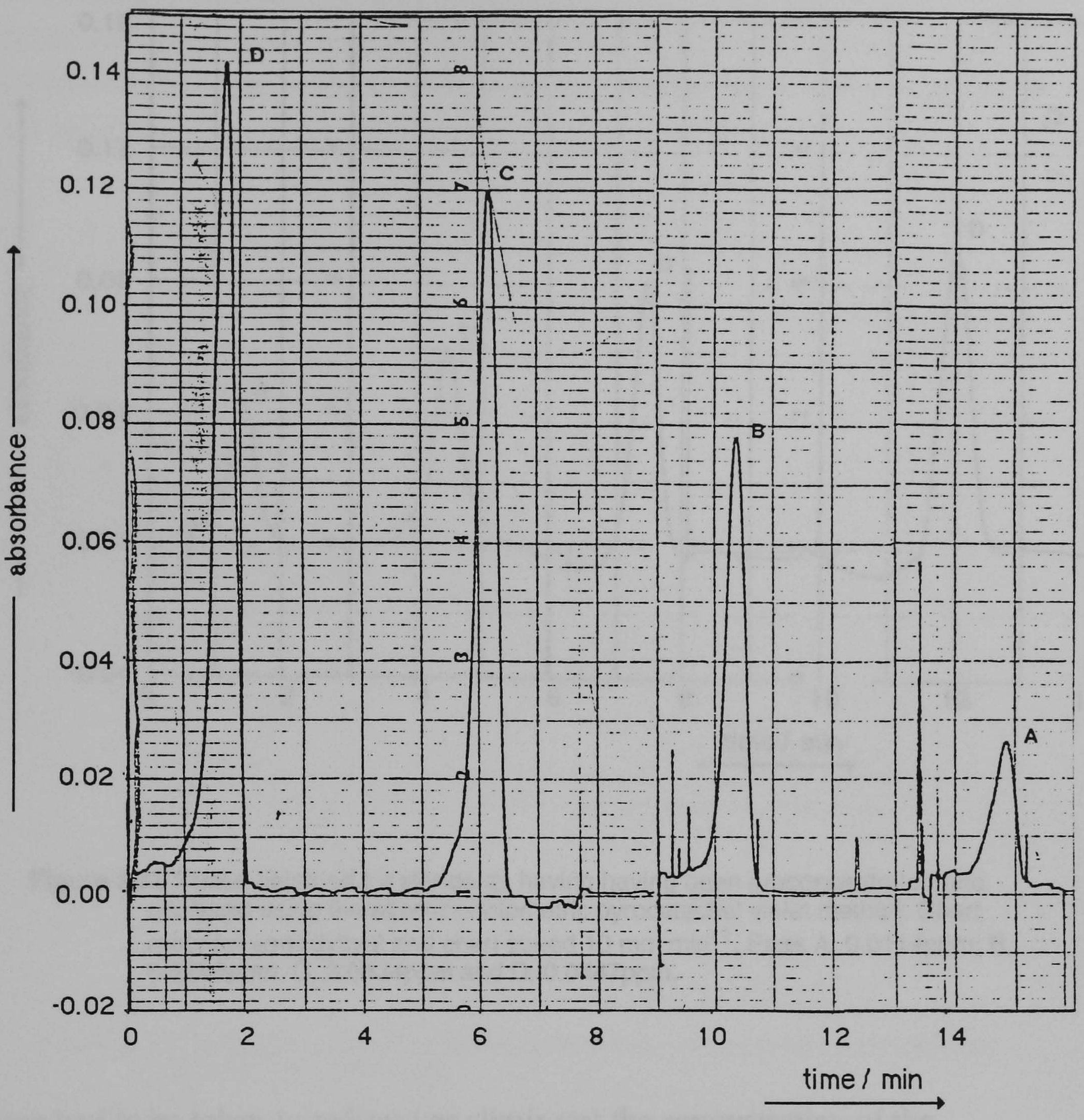

Figure 3.25 Peaks obtained for aluminium standards using the pyrocatechol violet spectrophotometric method. Chart recorder sensitivity, 1; chart speed, 10 mm min^{-1}. Peak A, 0.114ppm; B, 0.226 ppm; C. 0.334ppm and D, 0.447 ppm.

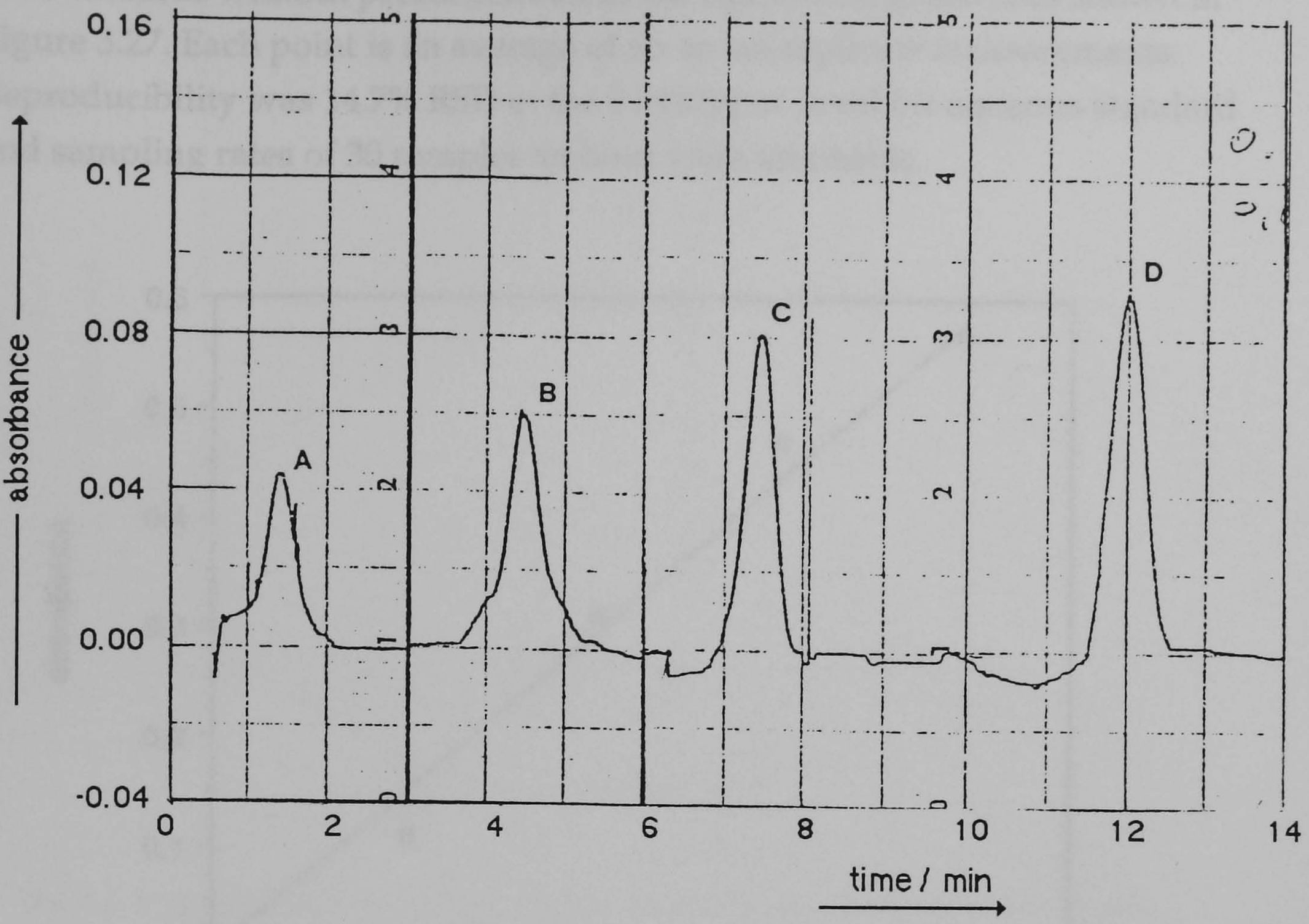

Figure 3.26 Peaks obtained for standards having having been preconcentrated and analysed using the spectrophotometric pyrocatechol violet method. Chart recorder sensitivity,2 and chart speed 10 mm min^{-1}. Peak A, 0.0114ppm; B, 0.0226ppm; C, 0.0334ppm and D, 0.0447ppm.

Care had to be taken to reduce (or eliminate) the concentration of the hydrochloric acid in the preparation of the standards to be preconcentrated, since on passing these through the membrane, the acid was also concentrated tending to off-set the effect of the hexamine buffer. Reaction of the aluminium and the pyrocatechol violet was thus reduced resulting in reverse peaks. When the standards were prepared in distilled water, normal peaks were obtained, since well controlled pH conditions were achieved, so that the concentration profile formed in the continuous flow system became the governing factor of the response curve.

In conjunction with the electrothermal atomiser, the membrane unit was employed off-line and in this case increased the detection limit from 0.0158ppm (without preconcentration) to 0.00303ppm (with preconcentration).

For standards without preconcentration the calibration graph is as shown in Figure 3.27. Each point is an average of six to ten replicate measurements. Reproducibility was 14.7% RSD at the 0.0447ppm level for aqueous standard and sampling rates of 30 samples an hour were attainable.

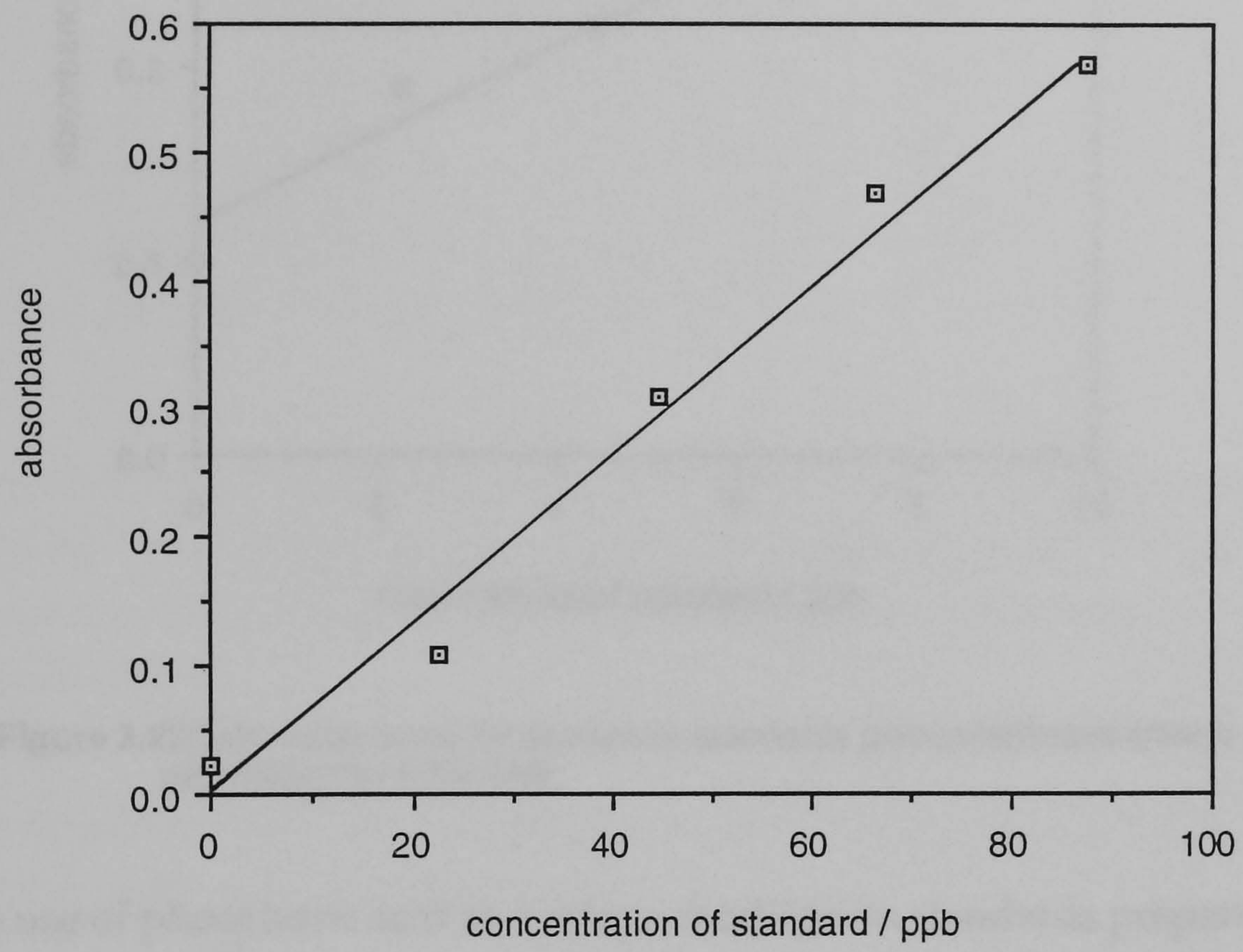

Figure 3. 27 Calibration curve for aluminium standards without preconcentration and determined by ETA-AAS.

For standards with preconcentration, the calibration curve is shown in figure 3.28. The reproducibility in this case was 29.4% RSD at the 0.00447 ppm level for aqueous standards. The sampling rate was similar to that for non-preconcentrated standards once the preconcentration step had been undertaken.

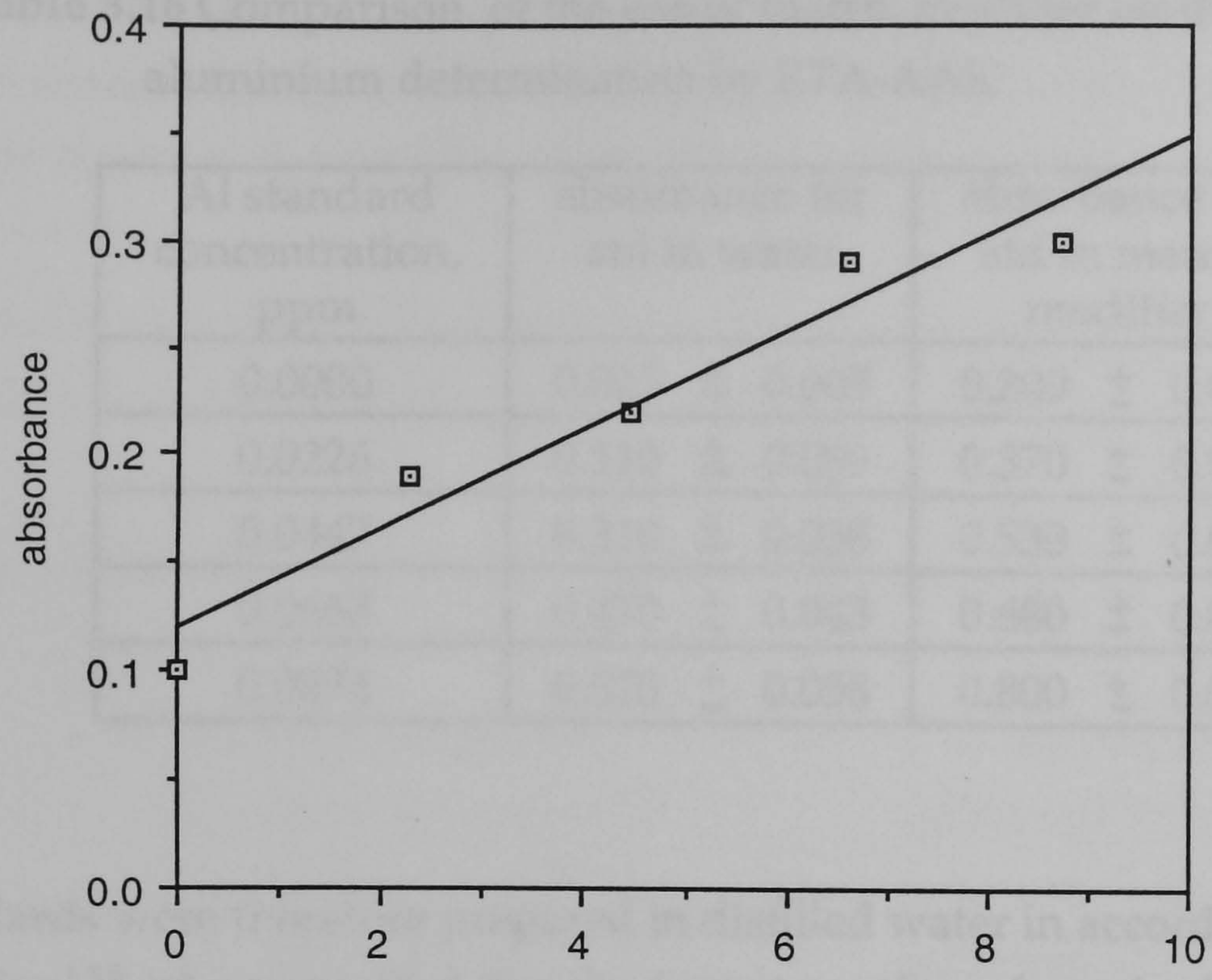

Figure 3.28 Calibration curve for aluminium standards preconcentrated off-line and determined by ETA-AAS.

The use of phosphoric acid as a matrix modifier on standards prepared in 0.01 M nitric acid [105] was attempted. The absorbances obtained when the modifier was used are compared with those without modifier, Table 3.16.

The micro molar concentrations of phosphoric acid added improved significantly the trace level aluminium determinations as Craney *et al* [105] pointed out, giving a limit of detection of 0.0059 ppm for straight aluminium standards and a correlation coefficient of 0.999. The detection limit is better than for standards prepared in deionised water. However the reagents introduced a high background absorbance reading, since even the Aristar grade reagents had about 0.05 ppm of aluminium in them.

Table 3.16 Comparison of the use of matrix modifier on the signal in aluminium determination by ETA-AAS.

Al standard concentration, ppm	absorbance for std in water	absorbance for std in matrix modifier
0.0000	0.023 ± 0.005	0.200 ± 0.057
0.0226	0.110 ± 0.059	0.370 ± 0.088
0.0447	0.310 ± 0.038	0.530 ± 0.076
0.0663	0.470 ± 0.043	0.680 ± 0.061
0.0874	0.570 ± 0.058	0.800 ± 0.094

Standards were therefore prepared in distilled water in accordance to Sperling[118] who suggested that the fewest number of manipulations and chemical additions are desirable when dealing with trace levels of determinations.

The membrane unit was incorporated in the simplified speciation scheme and the water sample was analysed.

The total aluminium content was determined using ETA-AAS, with no sample pre-treatment other than diluting 10 times to bring the absorbances within the range of the standards. The sample gave a mean absorbance of 0.40 for six measurement. The concentration of aluminium (A) was found to be 0.59 ppm.

The concentration of the total monomeric fraction was estimated by the pyrocatechol violet-flow injection method. The mean absorbance for for five sample injections was 0.096 and the concentration (B) was found to be 0.28 ppm.

By difference the total polymeric fraction (C) was calculated to be 0.31ppm.

The non-labile fraction (E) was determined by removing the free Al^{3+} of the monomeric fraction using Amberlite resin (cation desalting). This fraction

was below the detection limit of the pyrocatechol violet method (0.0398ppm) and preconcentrating it helped bring it to detectable levels. The fraction sample absorbance was 0.046, equivalent to a concentration of 0.027ppm.

The labile Al^{3+} (D) can then be obtained by subtracting (E) from (B), giving a concentration of 0.25ppm.

The results for the water sample can be summarised as:

A - total aluminium :	0.59 ± 0.049ppm
B - total monomeric Al:	0.28 ± 0.0025ppm
C - total polymeric Al :	0.31ppm
D - labile free Al^{3+} :	0.25ppm
E - non-labile monomeric Al :	0.027ppm

The pH of the water sample (pH 4) falls within the pH range where both monomeric and polymeric aluminium complexes are present. The results of the speciation are in agreement with this fact. Furthermore, the monomeric fraction consists mainly of the labile free Al^{3+} since the pH is on the lower end of the range. This labile free Al^{3+} accounts for the toxicity of aluminium since the toxicity of a metal ion is related to the aqua ion concentration as proposed by the so called " free metal ion " hypothesis [119,120]. It should also be noted that the distribution of metal species varies from sample to sample[121], being very much pH dependent.

3.5 Conclusion

A qualitative model to characterise a PTFE membrane as a preconcentrator device has been developed which describes vapour losses through the membrane under a variety of operating conditions. The model shows that the rate of loss is governed by the difference in water vapour pressure inside and the surrounding atmosphere, the surface resistance of the membrane to diffusive transport and the thickness of the boundary layer attached to the membrane surface. Estimation of the magnitude of these resistances is necessary for quantitative prediction of operating conditions and this will be the subject of future work.

The PTFE membrane has been successfully applied as preconcentration device for the determination and speciation of aluminium in natural water samples. It has high potential as a universal preconcentrator, increasing the levels of all elements in the sample on passing through it without chemical modification.

Adaptation of the preconcentration devices to FIA systems was aimed at producing a rugged, reproducible, rapid and sensitive device, whose main application would be for the determination of trace levels of elements in water. The reported method met with all the above aims except speed. The preconcentration step slowed down the whole analytical procedure and significantly lowered the rate of sample throughput. Investigations need to be undertaken to improve the throughput of the technique before it could be used for routine work.

A close examination of the use of the membrane indicated that results obtained using it can be affected by interferences because all the sample constituents are concentrated. This was exemplified by the preconcentration of hydrochloric acid, which caused the reagents in the spectrophotometric method to react only partially on passing through the membrane.

Therefore, it could be suggested that the membrane unit could only be used as a preconcentrator device for samples containing low levels of salts (potable waters). The use of the membrane unit could avoid contamination at very low levels that might occur during evaporation in open vessels.

In general, it can be concluded that the membrane preconcentration device enhances the detection limits and has potential as a tool in the speciation of aluminium. , However, it is difficult to use on a routine basis because it takes a long time to stabilise and has poor reproducibility between experiments.

CHAPTER FOUR
A MICROPOROUS MEMBRANE DEVICE FOR GENERATING ANALYTES IN GASEOUS FORM

In GD-FIA systems the gas diffusing through the membrane is usually transferred into a liquid acceptor stream. In cases where a gaseous acceptor stream is used, the method is called Dual Phase Gas Diffusion Flow Injection Analysis (DPGD-FIA)[20]. Most applications of this method is relate to its use in analytical methods utilising hydride generation followed by atomic spectroscopy. In the present investigation, a DPGD-FIA manifold was developed to generate and separate gaseous samples for analysis by mass spectrometry. The direct interfacing of a GD-FIA system to a mass spectrometer presents several advantages. The low detection limit of the mass spectrometer coupled to FIA provides a system capable of detecting very small amounts of volatile analytes and it would also be expected that the precision in any quantitative mass spectral analysis would be higher than in other common analytical inlet systems for mass spectrometers.

The GD-FIA-MS technique developed here was used for the determination of total nitrogen and $^{15}N/^{14}N$ isotopic ratios in agricultural samples. The versatility of the method has also been demonstrated for other nitrogen species determination such as, nitrite and nitrate.

4.1 Determination of nitrogen

The determination of nitrogen content in biological and agricultural samples is common both in research and on a routine basis. For example, nitrogen is important in crop production and the fate of fertiliser nitrogen applied to soils is often studied. Nitrogen does not have a radioactive isotope of sufficiently long half life for radioactive tracer experiments, therefore the stable isotope ^{15}N is used, and the $^{15}N/^{14}N$ ratio is normally determined by mass or emission spectrometry, the nitrogen gas is generated from the sample via a Kjeldahl-Rittenberg method, a Dumas combustion or a combination of the two. Today routine analysis of biological and agricultural samples are based on the modified Dumas combustion technique, known as automated nitrogen carbon analysis mass-spectrometry - ANCA-MS. It involves converting the

nitrogen in the samples into N_2 gas by catalytic combustion, through a furnace containing chromium oxide and silvered cobalt oxide. The nitrogen oxides, water and carbon dioxide produced, pass through to a reduction column (copper filings) where the oxides of nitrogen are reduced to N_2 gas, then through traps to remove H_2O and CO_2 and a GC column to remove any interfering trace impurities. The resultant N_2 gas is then swept into the mass spectrometer. The disadvantage of this technique is that both the combustion and reduction columns need replacing regularly, which involves shutting down the system to replace the packing which is inconvenient and undesirable.

The FIA technique has much to offer in improving the efficiency and in the automation of various separation and preconcentration processes, and it can be used either for direct introduction of an analyte to a mass spectrometer or to convert the analyte to a suitable form for detection.

4.1.1 Determination of total nitrogen

The determination of total nitrogen in a complex sample involves three steps: a - definition of the term "total nitrogen", b - conversion of all nitrogen included in this definition to a single measurable form and c - measurement. Usually certain forms of nitrogen, such as nitrate, cyanide, are excluded from the estimate of "total nitrogen"[122].

In general, the different forms of nitrogen present are converted to ammonia or nitrogen gas which is extracted from the matrix prior to determination.

4.1.1.1 Convertion of total nitrogen to ammonia

Ammonia is an easily measurable and easily extracted form of nitrogen compound. It can be extracted by distillation and its determination does not require elaborate apparatus being carried out by a large variety of methods such as titrimetry, spectrophotometry, potentiometry, etc. Combined nitrogen can be converted into ammonia by a number of methods such as Kjeldahl, Ter Meulen or caustic fusion.

Kjeldahl method - It is the most popular method used. The majority of nitrogen-containing compounds are amenable to this method, but ring structures such as pyrazolones, diazines and triazoles are not easily converted into ammonia.

In this procedure, the organic and inorganic nitrogen present in the sample are oxidised by digestion in sulphuric acid, in the presence of a catalyst (selenium, mercury(II) oxide or copper sulphate). Carbon and hydrogen are expelled as carbon dioxide and water whereas the convertible nitrogen present (aminoid nitrogen) is converted and retained in the digest as ammonia. Several procedures used for the quantitative determination of nonaminoid nitrogen (N-N; N=N; N-O; NO_2^- and NO_3^-) have been published[122]. Once the conversion is complete, the digest is made alkaline and ammonia is steam-distilled into a standard acid solution for determination.

Although this digestion method has been used for about 90 years, there is still no universally accepted digestion method; i.e. the best compromise seems to be to adapt the digestion technique to the nature of the sample material.

The Ter Meulen Method - In this procedure, the organic nitrogen present in the sample is combusted in a hydrogen atmosphere and all nitrogen is converted to ammonia over a nickel-magnesium catalyst at 320 ° C. The ammonia produced is absorbed in a standard acid solution as for the Kjeldahl method.

Although this method can be applied to all organic compounds, it has not received much attention because the catalyst is easily poisoned by sulphur or halogens. The use of calcium oxide to absorb hydrogen sulphide and halogen acids can improve the lifetime of the catalyst. This method is reported to be more sensitive than the Kjeldahl method[123].

Caustic fusion method - This method can be applicable to both aminoid and nonaminoid nitrogen. It involves fusion of the matrix with caustic

compounds such as sodium carbonate, sodium or potassium hydroxide. This method has received little attention recently.

4.1.1.2 Conversion of total nitrogen to molecular nitrogen

The Dumas method is the most widely used and involves the pyrolysis of the sample with copper oxide in an atmosphere of carbon dioxide which is passed through a strong potassium hydroxide solution. Ideally, all the elements present are converted to forms which either react with copper oxide or are very soluble in potassium hydroxide solution, except nitrogen which can be collected. Although this method is reported to work very well with inorganic and simple organic samples, complex samples such as biological materials can give lower recovery due to incomplete combustion[124, 125].

Several modifications has been proposed to improve the efficiency of the method [126, 127, 128,128]. Simultaneous determination of carbon, hydrogen and nitrogen can be made by combustion of the sample in a helium atmosphere with silver oxide-manganese oxide as the oxygen supplier. Heated copper then reduces nitrogen oxides and removes the excess of oxygen.

In the classical Kjeldahl method, ammonia is extracted from the digest and collected in a standard acid solution (hydrochloric or boric acid) and back titrated with standard alkaline solution. Among the spectrophotometric methods, the Nessler, indophenol and byspyrazolone methods are the most used. The use of an ammonium selective electrode enables the determination of ammonia concentration by potentiometry.

Recently, efforts have been made to automate this determination using flow injection and separation of the ammonia by gas diffusion through a PTFE membrane followed by conductometric[43], spectrophotometric or potentiometric detection [61], isothermal distillation or spectrophotometric determination[130, 131, 132].

When the total nitrogen is converted to nitrogen gas, it is usually determined by physical means such as gas chromatography or emission spectrometry.

4.1.2 Nitrogen-15 - analytical importance and methods of determination .

The use of tracer methods to investigate chemical, physical or biological processes in agricultural, biological and medical research, is widespread. As a basic prerequisite of this method, the tracer should behave in the same manner as does the original element, but its different isotopic composition makes it possible to identify the element at any stage of the process. Quantitative evaluation is based on the isotope dilution law. According this law, in a system in equilibrium, the ratio of tracer to carrier isotope is constant. Obviously, isotope effects and exchange reactions which would reduce the specific activity of the compound must be absent.

In the majority of cases, a radioactive isotope is used as the tracer which facilitates its determination using radiochemical techniques. Usually the determination of the carrier (inactive) element is also necessary and the ratio of radioactive to the inactive element is referred to as the specific activity.

Nitrogen does not have a radioactive isotope of sufficiently long half-life (as can be seen in Table 4.1) to enable radioactive tracer experiments of reasonable duration. So, any practical experiment which needs a nitrogen tracer should use a stable isotope.

The ^{15}N isotope matches all the conditions necessary to be used as tracer, i.e.; it does not easily exchange with nitrogenous compounds, all of its compounds can be produced and stored under normal conditions; many of its organic compounds can be produced directly from a few inorganic compounds. Several publications deal with its use for these purposes[133, 134, 135].

Table 4.1 Nitrogen nuclides.

nuclide	% abundance	nuclide mass	half life, s
^{12}N		12.01871	0.011
^{13}N		13.005739	600
^{14}N	99.634	14.0030744	
^{15}N	0.3663	15.000108	
^{16}N		16.00609	7.38
^{17}N		17.00845	4.14

In agronomic research, for example, ^{15}N is used as tracer in laboratory, greenhouse and field experiments. It is used to study the fate of fertiliser nitrogen applied to soil, transformations and movement of soil and fertiliser nitrogen , biological nitrogen fixation, uptake and utilisation of this element by crops and metabolism in plants.

In nature, nitrogen is a mixture of two stable isotopes; ^{14}N and ^{15}N. The concentration of ^{15}N is usually expressed as the abundance (atom%) as given in Eq. 4.1

$$\text{Atom\% } ^{15}\text{N} = \frac{\text{nº of } ^{15}\text{N atoms}}{\text{total nº of N atoms}} \times 100 \qquad \text{(eq.4.1)}$$

The natural abundance of the ^{15}N isotope in atmospheric nitrogen is (0.3663 + 0.0004) atom% [136]. Because of naturally occurring isotopic effects, not all nitrogen-containing compounds have the same value; some are enriched and some depleted by + 1.5%.

The ^{15}N % enrichment of a sample represents the % ^{15}N above the natural abundance as given in Eq. 4.2.

$$\%\ ^{15}\text{N excess (enrichment)} = \%\ ^{15}\text{N abundance} - 0.3663 \qquad \text{(eq.4.2)}$$

Small variations in ^{15}N abundance e.g. variation in the ^{15}N content of naturally occurring sample components, are often measured in terms of parts per thousand differences ($\partial\ ^{15}N$) from a reference gas, usually atmospheric N_2

$$\partial\ ^{15}N = \frac{R_{sample} - R_{reference}}{R_{reference}} \times 1000 \quad \text{(eq.4.3)}$$

where

R = ^{15}N / ^{14}N (number of atoms ratio)

with this system, one $\partial\ ^{15}N$ "unit" is equivalent to 3.7×10^{-4} atom% ^{15}N. Some authors [137, 138] use a slightly different definition of $\partial\ ^{15}N$ in that they use ^{15}N concentrations in their calculation rather than R. Close to natural abundance, the difference in $\partial\ ^{15}N$ values calculated using the two procedures is very small. Equation 4.3 can be written in the.

$$\partial^{15}N = \frac{(^{14}N\,^{15}N + 2\,^{15}N) \times 100}{2\,^{14}N_2 + 2\,^{14}N\,^{15}N + 2\,^{15}N_2} \quad \text{(eq. 4.4)}$$

Generally two kind of analytical techniques are used in order to determine the concentration of nitrogen-15 or the ^{15}N /^{14}N ratio present in the sample; mass spectrometry or emission spectroscopy. For both methods, the organically and inorganically bounded nitrogen present in the sample must be converted to nitrogen gas as both instruments exploit a physical property of the nitrogen molecule, N_2, to determine the relative amounts of each of the three possible species, $^{14}N_2$, $^{14}N^{15}N$ and $^{15}N_2$. In optical emission spectrometry, N_2 molecules are separated on the basis of their vibrational properties, whereas in mass spectrometry, charged ions are separated according to their mass charge (m/e) ratio.

Nitrogen gas is preferred because it is easier to generate from different compounds, it is easier separated form the samples matrix, it is almost inert

with respect to all the materials used and the interpretation of the isotopic data is simple as there are no interferences from others elements.

The ^{14}N and ^{15}N atoms in the nitrogen gas are paired to form nitrogen molecules $^{14}N_2$, $^{14}N^{15}N$ or $^{15}N_2$, but both methods provide output signals which are proportional to the number of the three types of molecules present in the gas.

Mass spectrometry is the preferred method since emission spectroscopy suffers lack of precision.

4.1.2.1 Mass Spectrometry

A mass spectrometer designed for gas analyses essentially comprises 5 units (Figure4.1): (1) an inlet system responsible for accepting the sample and converting it to a gas; (2) an ion source where the nitrogen molecules, bombarded with electrons, become charged and accelerated; (3) a mass analyser to separate the gaseous ions according to m/e. A magnetic analyser is normally used in nitrogen determinations in which the charged molecules are separated into different paths according to their momentum; (4) a collector placed at the end of the flight tube where the molecules are discharged, and the discharge currents are amplified; and (5) a recorder which registers the amplified discharged currents as peaks as the mass range is scanned. The heights of the peaks are proportional to the concentrations of the three atomic species in the gas mixture. By simply measuring the peak heights, the ^{15}N % abundance can be determined.

Although the principle is simple, the practice of mass spectrometry is complicated. The whole system must be maintained under high vacuum. Vacuum techniques are an integral part of the preparation of samples and are also involved in the operation of the spectrometer. The electric and electronic components must be highly stabilised.

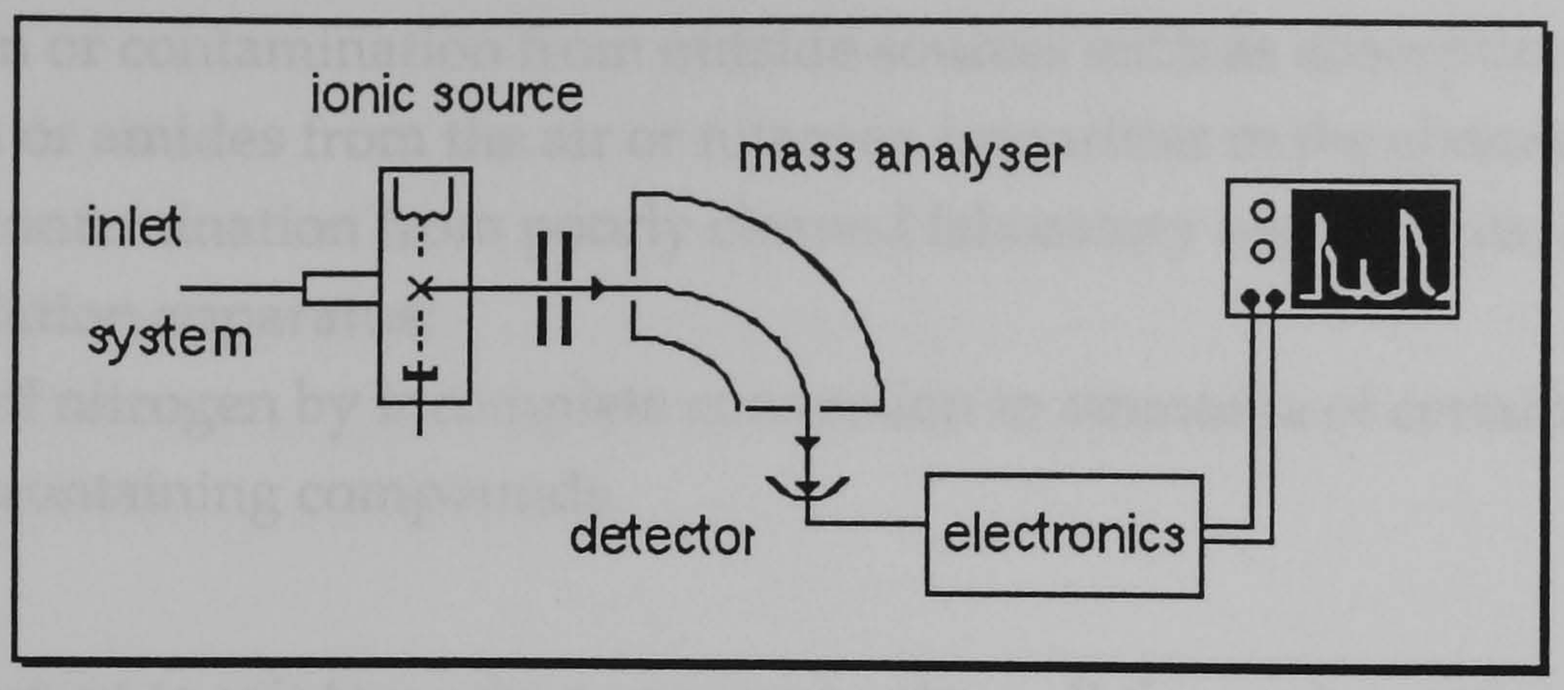

Figure 4.1 Diagram of a mass spectrometer. the arrows indicate the direction in which the sample passes through the instrument.

4.1.2.2 Sample preparation

The method for the conversion of nitrogen compounds to nitrogen gas should be applicable to all kind of compounds, should be simple, fast and with minimal possibility of cross-contamination, with would alter the ^{15}N abundance in the sample.

Several procedures can be found in the literature for this step but most of them are based on the Kjeldahl or Dumas method.

One of the most used methods is the Kjeldahl-Rittenberg[139]. This method uses the Kjeldahl method to convert nitrogen to ammonia followed by oxidation of the ammonia to nitrogen gas by alkaline hypobromite. It involves the following steps:

a) digestion of the sample with concentrated sulphuric acid in the presence of a catalyst;

b) separation of the ammonia by steam distillation after addition of alkali;

c) determination of the ammonia by back titration or colorimetrically;

d) acidification;

d) evaporation to a small volume;

e) oxidation of the ammonia to nitrogen gas by using hypobromite;

f) determination of the nitrogen content.

Some interferences have been reported for the $^{15}N/^{14}N$ ratio determination associated with the Kjeldahl digestion/distillation steps:

a) dilution or contamination from outside sources such as absorption of ammonia or amides from the air or nitrogen impurities in the chemicals ;
b) cross-contamination from poorly cleaned laboratory equipments, specially the distillation apparatus;
c) losses of nitrogen by incomplete conversion to ammonia of certain resistant nitrogen-containing compounds.

It is important to reinforce the necessity to clean all the equipments with detergents and acids prior the use to avoid cross contamination. Distillation of 10-20 ml of ethanol between samples is also reported to be efficient to prevent this kind of contamination [140].

Ammonia is oxidised in alkaline conditions in an evacuated container to nitrogen gas by means of sodium hypobromite solution (Rittenberg reaction)[141], according to the reaction:

$$2\,NH_3 + 3\,OBr^- = N_2 + 3\,H_20 + 3\,Br^-$$

Usually this step is carried out in special Rittenberg vessels.

Special care must to be taken to avoid air leak in the Rittenberg vessel, leak in the vacuum line or cross contamination from the vessels. In addition, hypobromite is a rather unstable compound and the reagent should be kept in a strong alkaline medium, stored in a refrigerator and used within a week after prepared[139].

The Dumas method, its advantages and disadvantages were previously described.

As the final step, the amount of nitrogen gas produced or the $^{15}N/^{14}N$ ratio is determined by mass spectrometry or emission spectrometry.

Although the principles of gas preparation are identical for both analytical techniques, the amount of sample required is different; mass spectrometry

requires 30 μg - 3 mg of nitrogen whereas emission spectroscopy requires only 0.2 - 10 μg.

Additional care must be taken to avoid the dilution of the ^{15}N in the sample with atmospheric nitrogen (better done in vacuum) or dilution with nitrogen present in the chemical reagents used.

An excellent review focusing the practical aspects of the two methods has been published[141].

Although ^{15}N has been used as tracer, its routine use has been restricted. The reason is that the conventional methods are slow and require tedious extensive labour. Biological variability results in additional problems since using high precision instrumentation is not as important as the ability to run a large number of samples with adequate precision in order to make biological experiments more meaningful.

As a consequence, automatic analysers have been developed. An automatic analyser for nitrogen isotope-ratio determinations using the Rittenberg technique has been reported[142]. The proposed equipment is computer controlled and uses a lithium hypobromide solution kept in a refrigerated vessel to oxidise ammonia to nitrogen gas prior to injection into the mass spectrometer. Air is removed by purging with Freon and the nitrogen liberated was allowed to flow through a liquid nitrogen trap for removal of Freon before the introduction into the mass spectrometer.

Modern designs of nitrogen analysers, which are essentially a GC operated on the basis of the Dumas method, using helium as carrier offer some advantages. A continuous-flow isotopic ratio mass spectrometer (IRMS) which involves sample preparation integrated with a mass spectrometry is now available and it is known as Automated Nitrogen Carbon Analysis-Mass Specttrometry (ANCA-MS)[143, 144].

The main disadvantage of this system is that both the combustion and reduction columns need replacing regularly, which involves shutting down the system to replace the packing which is inconvenient and undesirable.

One possibility of overcoming these problems is the use of flow injection analysis (FIA) coupled with a semi-permeable membrane as a means of producing gas samples for the determination of total nitrogen or for using isotope ratio mass spectrometry.

4.2 Determination of nitrogen contents in agricultural samples after Kjeldahl digestion by oxidation with hypobromite by DPGD-FIA system.

Nitrogen gas can be produced by oxidation of ammonia in alkaline conditions by hypobromite according to the reaction:

$$3BrO^- + 2NH_3 = N_2 + 3Br^- + 3H_2O$$

This reaction was first used as a basis for quantitative ammonia determination (volumetric) of inorganic and nitrogenous organic materials, after a Kjeldahl digestion, but it is reported to be slow so that a direct titration is not practical. Excess of reagent is added and back titrated either by iodometry or by means of naphthyl red which is decolorized by hypobromite in a directly proportional manner [145]. As direct titration is not possible, other methods for quantitative determination of the evolved nitrogen were proposed, such as manometric measurement.

For accurate results, the alkalinity has to be properly adjusted (from pH 7.5 to 9.5), the hypobromite solution must be freshly prepared, the temperature should not rise above 18° C and exposure to sunlight should be avoided[122]. The sodium hypobromite solution should therefore be stored in amber bottles at low temperatures. According to the same source, errors arise from the instability of the reagents, the rates at which the residual nitrogen reacts and possibly to the presence of unsuspected catalyst.

Solutions containing hypobromite of the alkali metals can be prepared by two different ways: (a) dissolving bromine in aqueous solution of the appropriate base or (b) adding an excess of bromide to a sample of hypochlorite at the pH range 9-14, according to:

(a) $Br_2 + 2OH^- \text{----------} Br^- + BrO^- + H_2O$

(b) $Br^- + ClO^- \text{----------} BrO^- + Cl^-$

The reaction (a) is rapid and must be carried out at or below 0°C in order to minimise the disproportionation of hypobromite ions into bromide and bromate. This disproportionation is catalysed by traces of copper(II) ions[146].

The reaction (b) is a second order reaction and proportional to the concentrations of bromide and hypochlorite. In general, bromide-free hypobromite solutions can be prepared by reacting equivalent amounts of bromide and hypochloride at pH 9 - 9.5 at room temperature. After 5 minutes, sodium hydroxide is added to bring the pH to 13 at which the formation of bromide and bromate is low. The reaction rate is also dependent on the pH and at pH lower than 10 the oxidation of bromide is very rapid. At pH values 7 - 9, the formation of hypobromite is extremely rapid, but if hypochlorite is in excess other reactions can take place producing chlorate, bromate and chloride.

The composition of these solutions as well as their oxidising capacity at different pH can be seen in the Figures 4.2 and 4.3 [147]. Figure 4.2 shows the composition of hypobromide solution at several pHs and at $[Br^-]$ equal to 10^{-3} M. It can be seen that at low pHs (pH<4.0) the main components are bromine and tribromide ions and in at this region the oxidising capacity is due mainly to the presence of bromine. At the pH range between 5.5 and 8.5 the most important oxidising agent present is hypobromous acid and at pH > 8.5 hypobromite is the main oxidising species present. In Figure 4.3 the composition of hypobromite and hypochlorite solutions at pH range 0 - 14 and halide $[X^-]$ concentration equal to 0.01 M is shown.

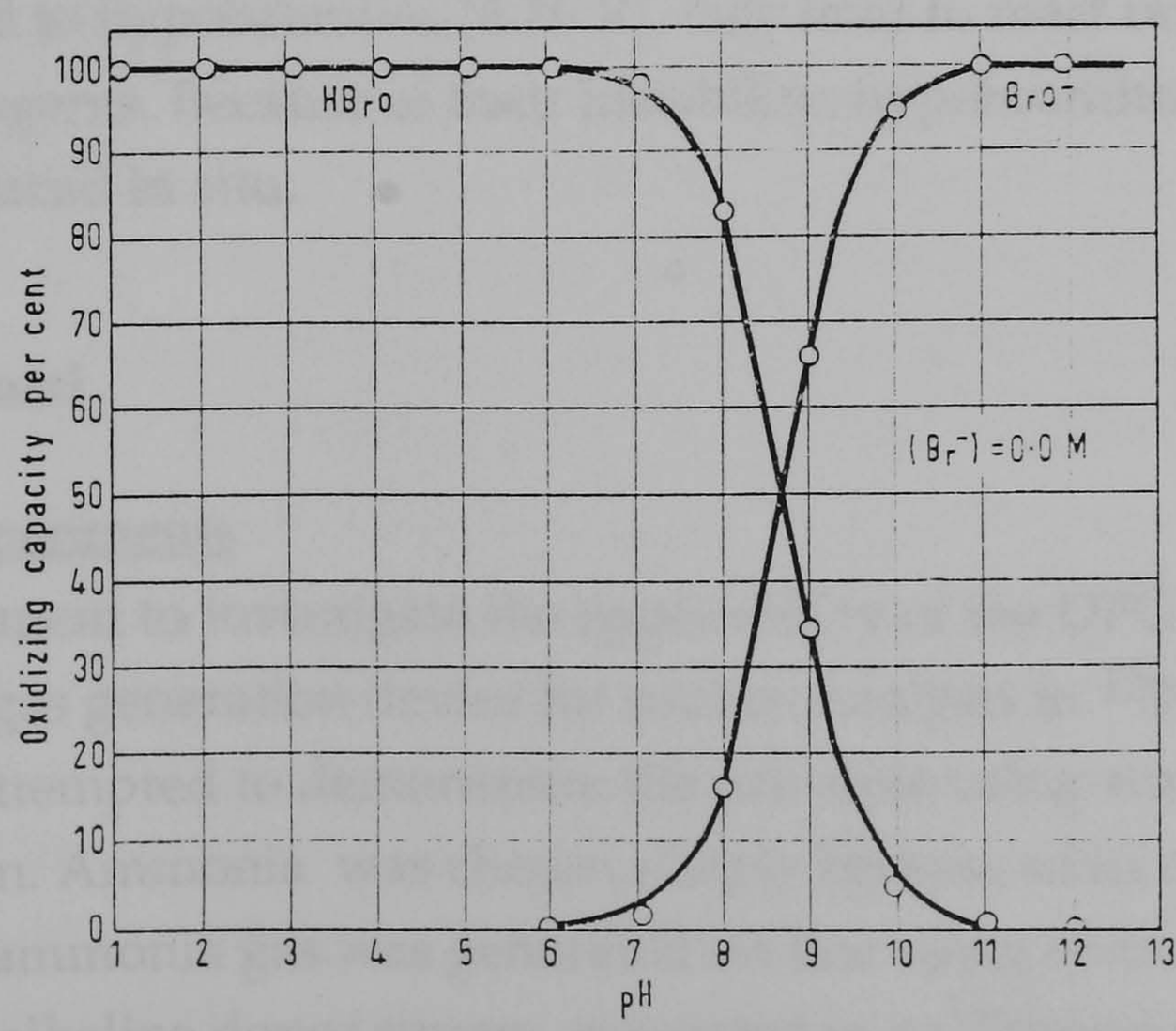

Figure 4.2 The composition of hypobromite solutions at pH 0-14 and $[Br^-]$ = 0.0 M (ref.146).

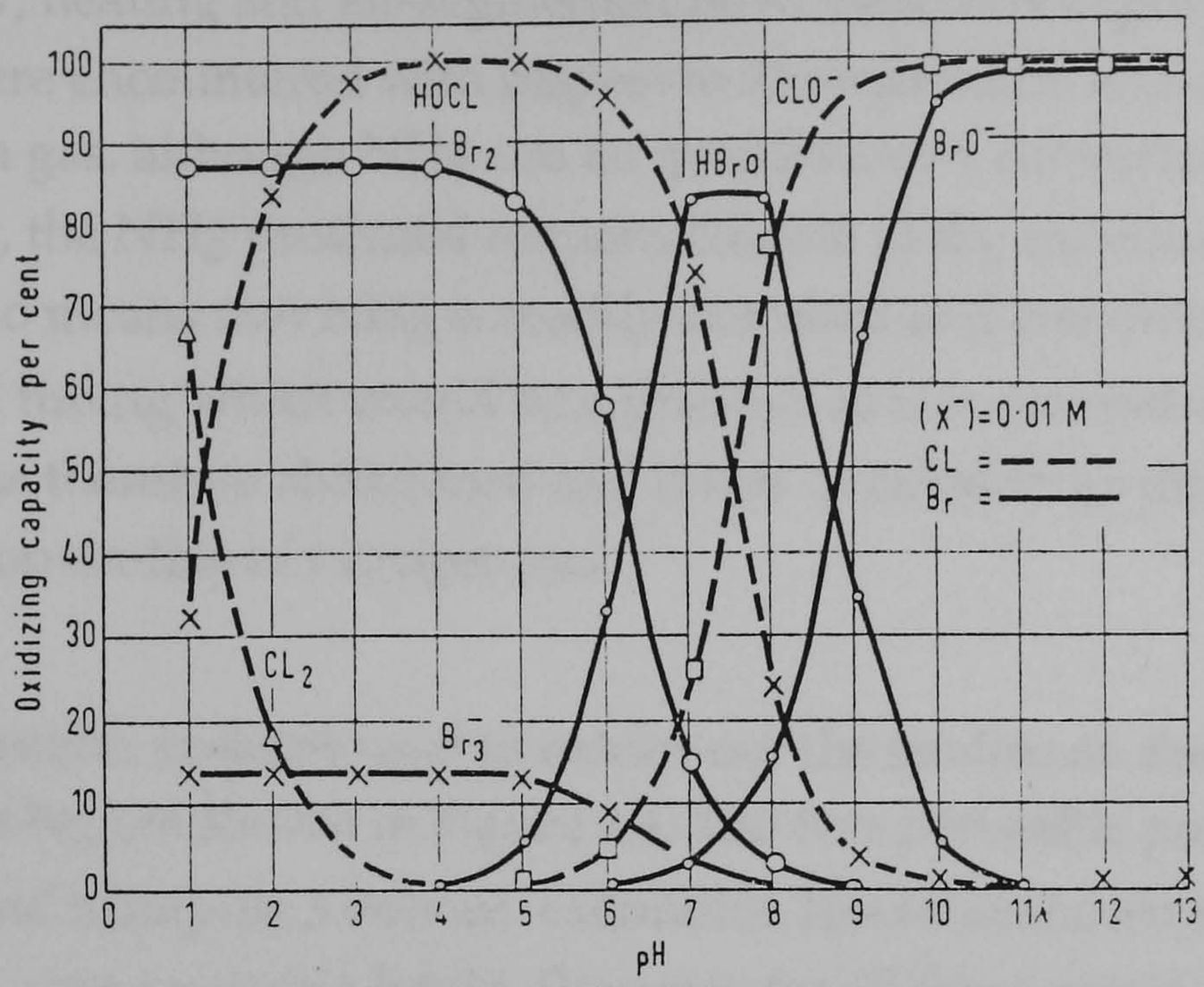

Figure 4.3 The composition of hypobromite and of hypochlorite solutions at pH 0-14 and $[X^-] = 0.01$ M (ref. 146).

It can be seen that the hypochlorous acid has its maximum concentration at pH 4-5 as compared to pH 7 - 8 for the hypobromous acid. As expected, the range of predominance of hypobromite ions is located at higher pH values (pH > 10). Although hypochlorites possess higher standard potential (0.89 V) when compared to hypobromites (0.76 V), they tend to react rather slowly with reducing agents. Because of their instability, hypobromites should be invariably prepared in situ.

4.2.1 Experimental

Preliminary experiments

The first experiment to investigate the applicability of the DPGD-FIA technique as a gas generation device for routine analysis in ^{15}N mass spectrometry attempted to demonstrate the principle using ammonia gas instead nitrogen. Ammonia was chosen simply because of its ease of detection. The ammonia gas was generated on-line using sodium hydroxide solution as the alkaline donor stream, separated in a GD-separator unit to an acceptor gaseous stream, collected and then determined using an ammonia gas sensing electrode. The effects of increasing the length of membrane, using

stopped flow, heating and air-segmented flow, were investigated. Several problems were encountered with respect to the separation and collection of the ammonia gas. although NH_4 can be quantitatively converted to NH_3 gas above pH 10, the NH_3 produced remains soluble in the aqueous phase. This solubility also means that NH_3 is readily absorbed and lost onto the walls of the manifold tubing which would be a problem at low concentrations. This approach was therefore abandoned and it was decided to go directly to study the generation on-line of nitrogen gas.

The flow injection systems used to carrier out the studies on the direct generation of N_2 are shown in Figure 4.4. The two peristaltic pumps, Gilson Minipuls 2 and Minipuls 3 (whose calibration has been shown in Chapter 3) were used to give a suitable liquid flow rate for all three manifolds. The standards and sample solutions were injected using 6 port low pressure Teflon valve, Rheodyne model 5041, with a pneumatic actuator, Universal. The manifolds were made from 0.80mm Teflon tubing and different loop sizes were used.

The systems were coupled to a thermal conductivity detector, Pye Unicam-Model 34. It was operated at 200 mA bridge current and 20 and 50 ml/min for both reference and sample helium flow. An integrator, Spectra-Physics-SP4290 and a chart recorder, Linseis- L6512, were used to register the response from the detector.

Both sheet and a tubular membranes were used to separate the gas generated on-line. The characteristics of each membrane are shown in Table 4.2. When the sheet membrane was used it was pressed between two polypropylene plates, diameter 100mm, with two matching grooves machined out, 72mm long, 2mm wide and 0.5mm deep. The liquid stream was passed into one side of the groove flowing on to waste, and the gas generated in the reaction diffused freely through the microporous PTFE- membrane and was purged with helium gas directly to the sample flow line of the detector. The tubular membrane was inserted into a glass tube, bore 2.5 cm, with connections that allowed the liquid stream to run through the core of the tubing and the gas generated to pass into the carrier gas flowing around the membrane. Three way connectors , OMNIFIT model 1010, were used for the connections.

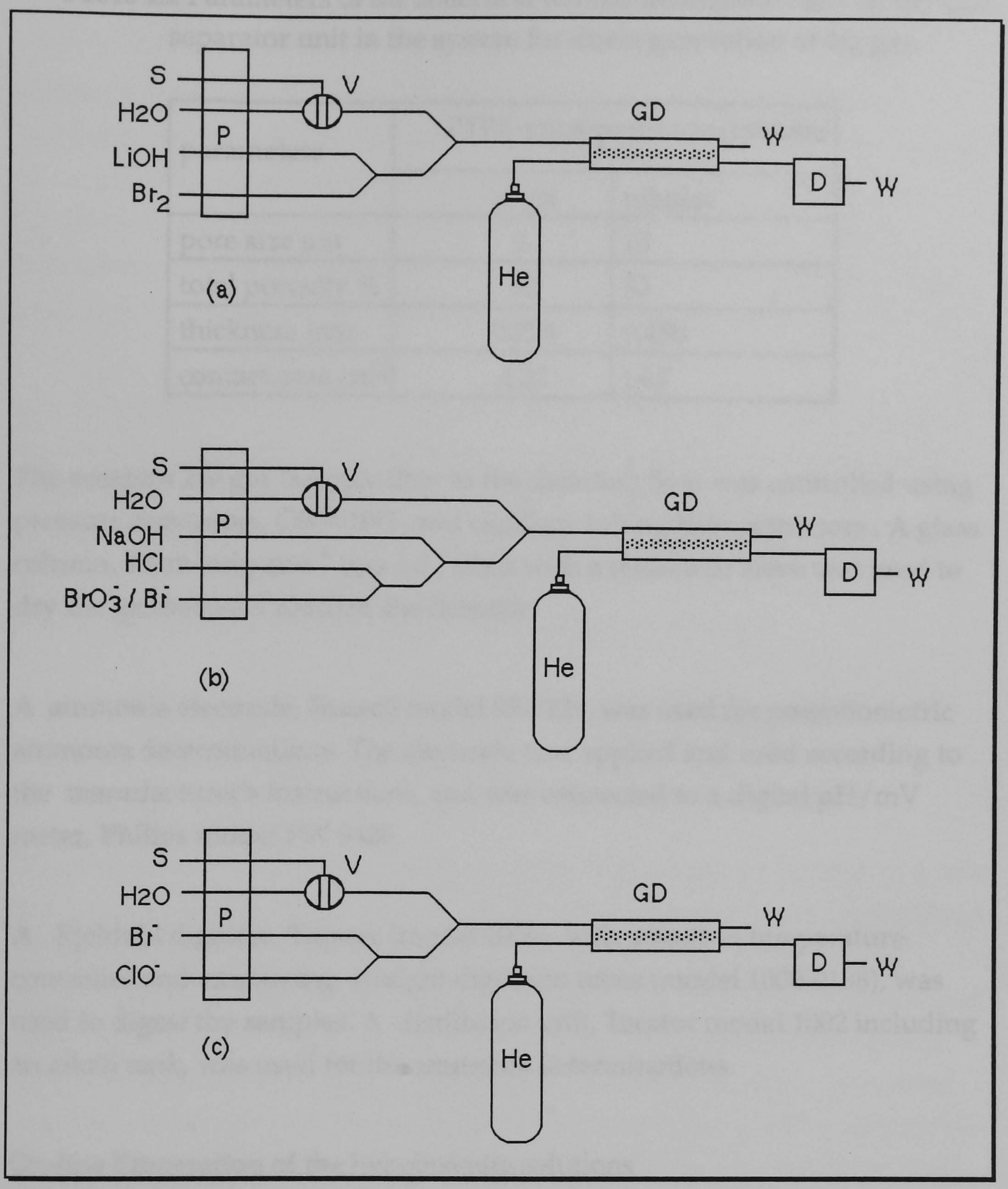

Figure 4.4 The three manifold used to produce hypobromite on-line before generating nitrogen gas. a)system used for hypobromite production by reacting bromine with lithium hydroxide. b)system used for hypobromite production on-line after producing bromine also on-line. c)system used for hypobromite production by reacting hypochlorite with bromide

Table 4.2 Parameters of the sheet and tubular membrane used on the GD-separator unit in the system for direct generation of N_2 gas.

parameters	PTFE-microporous membrane	
	sheet	tubular
pore size µm	1	10
total porosity %	50	50
thickness mm	0.275	0.450
contact area cm^2	4.37	14.7

The acceptor He gas (sample flow to the detector) flow was controlled using pressure regulators, OMNIFIT, and capillary tubing flow restrictors.. A glass column, 10cm long and 7 mm i.d., filled with a molecular sieve was used to dry the gas before it reached the detector.

A ammonia electrode, Russell model 95-5129, was used for potentiometric ammonia determinations. The electrode was applied and used according to the manufacturer's instructions, and was connected to a digital pH/mV meter, Philips model PW 9420.

A Kjeldahl digester, Tecator (model 1009), with a built-in temperature controller and employing straight digestion tubes (model 1000-0158), was used to digest the samples. A distillation unit, Tecator model 1002 including an alkali tank, was used for the ammonia determinations.

<u>On-line Preparation of the hypobromite solutions</u>

In order to avoid the problems caused by the instability of the hypobromite solutions, this reagent was prepared directly "on line" just before its use. Both methods of preparation, as described above were used and the performance of each was examined.

a - Dissolution of bromine in alkali metal hydroxide solution (system Br_2 + LiOH)

a.1 - Initially the hypobromite solution was produced by direct mixing of bromine and lithium hydroxide solutions according to :

$$Br_2 + LiOH = BrO^- + Br^- + H_2O$$

Solutions containing 1.3×10^{-1}M of bromine and 2.4×10^{-1}M of lithium hydroxide were prepared and used in all experiments. A solution containing an excess of hypobromite 1000 times higher than that stoichiometrically necessary to convert the ammonium ions into nitrogen gas, was used. Parameters of the system such as He carrier flow rate, loop size, liquid flow rates and concentration of the reagent solutions were studied.

a.2 - Because of the difficulty of obtaining bromine solutions with exactly known and stable concentrations and in order to avoid direct contact with bromine gas, a second procedure was tried. In this case, bromine was produced direct on line by adding hydrochloric acid to a solution containing bromide and bromate ions in a proportion of
1: 5 respectively, prior to the addition of alkali :

$$5Br^- + BrO_3^- + H^+ = 3Br_2 + 3H2O$$
$$Br_2 + 2OH^- = BrO^- + Br^- + H_2O$$

The system was very similar to that used initially with the difference of a new line introduced to produce the bromine before the reaction with hydroxide. A Solution containing 0.2M of KBr and 3.6×10^{-2}M of $KBrO_3$ to produce approximately 0.1 M of bromine (equivalent to 0.1M BrO^-) was prepared and run on the system. A study of the minimum concentration of hydrochloric acid necessary to produce the same amount of bromine on-line was carried out. The amount of bromine produced on-line was determined by iodometric titration[145]. The possibility of replacing the lithium hydroxide with sodium hydroxide was also studied for this system.

Although lithium hydroxide is preferred in the preparation of hypobromite in the conventional Rittenberg oxidation procedure, because of its greater stability, sodium hydroxide (which is less expensive and ease to prepare) is perfectly satisfactory for on-line preparation of hypobromite. No significant differences in performance were found between reagents prepared by these different routes.

The manifold was optimised with respect to physical layout and and in particular the use of reaction coils was investigated. It was found that they were unnecessary in the hypobromite line and positively deleterious to performance when used after stream mixing had occurred. This experiment showed an unexpected aspect of membrane operations. When high concentrations of the standards were used, or when reaction coils were present the N_2 gas tended to form bubbles in the liquid stream. These bubbles were not efficiently removed by the membrane probably because they break through the liquid boundary layer on the inner surface of the membrane. Best results were obtained when N_2 was generated at a slower rate and allowed to diffuse through the membrane is it was produced. For this reason high excess concentration of reagents were also unhelpful because it tended to result in a rapid generation of N_2 and the formation of bubbles.

b - Reaction between hypochlorite and bromide (system $ClO^- + Br^-$)
Equivalent amounts of bromide ions were added to a hypochlorite solution at pH 9 - 9.5, at room temperature, to produce equal amount of hypobromite:

$$ClO^- + Br^- = BrO^- + Cl^-$$

The concentrations of the hypochlorite and bromide solutions were those necessary to produce 0.1 molar BrO^-. A study of the best pH and of the best $[ClO^-]$ to $[Br^-]$ ratio was carried out to optimise the preparation of hypobromite using this method.

The results obtained for the three different reactions to produce hypobomite were compared and one was chosen to be used in the manifold for generating nitrogen. Once the system was chosen, the effect of external factors affecting the gas transfer efficiency such as temperature and length of the tubular membrane on the analytical signal were investigated.

<u>Study of the efficiency of oxidation by hypobromite solution</u>
The efficiency of the oxidation to produce N_2 gas was initially studied using the system Br_2 + LiOH. The investigation was carried out using two types of PTFE membranes: sheet and tubular. The efficiency was investigated by determination of the amount of ammonia generated in the reagent stream

after 0.2 ml of 50ppm standard solution were injected. This method shows how much of the NH_4^+ has been converted to N_2 and how much remains in solution as NH_3 (g) enabling the efficiency of the reactions to be calculated. The ammonia containing solution was collected in an acidic solution and then made alkali again to enable its determination by an ammonia electrode. Excess of reagent on-line, Br_2 and BrO^-, was found to interfere in the potentiometric measure and a reducing agent, $FeSO_4$, was then added to the collector flask before the interest sample be collected. The measure was compared with a calibration graph previously prepared in a range of 0.25-2.00 ppmN.

Agricultural sample preparation

Samples were prepared by Kjeldahl digestion and the total nitrogen determined by two methods: (a) distillation of NH_3 followed by titration and (b) using the GD interface coupled to a thermal conductivity detector (TCD). The results for total nitrogen content in different aliquots of same herbage samples were compared.

The Kjeldahl digestion was carried out using 0.5g dried sample. The aliquots were weighed on a weighing boat and quantitatively transferred to digestion tubes. Into each digestion tube was added 1 "Kjeltab" catalyst tablet and 4 ml of concentrated H_2SO_4. The digestion tubes were placed in the pre-heated digester where the temperature was kept at 400°C for 1 hour. After this time, the digestion tubes were taken out of the digester and left to cool. Ten aliquots and 5 blank solutions were prepared.
Five of the 10 aliquots digested were distilled for 10 min with NaOH and the distillate produced received in 25 ml of a boric acid 2% solution which was then back titrated with 0.1 M HCl.

Five blank solutions were also prepared under the same conditions as the sample aliquots. The total nitrogen was calculated using the formula:

$$\% N = \frac{14.01 \times \text{ml of titrant of sample - ml of titrant of blanks} \times \text{mol of std acid}}{\text{g of sample} \times 10}$$

Before injection into the DPGD-FIA system the pH of the digested solutions had to be adjusted to 5.0 and degassed for 2 min with helium. The contents of nitrogen determined in the sample aliquots for both analytical methods were then compared applying the t-test.

Reagents

All reagents run on-line were degassed for 10 minutes with helium and kept in sealed bottles.

Reagents for hypobromite generation on-line investigations

- bromine, 1.3 x 10^{-1}M solution
-Lithium hydroxide (AR), 2.4 x 10^{-1}M solution:
- bromate/bromide solution: 6g of potassium bromate (AR) add to 20.5g of sodium bromide in 1 litre of water.
-sodium hypochlorite (FSA), 0.1M solution: 19.5ml hypochlorite commercial solution prepared with 1.9g B_4O_7(borax) salt in 500 ml.
-sodium hydroxide pellets (FSA), different concentration solutions depending on the system.
-sodium iodide (FSA) salt.
-Sodium thiosulphate, 1N solution
-drier agent: - molecular sieves (J & W Scientific) or magnesium perchlorate dried(80% BDH)
-ammonium sulphate (AR) solutions: 1000 ppm in nitrogen stock solution was prepared by weighing 2.36g of the salt and dissolving in 500ml water. The preparation of standards was done by appropriate dilution of the stock solution.

Reagent for potentiometric determination of ammonia

-Sodium hydroxide, 10M solution.
-Ammonium chloride, 0.1M standard solution
-buffers, pH 4.00 and pH 7.00
-Iron(II) sulphate, 4.3 x 10^{-2}M., prepared by dissolving 1.2g of the salt in 500ml water.
-Internal electrode filling solution- Russel 952021.

Reagents for Kjeldhal digestion and ammonia determination

-sulphuric acid, (AR- grade, N-free),

-Kjeltabs,(FSA), each tablet contains 1g $(Na)_2SO_4$ and 0.05g Se.
-sodium hydroxide, 40% solution.
-boric acid, 2% solution - prepared with bromocresol green indicator as indicated on the Tecator leaflet.
-hydrochloric acid, 0.1M solution.

Herbage sample

The sample was provided by Macaulay Land Use Research Institute. It was oven dried and milled to 1mm . The calculation involved in the preparation of the sample solutions are in Table 4.3.

Table 4.3 Preparation of the aliquots to be analysed by DPGD-FIA system.

aliquot	weight / g	final weight of digest / g	dilution factor after pH adjust
1	0.5003	86.0086	1.0000
2	0.5191	71.6992	1.7886
3	0.5014	64.0882	1.4373
4	0.5042	61.6275	1.4457

4.2.2 Results and discussion

The amounts of ammonia determined in the carrier stream waste for different reactions on-line are shown in Table 4.4 . When the strong oxidising agent, hypobromite,was present, nitrogen gas was generated instead of ammonia and conversion efficiency of 85% was achieved.

Experiments using the sheet membrane and a 48 cm long tubular membrane gave results with poor sensitivity. These results could be explained by the small effective contact area of the membranes and therefore a separation unit with a 1 metre long piece of tubular membrane was used in all subsequent experiments.

Table 4.4 Efficiency in generating ammonia for different reactions on-line.

chemicals on-line	efficiency to generate ammonia %
only water	99.9*
water + LiOH	100
LiOH + Br_2	15

* NH3 (g) generated at time of analysis.

The first reagent system studied with the longer membrane was Br_2+LiOH. The water carrier and the reagent flow rates were studied separately and the results are shown in Figures 4.5 and 4.6. After this, the effect of the total liquid flow rate was investigated, keeping the ratio of the independent reagent flow rates constant (H_2O:Br_2:LiOH; 0.9:1.0:1.0)The results are shown in Figure 4.7.

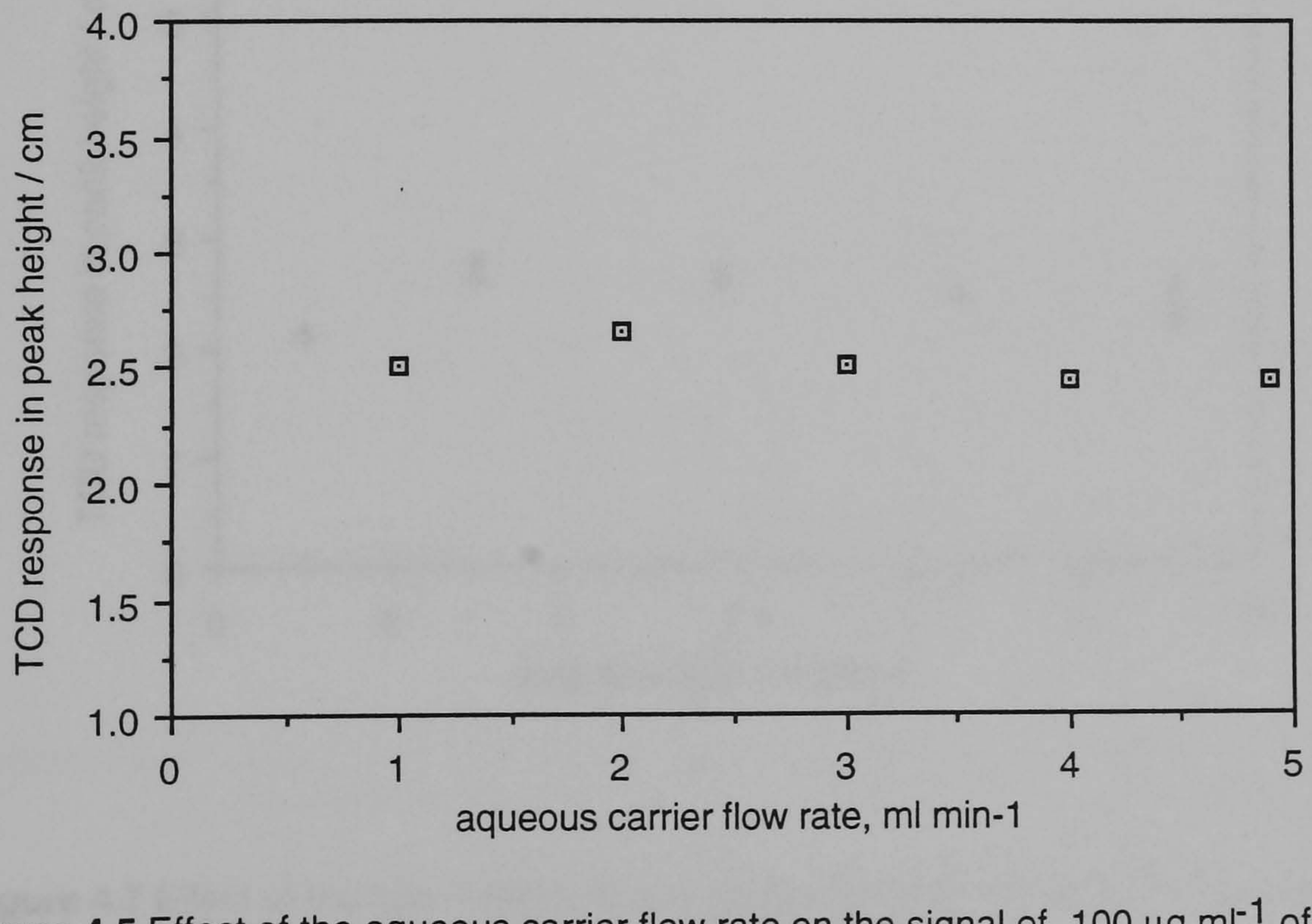

Figure 4.5 Effect of the aqueous carrier flow rate on the signal of 100 μg ml^{-1} of N. Loop size, 0.2 ml; Chemicals flow rate, 2..12 ml min^{-1}.

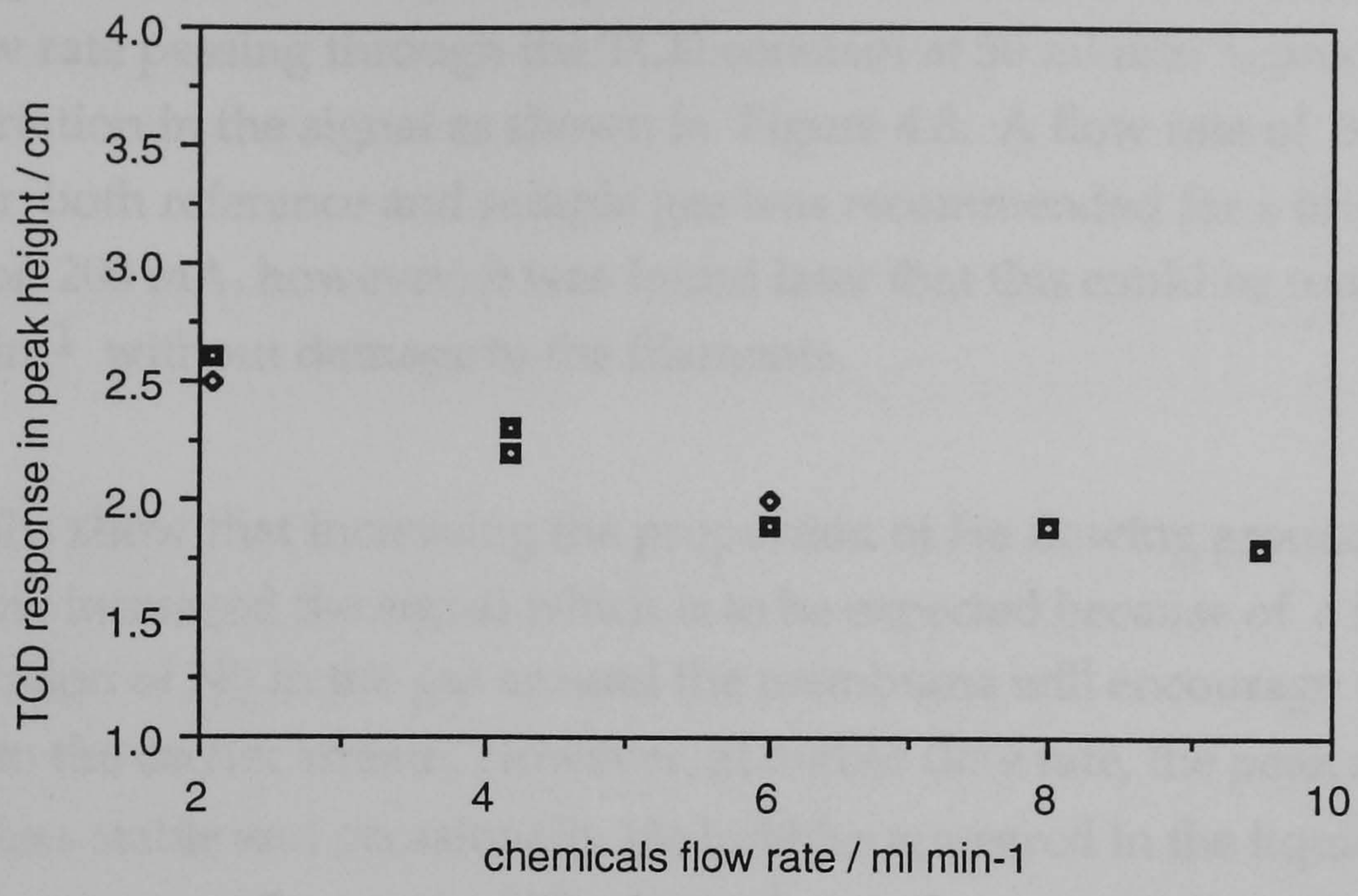

Figure 4.6 Effect of the reagents flow rate on the signal of 100 µg ml^{-1} of N. Loop size, 0.2ml; water carrier flow rate, 0.9 ml min^{-1}.

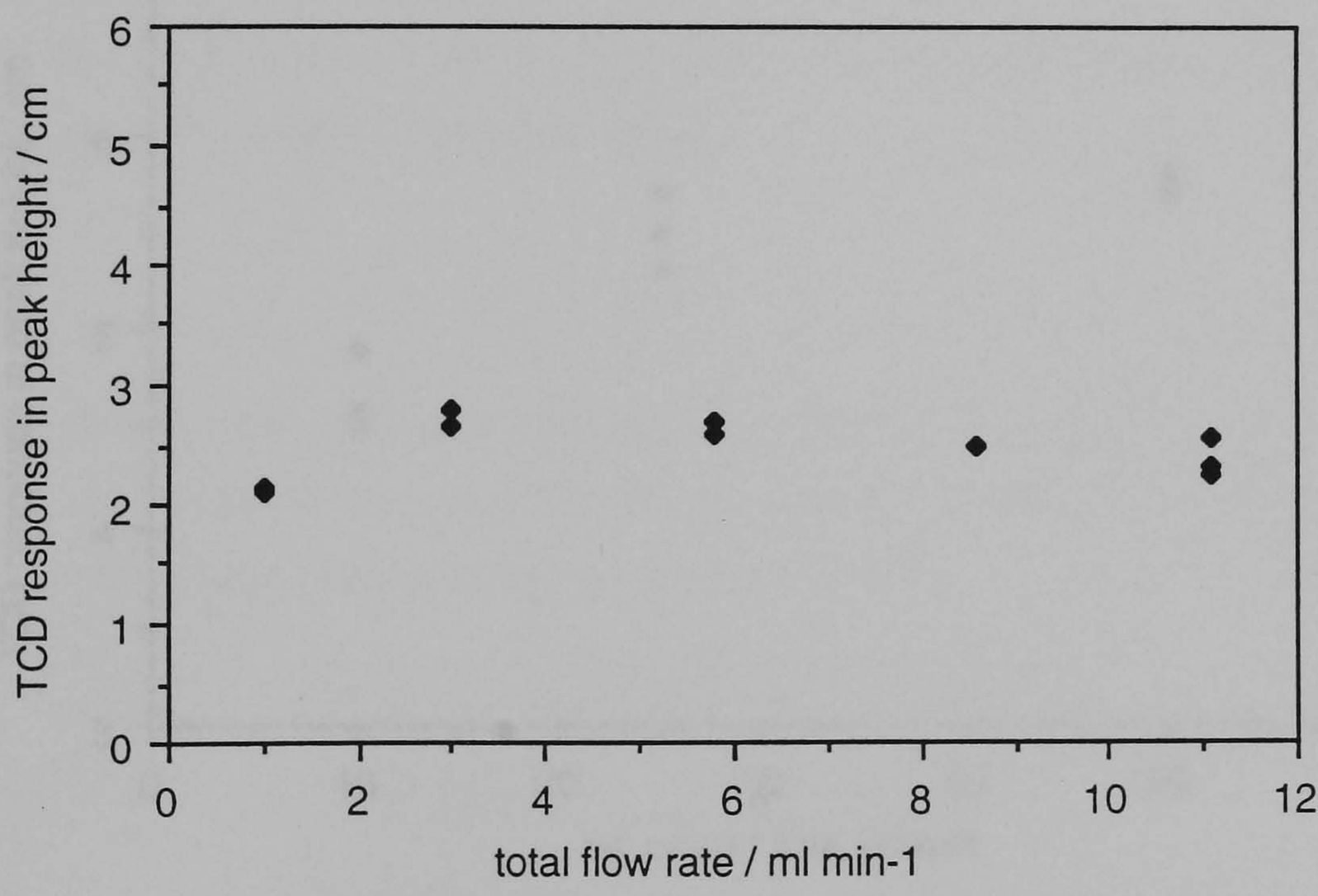

Figure 4.7 Effect of the total liquid flow rate on the signal of 100 µg ml^{-1}. Loop size 0.2 ml; reagents flow rate H_2O: Br_2: LiOH; 0.9: 1.0: 1.0.

The results shown that non of the flow rates was particularly critical provided that the correct stochiometry was maintained. Them was evident that reducing the flow rate was increasing the peak height (perhaps due to increased residence time), however, a total flow rate of ca 3 ml min^{-1} gave satisfactory sensitivity combined with good peak shapes.

Changing the He flow rate passing around the membrane, whilst keeping the total flow rate passing through the TCD constant at 50 ml min^{-1}, produced some variation in the signal as shown in Figure 4.8. A flow rate of 50 ml min^{-1} for both reference and sample gas was recommended for a bridge current of 200 mA, however, it was found later that this could be reduced to 20 ml min^{-1} without damage to the filaments.

The results show that increasing the proportion of He flowing around the membrane increased the signal which is to be expected because of a low concentration of N_2 in the gas around the membrane will encourage diffusion of N_2 into the carrier stream. However, at higher flow rate, the peak shape become less stable and occasionally He bubbles appeared in the liquid stream. For these reasons a flow rate of 10 ml min^{-1} was chosen.

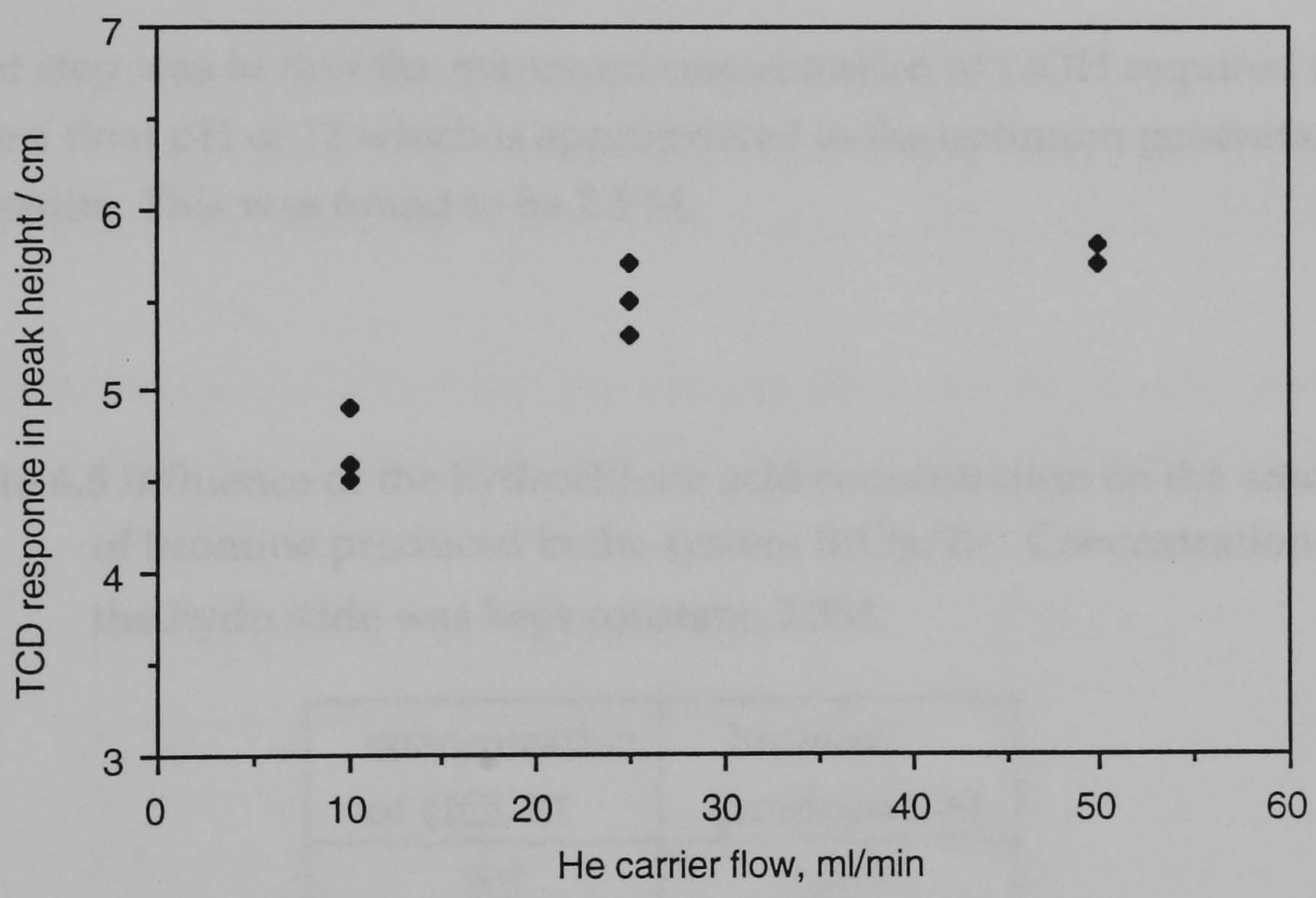

Figure 4. 8 Effect of the He carrier (acceptor stream) gaseous flow rate (3 replicated) on the signal of 100 μg ml^{-1} of N. Reference and sample flow to the TCD, 50 ml min^{-1}; loop size, 0.5 ml; total liquid flow rate, 3.2 ml min^{-1}.

The optimum injection loop size was determined by injecting the sample continuously into the system. The volume necessary to reach the plateau region, indicating that the dispersion was unity, was calculated to be 0.5 ml.

The effect of the size of the drier column was found to be negligible. Columns of 5 - 20 cm long, 7 mm id. were investigated and 10 cm long column was chosen for subsequent use.

Having established operating parameters for the $LiOH/Br_2$ chemistry, the optimum conditions for the alternative chemistries were investigated.

The effect of the concentration of the hydrochloric acid solution was investigated for the reagent system BrO_3^-/Br^-. The experiment was run using constant concentrations of BrO_3/Br^- solution and lithium hydroxide. The amount of bromine generated was determined by titration. The results are shown in Table 4.5. The minimum concentration of the hydrochloric acid required to generate the expected amount of bromine (0.1M).was 2.5 M.

The next step was to find the minimum concentration of LiOH required to produce a final pH of 12 which is appropriated to the optimum generation of hypobromite. This was found to be 2.5 M.

Table 4.5 Influence of the hydrochloric acid concentration on the amount of bromine produced in the system BrO_3/Br^-. Concentration of the hydroxide was kept constant, 2.5M.

concentration of HCl, M	bromine produced, M
5.0	0.097
2.5	0.092
1.25	0.085
0.5	0.048
0.25	0.037

For the ClO^-/Br^- reagent system to produce Br_2, the hypochlorite solution must be adjusted to a pH between 11.94 - 9.14. The effect of the pH of the individual reagents was investigated by studying the generation of N_2 gas directly. Titration of Br_2 was not appropriated in this case because of

potential errors from excess ClO^-. The optimum pH range of the final solution was between 9.9 - 10.2. Subsequently, for simplicity, hypochlorite solution was prepared in a borax buffer at pH 11. The stoichiometric ratio for $[ClO^-]/[Br^-]$ should be unity and this is confirmed by the results shown in Table 4.7 which shows the effect of varying $[Br^-]$ whilst maintaing $[ClO^-]$ constant. These findings are in accordance with the diagram shown in Figure 4.3.

Table 4.6 Influence of the pH on the generation of nitrogen sample. The bromide solution pH is constant and equal to 4.47.

pH of 0.1 M ClO^-	pH of 0.1 M BrO^-	pH of final solution	peak height / cm	peak area /counts
12.9	12.56	12.4	1.60	53830
11.9	11.42	10.9	2.15	69329
11.0	10.40	10.1	2.17	70813
9.8	10.00	9.8	2.15	70169
9.1	9.96	9.8	2.13	71263
7.9	9.38	9.3	2.20	65919
6.9	8.48	8.5	1.65	51732

Table 4.7 Influence of the concentration of the bromide solution on the peak height and peak area. The concentration of the hypochlorite solution was kept constant, 10^{-1}M.

$[Br^-]$ / M	peak height* / cm	peak area* /counts
-	1.75	48528
1×10^{-4}	1.95	53150
1 x 10-3	2.00	60228
1 x 10-2	2.05	65881
1 x 10-1	2.15	63599
1	1.83	59441

* figures are mean of two determinations.

The optimised operating conditions for all three chemistries are shown in Table 4.8.

Table 4.8 Summary of the optimised variables for the three DPGD-FIA manifolds used for generating of N_2 gas on-line. Manifold using loop size 0.5 ml; drier column, 10 cm; He carrier flow rate, 10 ml min^{-1}.

reagent	concentration	flow rate, ml min^{-1}
(I) $LiOH/Br_2$		
H2O carrier	-	0.9
Br_2	0.15	1.05
LiOH	0.24	1.05
(II) BrO_3/Br^-		
H2O carrier	-	1.5
BrO_3/Br^-	0.036/0.2	0.5
HCl	2.5	0.5
NaHO	2.5	0.5
(III) ClO^-/Br^-		
H2O carrier	-	1.0
ClO^-	0.1	1.0
Br^-	0.1	2.0

Calibration graphs were obtained using the three different methods of producing hypobromite and these are shown in Figure 4.9. The calibration graph for the ClO^-/H^+ chemistry showed lower sensitivity and a narrower linear range than the other two. Although the BrO_3/Br^-chemistry involves using a more complex manifold, it offers the best sensitivity and retains the advantage of generating the bromine on-line. This was therefore chosen for nitrogen gas generation and a more detailed investigation of the operating parameters were carried out.

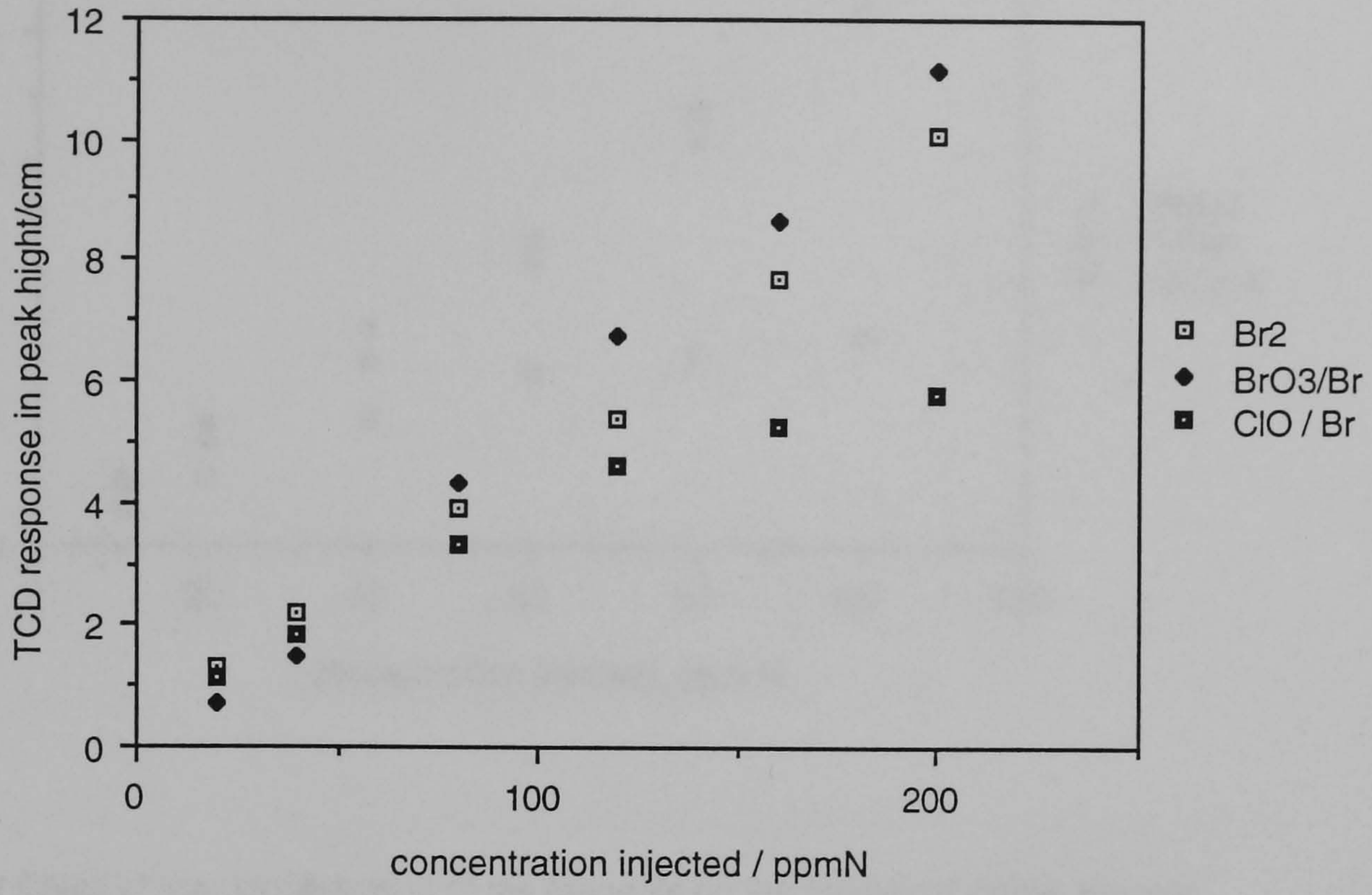

Figure 4.9 Comparison of the three methods of producing hypobromite on-line. All chemicals were prepared to produce about 0.1M BrO^-. All other parameters in Table 4.8.

The total liquid flow and reagent flow was investigated as before and the previous optimum flow rates were confirmed (see Table 4.8).

The relationship between the reagent concentrations and the resulting peak-areas was investigated and the results are shown in Figure 4.12. All reagents were diluted or concentrated twice thereby keeping the concentration ratio constant, in the proportions used previously. It can be seen from Figure 4.12 that there was no increase in sensitivity when the higher concentrations were used and therefore the previous values were retained

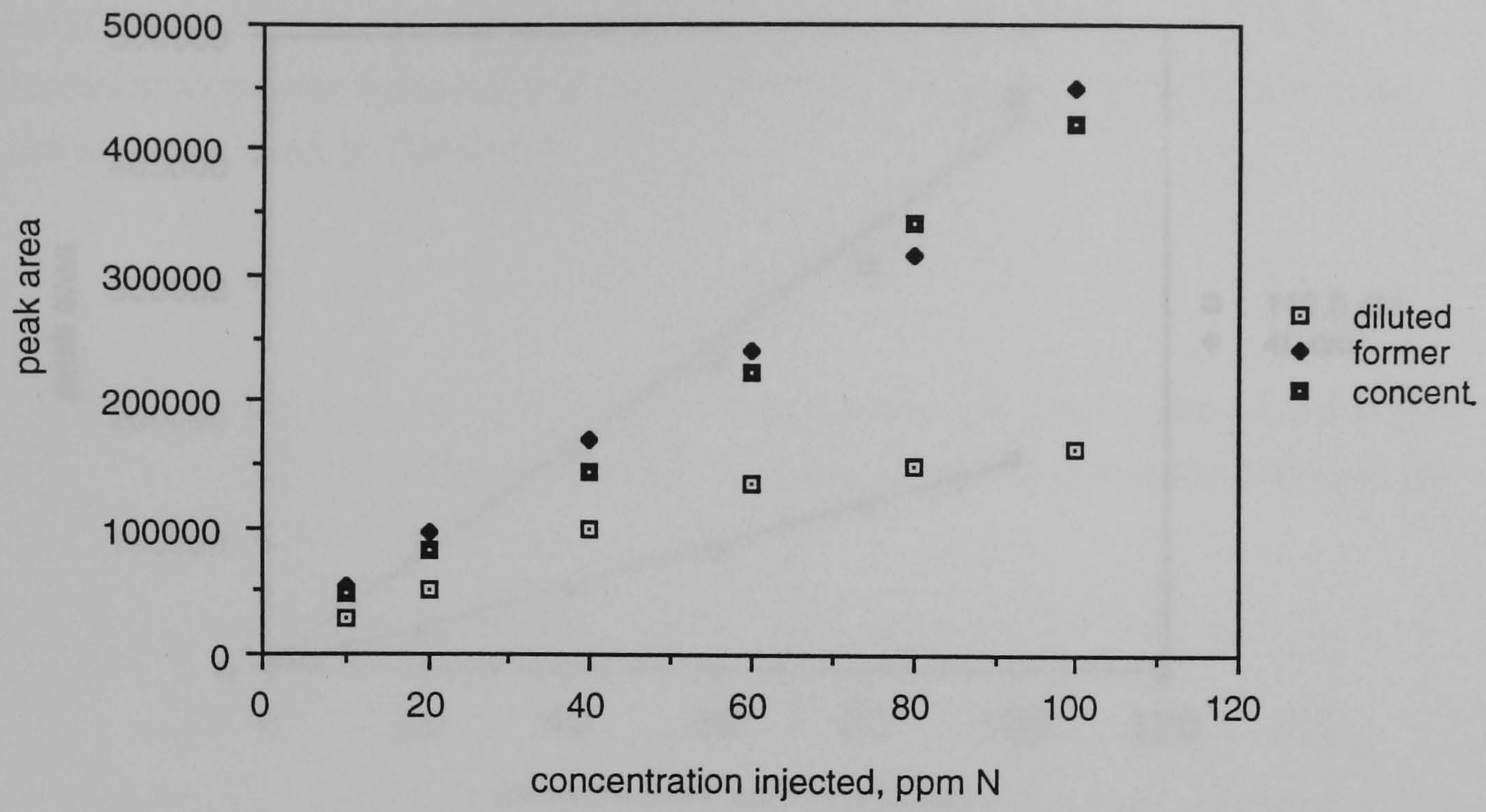

Figure 4.12 Effect of the concentration of the reagents on the analytical signal. Former reagent concentrations: HCl, 2.5M; NaOH, 2.5M; BrO_3, 3.6 x 10^{-2}M; Br^-, 0.2 M.

The Figure 4.13 shows two calibration graphs prepared with separator units containing the same type of tubular membrane with different lengths. In the same way, the Figure 4.14 presents calibration graphs obtained when the separator unit is kept in a water bath under three different temperatures. The length of the membrane and the temperature are factors which are directly related to the mass transfer process. Both variables are present in the diffusion equation and an increase in them will improve the gas transport efficiency through the membrane. The increase of temperature indeed improved the sensitivity but temperatures higher than 50 °C are not recommended due to necessitating more frequent replacement of the filling of dryer column.

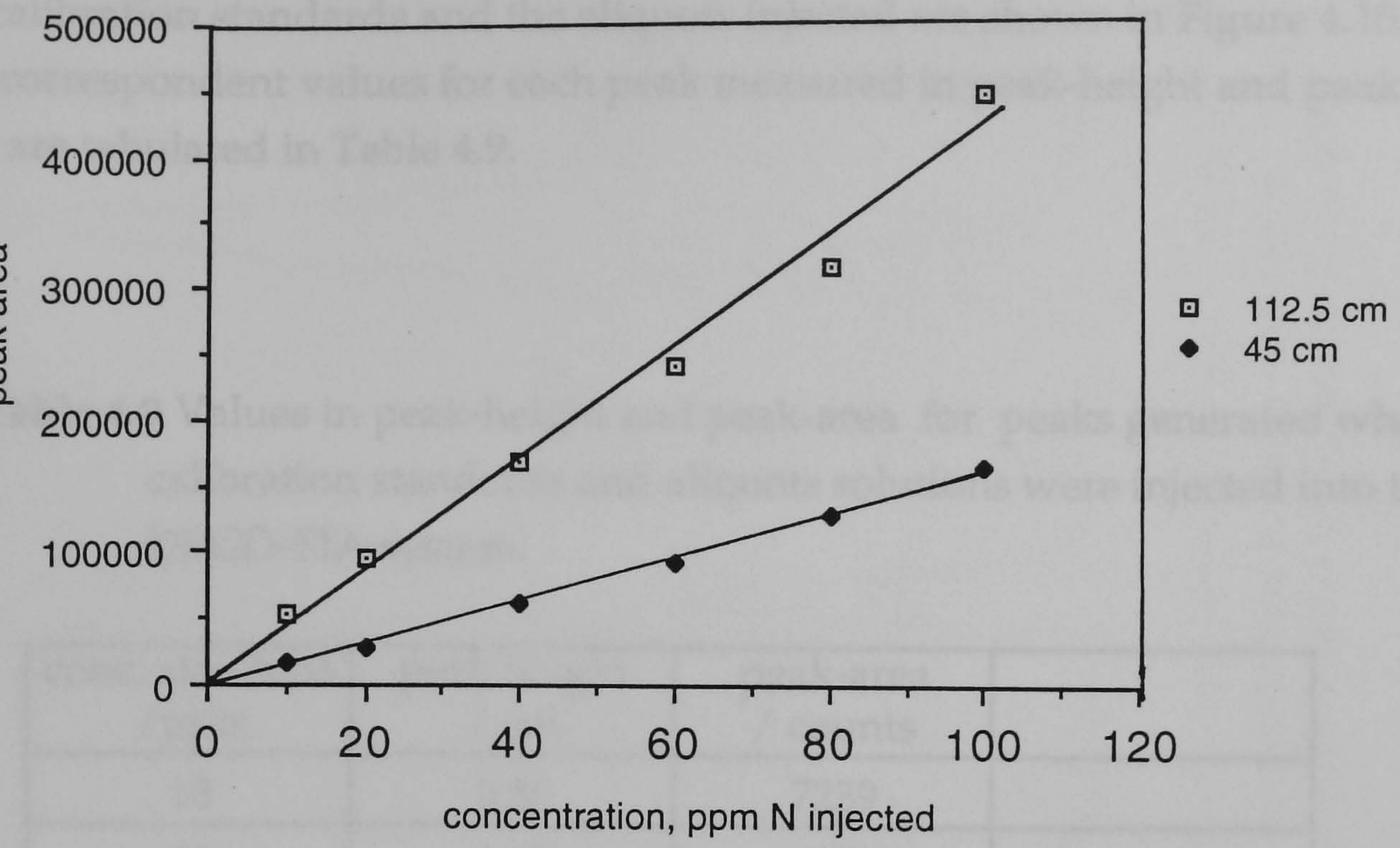

Figure 4.13 Influence of the length of the gas diffusion separator on the analytical signal. Loop size, 0.5 ml; He flow to TCD, 20 ml min^{-1}; all other variable as in Table 4.5 (II).

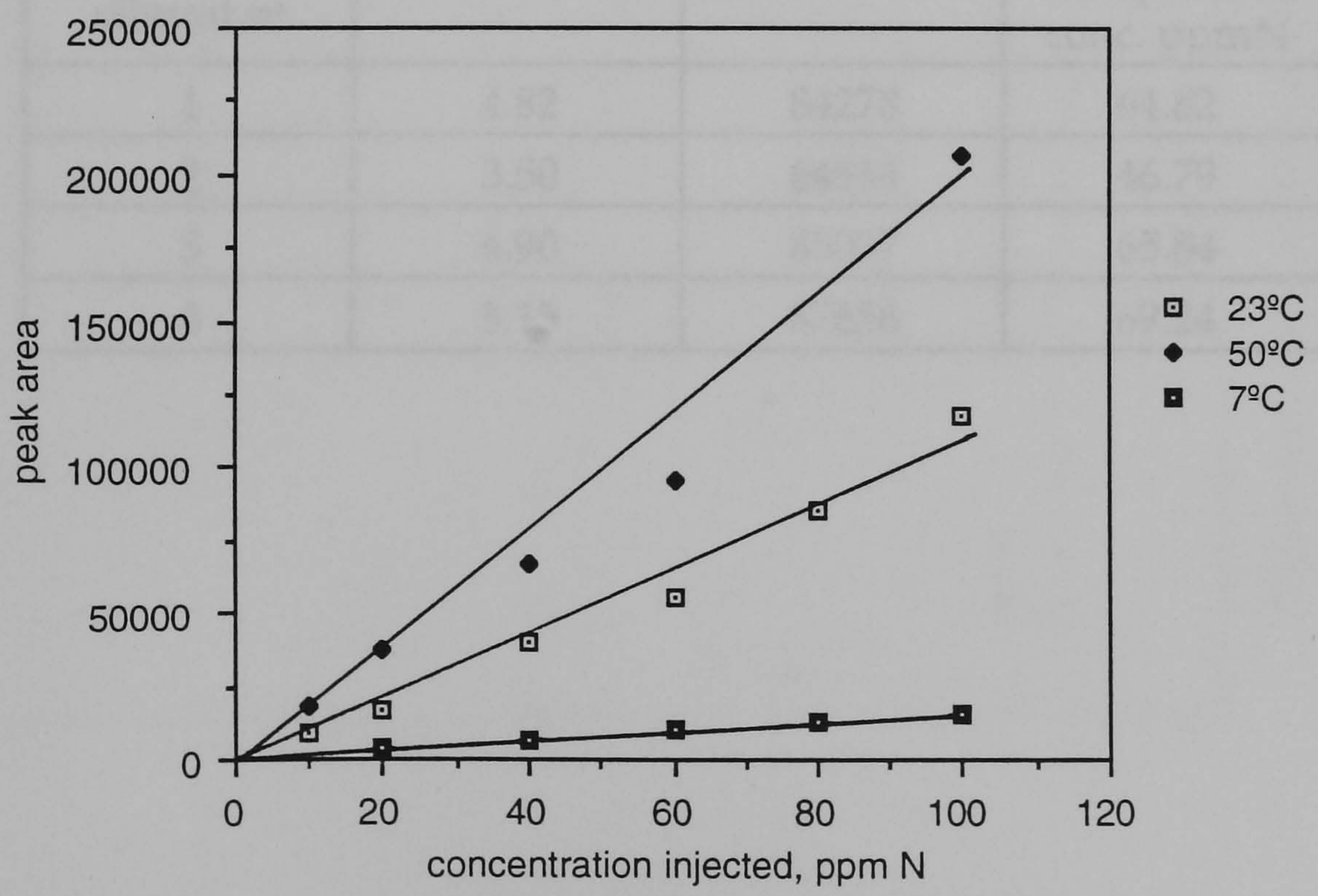

Figure 4.14 Effect of the temperature on the analytical signal. Loop size,0.5 ml; He flow rate to TCD, 50 ml min^{-1}; all other variables as in Table 4.5 (II).

The herbage sample was analysed and the characteristic peaks obtained for the calibration standards and the aliquots injected are shown in Figure 4.15. The correspondent values for each peak measured in peak-height and peak-area are tabulated in Table 4.9.

Table 4.9 Values in peak-height and peak-area for peaks generated when calibration standards and aliquots solutions were injected into the DPGD-FIA system.

conc. standard /ppm	peak height / cm	peak-area / counts	
10	0.80	7239	
20	1.45	20816	
40	3.10	51450	
60	4.40	83102	
80	6.10	112067	
100	7.30	135287	
detection limit	4.58 $\mu g\ g^{-1}$	9.54 $\mu g\ g^{-1}$	
aliquot nº			sample sol. conc. ppmN
1	4.82	84278	64.82
2	3.50	64914	46.79
3	4.90	85037	65.84
4	5.15	87656	69.24

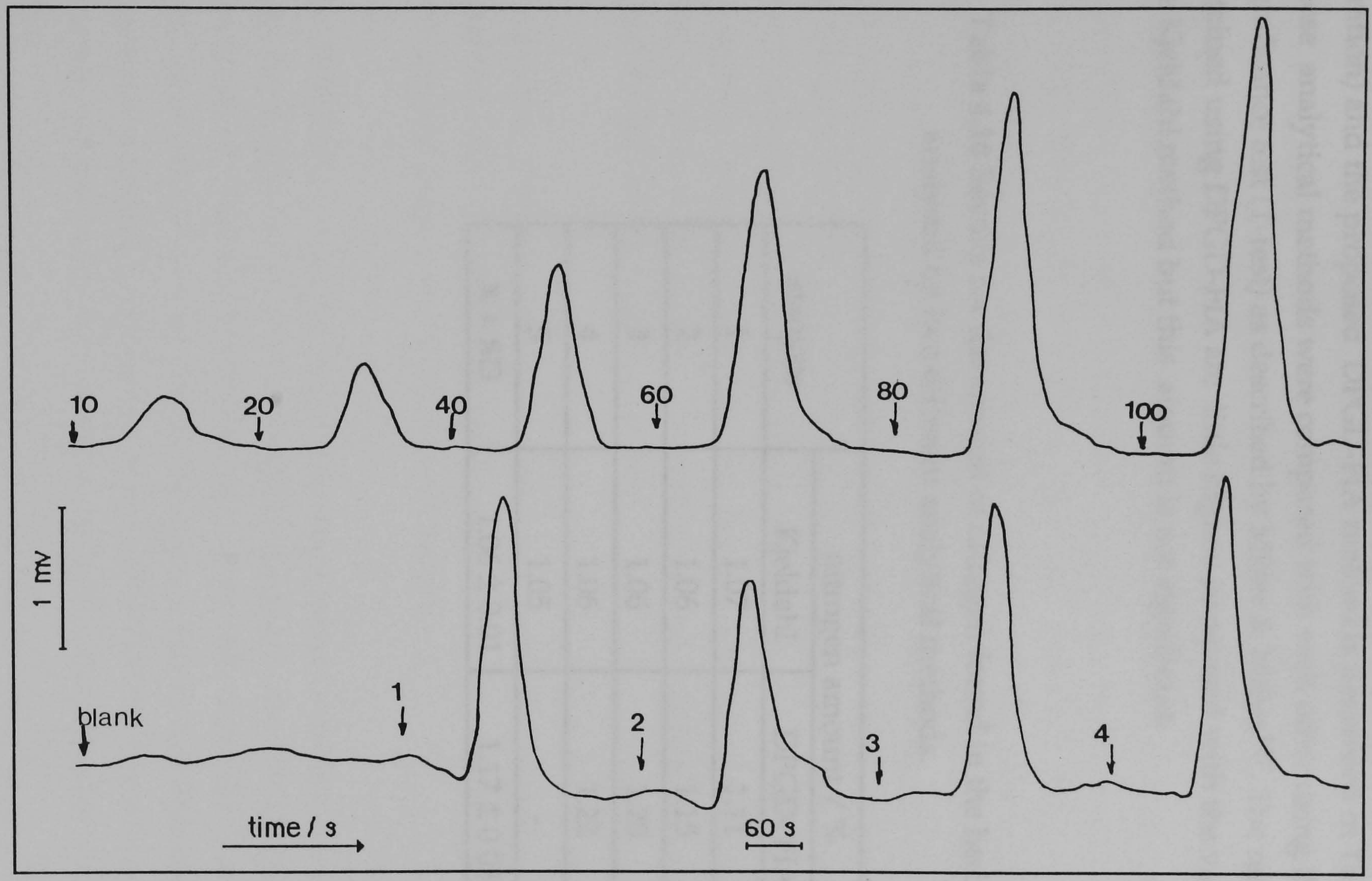

Figure 4.15 Characteristic peaks obtainded when concentration standards and sample solutions are injected into the DPGD-FIA system for generating nitrogen. He flow to the detector, 50 ml min; all other conditions as shown in Table 4.8(II)

The comparison between the content of nitrogen in the herbage sample found by the former Kjeldahl method (distillation of the ammonia and titration) and the proposed DPGD-FIA method is presented in Table 4.10. These analytical methods were compared with each other using the significance test (T-test) as described by Miller & Miller[117]. The results obtained using DPGD-FIA are little higher compared with the value from the Kjeldahl method but this amount is not significant.

Table 4.10 Results for the amount of nitrogen found in the herbage sample analysed by two different analytical methods.

analysis	nitrogen amount / %	
	Kjeldahl	DPGD- FIA
1	1.07	1.11
2	1.06	1.15
3	1.06	1.20
4	1.06	1.22
5	1.05	-
X + SD	1.06 ± 0.01	1.17 ± 0.05

4.3 Determination of $^{15}N/^{14}N$ by isotope ratio mass spectrometry using a DPGD-FIA interface.

4.3.1 Experimental

The DPGD-FIA system developed as a nitrogen gas generator was coupled to a mass spectrometer (MS) for $^{15}N/^{14}N$ isotope ratio determination. The connection of the FIA system to the MS was made by inserting the sample inlet capillary of the MS into the TCD sample flow outlet. A split ratio (flow from TCD: flow to MS) of approximately 200:1 was used. The procedure for the measurements with the mass spectrometer was the same for all experiments: the mass spectrometer was tuned to monitor masses 28, 29 and 30 ; the peristaltic pumps from the FIA system were switched on; the sample inlet capillary for the MS was connected to the TCD sample flow outlet and the MS inlet valve opened to ingress of the effluent gas. Reference N_2 gas of known isotopic abundance was injected twice before and after a set of standards to monitor the background. Experiments were carried out injecting solutions containing different concentrations and different isotopic ratios of N_2 on the system in a random order.

A schematic of the equipment is shown in Figure 4.16. The MS used was a research instrument, based on the VG Optima, isotope ratio mass spectrometer, located at the VG Isotech factory.

The DPGD-FIA system produced a constant background level of N2 due to outgassing of the reagent streams across the membrane. This was not a significant problem for TCD detectors, but with MS detection, the effect was to raise the background ion current by approximately two orders of magnitude compared with that obtained with pure He. Procedures were, therefore, adopted (described later) to reduce the background to acceptable levels.

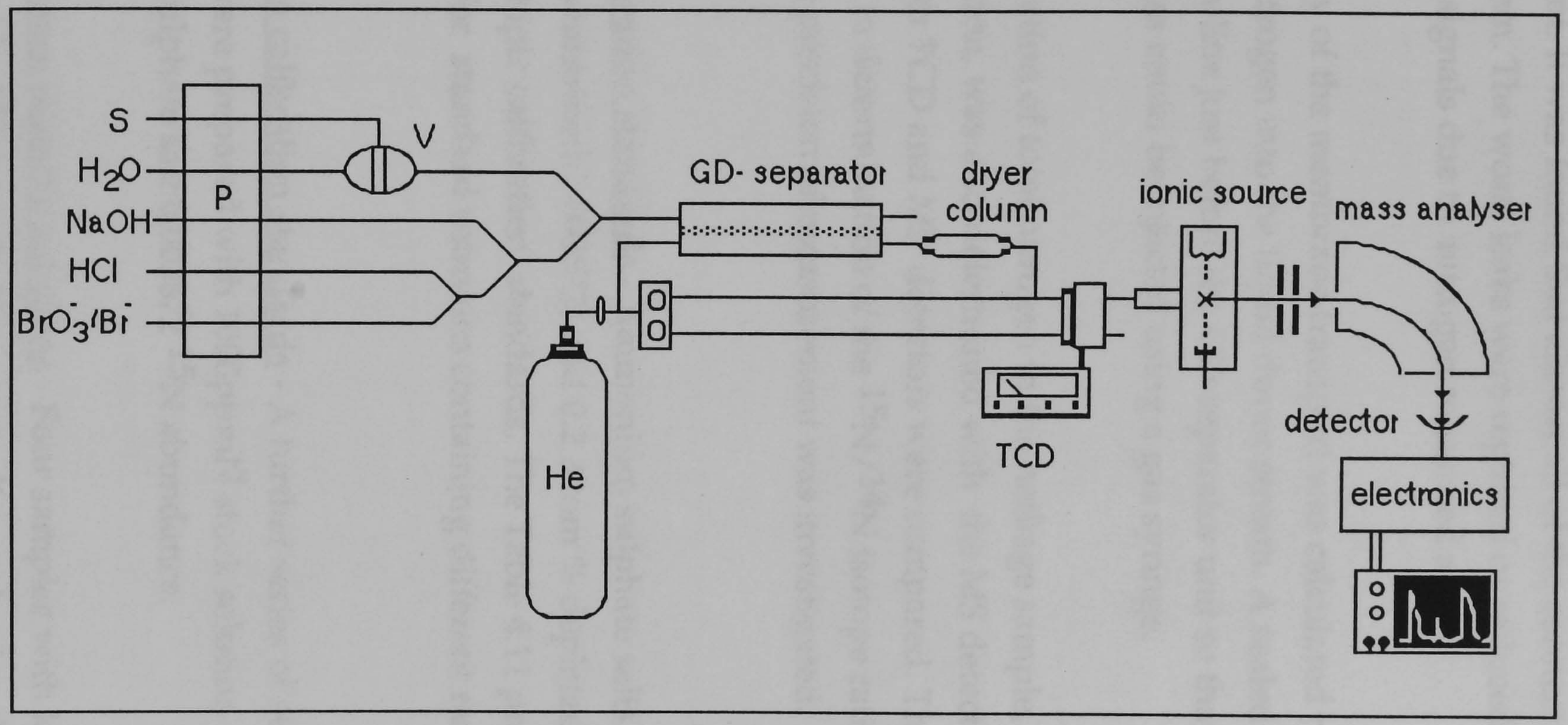

Figure 4.16 System used for generation and determination of $^{15}N/^{14}N$ isotope ratios.

The entire flow injection system was tested for leaks by re-tuning the MS and observing the background signal whilst blowing a stream of argon gas over the equipment. It was found that almost all of the connections leaked argon into the system. The worst leaks were repaired or reduced and the background signals due to nitrogen measured again.

The efficiency of the membrane transport was calculated by injecting a known amount of nitrogen into the liquid donor stream. A sealed T-piece was connected on-line just before the GD-separator unit so that different amounts of nitrogen gas could be injected using a gas syringe.

The concentration of total nitrogen in the herbage sample, as analysed in the previous section, was also determined with the MS detector. The results found for both TCD and MS detectors were compared. The apparatus was then applied to determination of the $^{15}N/^{14}N$ isotope ratios in reference samples. The precision of measurement was investigated.

Reagents

Isotopic calibration standards - Ammonium sulphate salts, ^{15}N abundance previously determined(0.003672) and 0.2 Atom % depleted were mixed to make the isotopic calibration standards. The Table 4.11 present the calculations for standard solutions containing different range of isotopic ratio.

Concentration calibration standards - A further series of standards, range 10 - 100 ppmN, were prepared with 1000ppmN stock solution prepared with ammonium sulphate salt 0.003672 ^{15}N abundance.

Isotopic reference material solutions - Four samples with known isotopic ratio were provided by VG-Isotech. They were digested using the Kjeldahl digestion and the digested solutions were diluted as necessary and adjusted to pH 5 prior to injection into the DPGD-FIA system. The Table 4.12 contains the specification for each material and Table 4.13 presents the calculations involved in of the relevant isotopic ratios.

Table 4.11 Isotopic ratio standards preparation and calculations for ratio and delta.

standard code	volume 0.3672 At% std / ml 344ppm	std / ml volume of depleted 688 ppm	final volume / ml	conc. / ppm N	ratio $^{15}N/^{14}N$	abundanc Atom %	delta value
I1	10	-	100	34.4	0.0036855	0.0036720	2.466
I2	7.5	2.5	100	43.0	0.0030122	0.0030030	-182.69
I3	5	5	100	51.6	0.0025638	0.0025572	-304.34
I4	2.5	7.5	100	60.2	0.0022438	0.0022388	-391.17
I5	-	10	100	68.8	0.0020040	0.0020000	-454.91
	ml std I1 34.4ppN	ml std I2 43ppmN					
I6	6	2	8	36.55	0.0036585	0.0036452	-7.31
I7	4	4	8	38.70	0.0036106	0.0035976	-20.31
I8	2	6	8	40.85	0.0035018	0.0034895	-49.85
	std.At% 0.3672 344 ppm	std depleted 11 ppm					
I10	10	-	100	34.40	0.0036855	0.0036720	2.466
I11	9	1	100	31.07	0.0036795	0.0036660	0.843
I12	8	2	100	27.74	0.0036721	0.0036587	-1.167
I13	7	3	100	24.41	0.0036627	0.0036493	-3.728
I14	6	4	100	21.08	0.0036503	0.0036370	-7.097
I15	5	5	100	17.75	0.0036333	0.0036201	-11.730
I16	4	6	100	14.42	0.0036084	0.0035954	-18.503
I17	3	7	100	11.09	0.0035685	0.0035558	-29.343
I18	2	8	100	7.76	0.0034945	0.0034823	-49.483
I18.5	1.5	8.5	100	6.09	0.0034271	0.0034157	-67.55
I19	1	9	100	4.43	0.0033092	0.0032983	-98.794
I20	-	10	100	1.10	0.0020040	0.0020000	-454.91

Table 4.12 Reference materials supplied by VG-Isotech to certify the DPGD-FIA-MS method for $^{15}N/^{14}N$ isotopic ratio determinations.

Compound	Assay (Carlo Erba)		
	Delta	Ratio	At%
nicotine	-4.11	0.00366136	0.3648%
pyrazine	-1.09	0.00367244	0.3659%
quinoxaline	-3.01	0.00366539	0.3652%
tripropylame	6.57	0.00370064	0.3687%
$(NH_4)_2SO_4$	-0.27	0.00367600	0.3662%

Table 4.13 Preparation of the reference material solutions for $^{15}N/^{14}N$ isotopic ratio determination by DPGD-FIA-MS.

reference material	Mass weight	sample size	final volume / ml	dilution factor	final conc. /ppm N	$^{15}N/^{14}N$ ratio expected
pyrazine 1	80.09	0.1215 g	96.4556	9.92	44.40	0.00367244
pyrazine 2	80.09	0.1752 g	95.2445	7.07	91.00	0.00367244
quinoxal3	130	0.1470 g	97.2009	7.29	44.66	0.00366539
quinoxal4	130	0.1725 g	97.0656	6.8646	55.76	0.00366539
nicotine 5	162	0.2 ml	95.6350	6.4602	55.95	0.00366136
nicotine 6	162	0.2 ml	96.9013	6.3894	55.83	0.00366136
t-pplmin7	143	0.2 ml	97.8400	7.6383	26.91	0.00370064
t-pplmin8	143	0.2 ml	95.2490	8.1543	24.91	0.00370064
NH_4SO_2	132	3.3287	500	20	71.38	0.00367600

4.3.3 Results and discussion

The described peaks were considerably wider than those obtained when the standard GC interface ("Isochrom " system)was connected, but they were nevertheless successfully integrated by the data system. The results, tabulated in Table 4.14 show good precision and compare favourably with those that might be obtained from a combustion analyser. The first results obtained using the system described are shown in Figure 4.17. The three lines shown on each trace correspond to mass channels: 28, 29 and 30.

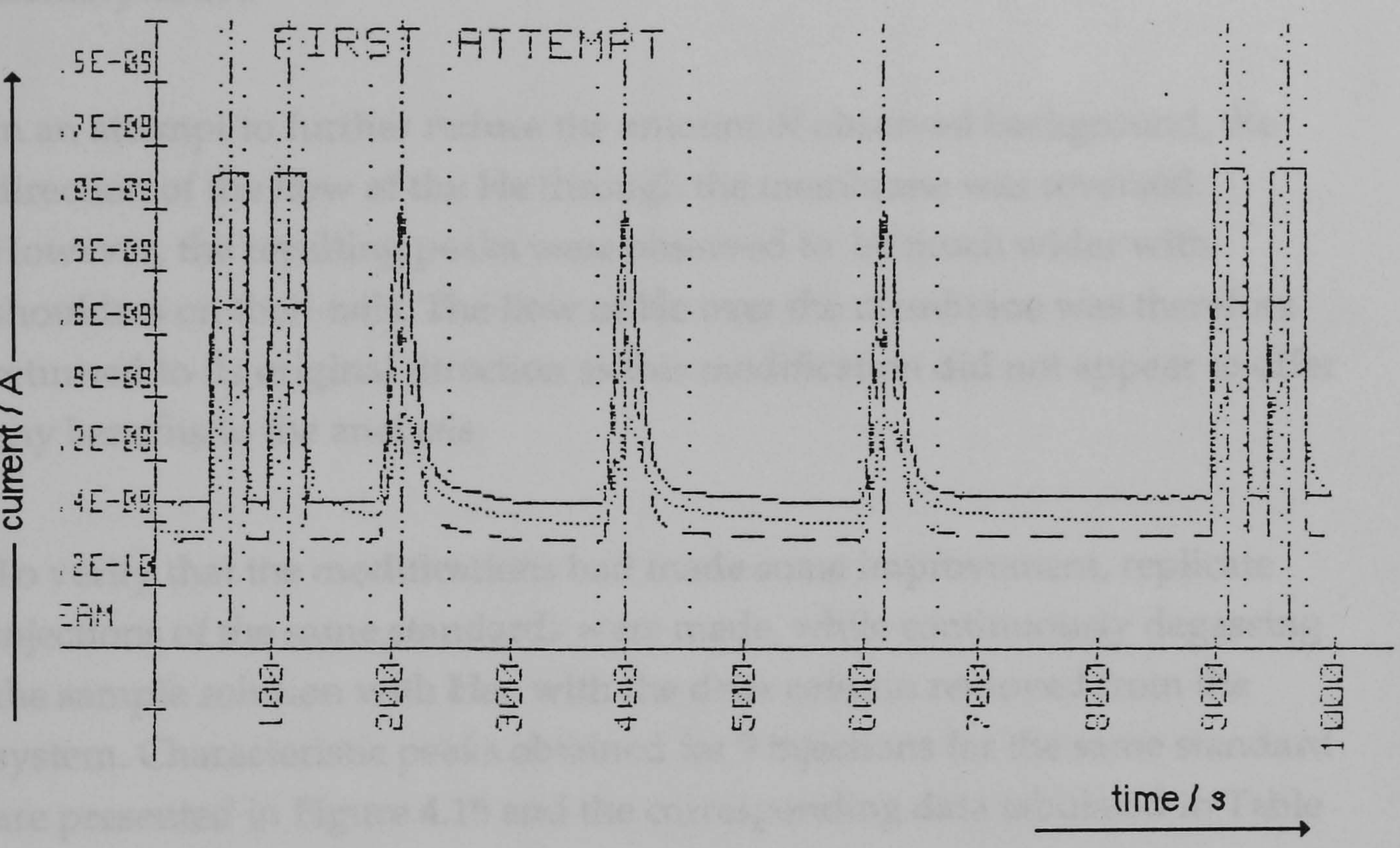

Figure 4.17 Characteristic peaks for three injections of 60ppmN. The first and last two peaks are reference gas injections. .....$30N_2$ – – $29N_2$ — $28N_2$

Table 4.14 Results found for the three injections shown in Figure 4.17.

peak number	major area	ratio
1	7.52×10^{-7}	3.59×10^{-3}
2	7.53×10^{-7}	3.59×10^{-3}
3	6.98×10^{-7}	3.59×10^{-3}
average	7.34×10^{-7}	3.59×10^{-3}
RSD	4.47%	0.01%

To increase the size of the peaks from the mass spectrometer , the total gas flow through the sample and reference streams of the TCD was reduced to 20 ml min^{-1} from 50 $mlmin^{-1}$ However, It was noticed that the background increased substantially and was not stable, presumably because the effect was greater for reduced He flow. All the connections on the manifold therefore were tested again for leakage and some connections improved. The injection valve was cleaned and serviced. Additionally, the drier column was taken out of the system as it was suspected that this column was either introducing air or retaining some of the original sample and causing a memory effect.

In an attempt to further reduce the amount of observed background, the direction of the flow of the He through the membrane was reversed. However, the resulting peaks were observed to be much wider with shoulders on their tails. The flow of He over the membrane was therefore returned to its original direction as this modification did not appear to offer any benefits to the analysis.

To verify that the modifications had made some improvement, replicate injections of the same standards were made, while continuously degassing the sample solution with He, with the drier column removed from the system. Characteristic peaks obtained for 9 injections for the same standard are presented in Figure 4.18 and the corresponding data tabulated in Table 4.15.

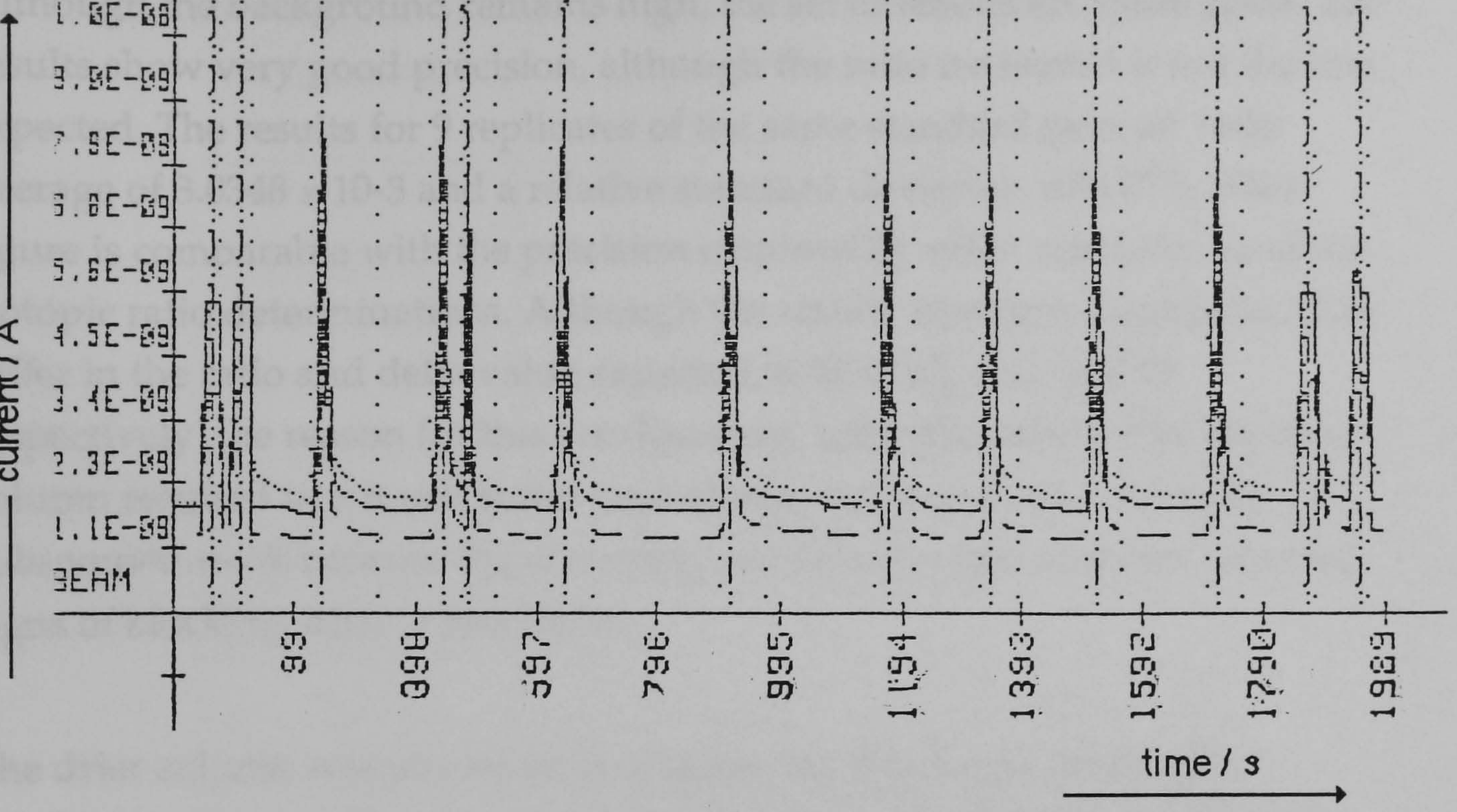

Figure 4.18 Characteristic peaks for 9 injections of standard I 2. (....$30N_2$ – $29N_2$ – $28N_2$

Table 4.16 Results found for 9 injections of standard I2. Isotopic ratio expected, 0.003012; delta expected, -182.69.

injection n°	$^{15}N/^{14}N$ ratio	delta
1	0.003000	-160.6
2	0.003001	-160.2
3	0.003521	-147.0
4	0.002983	-165.3
5	0.003009	-158.1
6	0.002967	-169.6
7	0.002946	-175.4
8	0.002945	-175.5
9	0.002942	-176.4
average	0.003035	-165.3
RSD	6.06%	5.98%

Although the background remains high, the set of results are quite good. The results show very good precision, although the ratio measured is not the one expected. The results for 9 replicates of the same standard gave an ratio average of 3.0348 x 10-3 and a relative standard deviation of 6.07% .This figure is comparable with the precision obtained by other methods used for isotopic ratio determinations. Although the results have good precision, they differ in the ratio and delta value expected, 0.0030122 and -182.69 respectively. the reason for this are discussed later. The removal of the drier column resulted in a much better peak shape, but it was not omitted in subsequent work because the water trap on the mass spectrometer showed signs of blocking after a few hours.

The drier column was placed on-line again, but filled with magnesium perchlorate instead of molecular sieve. Isotopic ratio calibration standards, continuously degassed with He, were injected into the manifold. The peaks generated are shown in Figure 4.19 and the data tabulated in Table 4.16.

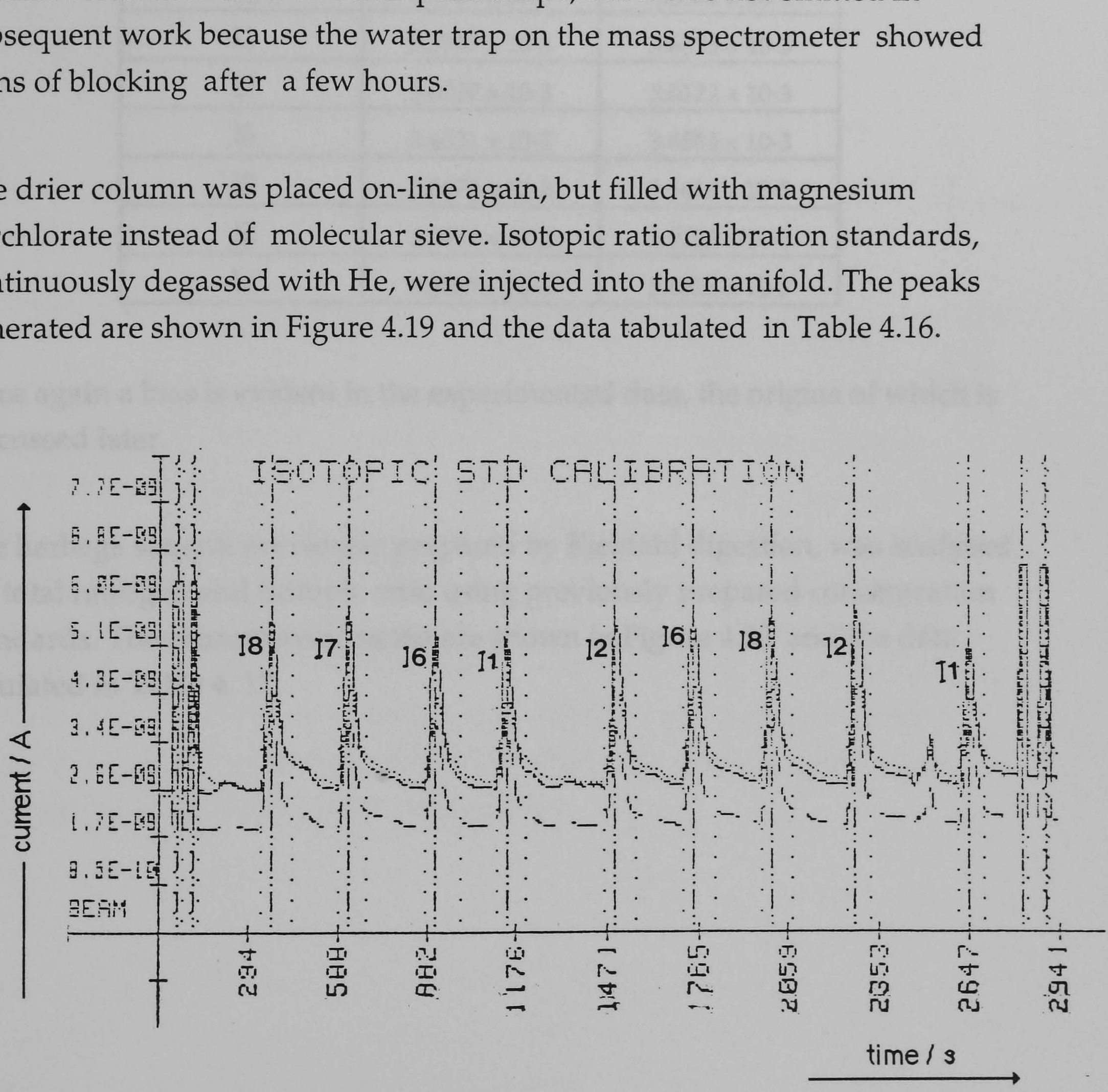

Figure 4.19 Characteristic peaks for isotopic ratio standards. Standards preparation shown in table 4.11.($^{30}N_2$–$^{29}N_2$–$^{28}N_2$

Table 4.16 Results found for the isotopic $^{15}N/^{14}N$ratio standards injected on the system:

standard code	15N/14N ratio	
	measured	actual
I8	3.3808 x 10-3	3.5018 x 10-3
I7	3.2327 x 10-3	3.6106 x 10-3
I6	3.4550 x 10-3	3.6585 x 10-3
I1	3.5887 x 10-3	3.6855 x 10-3
I2	3.0737 x 10-3	3.0122 x 10-3
I6	3.4631 x 10-3	3.6585 x 10-3
I8	3.3670 x 10-3	3.5018 x 10-3
I2	3.0671 x 10-3	3.0122 x 10-3
I1	3.5889 x 10-3	3.6855 x 10-3

Once again a bias is evident in the experimented data, the origins of which is discussed later.

The herbage sample previously prepared by Kjeldahl digestion, was analysed for total nitrogen and isotopic ratio using previously prepared concentration standards. The characteristic peaks are shown in Figure 4.20 and the data tabulated in Table 4. 17.

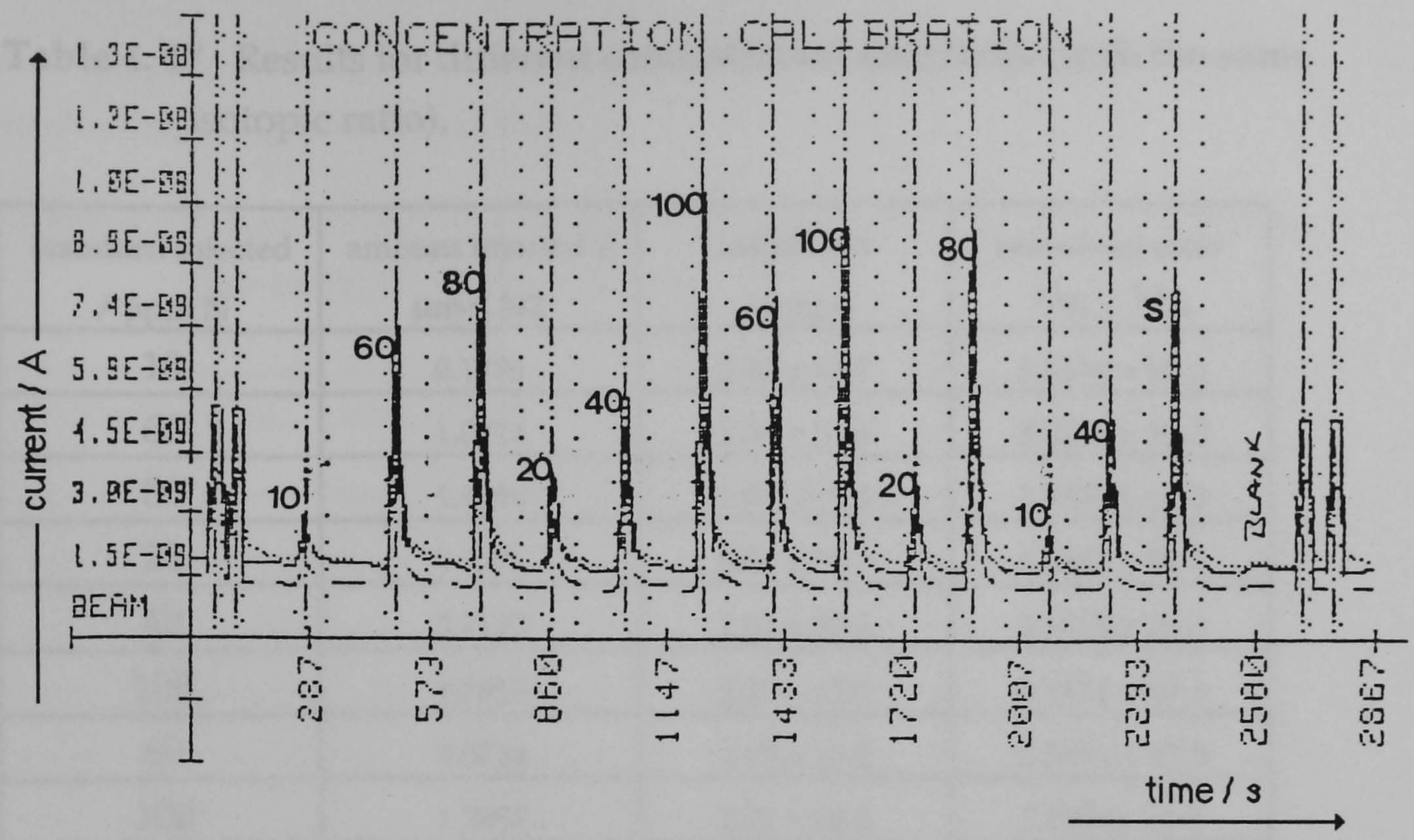

Figure 4.20 Characteristic peaks obtained from injecting 0.5 ml of different concentration standards (with the same isotopic ratio) and the herbage sample. 30 N2
---29N2
—28N2

The results for the isotopic ratio show that continuous degassing of the sample solution brings a dramatic improvement in precision from ca 6% - 0.03%. The improvement is evident from a visual comparison of the peak shapes in Figure 4.19 (sample not degassed) and Figure 4.20 (sample continuously degassed). These results emphasis the importance of avoiding external contamination with gaseous N_2 from the atmosphere. additionally the data do not show a trend in the measured ratio which might indicate some discrimination from concentration effects. the resultant calibration graph, gives a correlation coefficient of 0.989.

Table 4. 17 Results for different concentration standards (with the same isotopic ratio).

standard injected / ppm N	amount injected / µmol N2	major area /counts	measured ratio ^{15}N / ^{14}N
10	0.1786	3.40 x 10-7	3.5836 x 10-3
60	1.0714	1.56 x 10-6	3.5845 x 10-3
80	1.4286	1.96 x 10-6	3.5832 x 10-3
20	0.3571	6.56 x 10-7	3.5851 x 10-3
40	0.7143	1,04 x 10-6	3.5855 x 10-3
100	1.7857	2.20 x 10-6	3.5824 x 10-3
60	1.0714	1.48 x 10-6	3.5851 x 10-3
100	1.7857	2.21 x 10-6	3.5824x 10-3
20	0.3571	5.68 x 10-7	3.5857 x 10-3
80	1.4286	1.89 x 10-6	3.5841x 10-3
10	0.1786	2.73 x 10-7	3.5849 x 10-3
40	0.7143	9.99 x 10-7	3.5852 x 10-3
average	-	-	3.5843 x 10-3
RSD	-	-	0.032%
Sample	-	1.55 x 10-6	3.5845 x 10-3

The sample solutions analysed during this experiment gave a value of 65.1ppm for total N concentration and an isotope ratio of 0.003585. The blank produced a peak, but it was too small to be integrated by the data system (see Figure 4.20). The content of nitrogen in the sample was calculated to be 1.12% N and can be considered to be the same value as obtained when using the TCD as a detector (1.17% N).

The efficiency of the membrane was estimated after calibrating the detector(s) by injecting nitrogen gas into the helium flow directly after the GD-separator unit. All other parameters were kept the same. The amount in µl injected was converted in µmol of N_2 and the results are shown in Table 4.18 and the signal from this amount of pure N_2 injected was then compared with those obtained from the injection of concentration standards. The data tabulated in Table 4.19 and plotted in Figure 4.21 shows a comparison between the

calibration graph obtained for N_2 gas injected directly and N_2 gas was generated from aqueous standards.

Table 4. 18 Results for the amount of N_2 gas injected after the membrane unit to calibrate the detector.

amount injected, / µl N2	amount injected, / µmol N_2	major area / counts	measured ratio $^{15}N/^{14}N$
20	0.8928	1.54 x 10-6	3.5658 x 10-3
5	0.2235	4.35 x 10-7	3.5692 x 10-3
15	0.6696	1.19 x 10-6	3.5660 x 10-3
25	1.1161	1.93 x 10-6	3.5630 x 10-3
10	0.4464	7.65 x 10-7	3.5679x 10-3
average	-	-	3.5663 x 10-3
RSD	-	-	0.066%

Table 4.19 Data for estimating the mass transfer through the membrane for different amount of N_2 generated from aqueous standards.

std injected /ppm N	amount injected /µmol N_2	major area	amount found /µmol N_2
10	0.17731	3.40×10^{-7}	0.19922
10	0.17731	2.73×10^{-7}	0.16118
20	0.35462	6.56×10^{-7}	0.38824
20	0.35462	5.68×10^{-7}	0.33570
40	0.70925	1.04×10^{-6}	0.61606
40	0.70925	9.99×10^{-7}	0.59082
60	1.06390	1.56×10^{-6}	0.92158
60	1.06390	1.48×10^{-6}	0.87635
80	1.41850	1.96×10^{-6}	0.11618
80	1.41850	1.89×10^{-6}	0.11910
100	1.77310	2.20×10^{-6}	1.29970
100	1.77310	2.21×10^{-6}	1.30450

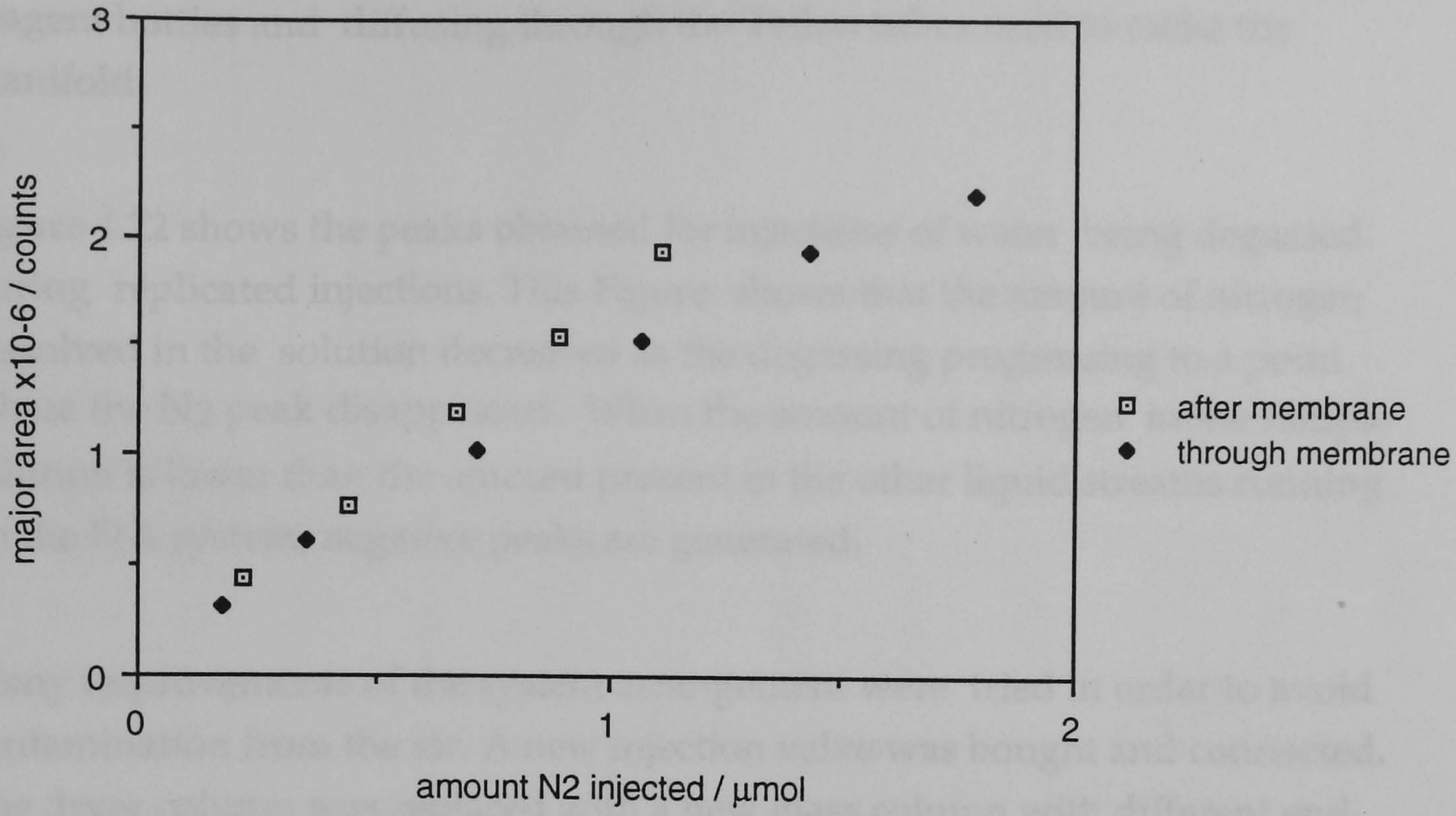

Figure 4.21 Calibration graphs of pure N_2 injected directly and N_2 generated from aqueous standards. injected as a gas straight to the detector.

The stability of isotopic ratio data is acceptable for the instrument indicating that the drier and the TCD were not producing any discrimination. The peak areas for the injections of N_2 gas produced a slope of 1.689455 A mol^{-1} and a correlation coefficient of 0.999. Similarly, the sensitivity for N_2 generated from the aqueous standards was 1.88146 Amol^{-1}. The ratio of these slopes yields an estimate for the membrane transport efficiency of 89.8 %. It appears from Figure 4.21 that the efficiency may be reducing at higher concentrations, but as all other calibration graphs were linear over this concentration range, this apparent curvature was considered to be an artefact of this experiment.

Contamination with atmospheric N_2 was the reason why the FIA system generated high background signals and also probably the bias in the measured isotopic ratios. Nitrogen has high solubility in aqueous solutions, 1.83ml in 100ml. However, background level per se is not the problem rather the temporal variation in background as discussed later. Even with this closed

system , it was not sealed enough to avoid some nitrogen ingressing into the reagent bottles and diffusing through the Teflon tubes used to make the manifold.

Figure 4.22 shows the peaks obtained for injections of water being degassed during replicated injections. This Figure shows that the amount of nitrogen dissolved in the solution decreased as the degassing progressing to a point where the N_2 peak disappeared. When the amount of nitrogen in the sample solution is lower than the amount present in the other liquid streams running on the FIA system, negative peaks are generated.

Many improvements of the system arrangement were tried in order to avoid contamination from the air. A new injection valve was bought and connected. The dryer column was replaced with a new glass column with different end connection. But, inaccurate results continued being produced.

The presence of the dryer column was detrimental to peak shapes, the drying reagent needs periodic replacement and the connections are a potential source of leaks. As an alternative, the wet gas from the GD-separator unit was continuously dried by using a hygroscopic Nafion (DuPont) membrane (described in the chapter 1) as a dryer unit. The arrangement for this dryer unit was similar that used for the GD-separator unit. The outer containing tube was a stainless- steel tube having T-piece connectors on the ends. As the wet gas from the acceptor stream passes through the inner membrane, the moisture is removed and transferred to its outer surface. A dry flow of He gas flows was directed in a direction opposite to that of the wet gas thus removing the moisture on the outer surface of the membrane[51, 79]. The peaks generated when isotopic ratio standards were injected with the system using each dryer unit are shown in Figure 4.23 and the results are tabulated and compared in Table 4.20.

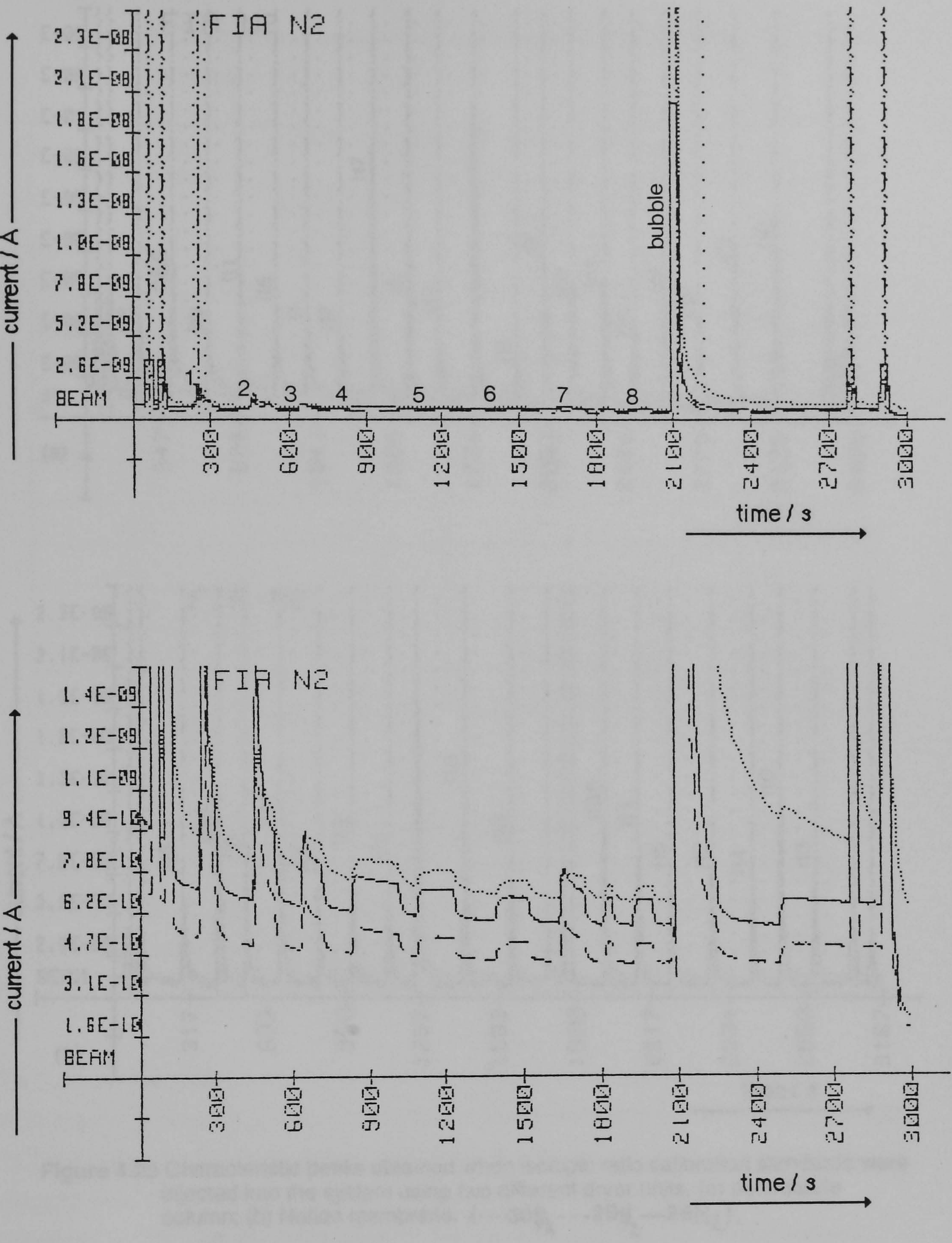

Figure 4.22 Characteristic peaks obtained when water is injected without be degassed and after being continuously degassed.(a) normal size of trace peaks; (b) expansion of the trace peaks.

....$30N_2$
- - -$29N_2$
—$28N_2$

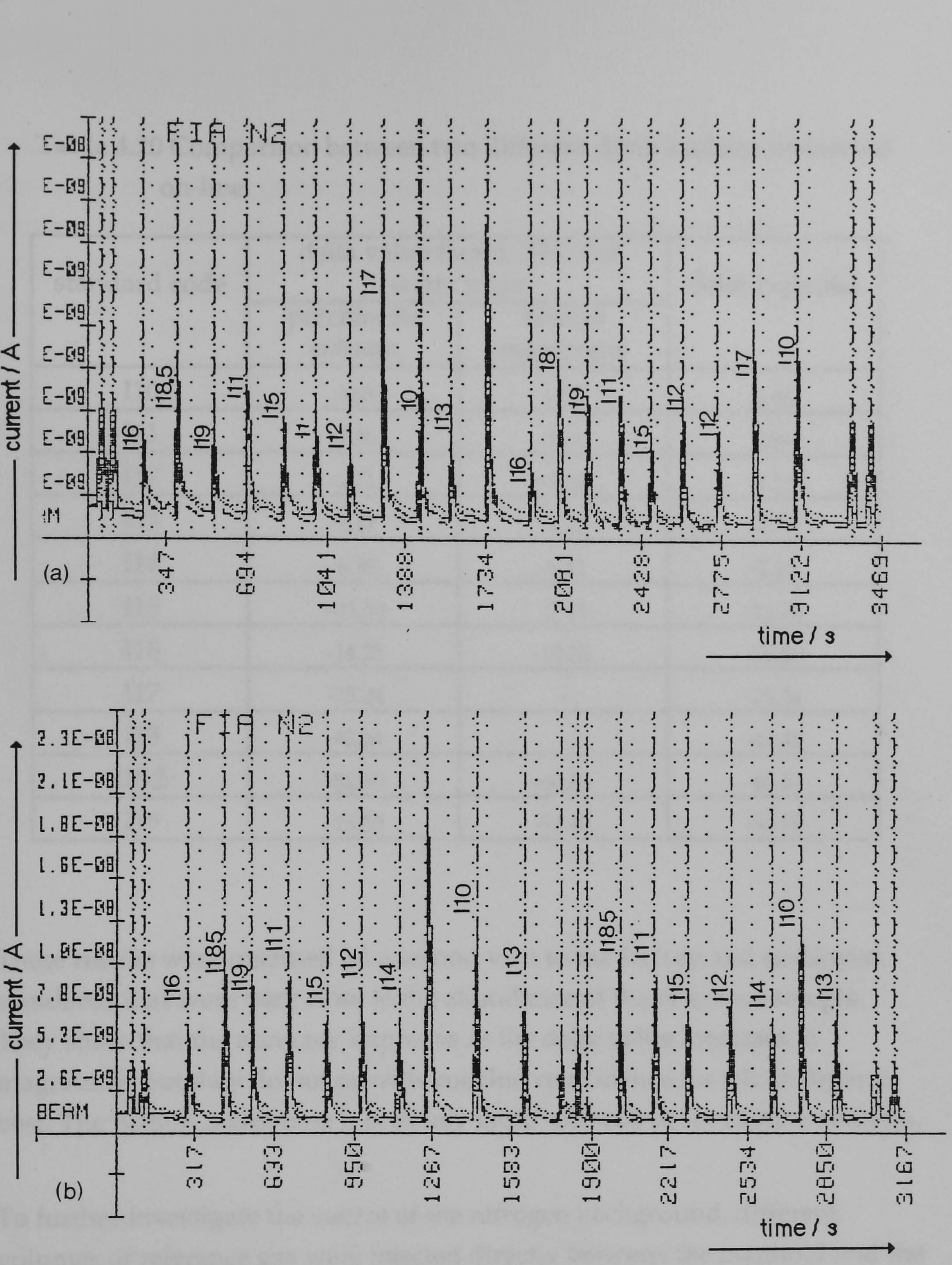

Figure 4.23 Characteristic peaks obtained when isotopic ratio calibration standards were injected into the system using two different dryer units. (a) perchlorate column; (b) Nafion membrane. (···$^{30}N_2$ - - -$^{29}N_2$ —$^{28}N_2$).

Table 4.20 Comparison between two different dryer systems connected on-line.

standard code	delta value found different water traps		delta expected
	perchlorate column	Nafion membrane	
I10	0.50	1.33	2.46
I11	-1.36	-1.69	0.84
I12	-1.71	-1.28	-1.17
I13	-4.17	-4.42	-3.73
I14	-6.35	-6.41	-7.10
I15	--11.34	-7.59	-11.73
I16	-14.25	-10.55	-18.50
I17	-25.24	-	-29.34
I18	-43.64	-	-49.48
I18.5	-52.59	-60.82	-65.61
I19	-75.38	-87.40	-98.79

These results were obtained on a second visit to the factory and employed standards that were very close to the abundance of the reference sample. They show that the accuracy improves as the delta value increases in magnitude, but they do not provide conclusive evidence for which dryer is best. The Nafion membrane is certainly more convenient for routine analysis.

To further investigate the source of the nitrogen background, different volumes of reference gas were injected directly between the manifold and the TCD: (i) reagent flows stopped, but He flowing around the membrane; (ii) reagent flows running (no sample injection) and He flowing around the membrane. The results are shown in Figure 4.24 and the measured values tabulated in Table 4.21. The background signals are the same order of magnitude changing only from 4.17×10^{-10} for the liquid flow off to 9.6×10^{-10} for the liquid flow on. The stopped liquid flow should be rapidly completely degassed and therefore the background should have been considerably reduced. That it was not suggest that in this experiment some nitrogen was present in the He flow. The results for delta values are

contradictory in that the stopped flow conditions produced a greater deviation from the expected value when the liquid flow was on. No explanation can be offered for this values then was some residual contamination from a previous positive delta sample remaining in the liquid flow line.

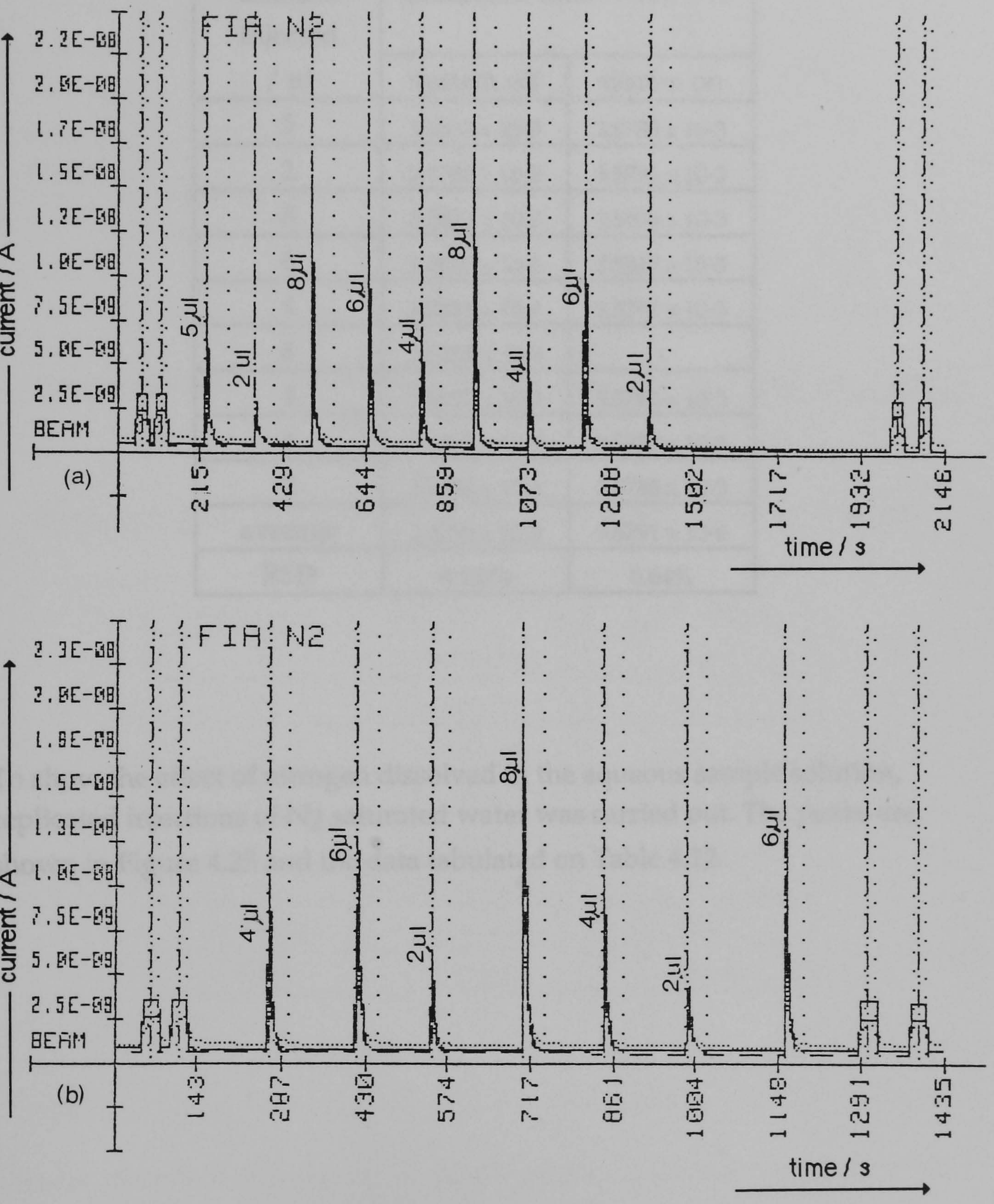

Figure 4.24 Characteristic peaks obtained for different volumes of reference gas injected into the acceptor gaseous helium stream; (a) liquid streams off; (b) liquid streams on. ...30N_2; - 29N_2 - 28N_2.)

Table 4.21 Comparison between the delta values found when reference gas was injected into the acceptor gaseous stream with and without running the liquid streams. Expected value for the $^{15}N/^{14}N$ ratio in the reference gas 0.003664.

amount injected / µl	measured ratio $^{15}N/^{14}N$	
	system off	system on
5	3.5832 x 10-3	3.5788 x 10-3
2	3.5785 x 10-3	3.5790 x 10-3
8	3.5822 x 10-3	3.5806 x 10-3
6	3.5810 x 10-3	3.5813 x 10-3
4	3.5811 x 10-3	3.5794 x 10-3
8	3.5814 x 10-3	-
4	3.5807 x 10-3	3.5762 x 10-3
6	3.5739 x 10-3	3.5788 x 10-3
2	3.5782 x 10-3	3.5788 x 10-3
average	3.5790 x 10-3	3.5791 x 10-6
RSD	0.137%	0.04%

To show the effect of nitrogen dissolved in the aqueous sample solution, replicated injections of N_2 saturated water was carried out. The peaks are shown in Figure 4.25 and the data tabulated on Table 4.22.

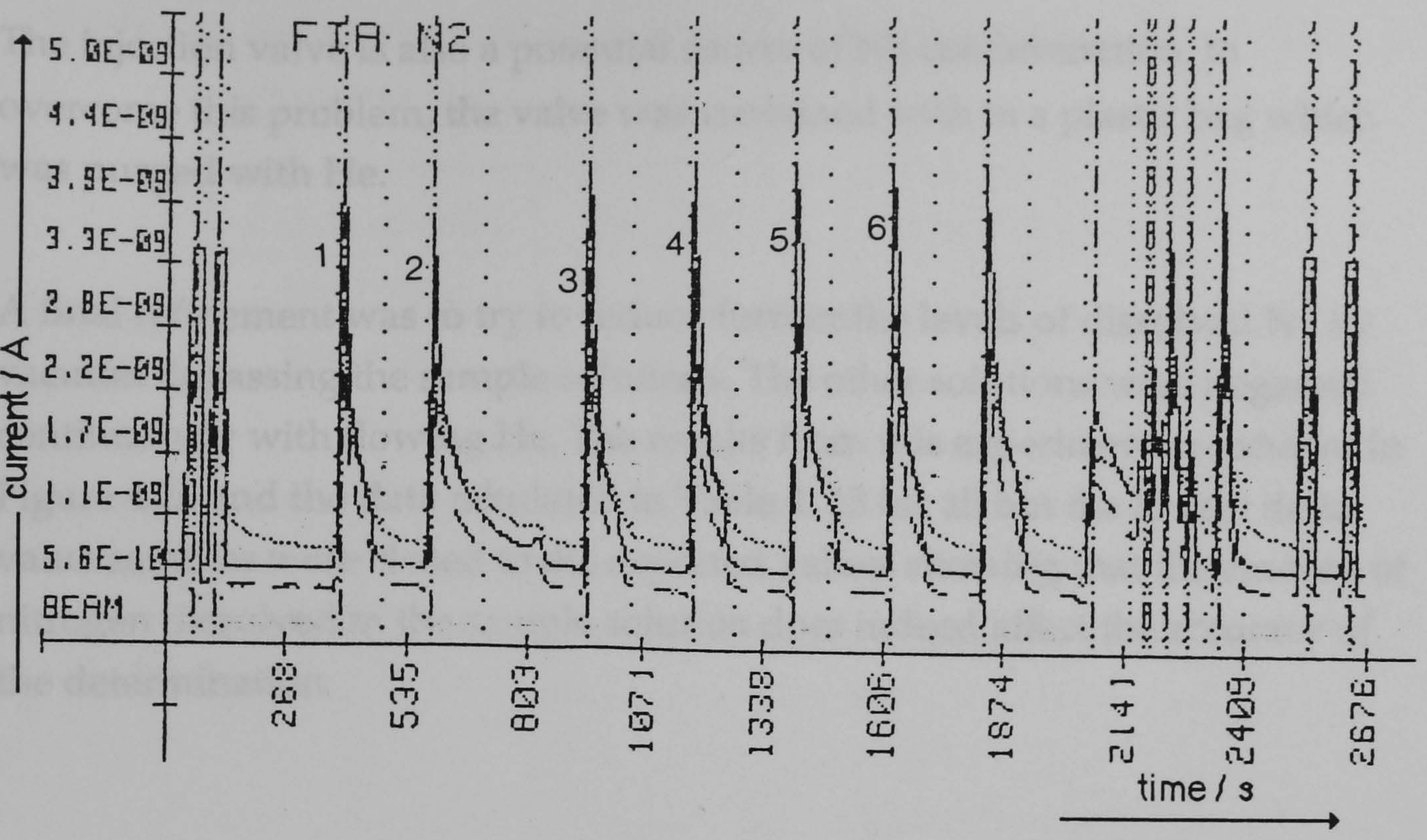

Figure 4.25 Peaks for replicates injections of N_2 saturated water .(···30N_2- 29N_2-28N_2) .

Table 4.22 Delta values found when N_2 saturated water was injected.

replicate n°	ratio measured	delta found
1	3.5951 x 10-3	1.25
2	3.5946 x 10-3	1.21
3	3.5940 x 10-3	0.91
4	3.5935 x 10-3	0.65
5	3.5924 x 10-3	1.10
6	3.5940 x 10-3	0.67
average	3.5939 x 10-3	0.96
RSD	0.026%	0.027%

Clearly, dissolved nitrogen in the sample solution behaves as an additional sample component whose isotope ratio may bias the observed result for the true sample. The expected delta values for atmospheric N_2 should be close to zero as are there shown in Table 4.22 remembering that a unit change in delta is only a 1 part per 1000 change in the isotopic ratio.

The injection valve is also a potential source of N_2 contamination. to overcome this problem, the valve was contained with in a plastic bag which was purged with He.

A final refinement was to try to reduce further the levels of dissolved N by vacuum degassing the sample solutions. The other solutions were degassed continuously with flowing He. The results from this experiment are shown in Figure 4.26 and the data tabulated in Table 4. 23 for all but the lowest delta value samples were closed to the expected values showing that the amount of nitrogen dissolved in the sample solution does indeed affect the accuracy of the determination.

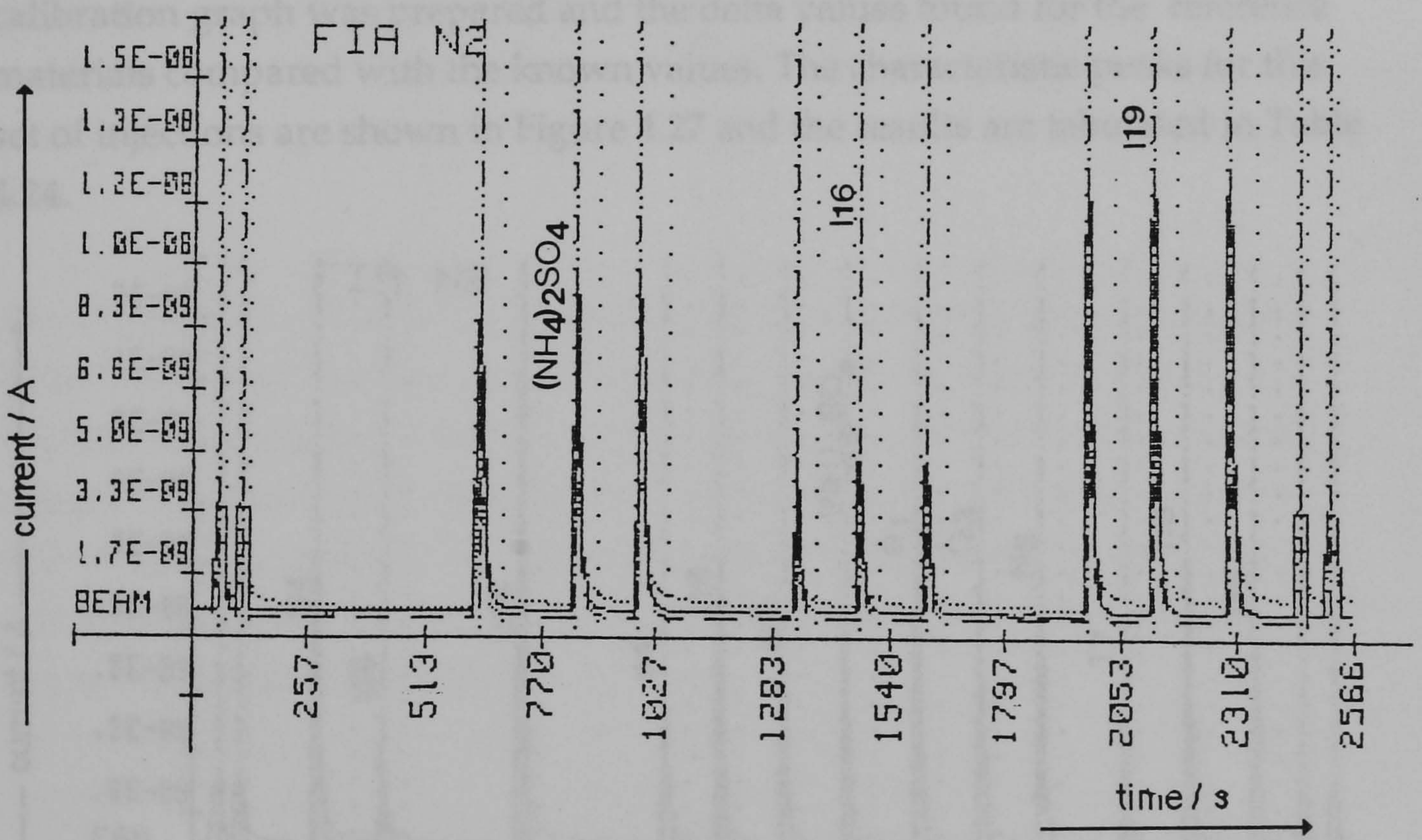

Figure 4.26 Characteristic peaks for different injections after vacuum degassing of the sample solution. (··· $30N_2$ - $29N_2$ - $28N_2$).

Table **4.23** delta values obtained after vacuum degassing of the sample solution.

standard code	delta found	delta expected
$(NH_4)_2SO_4$	-0.052	-0.27
$(NH_4)_2SO_4$	-0.066	-0.27
I16	-16.15	-17.78
I16	-16.25	-17.78
I19	-96.24	-96.96
I19	-94.09	-96.96

Having obtained some encouraging results, the reference materials were then analysed using vacuum degassing of the standards and sample solutions. A calibration graph was prepared and the delta values found for the reference materials compared with the known values. The characteristic peaks for this set of injections are shown in Figure 4.27 and the results are tabulated in Table 4.24.

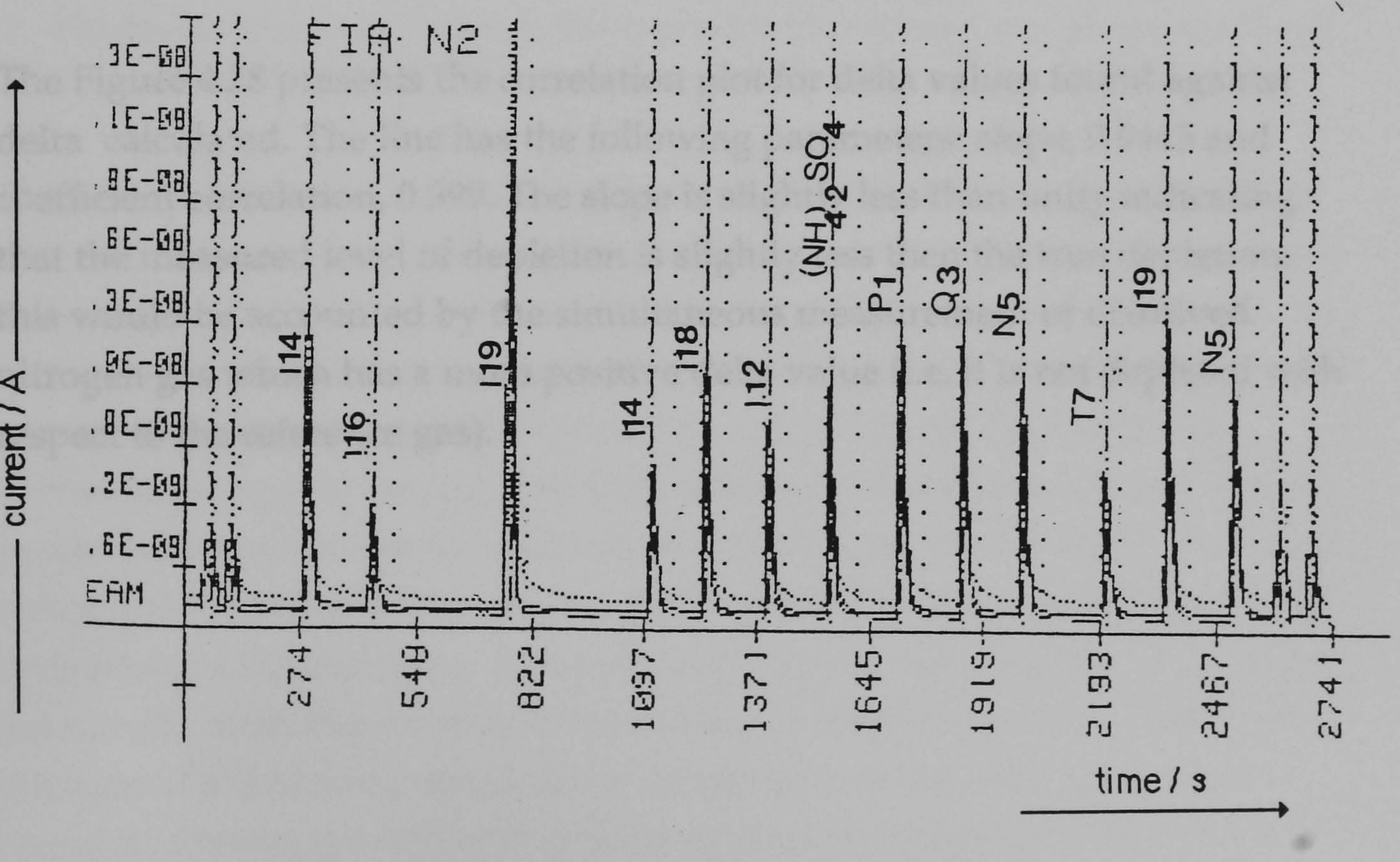

Figure 4. 23 Characteristic peaks for the calibration isotopic ratio standards and reference material solutions.(···$30N_2$-$29N_2$-$28N_2$).

Table 4.24 Values found for isotopic standards and reference material. All sample solution were vacuum degassed before injection.

solution injected code	delta found	delta expected
I10	2.66	2.47
I16	-15.28	-18.50
I14	-5.69	-7.10
I18	-45.46	-49.48
I12	-0.55	-0.84
$(NH_4)_2SO_4$	-0.19	-0.27
P1	-1.13	-1.09
Q3	-2.60	-3.01
N5	-3.15	-4.11
T7	7.01	6.57
I19	-93.45	-99.89
N5	-3.34	-4.11

The Figure 4.28 presents the correlation plot for delta values found against delta calculated. The line has the following parameters: slope, 0.9445 and coefficient correlation, 0.999. The slope is slightly less than unity indicating that the measured level of depletion is slightly less then the true depletion. this would be accounted by the simultaneous measurement of dissolved nitrogen gas which has a more positive delta value (i.e. it is not depleted with respect to the reference gas).

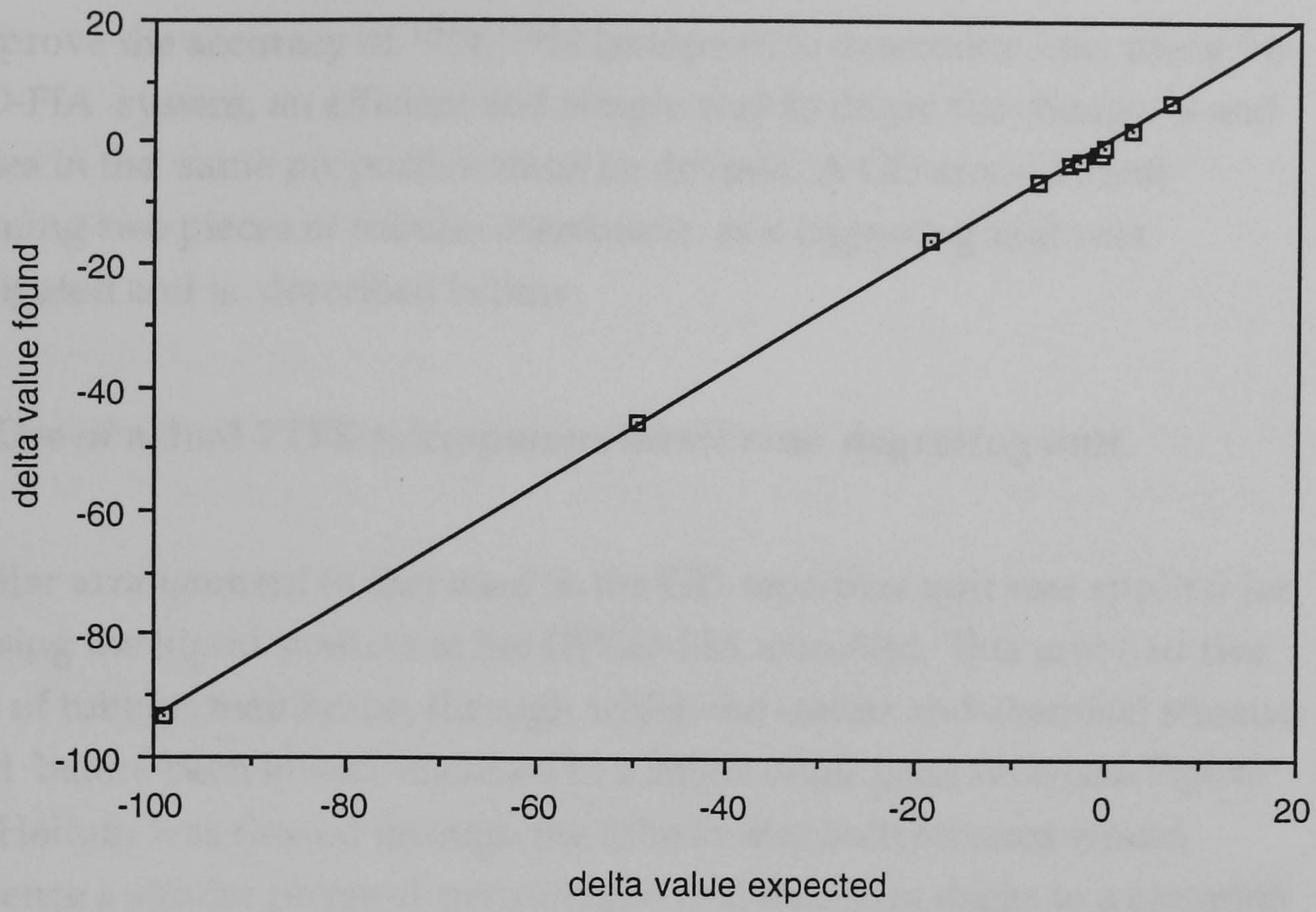

Figure 4.28 Comparison between the delta found and expected. Using a vacuum line to degas the solutions.

The results obtained for the determination of $^{15}N/^{14}N$ isotope ratios have shown that the amount of external nitrogen dissolved in the sample solutions is the most critical factor affecting the accuracy of the results. Contaminations of the sample with dissolved nitrogen cause its apparent abundance to become enriched or depleted depending on its original ^{15}N abundance. However, a constant background level of dissolved nitrogen is not of itself a problem because the background count is subtracted from the total ion count before isotope ratios are computed. It is important that the all background level must be stable during the appearance time of the ion peak. Therefore, the sample solutions must have the same quantities of nitrogen (ideally no nitrogen at all) as that present in the carrier stream because if any of the chemical streams are different in concentration of nitrogen, the baseline will change during the appearance time of the peak. The software can make no

allowance for such changes and positive or negative deviations from the true abundances will occur.

To improve the accuracy of $^{15}N/^{14}N$ isotope ratio determinations using the DPGD-FIA system, an efficient and simple way to degas the chemicals and samples in the same proportion must be devised. A GD arrangement containing two pieces of tubular membrane as a degassing unit was investigated and is described bellow.

4.3.3 Use of a dual PTFE-microporous membrane degassing unit.

A similar arrangement to that used in the GD-separator unit was applied for degassing the liquid streams in the DPGD-FIA manifold. This unit had two pieces of tubular membrane, through which the carrier and chemical streams passed before been mixed, enclosed in a single onter glass tube (see Figure 4.29). Helium was flowed through the tube so that both streams would experience a similar physical environment and therefore degas to a common level.

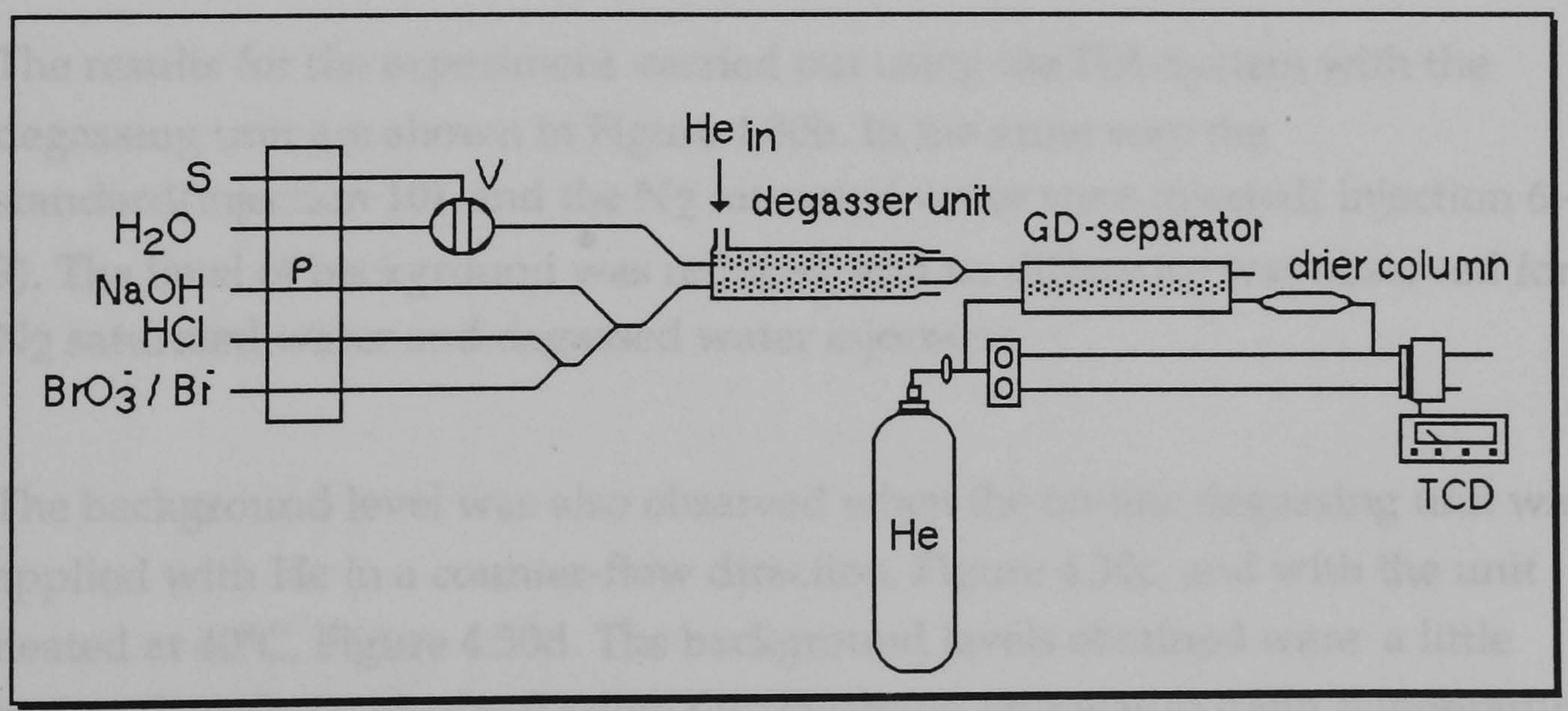

Figure 4.29 DPGD-FIA manifold containing a degasser unit on-line.

The investigation was carried out using the DPGD-FIA system with the TCD detector. Levels of background were monitored under different operating conditions. The background produced by the FIA system with and without the degassing unit were compared with that level measured when only He was flowing in both reference and sample streams of the detector. The investigation was carried out injecting N_2 saturated and degassed water samples and a standard solution containing 60ppm total nitrogen.

4.3.3.1 Results and discussion

The first result was obtained with the FIA system coupled to the detector, but without the degassing unit. The results are shown in Figure 4.30a. The first injection of 0.5ml of N_2 saturated water into a saturated reagent stream generated no peak (injection 1) but when the water started to be degassed with a He probe (injections 3, 4, and 5) negative peaks appeared. These negative peaks show that the sample plug contained less nitrogen than the carrier stream. The amount of nitrogen degassed from the water could be calculated by comparison of the height of the negative peak(1.6cm) with that obtained by injecting a 60ppm N standard (injection 2) that produced a peak 8.5 cm high. The negative peak corresponds to 11.3ppmN. This result is in concordance with the solubility of this gas in water, i.e. 1.9ml in 100 ml H_2O, which translated to 11.7 ppm of N in the N_2 saturated water.

The results for the experiment carried out using the FIA-system with the degassing unit are shown in Figure 4.30b. In the same way the standard(injection 10) and the N_2 saturated water were injected(injection 6 - 9). The level of background was reduced and no difference was observed for N_2 saturated water and degassed water injections.

The background level was also observed when the on-line degassing unit was applied with He in a counter-flow direction, Figure 4.30c, and with the unit heated at 40°C, Figure 4.30d. The background levels obtained were a little higher than those obtained when the degassing unit was at room temperature and the He flow was in the same direction as the liquid flow. These results suggest that, contrary to expectation, no benefits were gained from these modifications.

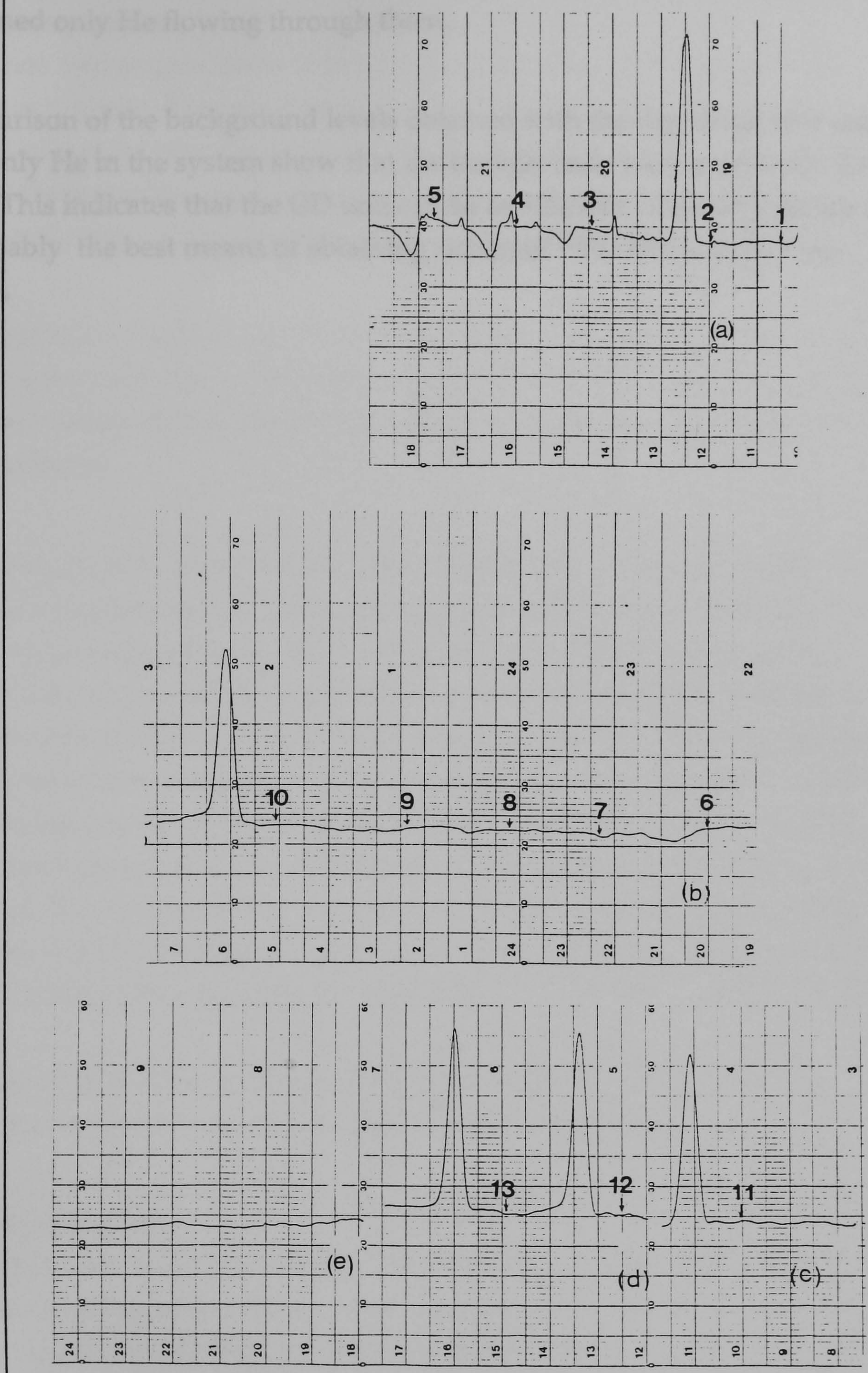

Figure 4.30 Background levels for different manifold arrangements; (a) without degassing unit; (b) with degassing unit; (c) degassing unit heated at 40ºC; (d) counter He flow and (e) without FIA system (pure He flowing).

Figure 4.30 (e) shows the background level obtained when the TCD channels contained only He flowing through them..

Comparison of the background levels obtained with the degassing unit and with only He in the system show that the backgrounds were essentially the same. This indicates that the GD unit can be an efficient degassing device and is probably the best means of obtaining accurate $^{15}N/^{14}N$ isotope ratio results.

4.4 Determination of inorganic forms of nitrogen by DPGD-FIA system - preliminary results.

The other two majors forms of inorganic nitrogen in natural samples are nitrate and nitrite. They are found together in soils, waters, effluents, biologically active materials and in some food products. Determination of the ratio of these species in environmental samples, is of vital importance because of potential toxicity even when present in micro amounts.

Although many methods are available for the determination of nitrates or nitrites separately, their simultaneous determination in binary mixtures has not been widely studied and little attention has been given to isotope ratio measurements.

It was recently demonstrated that nitrate and nitrite can be reduced to ammonia by passing them solutions through a column filled with metallic zinc. The procedure has been automated by the use of a steady-state, air-segmented, continuous-flow method [147]. Alternative methods make use of the reduction of nitrate to nitrite with homogeneous [148, 149] or heterogeneous [150, 151] reductants followed by a diazotization and coupling colour reaction. Ammonium ion can be determined by the well known Berthelot reaction. Therefore to determine total nitrogen at least two separate manifolds are required. A recently reported computer-controlled continuous-flow analyser has been used for this task, but the total inorganic nitrogen could be found only indirectly after summing the contributions of NO_3-N, NO_2-N and NH_4-N [152].

Using the DPGD-FIA technique, the form of nitrogen under analysis is converted to ammonium and is determined as nitrogen gas.

4.4.1 Experimental

The DPGD-FIA system developed for nitrogen gas generation was used with an additional line where the inorganic forms of nitrogen (nitrite and nitrate) present in the sample were reduced to ammonia before the oxidation to N_2 takes place. This proposed DPGD-FIA arrangement is shown in Figure 4.29.

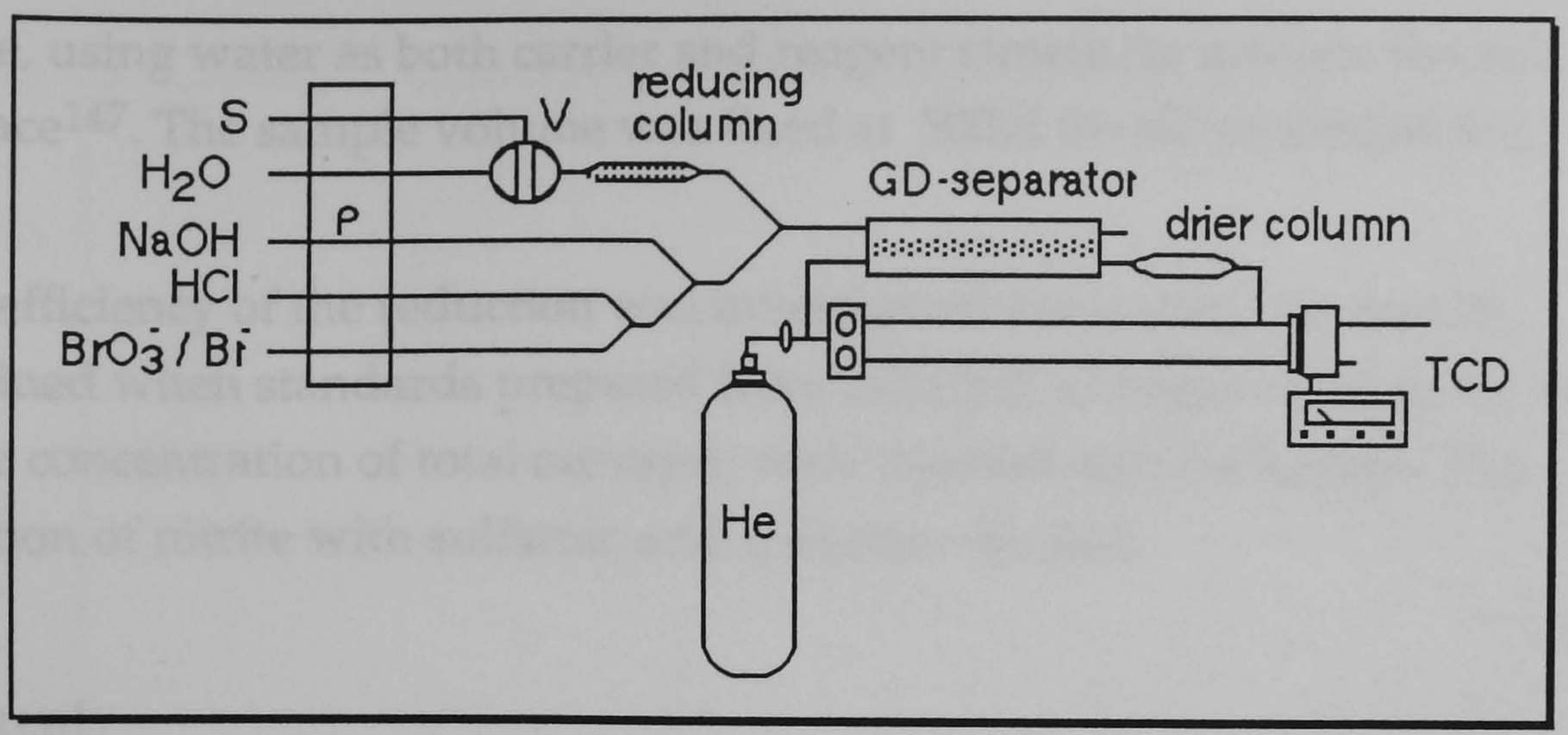

Figure 4.29 DPGD-FIA manifold used for determination of different inorganic forms of nitrogen.

One approach to the determination of nitrate in the presence of nitrite depends on the fact that sulfamic acid decomposes nitrite rapidly and quantitatively to nitrogen at room temperature, but does not react with ammonium or nitrate or interfere with the on-line reducing step (NO_3/NO_2 -- NH_4)[129]. The convertion of nitrite to nitrogen by sulfamic acid is given by[153]:

$$KNO_2 + HSO_3NH_2 \quad \text{----} \quad N_2 + KHSO_4 + H_2O$$

This reaction could be used to generate nitrogen gas for mass spectrometry, but due the requirement fo isotopic ratio determination it is not a good choice because the nitrogen molecules produced contain 1 nitrogen atom from the sample and one from the reagent.

The alternative is to produce nitrogen via the intermediate of ammonium ion as described before.

Preliminary investigations were carried out using two different sizes of reducing columns filled with metallic zinc. One was made with 50 cm Tygon tube of 2mm i.d. containing a zinc wire of 1 mm diameter; the other was made with a glass tube, 5.5 mm i.d. and 10 cm long, filled with 20 mesh zinc granules. Glass-wool was employed to retain the zinc inside the column. Before using the column, 0.1M aqueous CuSO4 solution was injected once or

twice, using water as both carrier and reagent stream, to activate the zinc surface[147]. The sample volume was fixed at 500µl for all investigations.

The efficiency of the reduction was investigated comparing the results obtained when standards prepared from different nitrogen species, but with same concentration of total nitrogen, were injected into the system. The reaction of nitrite with sulfamic acid was also studied.

Reagents

The reagents used for nitrogen generation are described in section 4.2.2.1

-standard nitrite stock solution containing 1000ppmN (or 3287ppm NO_2)was prepared from analytical reagent grade potassium nitrite; 3.037g into 500ml water. Calibration standards were prepared daily.

-standard nitrate stock solution containing 1000ppmN (or 4430ppmNO_3) was prepared from analytical reagent grade potassium nitrate. Calibration standards were prepared daily.

-metallic zinc (20-mesh), supplied by Aldrich.

-zinc wire, 99.99% pure, 1mm diameter

-copper sulphate solution, 0.1M

-sulfamic acid solution, 8% (w/v)

4.4.2 Results and discussion

The experiments carried out using the Zn wire as a reductor showed good efficiency for the nitrite, but poor results were obtained for nitrate. Figure 4.30 shows the calibration graphs prepared when standards containing the same amount of nitrogen, but prepared from different salts were injected into the system with this reductor present.

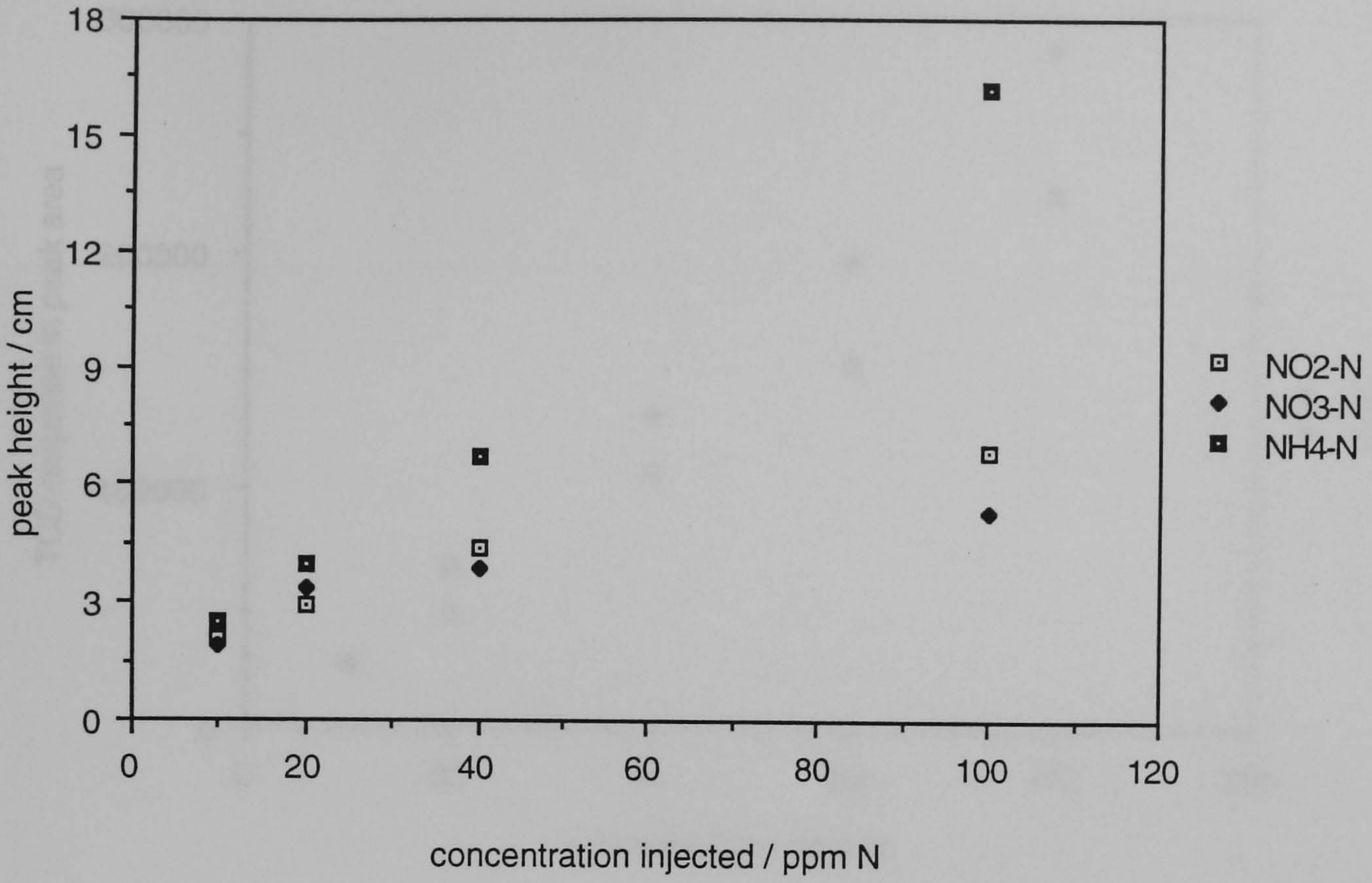

Figure 4.30 Calibration graphs obtained for standards prepared from different forms of nitrogen .

The reduction column containing zinc granules was then placed on-line and standards of NO_3-N and NH_4-N injected. The Figure 4.31 shows the calibration graphs obtained.

The zinc granules allow a larger contact area and showed greater efficiency than the zinc wire. Due the low sensitivity of the TCD detector, a high concentration range was used that saturated the reducing column and it had to be re-activated with $CuSO_4$ solution after each run.

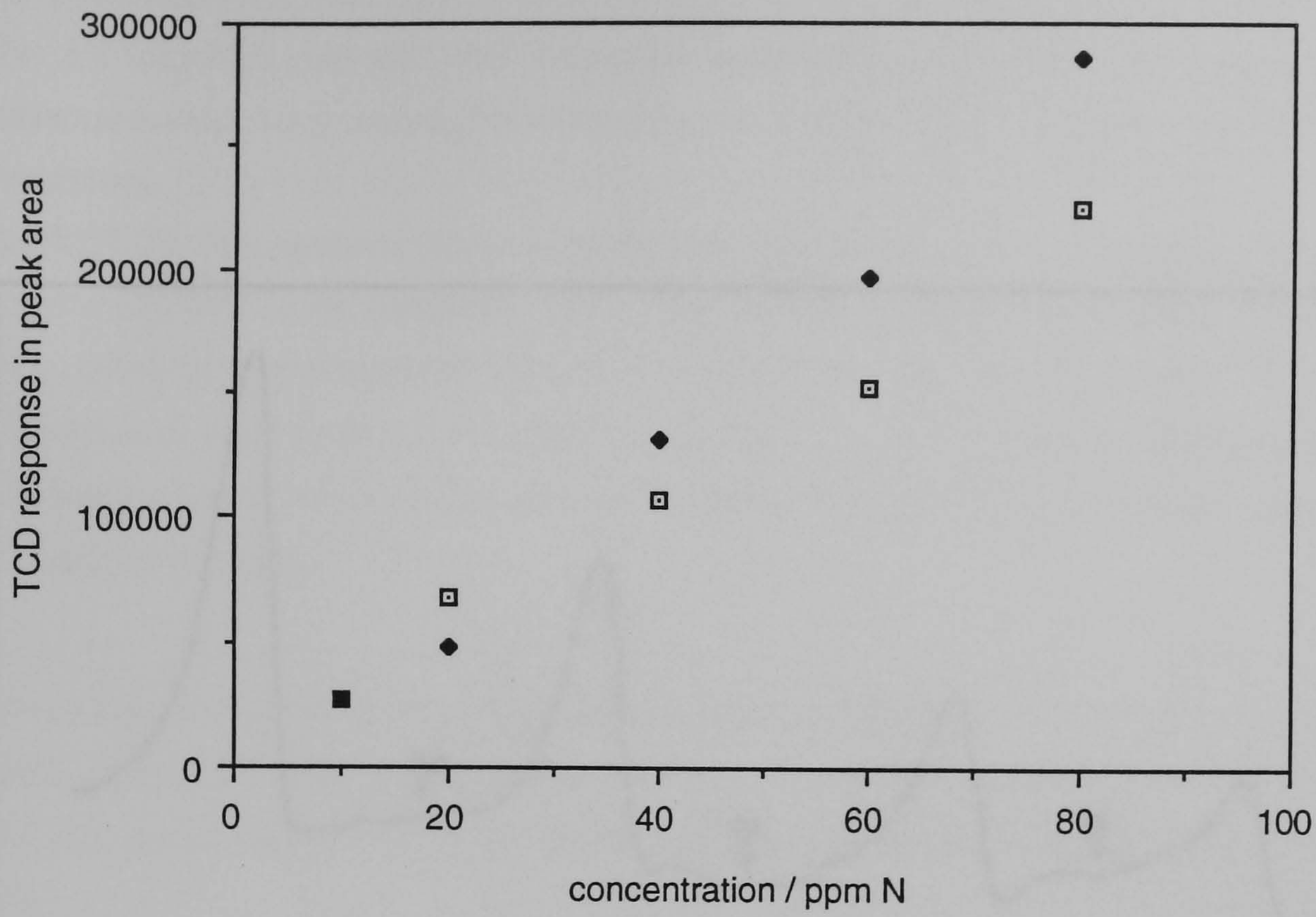

Figure 4.31 Calibration graphs obtained from injecting different forms of nitrogen using a reducing column prepared from zinc granules.

The use of sulfamic acid to reduce the nitrite to nitrogen was also investigated and was found to be simple and effective reaction. The characteristic peaks obtained when nitrite was mixed with this acid on-line are shown in Figure 4.32 and are compared with peaks obtained when NH_4-N was injected on-line. Higher peaks were found for the determination carried out with sulfamic acid due the stoichiometry of the reaction. This result is an amplification factor of 2 because of the additional nitrogen from the reducing acid.

The preliminary results show that the DPGD-FIA system used for nitrogen gas generation can be successfully explored for inorganic nitrogen speciation. However, the concentration of these species present in environmental samples is in the range of 0.2-1.5 $\mu g\ ml^{-1}$ for NO_3^- and NO_2^-. This is about 10 times smaller than the detection limit of the TCD detector, but such determinations would be feasible with mass spectrometric detection.

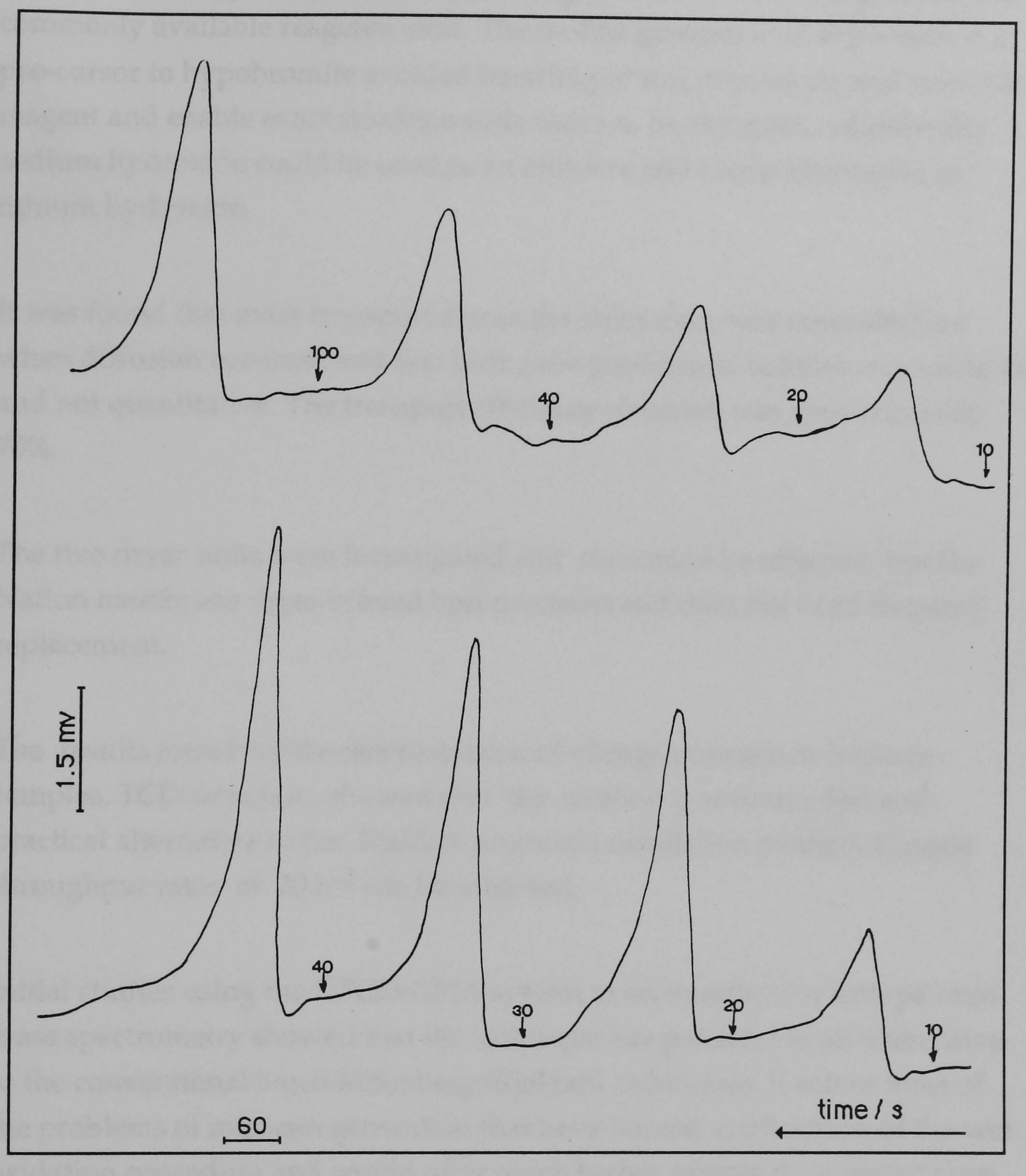

Figure 4. 32 Characteristic peaks obtained when nitrogen gas is generated by (a) reducing NO_2-N first to ammonia and then oxidation and (b) reducing NO_2-N with sulfamic acid.

4.5 Conclusion

The DPGD-FIA system was found to be an efficient method for generating gaseous sample for nitrogen determinations with TCD or mass spectrometry detection.

The DPGD-FIA system has a simple configuration and was inexpensive and commonly available reagents used. The on-line generation of Br_2 which is a pre-cursor to hypobromite avoided handling of this unpleasant and unstable reagent and enable exact stoichiometric ratios to be obtained. Additionally, sodium hydroxide could be used as an effective and cheap alternative to lithium hydroxide.

It was found that mass transport across the membrane was most efficient when diffusion occurred and that bulk flow pre-formed bubbles was unstable and not quantitative. The transport efficiency obtained was approximately 90%.

The two dryer units were investigated and showed to be effective but the Nafion membrane dryer offered best precision and does not need frequent replacement.

The results found for the determination of nitrogen content in herbage samples, TCD detection, showed that the method is accurate, fast and practical alternative to the Kjeldahl ammonia distillation method. Sample throughput rates of 20 h^{-1} can be achieved.

Initial studies using the DPGD-GFIA system as an interface for isotope ratio mass spectrometry showed that the technique has potential as an alternative to the conventional batch Rittenberg/Kjeldahl techniques. It solves most of the problems of nitrogen generation that have limited applications of the wet oxidation procedure and would offer much higher sample throughput rates.

The technique also offers a low cost alternative to the Dumas combustion type system and incorporates the possibility of speciation. However, it does not yet achieve the same levels of accuracy although precision compares favourably. There is no evidence of mass discrimination occurring in the membrane as might be expected since the pore size is large (10µm) compared with

molecular dimensions. Inaccuracy appears to derive from residual differences in the dissolved N_2 gas status of the different liquid streams. A dual membrane degassing unit has been developed that appears to overcome this problem, at least using TCD detection, and future work will involve testing its use with mass spectrometry.

CHAPTER FIVE
CONCLUSIONS AND SUGGESTIONS FOR FURTHER WORK.

5.1 Conclusions.

It has been shown that the mass transport through a microporous membrane is a process involving diffusive and convective forces. The rate of transport is dependent on diffusive resistances caused by the size and distribution of the membrane pores (effective area) and by the external atmospheric conditions. Convective forces caused by the air movement surrounding porous media can break up the boundary layer between the membrane surface and the external atmosphere. These convective forces are critical because they control the concentration gradient which is the driving force for the transport process.

The tubular membrane studied was demonstrated to have potential as a universal preconcentration device for samples in aqueous solutions. This type of preconcentrator can be successfully applied when the fewest number of sample manipulations and chemical additions are desirable such as in trace analysis.

The tubular membrane exhibits substantial dispersion effects associated with its length and internal volume. However, due its concentrating action and using appropriate sample loop size, liquid flow rate and temperature, this effect can be reduced and high preconcentration factors achieved.

Although the membrane preconcentrator unit improved detection limits, it had the disadvantage of low stability that resulted in poor reproducibility when it was used in flow injection analysis.

The DPGD-FIA system developed showed a considerable potential for generating N_2 gas for routine analysis. It facilitated the on-line preparation of reagents, introduction and change of samples and solved problems of separating the analyte from other species allowing the use of a non-selective detector for nitrogen determination. The on-line oxidation reaction was shown to be efficient, 85%, and the 1m piece of the tubular membrane provided a contact area that allowed efficient separation of N_2 generated

from up to 50μgN in the sample solution. The separation efficiency was 92%. The method was precise and accurate for the determination of total nitrogen with both detectors (MS and TCD). The precision was good for $^{15}N/^{14}N$ isotope ratio determinations but the accuracy of the results was affected by contamination from atmospheric N_2.

A membrane degassing unit has been described as a means of avoiding such contamination. Its use drastically decreased the background N_2 levels detected from the FIA system.

It was also shown that the DPGD-FIA system is versatile and can be readily adapted to enable different forms of nitrogen eg NO_3^-, NO_2^-, NH_4^+ to be determined using the same manifold as that for total nitrogen.

The DPGD-FIA interface for isotopic ratio mass spectrometry has advantages over the conventional Kjeldahl/Rittemberg method. These include speed of analysis, ease automation and interfacing to the MS and the ability to determine other forms of nitrogen. Similar advantages exist with respect to continuous flow combustion isotope ratio analysis, but the accuracy is not yet as high as that obtained with these systems.

5.2 Suggestions for further work.

5.2.1 Study of the resistances involved in the mass transport through a microporous membrane.

To be able to predict the mass loss through microporous membranes at known conditions it is necessary to investigate the resistances produced by the boundary layer and the surrounding atmosphere. The factors influencing these resistances are complex involving many variables including turbulence levels in the atmosphere and surface roughness. A practical means of estimating the magnitude of the resistance contribution could be to develop a parametric model similar to the atmospheric deposition model described by Fowler[85]. This would involves replacing the unknown parameters (e.g. A and L) in the diffusion equation by measured values of the resistance.

5.2.2 Application of the DPGD-FIA system using the dual PTFE-microporous membrane degassing unit.

The results obtained for the experiment carried out using a GD unit as a degassing system showed that the background levels associated with dissolved N_2 decreased. The TCD was used as the detector. The next step is to prove the capability of this unit for degassing samples prior to isotopic ratio measurements.

Further improvements in accuracy for isotope ratio measurements might be obtained by replacing the Teflon tubes and connectors, after the degassing unit, with devices made from stainless steel. This way, diffusion of atmospheric nitrogen through the Teflon material could be avoid.

5.2.3 DPGD-FIA system for speciation and total nitrogen determination.

Nitrite and nitrate can be transformed into ammonia by reduction with zinc and this can be oxidised to nitrogen gas. Some investigations were carried out and the results showed (in section 4.4) that the same manifold could be used for both speciation and the determination of total nitrogen.

The possibility for speciation of NO_3^- in presence of NO_2^- has also been discussed based on the reaction of NO_2^- with sulfamic acid. The manifold shown in Figure 5.1 allows for NO_2^- to be removed as N_2 after reaction with sulfamic acid before the reduction to ammonium ion takes place.

5.2.4 Use of the DPGD-FIA system for generating different gaseous analytes.

The DPGD-FIA technique could also be used for generating other gaseous analytes. As discussed in Chapter 2, gaseous species such as: H_2S, HCN, CO_2 etc. could also be generated on-line for IRMS determinations. If the TCD detection is used, it might be necessary to incorporate a circulating loop preconcentration step into the manifold in order to increase the sensitivity of the determination.

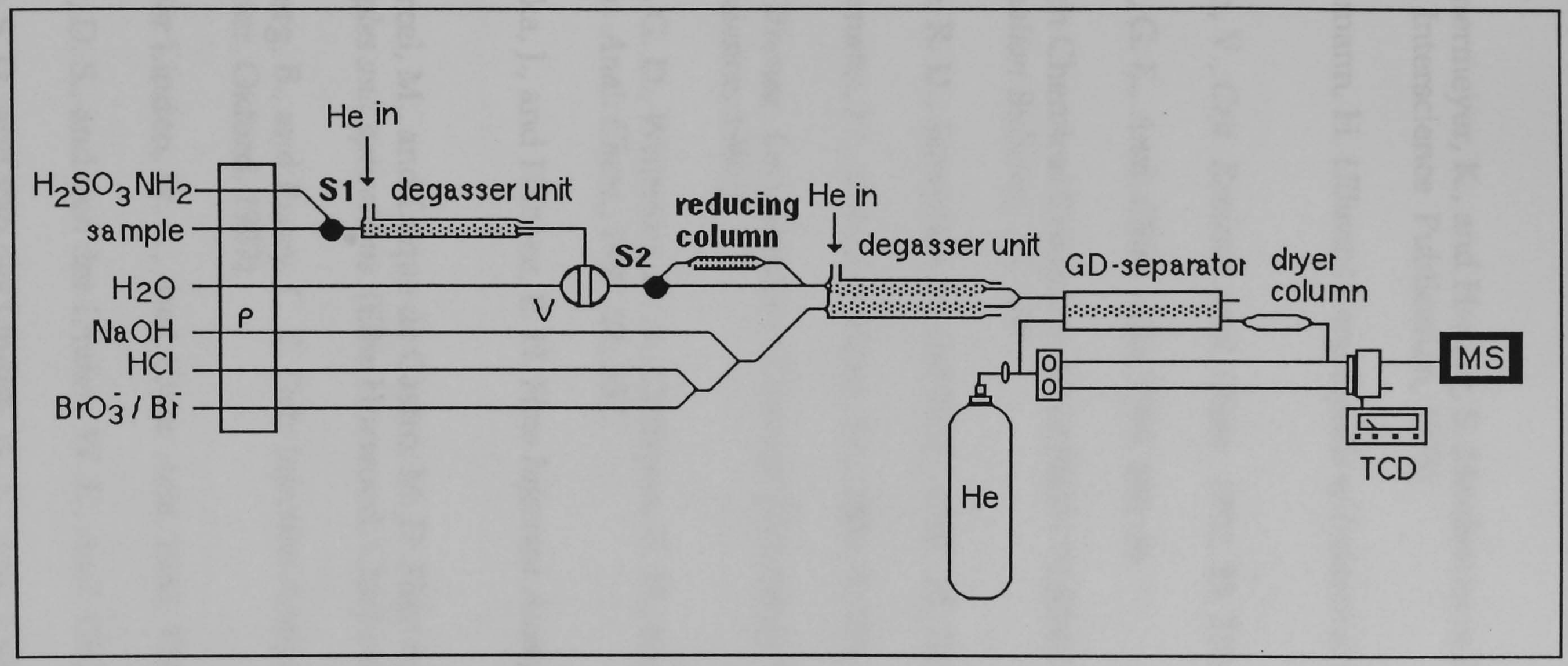

Figure 5.1 DPGD-FIA manifold for determination and speciation of nitrogen. S1 and S2 represent segmented valve to allow the sample to react with sulfamic acid or pass through the reducing column.

REFERENCES

1. Moskin, L. N., and Gurskii, V. S., *Journal of Anal. Chem. USSR*, 1988, **43**, 449.

2. Kammermeyer, K., and Hwang, S. *Membranes in Separations* 1-559 (A Wiley Interscience Publication, 1975).

3. Strathmann, H. *Ullmans Encyclopedia of Industrial Chemistry* (VCH, 1990).

4. Kubán, V., *Crit. Reviews Anal. Chem.*, 1992, **23**, 323.

5. Pacey, G. E., *Anal. Chim. Acta*, 1986, **180**, 36.

6. Aldrich Chemical Company, I. NAFION RESINS - *Technical Information Bulletin*, AL-163 .

7. Noble, R. D., *Separation Sc. and Tech.*, 1987, **22**, 731.

8. Strathmann, H., *Journal of Memb. Sc..*, 1981, **9**, 121.

9. Kirk-Othmer. *Encyclopedia of Chemical Technology* 1-92 (Wiley-Interscience, 1981).

10. Clark, G. D., Whitman, D. A., Christian, G. D., and Ruzicka, J., *Crit. Review Anal. Chem.*, 1990, **21**, 357.

11. Ruzicka, J., and Hansen, E. H. *Flow Injection Analysis* (John Wiley, 1988).

12. Valcárcel, M., and Luque de Castro, M. D. *Flow Injection Analisys. Principles and aplications* (Ellis Horwood, Chichester, 1987).

13. Karlberg, B., and Pacey, C. E. *Flow Injection Analysis - a practical guide* (Elsevier, Oxford, 1989).

14. Van der Linden, W. E., *Anal. Chim. Acta*, 1983, **151**, 359.

15. Kolev, D. S., and van der Linden, W. E., *Anal. Chim. Acta*, 1991, **247**, 51.

16. Kolev, S. D., and van der Linden, W. E., *Anal. Chim. Acta*, 1992., **257**, 317.

17. Kubán, V., *Anal. Chim. Acta*, 1992, **259**, 45.

18. Kubán, V., Dasgupta, K., and Marx, J., *Anal. Chem.*, 1992, **64**, 36.

19. Zhu, Z., and Fang, Z., *Anal. Chim. Acta*, 1987, **198**, 25.

20. Canham, J. S., Gordon, G., and Pacey, G. E., *Anal. Chim. Acta*, 1988, **209**, 157.

21 Attalah, R. H., Rusicka, J., and Christian, G. D., *Anal. Chem.*, 1987, **59**, 2909.

22. Ramasamy, S. M., and Mottola, A., *Anal. Chem.*, 1982, **54**, 283.

23. Rios, A., Luque de Castro, M., and Valcarcel, M., *Anal. Chem.*, 1987, **59**, 666.

24. Kubán, V., and Dasgupta, K., *Anal. Chem.*, 1992, **64**, 1106.

25. Van der Linden, W. E., Reijn, J. M., and Poppe, H., *Anal. Chim. Acta*, 1980, **114**, 105.

26. Kubán, V., *Anal. Chim. Acta*, 1992, **260**, 45.

27. Nakata, R., Kauamura, T., Sakashita, H., and Nitta, A., *Anal. Chim. Acta*, 1988, **208**, 81.

28. Motomizu, S., Toei, K., Kuwaki, T., and Oshima, M., *Anal. Chem.*, 1987, **59**, 2930.

29. Tanaka, A., Mashiba, K., and Deguchi, T., *Anal. Chim. Acta*, 1988, **214**, 259.

30. Ruzicka, J., and Hansen, E. H., *Anal. Chim. Acta*, 1985, **173**, 3.

31. Melcher, R. G., *Anal. Chim. Acta*, 1988, **214**, 299.

32. Baadenhuijsen, H., and Seuren-Jacobs, H. E. H., *Clin. Chem.*, 1979, **25**, 443.

33. Kenny, M. A., and Cheng, M. H., *Clin. Chem.*, 1972, **18**, 352.

34. Linares, P., Luque de Catro, M. D., and Válcarcel, M., *Anal. Chim. Acta*, 1989, **225**, 443.

35. Carlson, R. M., *Anal. Chem.*, 1978, **50**, 1528.

36. Rohwedder, J. J. R., and Pasquini, C., *Analyst*, 1991, **116**, 841.

37. Blet, V., Pons, M. N., and Greffe, J. L., *Anal. Chim. Acta*, 1989, **219**, 309.

38. Spinks, T. L., and Pacey, G. E., *Anal. Chim. Acta*, 1990, **237**, 503.

39. Chang, Q., *Anal. Chim. Acta*, 1986, **186**, 81.

40. Aoki, T., Uemura, S., and Munemori, M., *Bunseki Kagaku*, 1984, **33**, 505.

41. Marstorp, P., Anfalt, and Andersson, *Anal. Chim. Acta*, 1983, **149**, 281.

42. Van Staden, J. F., and Bassen, W. D., *Lab. Pract,,* 1980, **29**, 1279.

43. Pasquini, C., and Cardoso de Faria, L., *Anal. Chim. Acta*, 1987, **193**, 19.

44. Bartroli, J., Escalada, M., Jorquera, C. J., and Alonso, J., *Anal. Chem.*, 1991, **63**, 2532.

45. Ohura, H., Imato, T., Asano, Y., Yamasaki, S., and Ishibashi, N., *Anal. Sci.*, 1990, **6**, 541.

46. Kunnecke, W., and Schmid, R. D., *Anal. Chim. Acta*, 1990, **234**, 213.

47. Van Son, M., Schothorst, M., and Den Boef, G., *Anal. Chim. Acta*, 1983, **153**, 271.

48. Straka, M. R., Gordon, G., and Pacey, G. E., *Anal. Chim. Acta*, 1985, **57**, 1799.

49. Hara, H., Motoike, A., and Okazaki, S., *Analyst*, 1988, **113**, 113.

50. DeFaria, L. C., and Pasquini, C., *Anal. Chim. Acta*, 1991, **245**, 183.

51. Fernández, B. A., Fernández de la Campa, M. R., and Sanz-Mendel, A., *J. Anal. At. Spectrom.*, 1993, **8**, 1.

52. Nikolic, S. D., Milosavljevic, E. B., Hendrix, J. L., and Nelson, J. H., *Talanta*, 1993, **40**,1283.

53. Barnes, R. M., and Wang, X., *J. Anal. At. Spectrom*. 1988, **3**, 1083.

54. Aoki, T., Ito, K., and Munemori, M., *Bumseki Kagaku*, 1988, **37**, 133.

55. Van Staden, J. F., *Anal. Chim. Acta*, 1992, **261**, 453.

56. Marion, P., Rouillier, M. C., Blet, V., and Pons, M. N., *Anal. Chim. Acta*, 1990, **238**, 117.

57. Schulze, G., Brodowski, M., Elsholz, O., and Thiele, A., *Fresenius Z. . Anal. Chem.*, 1988, **329**, 714.

58. Sweileh, J. A., *Anal. Chim. Acta*, 1989, **220**, 65.

59. Martin, G. B., *Anal. Chim. Acta*, 1986, **19**, 1407.

60. Wolfbeis, O. S., Weis, M. J. P., Leiner, J. P., and Ziegler, W. E., *Anal. Chem.*, 1988, **60**, 2028.

61. Schulze, G., Liu, C. Y., Brodowski, M., Elsholz, O., Frenzel, W., and Moller, J., *Anal. Chim. Acta*, 1988, **214**, 121.

62. Aoki, T., Uemura, S., and Munemori, M., *Anal. chem.*, 1983, **55**, 1620.

63. Sonne, K., and Dasgupta, P. K., *Anal. Chem.*, 1991, **63**, 427.

64. Milosavljevic, E. B., Solujic, L., Hendrix, J. L., and Nelson, J. H., *Anal. Chem.*, 1988, **60**, 2791.

65. Barros, F. G., and Tubino, M., *Analyst*, 1992, **117**, 917.

66. Schondorf, G., and Engelhardt, H., *Fresenius Z. Anal. Chem.*, 1989, **333**, 719.

67. Hangos-Mahr, M., Pungor, E., and Kuznecov, V., *Anal. Chim. Acta*, 1985, **178**, 289.

68. Fang, Z., Zhu, Z., Zhang, S., Xu, S., L., G., and Sun, L., *Anal. Chim. Acta*, 1988, **214**, 41.

69. Figuerola, E., Florido, A., Aguilar, M., and de Pablo, J., *Frezenius Z. Anal. Chem.*, 1988, **331**, 620.

70. Hollowell, D. A., Pacey, G. E., and Gordon, G., *Anal. Chem.*, 1985, **57**, 2851.

71. Gord, J. R., Gordon, G., and Pacey, G. E., *Anal. Chem,*, 1988, **60**, 2.

72. Motomizu, S., and Yoden, T., *Anal. Chim. Acta*, 1992, **261**, 461.

73. De Andrade, J. C., Pasquini, C., Baccan, N., and Van Loon, J. C., *Spectroch. Acta*, 1983, **38B**, 1329.

74. Fang, Z., Xu, S., Wang, X., and Zhang, S., *Anal. Chim. Acta*, 1986, **179**, 325.

75. Wang, X., and Barnes, R. M., *J. Anal. At. Spectrom.*, 1988, **3**, 1091.

76. Chan, W. F., and Hon, P. K., *Analyst*, 1990, **115**, 567.

77. Pacey, G. E., Straka, M. R., and Gord, J. R., *Anal. Chem.*, 1986, **58**, 502.

78. Yamamoto, M., Takada, K., Kumamaru, T., Yasada, M., Yokoyama, S., and Yamamoto, Y., *Anal. Chem.*, 1987, **59**, 2446.

79. Corns, W. T., Ebdon, L., Hill, S. J., and Stockwell, P. B., *Analyst*, 1992, **117**, 717.

80. Canham, J. S., and Pacey, G. E., *Anal. Chim. Acta*, 1988, **214**, 385.

81. Reid, R. C., and Sherwood, T. K. *The Properties of Gases and Liquids* 1-646 (McGraw-Hill Book Company, New York, 1958).

82. Brown, H. T., and Escombe, F., *Ann. Sci. Nat.*, 1900, **3**, 223.

83. Penman, H. L., and Schofield, R. K. *Carbondioxide Fixation and Photosynthesis* 1-115 1951).

84. Monteith, J. L., *Soc. Exp. Biol. Symp.*, 1965, **19**, 205.

85. Fowler, D., *Phil. Trans. R. Lond.*, 1984, **305**, 281.

86. Ruzicka, J., and Hansen, E. H., *Anal. Chim. Acta*, 1973, **99**, 37.

87. Korenaga, T., *Anal. Chim. Acta*, 1992, **261**, 539.

88 Vanderslice, J. T., Stewart, K. K., and Rosenfeld, A. G., *Talanta*, 1981, **28**, 11.

89. Vanderslice, J. T., Beecher, G. R., and Rosenfeld, A. G., *Anal. Chem.*, 1984, **56**, 292.

90. Stults, C. L. M., Wade, A. P., and Crouch, S. R., *Anal. Chim. Acta*, 1987, **192**, 301.

91. Campbell, P. G. C., Bisson, M., Bougie, R., Tessier, A., and Villeneuve, J. P., *Anal. Chem.*, 1983, **55**, 2246.

92. Bertsch, P. M., and Anderson, M. A., *Anal. Chem.*, 1989, **61**, 535.

93. Driscoll, C. T., Baker, J. P., Bisogni, J. J., and Schofield, C. L., *Nature*, 1980, **284**, 9161.

94. Cai, Q., and Khaoo, S. B., *Anal. Chim. Acta*, 1993, **276**, 99.

95. Downard, A. J., Kipton, H., Powell, J., and Xu, S., *Anal. Chim. Acta*, 1991, **251**, 157.

96. Van den Berg, C. M. G., Murphy, K., and Riley, J. P., *Anal. Chim.Acta*, 1986, **188**, 177.

97. Lowe, R. D., and Snook, R. D., *Anal. Chim. Acta*, 1991, **250**, 95.

98. Nagaosa, Y., and Kawabe, H., *Anal. Chem.*, 1991, **63**, 28.

99. Royset, O., *Anal. Chem.*, 1987, **59**, 899.

100. Royset, O., *Anal. Chim. Acta*, 1986, **185**, 75.

101. Figura, P., and McDuffier, B., *Anal. Chem.*, 1979, **51**, 120.

102. Ambe, Y., and Nishikawa, M., *Anal. Chim. Acta*, 1987, **193**, 355.

103. Vilchez, J. L., Navalon, A., Avidad, R., and Garcia-Lopez, T., *Analyst*, 1993, **118**, 303.

104. Mohammed, B., Ure, A. M., and Littlejohn, D., *J. Anal. At. Spectrom.*, 1992, **7**, 695.

105. Craney, C. L., Swartout, K., Smith, F. W., and West, C. D., *Anal. Chem.*, 1986, **58**, 656.

106. Figura, P., and McDuffie, B., *Anal. Chem.*, 1980, **52**, 1433.

107. Porta, V., Sarzanini, C., Abollino, O., Mentasti, E., and Carlini, E., *J. Anal. At. Spectrom.*, 1992, **7**, 19.

108. Koropchak, J. A., and Dabek-Zlotorzynska, E., *Anal. Chem.*, 1988, **60**, 328.

109. Sugimae, A., and Mizoguchi, T., *Anal. Chim. Acta*, 1982, **144**, 205.

110. West, T. S., and Nurnberg, H. W. *The Determination of Trace Metals in Natural Waters* .(Wiley-Interscience, New York, 1981).

111. Seip, H. M., *Water, Air, Soil Pollut.*, 1984, **23**, 81.

112. Persson, J. A., Frech, W., and Cedergren, A., *Anal. Chim. Acta*, 1977, **89**, 119.

113. Hodges, S. C., *Soil Sc. Am. Journal*, 1987, **51**, 57.

114. Driscoll, C. T., *Int. J. Environ. Anal. Chem.*, 1984, **16**, 267.

115. Morrison, G. M., *Analyst*, 1990, **115**, 1371.

116. Dougan, W. K., and Wilson, A. L., *Analyst*, 1974, **99**, 413.

117. Miller, J. C., and Miller, J. N. *Statistics for Analytical Chemistry* 1-227 (Ellis Horwood Limited, Chichester, 1988).

118. Sperling, K., *Fresenius Z. Anal. Chem.*, 1982, **311**, 656.

119. Langford, C., and D.W., G., *Anal. Chim. Acta*, 1992, **256**, 183.

120. Lund, W., *Fresenius J. Anal. chem.*, 1990, **337**, 557.

121. Chakrabarti, C. L., Cheng, J., Back, M. H., and Schroeder, W. H., *Anal. Chim. Acta*, 1993, **267**, 47.

122. Drew, H. D., Streuli, C. A., and Averell, P. R. *The Analytical Chemistry of Nitrogen and Its Compounds* (Wiley-Interscience, New York, 1970).

123. Lake, R., *Anal. Chem.*, 1952, **24**, 1806.

124. Fiedler, R., and Proksch, G., *Anal. Chim. Acta*, 1972, **60**, 277.

125. Simon, H., Daniel, H., and Kleber, J. F., *Angew. Chem.*, 1959, **71**, 303.

126. Proksch, G., *Plant Soil*, 1969, **31**, 380.

127. Perschke, H., Proksch, G., Kero, E. A., and Muhl, A., *Anal. Chim. Acta*, 1971, **53**, 459.

128. Gunter, H., Floss, H. G., and Simon, H. Z., *Anal. Chem.*, 1966, **218**, 401.

129. Bremner, J. M. *Methods of Soil Analysis - part 2* (Inc. Madison, Winsconsin, 1965).

130. Zagato, E. A. G., Reis, B. F., F°, B., and Krug, F. J., *Anal. Chim. Acta*, 1979, **109**, 45.

131. Stewart, J. W. B., Ruzicka, J., Bergamin, H., and Zagatto, E. A. G., *Anal. Chim. Acta*, 1976, **81**, 371.

132. Stewart, J. W. B., and Ruzicka, J., *Anal. Chim. Acta*, 1976, **82**, 137.

133. Sorensen, P., and Jensen, E. S., *Anal. Chim. Acta*, 1991, **252**, 201.

134. Myrold, D. D., and Tiedje, J. M., *Soil Biol. Biochem.*, 1986, **18**, 559.

135. Ross, P.J., and Martin, A. E., *Analyst*, 1970, **95**, 817.

136. Smith, K. A. *Soil Analysis- Modern Instrumental Techniques* 1-659 (Marcel Dekker, Inc., Edinburgh, 1991).

137. Fried, D., and Middelboe, V., *Plant Soil*, 1977, **47**, 713.

138. Fried, M., and Broeshart, H., *Plant Soil*, 1981, **62**, 331.

139. Rittenberg, D. *Preparation and measurement of isotopic tracers* (Wilson, D.W. Nier, A.O.C., Michigan, 1948).

140. Huser, R., and Habfast, K., *Z. Anal. Chem.*, 1960, **176**, 429.

141. Fiedler, R., and Proksch, G., *Anal. Chim. Acta*, 1975, **78**, 1.

142. Mulvaney, R. L., Fohringer, C. L., and Bojan, V. J., *Rev. Sci. Instrum.*, 1990, **61**, 897.

143. Barrie, A., and Lemley, M., *Am. Lab.*, 1989, **21**, 54.

144. Barrie, A., Davies, J. E., and Workman, C. T., *Spectroscopy*, 1989, **4**, 42.

145. Vogel, A. I. *A Text-book of Quantitative Inorganic Analysis* ,1973.

146. Jolles, Z. E. *Bromine and its compounds* 1-940 (Ernest Benn Limited, London, 1966)

147. Carlson, R. M., *Anal. Chem.*, 1986, **58**, 1590.

148. Madsen, B. C., *Anal. Chim. Acta*, 1981, **112486**, 437.

149. Al-Wehaid, A., and Townshend, A., *Anal. Chim. Acta.*, 1986, **186**, 289.

150. Gine, M. F., Bergamin, H. F., and Zagatto, E. A. G., *Anal. Chim. Acta*, 1980, **114**, 191.

151. Van Staden, J. F., *Anal. Chim. Acta*, 1982, **138**, 403.

152. Malcome-Lawes, D. J., and Pasquini, C., *J. Autom. Chem.*, 1988, **10**, 192.

153. Hassan, S. S. M., *Anal. Chim. Acta*, 1972, **58**, 480.